

## II. PHASE DIAGRAMS

L. BREWER, R.H. LAMOREAUX  
Materials and Molecular Research Division,  
Lawrence Berkeley Laboratory,  
and Department of Chemistry,  
University of California,  
Berkeley, California,  
United States of America

### INTRODUCTION

This presentation of phase diagrams represents an attempt to supplement the meagre experimental phase diagram information with chemical bonding models in order to generate thermodynamic data which can be used to calculate the complete phase diagrams. A large fraction of the diagrams is original and has not been available before. Most of the previously available diagrams have been extensively modified to make them consistent with reasonable thermodynamic values. Within the limit of practical accuracy specified below in the section entitled Accuracy of Data, it has been possible to provide essentially complete phase diagrams for 100 of the 102 binary systems of molybdenum with the elements hydrogen to lawrencium.

The available experimental observations and the results of thermodynamic calculations are reviewed in alphabetical order of the chemical symbols of the elements. Unless otherwise specified, the diagrams are given for 1 atm pressure. In general, the figure displaying the phase diagram appears together with the discussion. There are four types of exceptions, all dealing with systems involving such small solubilities that they cannot be read from the diagram. For the systems with a liquid-liquid immiscibility gap, such as those of Mo with Ac and the lanthanide metals Er, Ho, Tb, Gd, and Pm to La, a representative diagram is given in Fig.II-1. The discussion for each system gives analytical equations for the phase boundaries. For the elements Bi, Pb, In, Tl, Cd, Hg, Ag, the lanthanides Yb, Tm, Dy, Eu and Sm, the actinides Bk to Am, the alkaline earth metals other than Be, and the alkali metals, the single diagram given in Fig.II-2 is used. All of these metals boil below the melting point of molybdenum and thus the diagram differs from Fig.II-1 in not having a liquid-liquid immiscibility gap at 1 atm pressure. The order of listing of these elements is in the standard order of the arrangement of the elements across the Periodic Table which is also used in Part I for listing of the thermodynamic values. Figure II-11 represents the phase diagram for the five actinides No to Cf which are predicted to sublime at 1 atm pressure. Finally, for

hydrogen and the noble gases which are gaseous even at room temperature, their type of phase diagram is shown in Fig. II-4. In all instances, the discussion of each binary system presents quantitative information about the boundaries of each of these systems.

#### Phase diagram figures

For all phase diagrams, the ordinate is temperature in degrees Celsius and the abscissa is the composition expressed in atomic per cent of the element added to molybdenum.<sup>1</sup> The phases are usually identified by the elemental symbol or by the ideal crystal formula, even if the actual composition range does not include the stoichiometric composition. The discussion of each diagram or the table associated with it gives the actual composition ranges of each phase.

When a substance exists in solid, liquid or gaseous forms, the designations Mo(s), Mo(l), MoCl<sub>4</sub>(g), etc. indicate the appropriate state. Particularly when there is a wide homogeneous composition range, a composition is not designated and a phase region may be indicated by S, L or G for solid, liquid or gas, respectively. For most diagrams, the pressure is 1 atm and the designation 1 atm gas is used. When the composition of the gas is well defined, the designations 1 atm S<sub>2</sub> or 850 atm N<sub>2</sub>, for example, are used to specify both the composition and the pressure of the gas. When there are miscibility gaps in a liquid or solid-phase regions, the designations L<sub>1</sub>+L<sub>2</sub> or  $\beta_1 + \beta_2$ , respectively, are used. When it is important to distinguish different elemental crystalline modifications, designations such as BCC Zr and HCP Zr, for example, are used. Particularly when there are wide homogeneous ranges, the designations BCC, HCP and CCP are used for body-centred cubic, hexagonal close-packed and cubic close-packed structures, respectively, with no designation of composition. In a few instances, when it is important to designate the structure of an intermediate phase, the Pearson classification symbols may be used, e.g. BMo(116) and BMo(oC8), as discussed in the section on Units and Symbols, or the common Strukturbericht symbols A15, B19, D0<sub>19</sub>, etc. may be used. In some instances, there has been agreement in the literature on the use of symbols to designate structures in a particular system and these have been used in the phase diagrams. For example, in the Mo-Fe system, the symbols  $\sigma$ ,  $\mu$ ,  $\lambda$  and R have been used to designate the four intermediate phases. In other systems,  $\alpha$ ,  $\beta$ ,  $\gamma$ ,  $\eta$ , etc. prefixes are used, for instance in the Mo-C system where the designations  $\alpha$ Mo<sub>2</sub>C,  $\beta$ Mo<sub>2</sub>C,  $\eta$ MoC<sub>1-x</sub>, and  $\alpha$ MoC<sub>1-x</sub> are widely used in the literature to characterize the phases. The text always provides an identification of these symbols as discussed in the section on Units and Symbols.

The diagrams have been kept as uncluttered as possible, with the minimum number of phase designations. In complicated systems, many of the phase boundary compositions and many of the temperatures are tabulated in the text rather than crowding the diagram. In all instances, the discussion of each binary system will

<sup>1</sup> In the diagrams representing molybdenum and only one alloying element, weight per cent scales have also been added.

#### PART II. PHASE DIAGRAMS

present quantitative information about the boundaries of each of these systems. Although the diagrams, for the most part, have been accurately drawn, artistic licence has been taken occasionally at the edges of the diagram to emphasize a change in slope or other details that would not have been apparent if the drawings were exactly to scale. In some instances, the text indicates that the diagram from literature data deviates somewhat from the diagram calculated using the thermodynamic data of Part I. If the uncertainties of both sets overlap, the boundaries indicated by the thermodynamic data are given in the text for the and the thermodynamic data are consistent with one another and the analytical equations in the text reproduce the boundaries shown in the diagram.

#### Units and symbols

In the analytical equations given in the text to represent the phase boundaries, composition is expressed as the mole fraction, x, and temperature is expressed as the temperature in kelvin, T. P represents the pressure in atmospheres. In the text, the compositions are given as mole fraction, or at.%, or atomic ratio, e.g. MoTe<sub>1.90</sub>, but sometimes it is convenient to quote a literature value given in wt%. In the phase diagrams and often in the text, the temperature is given in degrees Celsius. Most of the temperatures given in the literature are based on the 1948 International Practical Temperature Scale (IPTS). These have been retained and the few recent temperatures based on the 1968 IPTS have been corrected so that this review is consistent with the previous Atomic Energy Review Special Issues which have used the 1948 IPTS. If it is desired to convert to the 1968 IPTS, within an accuracy of 1 K, no correction is required below 1014 K. Add 1 K between 1014 and 1379 K. Add 2 K between 1380 and 1925 K. Add 3 K between 1926 and 2377 K. Add 4 K between 2378 and 2770 K. Add 5 K between 2771 and 3124 K. Add 6 K between 3125 and 3449 K.

All phases are characterized in the text by the designation of their crystal structure using the Pearson classification system [186]. For example, the designations BMo(116) and BMo(oC8) distinguish the BMo phase of the tetragonal crystal system with body-centred lattice containing 16 atoms per unit cell from the BMo phase of the orthorhombic crystal system, with one face-centred lattice containing 8 atoms per unit cell. These Pearson designations also serve as a cross-reference to the crystallographic information for the alloys of molybdenum tabulated in Part III of this monograph where each structure is identified by the Pearson symbol as well as the name of the structure type corresponding to the representative substance.

**Analytical expressions**

In recognition of the widespread availability of pocket calculators, the phase boundaries are expressed in analytical form. It is thus not necessary to measure boundary co-ordinates with a ruler. Also, as mentioned above, artistic licence was taken occasionally for some portion of the diagram to emphasize important features.

A variety of analytical formulations has been used. Sometimes  $x$  is given as a function of  $T$  and at other times  $T$  is given as a function of  $x$ . Sometimes  $x$  is given as a function of  $T_{\text{Mp}} - T$  or  $T - T'$ , where  $T_{\text{Mp}}$  is the melting point limit of a solidus or liquidus curve and  $T'$  is some temperature, usually even, designed to limit the magnitude of the variable. The different formulations were designed to fit the boundary as accurately as possible, with as few terms as possible and with constants involving as few digits as possible to simplify the calculations. The general procedure was to calculate the phase diagram boundaries using the thermodynamic values tabulated in Part I. If possible, the exact thermodynamic equation was then used to represent the boundary. In most instances the exact thermodynamic equation is too complicated to be expressed conveniently or may not be possible of representation in explicit form. The next choice was to use an approximation of the exact thermodynamic expression, with the deviation between the exact and approximate expressions being fitted by a simple analytical expression compatible with the approximate equation used. With such an expression, the constants still have some thermodynamic significance. Finally, if it seemed appropriate from the shape of the boundary, a simple power series or a logarithmic term or inverse power term combined with a power series was used. In all instances, only natural logarithms designated by  $\ln x$  have been used.

**Accuracy of data**

It is important for any user of data to know the accuracy of the data. When applying these data, it is important to know the range of possible values of the final result. In all instances, the uncertainty of the phase diagram information is indicated either in terms of uncertainty of the boundaries or in terms of uncertainty of the thermodynamic data of Part I that were used for the calculation of the phase diagrams. In many systems, no experimental data of any type were found and the diagram is based on calculations from thermodynamic data estimated from chemical bonding models in Part I. To be usable, these calculated results have to meet certain minimum standards.

In the centre of the phase diagrams, the calculated boundaries were not considered usable if there was a 50-50 chance that they could be in error by more than 50%. At the edges of a diagram with small solubilities, it was felt that values uncertain by as much as a factor of five could still be useful. At high temperatures

**PART II. PHASE DIAGRAMS**

near the melting point the vacancy or defect concentration for a solid phase is fixed by designating temperature, pressure and composition. However, at lower temperatures, the defect concentration depends upon the quenching history and is not fixed by the state variables. When the calculated solid solubilities at lower temperatures were of the order of the defect concentrations, e.g. a mole fraction of the order  $10^{-5}$ , depending upon the temperature, there was felt that such calculated solubilities would not have any significance. The observed solubilities reported solubilities were truncated at temperatures at which it was felt that the quenched defects were the determining factor in fixing the amount of retained solute. In handling the enormous mass of numbers used in calculating and describing the phase diagrams, it is inevitable that there will be errors in transcription. We would appreciate hearing of any corrections that we have missed.

**References**

The literature examined was based on a complete review of the entries in the Bulletin of Thermodynamics and Thermochemistry through No. 21 (August 1978) and Chemical Abstracts through Vol. 89 (1978); a few recent publications up to 1979 were also included. Many thousand references dealing with molybdenum systems were examined. A considerable fraction did not deal directly with the phase diagrams or thermodynamic properties. High-temperature phase diagrams are difficult to determine and many serious systematic errors are not readily detected. Of the references that did present phase diagram information, more than one half were found to have clearly inaccurate or misleading results by comparison with other references deemed reliable or by comparison with bonding theory models. Several of the systems had been reviewed previously in the literature. When our treatment of the literature agreed with the previous review, it was felt redundant to discuss the reviewed publications and only the review paper is referred to, unless a certain reference is specifically required for discussion of some aspect of the system. Otherwise, a complete listing of the references used in the evaluation is given.

Unless otherwise specified, melting points, transition temperatures and other properties of the elemental phases being added to molybdenum were taken from the critical compilation of Hultgren et al. [120]. The values of the elemental melting points, enthalpies of fusion and enthalpies of sublimation given by Hultgren et al. have been tabulated and updated where necessary by Lamoreaux [157] and Brewer [33]. The thermodynamic procedures, bonding models and calculation programs [32, 34] used to calculate phase diagrams when no phase diagram information was found or to correct reported experimental diagrams are referenced in Part I which presents the thermodynamic values for each system.

## ACKNOWLEDGEMENTS

This complete presentation of phase diagrams would not have been possible without the foundation of understanding of chemical bonding and molecular interactions developed by G.N. Lewis and J.H. Hildebrand, to which L. Pauling has added so importantly in his development of the valence-bond model for metals. N. Engel has combined the important empirical correlations of W. Hume-Rothery with the bonding concepts of L. Pauling in a description of metallic bonding that has made possible the conversion from theory to practical concrete results such as phase diagrams.

We are indebted to the Division of Materials Science, Office of Basic Energy Sciences, of the United States Department of Energy and its predecessors for their support of the research that provided the development and testing of the procedures for the present work. We wish to acknowledge the important contribution of K.M. Krushwitz to the reliable transcription and professional checking of the accuracy of the final results.

We are indebted to Gloria C. Pelatowski and R.G. Stevens for their skill and care in the accurate preparation of the phase diagram drawings. We wish to express our gratitude for information that was provided to us by authors in advance of publication, as indicated in the References. We are especially indebted to H. Weeks for his efficient retrieval of the multitude of the journal articles examined during the preparation of this review.

## PHASE DIAGRAMS

## Mo-Ac: molybdenum-actinium (Fig.II-1)

No data were found. The estimated thermodynamic equations of Part I have been used to calculate the phase boundaries of Fig.II-1.

The monotectic is at  $2790 \pm 5$  K and  $x_{Ac} = 1.5 \times 10^{-3}$ ,  $0.062 \pm 0.005$  and  $0.70 \pm 0.03$ . The molybdenum solidus and liquidus above the monotectic are calculated to be

$$x_{Ac} = 6 \times 10^{-4}(2890-T) - 4 \times 10^{-7}(2890-T)^2$$

with an uncertainty of  $\pm 10^{-4}(2890-T)$  for the liquidus, and

$$x_{Ac} = 1.5 \times 10^{-5}(2890-T)$$

with an uncertainty of a factor of 5 for the solidus.

## ACKNOWLEDGEMENTS

This complete presentation of phase diagrams would not have been possible without the foundation of understanding of chemical bonding and molecular interactions developed by G.N. Lewis and J.H. Hildebrand, to which L. Pauling has added so importantly in his development of the valence-bond model for metals. N. Engel has combined the important empirical correlations of W. Hume-Rothery with the bonding concepts of L. Pauling in a description of metallic bonding that has made possible the conversion from theory to practical concrete results such as phase diagrams.

We are indebted to the Division of Materials Science, Office of Basic Energy Sciences, of the United States Department of Energy and its predecessors for their support of the research that provided the development and testing of the procedures for the present work. We wish to acknowledge the important contribution of K.M. Krushwitz to the reliable transcription and professional checking of the accuracy of the final results.

We are indebted to Gloria C. Pelatowski and R.G. Stevens for their skill and care in the accurate preparation of the phase diagram drawings. We wish to express our gratitude for information that was provided to us by authors in advance of publication, as indicated in the References. We are especially indebted to H. Weeks for his efficient retrieval of the multitude of the journal articles examined during the preparation of this review.

## PHASE DIAGRAMS

## Mo-Ac: molybdenum-actinium (Fig.II-1)

No data were found. The estimated thermodynamic equations of Part I have been used to calculate the phase boundaries of Fig.II-1.

The monotectic is at  $2790 \pm 5$  K and  $x_{Ac} = 1.5 \times 10^{-3}$ ,  $0.062 \pm 0.005$  and  $0.70 \pm 0.03$ . The molybdenum solidus and liquidus above the monotectic are calculated to be

$$x_{Ac} = 6 \times 10^{-4}(2890-T) - 4 \times 10^{-7}(2890-T)^2$$

with an uncertainty of  $\pm 10^{-4}(2890-T)$  for the liquidus, and

$$x_{Ac} = 1.5 \times 10^{-5}(2890-T)$$

with an uncertainty of a factor of 5 for the solidus.

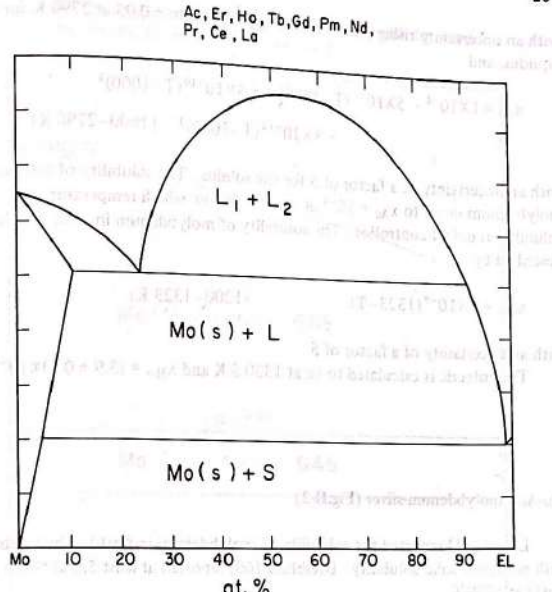


FIG.II-1. Phase diagram of a system Mo-El, where El is actinium or one of the lanthanides shown above.

The two-liquid phase boundaries from 2790 to 3100 K are represented by

$$x_{Ac} = 0.055 + 8 \times 10^{-5}(T-2700) + 10^{-8}(T-2700)^2$$

with an uncertainty of  $\pm 0.005$ , and

$$x_{Mo} = 0.275 + 3 \times 10^{-4}(T-2700) + 10^{-8}(T-2700)^2$$

with an uncertainty of  $\pm 0.03$ .

The phase boundaries between molybdenum and liquid actinium below 2790 K are described by

$$x_{Mo} = -0.015 + 8.2 \times 10^{-5}(T-1000) - 10^{-7}(T-1000)^2 + 8.3 \times 10^{-11}(T-1000)^3 \quad (1300-2790 \text{ K})$$

with an uncertainty rising from  $\pm 5 \times 10^{-4}$  at 1320 K to  $\pm 0.03$  at 2790 K for the liquidus, and

$$x_{Ac} = 1 \times 10^{-4} - 5 \times 10^{-7}(T-1000) + 5.5 \times 10^{-10}(T-1000)^2 \\ + 8 \times 10^{-14}(T-1000)^3 \quad (1800-2790 \text{ K})$$

with an uncertainty of a factor of 5 for the solidus. The solubility of actinium in molybdenum drops to  $x_{Ac} = 10^{-4}$  at 1800 K, below which temperature the solubility is defect-controlled. The solubility of molybdenum in solid actinium is described by

$$x_{Mo} = 9 \times 10^{-7}(1323-T) \quad (1200-1323 \text{ K})$$

with an uncertainty of a factor of 5.

The eutectic is calculated to be at 1320.5 K and  $x_{Mo} = (3.9 \pm 0.5) \times 10^{-3}$ .

#### Mo-Ag: molybdenum-silver (Fig. II-2)

Linel [163] reported the solubility of molybdenum in Ag( $\infty$ ) to be limited, with negligible solid solubility. Dreibholz [60] reported at least 5.6 at.% Mo in Ag( $\infty$ ) at 1600°C.

From the thermodynamic data of Part I, the phase diagram was calculated as follows: Between the eutectic and the melting point of silver, the silver liquidus is given by

$$x_{Mo} = 8.76 \times 10^{-4}(1234-T)$$

with an uncertainty of 0.5%, and the silver solidus is given by

$$x_{Mo} = 4 \times 10^{-4}(1234-T)$$

with an uncertainty of a factor of 5. The eutectic is calculated to be at  $959 \pm 2^\circ\text{C}$ , with the solid compositions  $x_{Ag} = 6 \times 10^{-5}$  and  $x_{Mo} = 1.5 \times 10^{-3}$ , in equilibrium with liquid  $x_{Mo} = 0.0033$ . The molybdenum solidus is given within a factor of four by

$$\ln x_{Ag} = -10700 T^{-1} - 0.06 - 1.98 \times 10^{-3} T + 1.29 \times 10^{-6} T^2 - 2.82 \times 10^{-10} T^3 \\ (1232-2501 \text{ K})$$

#### PART II. PHASE DIAGRAMS

Bi; Pb; In, Tl; Cd, Hg; Ag; Yb, Tm, Dy, Eu, Sm; Bk, Cm, Am; Mg, Ca, Sr, Ba, Ra; Li, Na, K, Rb, Cs, Fr

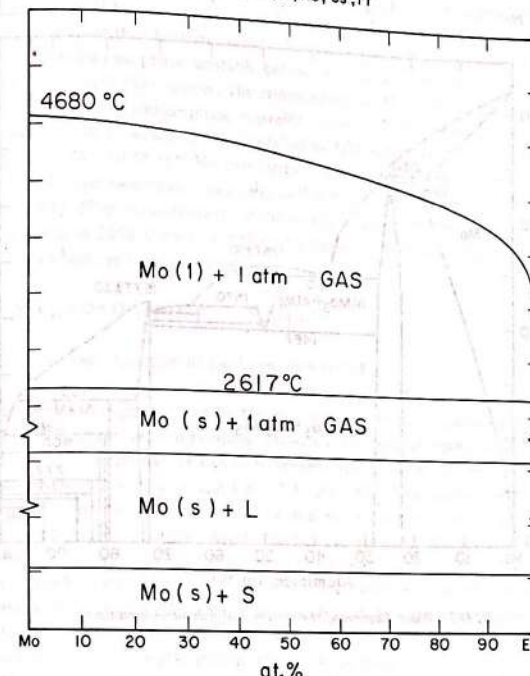


FIG. II-2. Phase diagram of a system Mo-El, where El is one of the elements shown above in M the sequence of the standard order of arrangement of the elements.

The molybdenum liquidus is given by  

$$T = \frac{5246 + 4100(1-x_{Mo})^2}{1.86 - \ln x_{Mo}} \pm 70^\circ \quad (1232-2501 \text{ K})$$

The liquidus is terminated at 2501 K, with molybdenum liquid;  $x_{Ag} = 0.38$ , in equilibrium with silver gas at 1 atm, and molybdenum solid, with  $x_{Ag} = 0.0035$ .

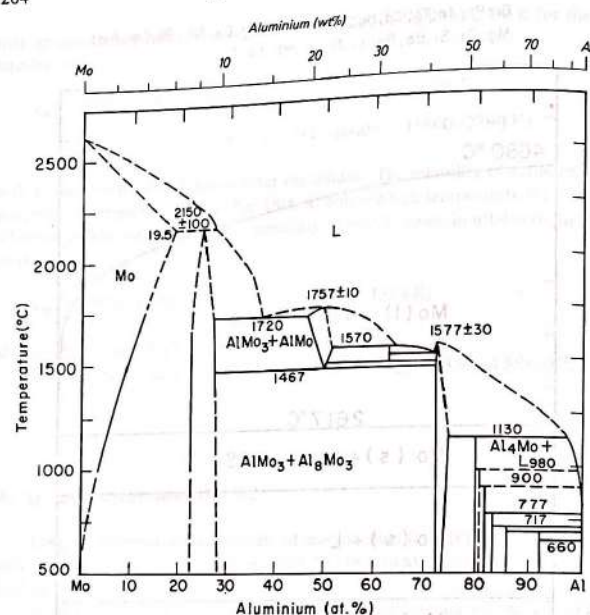


FIG.II-3. Phase diagram of the system molybdenum-aluminium.

Mo-Al: molybdenum-aluminium (Fig.II-3)

Part III reviews the many phases that have been reported for this system. Hansen and Anderko [109], Elliott [68] and Shunk [228] have covered the extensive phase diagram literature through 1964. Recent work has modified the diagram. All of the earlier work on the molybdenum-rich side had indicated the phase  $\text{AlMo}_3$ (cP8) with a homogeneous range of 73–78 at.% Mo and a peritectic at around 2150°C, in equilibrium with molybdenum, containing a maximum aluminium content of 19.5 at.% on one side and forming a eutectic at 1760°C and 50 at.% Mo on the other side. Two recent studies [15, 62] have confirmed the older work, but Kamei et al. [129] did not observe the  $\text{AlMo}_3$  phase, and their melting point determinations and metallographic examinations gave no evidence

for a eutectic. The boundary that they report for the bcc molybdenum phase is very close to the boundary reported for the  $\text{AlMo}_3$  phase. It appears that they have mistaken the  $\text{AlMo}_3$  phase for the bcc molybdenum phase, or  $\text{AlMo}_3$  did not nucleate and they have measured a metastable boundary. Kamei et al. [129] have reported a new phase, unstable below  $1465 \pm 25^\circ\text{C}$  and melting around  $1760^\circ\text{C}$ , to which they assigned the composition  $\text{Al}_3\text{Mo}_2$ . Rexer [201] has recently reported a similar phase, unstable below  $1470^\circ\text{C}$  and melting congruently at around  $1750^\circ\text{C}$ , which he has identified as  $\text{AlMo}(\text{cI}2)$ . It has a homogeneous range from 48.5 to 54 at.% Mo and forms a eutectic, with  $\text{AlMo}_3$  at  $1720^\circ\text{C}$  and 63 at.% Mo, corresponding reasonably well with the eutectic reported in earlier work [234]. Nine measurements of the molybdenum solvus between 1000 and  $1700^\circ\text{C}$  and at  $2150^\circ\text{C}$  by four different groups [15, 108, 201, 234] are in excellent agreement and can be represented by

$$\ln x_{\text{Al}} = 0.618 - 5040 T^{-1} - 5.2 \times 10^{-5} T$$

with the average deviation of  $x_{\text{Al}}$  being only 0.004.

The phase in equilibrium with  $\text{AlMo}_3$  below  $1467^\circ\text{C}$  has been in dispute. Sperner [234] designated it as  $\text{Al}_2\text{Mo}$ , and Belyaeva et al. [15] and Kamei et al. [129] presented diagrams in confirmation. However, the metallographic observations of Kamei et al. indicate two phases to be present at  $600^\circ\text{C}$  for the composition ranges  $\text{Al}/\text{Mo} = 2.47 - 1.75$  and  $1.6 - 1.1$ . At  $1000^\circ\text{C}$  and  $1300 - 1475^\circ\text{C}$ , they find two phases for  $\text{Al}/\text{Mo} = 2$  and for compositions richer in molybdenum. In addition to  $\text{Al}_2\text{Mo}$ , the phase  $\text{Al}_3\text{Mo}$  has been in question. Vengrenovich and Psarev [256] have suggested that the reported  $\text{Al}_3\text{Mo}$  is a metastable phase that transforms to stable  $\text{Al}_5\text{Mo}$ . Pötzschke and Schubert [192] report a phase, in addition to  $\text{Al}_8\text{Mo}_3$ , in alloys between 74 and 79 at.%, which may be this metastable  $\text{Al}_3\text{Mo}$  phase. A number of studies [62, 78, 192, 201, 259] have indicated that the phases designated as  $\text{Al}_2\text{Mo}$  and  $\text{Al}_3\text{Mo}$  should be assigned to portions of the  $\text{Al}_8\text{Mo}_3$  homogeneous range which, according to Forsyth and Gran [78], extends from  $\text{Al}/\text{Mo} = 2.2$  to 3. However, Rexer [201] fixes the molybdenum-rich boundary at  $\text{Al}/\text{Mo} = 2.57$ . He also indicates that the  $\text{Al}_8\text{Mo}_3$  phase melts congruently around  $1575^\circ\text{C}$ . In Fig.II-3, Rexer has been followed in indicating no stable phases below  $1467^\circ\text{C}$  between 27 and 72 at.% Al. However, at high temperatures, Rexer reports the phase  $\text{Al}_{6.7}\text{Mo}_{3.7}$ , which has a range of stability only between  $1490$  and  $1570^\circ\text{C}$ , and which forms a eutectic with  $\text{Al}_8\text{Mo}_3$  at  $1535^\circ\text{C}$  and 72 at.% Al.

There have been indications [62, 192] of unusual complexity in the region between 80 and 83 at.% Al. Van Tendeloo et al. [254] have recently demonstrated that a series of stacking variants with missing aluminium planes have the general composition  $\text{Al}_{5n+2}\text{Mo}_{n+1}$ . In the range  $600$  to  $740^\circ\text{C}$ , phases with  $\text{Al}/\text{Mo} = 4.05$ , 4.24 and 4.46 were found, corresponding to  $n = 2$  to 4.

TABLE II-1. PHASES OF THE Al-Mo SYSTEM

Phase (structure)	Maximum composition range (at.% Al)	Melting or peritectic temperature (K)
Mo (cI2)	0–19.5	m2890 ± 8
AlMo <sub>3</sub> (cP8)	22–27	p2423 ± 100
AlMo (cI2)	46–51.5	1740 ± 10 to m2030 ± 10
Al <sub>63</sub> Mo <sub>37</sub>	63 ± 0.5	1763 ± 10 to p1843 ± 10
Al <sub>8</sub> Mo <sub>3</sub> (mC22)	72–75	m1850 ± 30
Al <sub>4</sub> Mo (mC30)	80.2 ± 0.2	p1403 ± 20
Al <sub>17</sub> Mo <sub>4</sub>	80.9 ± 0.2	p1250 ± 100
Al <sub>22</sub> Mo <sub>5</sub>	81.7 ± 0.2	p1170 ± 80
Al <sub>5</sub> Mo (hP12)	83.3 ± 0.1	p1050 ± 20
Al <sub>6</sub> Mo (m)	86 ± 0.5	p990 ± 10
Al <sub>12</sub> Mo (cI26)	92.42 ± 0.05	p963 ± 10
Al (cF4)	99.95–100	m933.25

The number of aluminium-rich phases, their compositions and their peritectic temperatures have been in question because of difficulty of attaining equilibrium, and additional work is needed to clarify this portion of the diagram. Walford [259] has reviewed previous observations and has suggested a reassignment that is accepted here. The most aluminium-rich phase is Al<sub>12</sub>Mo(cI26) for which the peritectic temperature of 690 ± 10°C is based on reported values of 684°C [129], 700°C [234], 703°C [265] and 706°C [52]. The next phase is of unknown structure [52], but chemical analyses [259] indicate a composition Al<sub>6</sub>Mo. The second observed peritectic at 717°C [129] or 735°C [228] had been assigned to Al<sub>1</sub>Mo, but following Walford [259], the second peritectic is assigned to Al<sub>6</sub>Mo. The value of 717°C was accepted. This is consistent with the observation of Pötzschke and Schubert [192] that a melt of 87 at.% Al yields Al<sub>5</sub>Mo down to 720°C, while at 700°C the Al<sub>5</sub>Mo reacts with the melt to yield Al<sub>12</sub>Mo, and a second phase that is assigned to Al<sub>6</sub>Mo by Walford. Walford reviews data which indicate that Al<sub>5</sub>Mo is unstable at 800°C but stable at 750°C. On this basis the Al<sub>5</sub>Mo peritectic temperature is taken as 777 ± 20°C. Pötzschke and Schubert [192] report that 83 at.% Al samples yield Al<sub>4</sub>Mo at 1000°C but form a new phase at 870°C. On this basis, a peritectic temperature of 900 ± 80°C was assigned to

## PART II. PHASE DIAGRAMS

Al<sub>22</sub>Mo<sub>5</sub>, although it is possible that Al<sub>17</sub>Mo<sub>4</sub> was the phase observed. For Al<sub>17</sub>Mo<sub>4</sub>, a peritectic temperature of 980 ± 100°C was estimated. Sperner [234] had given the peritectic temperature of Al<sub>5</sub>Mo as 1130°C; Walford reassigned this temperature to Al<sub>4</sub>Mo. Table II-1 lists the present assignments for the phases of the Al-Mo system, their crystal structures, their maximum composition ranges and their melting or peritectic temperatures.

Part III gives references to quenched solid solutions of molybdenum in solid aluminium. The differential thermal analysis and metallographic measurements of Kamei et al. [129] indicate that the liquid in equilibrium with solid aluminium contains less molybdenum than  $x_{\text{Mo}} = 6 \times 10^{-4}$  and probably less than  $x_{\text{Mo}} = 3 \times 10^{-4}$ . The equilibrium solid solubility is not likely to be much higher. A eutectic is assumed, with the eutectic temperature 0.1°C below the melting point of pure aluminium. The Al<sub>12</sub>Mo liquidus extends from the eutectic with aluminium at 660–690°C, where  $x_{\text{Mo}} = 6 \times 10^{-4}$  [129]. Along the Al<sub>6</sub>Mo liquidus,  $x_{\text{Mo}}$  increases to  $9 \times 10^{-4}$  at 717°C [129]. The data of Yamaguchi and Simizu [265] join those of Kamei et al. [129] and indicate that  $x_{\text{Mo}} = (1.9 \pm 0.4) \times 10^{-3}$  for the liquid of the Al<sub>5</sub>Mo peritectic at 777°C. The closely related phases Al<sub>6</sub>Mo, Al<sub>22</sub>Mo<sub>5</sub>, Al<sub>17</sub>Mo<sub>4</sub> and Al<sub>4</sub>Mo should have very similar values for the partial molal enthalpies of molybdenum and only small changes in slope should occur at each peritectic. The data of Yamaguchi and Simizu were used to represent the combined liquidus curve for the four phases by

$$\ln x_{\text{Mo}} = 3.62 - 10460 T^{-1} \pm 0.09 \quad (990-1403 \text{ K})$$

The temperature given for the Al<sub>22</sub>Mo<sub>5</sub> peritectic, 1170 ± 80 K, is very uncertain, but at 1170 K,  $x_{\text{Mo}} = (4.9 \pm 0.4) \times 10^{-3}$ . Likewise,  $x_{\text{Mo}} = (9 \pm 1) \times 10^{-3}$  at 1250 ± 100 K, the Al<sub>17</sub>Mo<sub>4</sub> peritectic. Extrapolation to 1403 ± 20 K, the Al<sub>4</sub>Mo peritectic, yields  $x_{\text{Mo}} = (2 \pm 0.2) \times 10^{-2}$  as the liquid composition.

The aluminium-rich liquidus of the Al<sub>3</sub>Mo-Al<sub>8</sub>Mo<sub>3</sub> solid solution is calculated to be

$$x_{\text{Mo}} = 0.27 - 3.4 \times 10^{-4}(1850-T) - 2.23 \times 10^{-6}(1850-T)^2 \\ + 3.9 \times 10^{-9}(1850-T)^3 \pm 0.03 \quad (1403-1850 \text{ K})$$

Because of the small variations in the molybdenum and aluminium activities in the centre of the diagram, the thermodynamic data are not accurate enough to provide calculations of the AlMo or Al<sub>63</sub>Mo<sub>37</sub> liquidus boundaries. The boundaries shown in Fig.II-3 are rough estimates. The AlMo<sub>3</sub> liquidus is calculated to be

$$x_{\text{Al}} = 0.37 - 5 \times 10^{-5}(T-2000) - 2 \times 10^{-8}(T-2000)^2 \\ - 1.1 \times 10^{-9}(T-2000)^3 \pm 0.03 \quad (1993-2423 \text{ K})$$

The molybdenum liquidus is calculated to be

$$x_{Al} = 5.8 \times 10^{-4}(2890-T) - 3.8 \times 10^{-6}(2890-T)^2 + 2.05 \times 10^{-8}(2890-T)^3 - 2.67 \times 10^{-11}(2890-T)^4 \pm 10\% \quad (2423-2890 \text{ K})$$

The molybdenum solidus is calculated to be

$$x_{Al} = 1.75 \times 10^{-4}(2890-T) + 2.06 \times 10^{-6}(2890-T)^2 - 2.7 \times 10^{-9}(2890-T)^3$$

with an uncertainty of 5%. The equation for the molybdenum boundary saturated by  $AlMo_3$  has been given earlier.

#### Mo-Am: molybdenum-americium (Fig.II-2)

No data were found. The estimated thermodynamic equations of Part I have been used to calculate the phase boundaries of Fig.II-2.

The eutectic is calculated to be at  $1405 \pm 10$  K and  $x_{Mo} = 0.04 \pm 0.01$ . Above 1405 K the americium liquidus and solidus are calculated to be

$$x_{Mo} = 7 \times 10^{-4}(1447-T) + 3 \times 10^{-6}(1447-T)^2$$

with an uncertainty of  $2 \times 10^{-4}(1449-T)$  for the liquidus, and

$$x_{Mo} = 10^{-4}(1447-T)$$

with an uncertainty of a factor of 5 for the solidus.

The molybdenum solidus and liquidus between 1405 and 2200 K, the estimated normal boiling point of americium, are calculated to be

$$x_{Am} = 0.002 - 6 \times 10^{-6}(T-1000) + 2.2 \times 10^{-8}(T-1000)^2 - 8 \times 10^{-12}(T-1000)^3$$

and

$$x_{Mo} = -0.01 + 10^{-4}(T-1000) - 10^{-8}(T-1000)^2 + 1.1 \times 10^{-10}(T-1000)^3$$

The uncertainty in  $x_{Mo}$  rises from  $\pm 0.015$  at 1405 K to  $\pm 0.05$  at 2200 K. The uncertainty in  $x_{Am}$  is a factor of 5.

The solid solution phase boundaries below 1405 K are calculated to be

$$x_{Mo} = 6 \times 10^{-5} + 10^{-6}(T-800) + 3 \times 10^{-9}(T-800)^2 + 1.2 \times 10^{-11}(T-800)^3$$

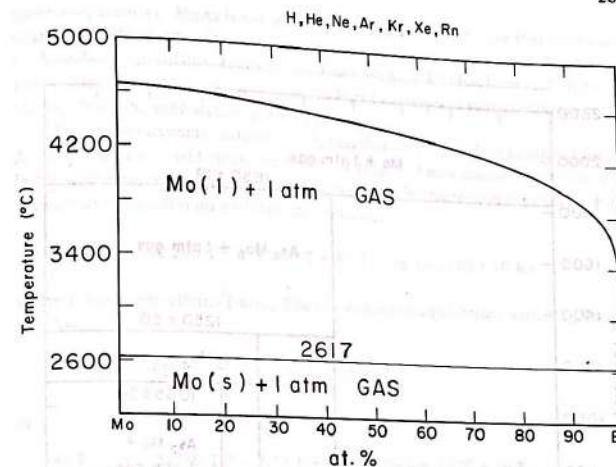


FIG.II-4. Phase diagram of a system Mo-El, where El is hydrogen or one of the noble gas elements shown above.

and

$$x_{Am} = 3 \times 10^{-5} + 4 \times 10^{-7}(T-800) + 8 \times 10^{-12}(T-800)^3$$

The solubility of americium in molybdenum falls to  $10^{-4}$ , with an uncertainty of a factor of 5 at 930 K, and the solubility of molybdenum in americium falls to  $10^{-4}$ , with an uncertainty of a factor of 5 at 840 K. Below these temperatures the solubilities are defect-controlled.

#### Mo-Ar: molybdenum-argon (Fig.II-4)

No experimental data were found; the phase diagram of Fig.II-4 was calculated from the theoretical thermodynamic data of Part I. Since the calculated solubilities in ideal molybdenum solid are much smaller than the defect concentrations which depend upon the quenching history, the solid solubilities have no thermodynamic significance. For liquid molybdenum at 2890 K, in equilibrium with 1 atm gas, the order of magnitude of the mole fraction of argon is calculated to be  $10^{-15}$ .

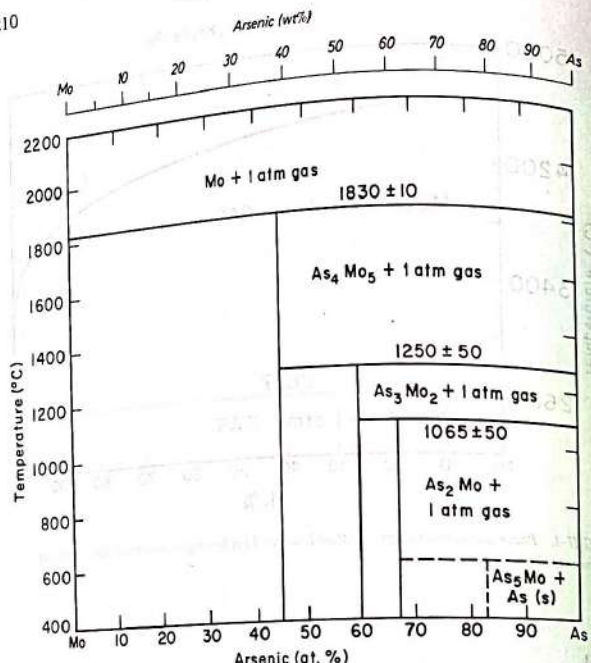


FIG.II-5. Phase diagram of the system molybdenum-arsenic.

**Mo-As:** molybdenum-arsenic (Fig.II-5)

No phase diagrams were found in the literature. Figure II-5 was calculated from the thermodynamic data of Part I. All studies [22, 35, 103, 124–126, 130, 246] of the molybdenum arsenide phases agree on  $\text{Mo}_3\text{As}_4$ (tI18),  $\text{Mo}_2\text{As}_3$ (mC20) and  $\text{MoAs}_2$ (mC12). X-ray data gave no evidence of significant homogeneous ranges for the intermediate phases or for the elements; any homogeneous range would thus be less than 2–3% in extent. Two studies [22, 130] indicate the existence of the phase  $\text{Mo}_{49}\text{As}_{51}$ (oP8) which is reported to be stable at 700°C and unstable at 1100°C. A recent study [103] has shown that the  $\text{MoAs}$ (oP8) phase can be stabilized at temperatures of 1050–1250°C by adding FeAs and other arsenides, but phases with more than 95% MoAs are unstable at

**PART II. PHASE DIAGRAMS**

these temperatures.  $\text{MoAs}$  is not shown as a phase in Fig.II-5; the thermodynamic values given for  $\text{MoAs}$  in Part I correspond to metastability of pure  $\text{MoAs}$  or, at most, stability up to 500–600°C. The phase  $\text{MoAs}_3$ (oP5) has been reported by Brown [35]. The thermodynamic data in Part I correspond to decomposition of  $\text{MoAs}_3$  above the sublimation point of arsenic.

The thermodynamic data of Part I, together with the values tabulated for  $\text{As}_2$  and  $\text{As}_4$  gases, yield values for the three ranges of dissociative vaporization. In the following equations, P gives the dissociation pressure in atmospheres. For the vapour in equilibrium with Mo and  $\text{Mo}_2\text{As}_4$ ,

$$\ln P_{\text{As}_2} = -42\,290 T^{-1} - 1.6 \ln T + 32.32 \quad (\text{up to } 2110 \pm 10 \text{ K})$$

where the pressure attains 1 atm. For the vapour in equilibrium with  $\text{Mo}_2\text{As}_4$  and  $\text{Mo}_2\text{As}_3$ ,

$$\ln P_{\text{As}_2} = -32\,890 T^{-1} - 1.6 \ln T + 32.34$$

or

$$\ln P_{\text{As}_4} = -40\,480 T^{-1} - 6 \ln T + 70.09 \quad (\text{below } 1520 \pm 50 \text{ K})$$

where the sum of  $\text{As}_4$  and  $\text{As}_2$  pressures attains 1 atm. For  $\text{Mo}_2\text{As}_3 + \text{MoAs}_2$ ,

$$\ln P_{\text{As}_4} = -38\,700 T^{-1} - 6 \ln T + 71.61 \quad (\text{below } 1340 \pm 50 \text{ K})$$

where the sum of  $\text{As}_4$  and  $\text{As}_2$  pressures reaches 1 atm.

**Mo-At:** molybdenum-astatin

No data were found and it was not possible in Part I to estimate accurate enough thermodynamic data to fix the phase diagram. A reasonable guess is that the phase diagram would be similar to Fig.II-22, the diagram for iodine, with only the single phase  $\text{MoAt}_2$  being stable.

**Mo-Au:** molybdenum-gold (Fig.II-6)

No liquidus data have been reported and the liquidus curves of Fig.II-6 were calculated from the estimated thermodynamic data of Part I. Geach and Summers-Smith [86] report solid solubilities of molybdenum in gold ranging from 0.65 at.% at 20°C to 1.2 at.% at 1000°C. They give a eutectic temperature of 1054°C. Raub [198] reports the eutectic at 1058°C. No detectable solid solubility

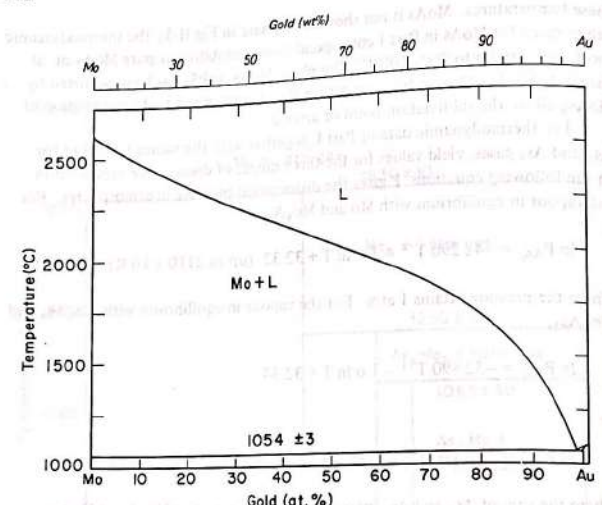


FIG.II-6. Phase diagram of the system molybdenum-gold.

of gold in molybdenum was found by either. Part III reviews data on metastable quenched alloys.

The data of Geach and Summers-Smith give much too negative partial molal entropies of molybdenum. The reported solubilities at lower temperatures should be much smaller and they were discarded. As a compromise, the solid solubility of molybdenum in gold can be represented by

$$\ln x_{\text{Mo}} = -3.6 - 1190 T^{-1} \pm 0.2 \quad (300-1327 \text{ K})$$

The gold liquidus is given by

$$x_{\text{Mo}} = 2.289 \times 10^{-3} (1336.15 - T) \pm 0.0002 \quad (1327-1336 \text{ K})$$

The gold solidus is given by

$$x_{\text{Mo}} = 1.34 \times 10^{-3} (1336.15 - T) \pm 1 \times 10^{-4} \quad (1327-1363 \text{ K})$$

## PART II. PHASE DIAGRAMS

The molybdenum liquidus is given by

$$T = \frac{5150 + 2450 (1 - x_{\text{Mo}})^2}{1.782 - \ln x_{\text{Mo}}} \pm 15^\circ \quad (1327-2890 \text{ K})$$

The molybdenum solidus is given by

$$\ln x_{\text{Au}} = \ln (2890 - T) - 9460 T^{-1} - 9.686 + 9.86 \times 10^{-4} T - 9.27 \times 10^{-8} T^2 \pm 0.5 \quad (1327-2890 \text{ K})$$

The maximum value of  $x_{\text{Au}} = 4 \times 10^{-3}$  occurs at 2400 K. At the eutectic temperature of 1054°C, the calculated solid compositions are  $x_{\text{Au}} = 2.5 \times 10^{-4}$  and  $x_{\text{Mo}} = 0.0125 \pm 0.001$ , together with  $x_{\text{Mo}} = 0.021 \pm 0.005$  in the liquid.

Mo-B: molybdenum-boron (Fig.II-7)

The crystallographic literature of the molybdenum borides is reviewed in Part III. The phase diagram given by Hansen and Anderko [109] and Elliott [68], based on work up to 1960, comes mainly from the work of Steinitz et al. [238] and of Giles and Pollock [88]. Since then, Rudy and Windisch [208] have made a detailed study of the complete system and Fig.II-7 is taken largely from their diagram. Portnoi et al. [191] have obtained results that are in good agreement.

In the following comparisons, the value of Portnoi et al. is given last. For the Mo-BMo<sub>2</sub> eutectic:  $2175 \pm 6^\circ \text{C}$  compared with  $2200 \pm 15^\circ \text{C}$ , and  $23 \pm 1$  at.% B versus  $> 20$  at.% B. For the BMo<sub>2</sub> peritectic:  $2280 \pm 12^\circ \text{C}$  versus  $2270 \pm 20^\circ \text{C}$ . For the BMo melting point:  $2600 \pm 8^\circ \text{C}$  versus  $2550^\circ \text{C}$ . For the B<sub>2</sub>Mo peritectic:  $2375 \pm 15^\circ \text{C}$  versus  $2350 \pm 15^\circ \text{C}$ . For the peritectoid formation of BMo(t116) from BMo<sub>2</sub> and BMo (oC8):  $2180 \pm 30^\circ \text{C}$  versus  $2000^\circ \text{C}$ . For the eutectoid formation of BMo(oC8) from B<sub>2</sub>Mo and BMo(t116):  $1800 \pm 80^\circ \text{C}$  versus  $1900^\circ \text{C}$ . For the B<sub>5</sub>Mo<sub>2</sub> peritectic:  $2140 \pm 15^\circ \text{C}$  versus  $2200 \pm 30^\circ \text{C}$ . For the decomposition of B<sub>2</sub>Mo to BMo and B<sub>3</sub>Mo<sub>2</sub>:  $1520 \pm 50^\circ \text{C}$  versus  $1500^\circ \text{C}$  (Storms and Mueller [241]) have recently fixed this temperature as  $1517 \pm 15^\circ \text{C}$ .

The only significant difference has to do with the highest boride which had been designated B<sub>12</sub>Mo by Rudy et al. [206]. However, Chretien and Helgorsky [48] had reported a phase of composition B<sub>4</sub>Mo, which Rudy and Windisch [208] found to be identical with the phase previously reported as B<sub>12</sub>Mo. Nowotny et al. [178] and Galasso and Pinto [81] have discussed this phase, and Lundström and Rosenberg [164] have established it as B<sub>3</sub>Mo<sub>1-x</sub> with a very small homogeneous range with x around 0.20. This corresponds to about 79 at.% B or just short of the composition B<sub>4</sub>Mo. The diagram of Portnoi et al. [191] shows a congruently melting phase at 92 at.% B which is rejected in view of the above results. Storms

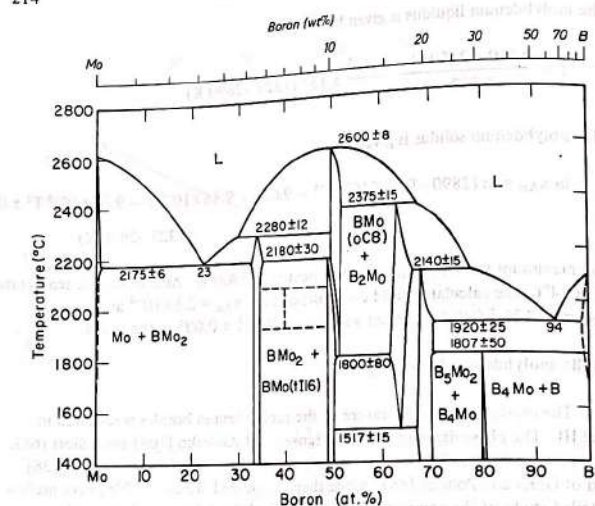


FIG.II-7. Phase diagram of the system molybdenum-boron.

and Mueller [241] were able to improve upon the very rough value of 1800°C for the peritectic temperature of  $B_3Mo_{0.8}$  given by Rudy and Windisch to obtain  $1807 \pm 50^\circ C$ .

There have been several reports [51, 88, 147, 238, 264] of  $B_2Mo_3$ (tP10 or tI32). The phase is reported to have a limited temperature range of stability. The work of Storms and Mueller excludes its existence below 1900°C, and the work of Rudy and Windisch excludes its existence above 2180°C. The phase is indicated in Fig.II-7 with dotted lines to indicate its uncertainty. Aronsson [12] has established the stability of  $Mo_2B_2Si$ (tI32). Since samples are often prepared in silica containers, the reported  $B_2Mo_3$  may be a ternary phase. Another possibility of a ternary phase would be  $Mo_2FeB_2$ (tP10), which was prepared by Rieger et al. [202]. Similar ternary phases are known with cobalt and titanium and can be expected with other transition metals that may be present as contaminants in high-temperature systems. Rudy and Windisch suggest carbide phases to account for the reported  $B_2Mo_3$  and they doubt its existence in the binary system.

The solubility of molybdenum in boron has not been established. Seybolt [226] reports that boron with 1 at.% Mo is a single phase. A number of determinations

## PART II. PHASE DIAGRAMS

TABLE II-2. PHASES OF THE B-MO SYSTEM

Phase (structure)	Maximum composition range (at.% B)	Melting or peritectic temperature (K)
Mo (cI2)	0–0.8	m2890 ± 8
BMo <sub>2</sub> (tII2)	33–34	p2553 ± 12
$B_2Mo_3$ (tP10)?	?	> 2223?, < 2400?
BMo (tI16)	48.5–50.0	tr, 2073 ± 80 to 2453 ± 50; m2873 ± 8
BMo (oC8)	49–52	d < 1790 ± 15, p2648 ± 15
$B_2Mo$ (hP3)	61–66	p2413 ± 15
$B_3Mo_2$ (hR21)	66.7–70	
$B_3Mo_{0.8}$ (hP20)	79 ± 0.5	p2080 ± 50
B (hR108)	~98–100	m2362 ± 15

of the solubility of boron in molybdenum were reported [51, 137, 138, 191, 271] which range over almost an order of magnitude from 1.75 at.% to 0.2 at.% at the eutectic. A value of 0.8 ± 0.4 at.% was accepted for the eutectic, and the equation  $\ln x_B = -12000 T^{-1} \pm 0.6$  was adopted for the solvus below 2448 K. The composition and temperature ranges of the phases are summarized in Table II-2.

The liquidus curves of Fig.II-7 were taken from Rudy and Windisch [208], since they are consistent with reasonable estimates of the thermodynamic behaviour of the melt. The various three-phase equilibria are summarized in Table II-3.

The molybdenum liquidus is given by

$$x_B = 5.7 \times 10^{-4} (2890-T) + 5.8 \times 10^{-7} (2890-T)^2 - 1.5 \times 10^{-9} (2890-T)^3 \pm 0.01 \quad (2448-2890 \text{ K})$$

The molybdenum solidus is given by

$$x_B = 6 \times 10^{-5} (2890-T) - 2.7 \times 10^{-7} (2890-T)^2 + 4 \times 10^{-10} (2890-T)^3$$

within a factor of two between 2448 and 2890 K. The BMo<sub>2</sub> liquidus is given by

$$x_B = 0.60 - 2.06 \times 10^{-3} (T-2000) + 2.75 \times 10^{-6} (T-2000)^2 \pm 0.02 \quad (2448-2553 \text{ K})$$

TABLE II-3. THREE-PHASE EQUILIBRIA OF THE B-Mo SYSTEM ( $x_B$  is given after each phase)

T (K)		
2448 ± 6	Mo, 0.008 ± 0.004	L, 0.23 ± 0.01
2553 ± 12	L, ~ 0.3	BMo <sub>2</sub> , ~ 0.34
2453 ± 30	BMo <sub>2</sub> , 0.34	BMo (t116), ~ 0.485
< 2400?	BMo <sub>2</sub> , 0.34	B <sub>2</sub> Mo <sub>2</sub> (tP10)?
> 2200?	BMo <sub>2</sub> , 0.34	B <sub>2</sub> Mo <sub>2</sub> (tP10)?
2648 ± 15	BMo (oC8), 0.52	B <sub>2</sub> Mo, ~ 0.63
2413 ± 15	B <sub>2</sub> Mo, 0.66 ± 0.005	B <sub>2</sub> Mo <sub>2</sub> , ~ 0.68
2193 ± 25	B <sub>5</sub> Mo <sub>2</sub> , 0.70 ± 0.01	L, 0.94 ± 0.04
2073 ± 80	BMo (t116), 0.500 ± 0.002	BMo(oC8), ~ 0.51
1790 ± 15	BMo (t116), 0.500 ± 0.002	B <sub>2</sub> Mo, 0.62 ± 0.005
2080 ± 50	B <sub>5</sub> Mo <sub>2</sub> , 0.68 ± 0.01	B <sub>4</sub> Mo, ~ 0.79

BREWER and LAMOREAUX

## PART II. PHASE DIAGRAMS

The BMo liquidus is given on the molybdenum-rich side by

$$x_B = 0.44 - 7.5 \times 10^{-4}(T-2000) + 9.4 \times 10^{-7}(T-2000)^2 \pm 0.02 \quad (2553-2873 \text{ K})$$

and on the boron-rich side by

$$x_B = 0.11 + 2.1 \times 10^{-3}(T-2000) - 1.89 \times 10^{-6}(T-2000)^2 \pm 0.03 \quad (2648-2873 \text{ K})$$

The B<sub>2</sub>Mo liquidus is given by

$$x_B = 0.87 - 4 \times 10^{-5}(T-2000) - 3.4 \times 10^{-7}(T-2000)^2 \pm 0.03 \quad (2413-2648 \text{ K})$$

The B<sub>5</sub>Mo<sub>2</sub> liquidus is given by

$$x_B = 1.02 - 3.1 \times 10^{-4}(T-2000) - 6 \times 10^{-7}(T-2000)^2 \pm 0.04 \quad (2193-2413 \text{ K})$$

Calculation of the boron liquidus is rather uncertain because of uncertainty of the solid solubility and of the eutectic composition.

## Mo-Ba: molybdenum-barium (Fig.II-2)

No data were found. The solubility of molybdenum in Ba(?) has been calculated using the estimated thermodynamic equations of Part I. From 1002 to 1950 K,

$$\ln x_{\text{Mo}} = -23190 T^{-1} + 2.2$$

The solubility of molybdenum in the liquid rises from  $x_{\text{Mo}} = 8 \times 10^{-10}$  at 1002 K to  $6 \times 10^{-5}$  at 1950 K, with an uncertainty of a factor of 5.

The solid solubilities of barium in molybdenum and of molybdenum in Ba(s) below 1002 K are less than the quenched defect concentrations and are not thermodynamic quantities.

## Mo-Be: molybdenum-beryllium (Fig.II-8)

Von Goldbeck [95] has used the results summarized by Hansen and Anderko [109] and Elliott [68] and more recent data to prepare a phase diagram. No significant data have been reported since then and Fig.II-8 is based on the diagram given by Von Goldbeck, with extensions calculated from the thermodynamic data estimated in Part I. The only significant change has been to extend the stability of Be<sub>22</sub>Mo to low temperatures on the basis of the thermodynamic

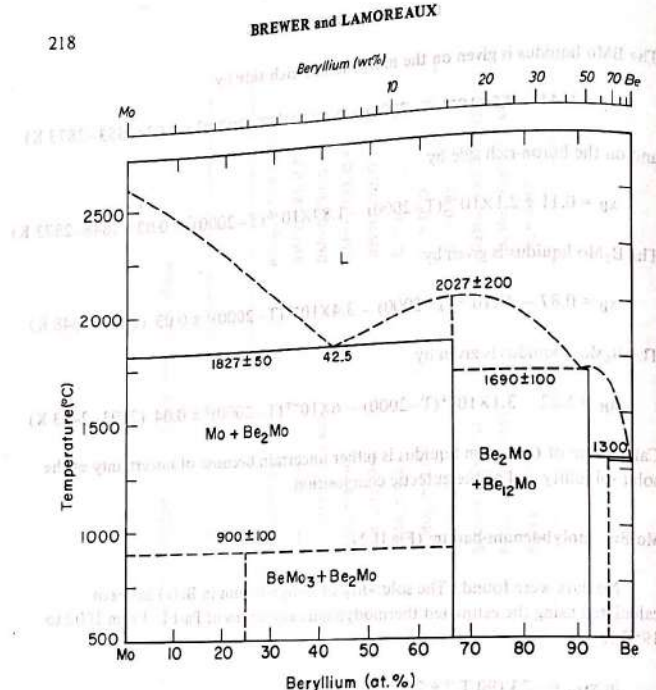


FIG.II-8. Phase diagram of the system molybdenum-beryllium.

The data for the liquidus curve of Fig. II-8 were taken from Part I. The literature on crystal structures for the four phases  $\text{BeMo}_3$ (cP8),  $\text{Be}_2\text{Mo}(\text{hP12})$ ,  $\text{Be}_{12}\text{Mo}(\text{II26})$  and  $\text{Be}_{22}\text{Mo}(\text{cF184})$  is reviewed in Part II.

The molybdenum solidus is given by

$$x_{\text{Be}} = 1.86 \times 10^{-5} (2890 - T) - 2.08 \times 10^{-8} (2890 - T)^2 \\ + 7 \times 10^{-12} (2890 - T)^3 \pm 0.001 \quad (2100 - 2890 \text{ K})$$

The molybdenum solvus is given by

$$\ln x_{\text{Be}} = -11000 T^{-1} \pm 0.1 \quad (2100 - 1000 \text{ K})$$

## PART II. PHASE DIAGRAMS

The molybdenum liquidus is given by

$$x_{\text{Be}} = 5.84 \times 10^{-4} (2890 - T) - 9 \times 10^{-10} (2890 - T)^2 \\ - 7.5 \times 10^{-11} (2890 - T)^3 \pm 0.01 \quad (2100 - 2890 \text{ K})$$

The molybdenum-rich  $\text{Be}_2\text{Mo}$  liquidus is given by

$$x_{\text{Be}} = 0.425 + 1.09 \times 10^{-3} (T - 2100) - 7.9 \times 10^{-6} (T - 2100)^2 \\ + 4.2 \times 10^{-8} (T - 2100)^3 \pm 0.02 \quad (2100 - 2300 \text{ K})$$

The beryllium-rich  $\text{Be}_2\text{Mo}$  liquidus is given by

$$x_{\text{Be}} = 0.991 - 1.5 \times 10^{-3} (T - 1900) + 6.7 \times 10^{-6} (T - 1900)^2 \\ - 1.24 \times 10^{-8} (T - 1900)^3 \pm 0.04 \quad (1967 - 2300 \text{ K})$$

The  $\text{Be}_{12}\text{Mo}$  liquidus increases from  $x_{\text{Be}} = 0.91 \pm 0.02$  at 1967 K to 0.923 at 1973 K. At higher  $x_{\text{Be}}$ , the liquidus is given by

$$\ln x_{\text{Mo}} = -9.64 + 2.7 \times 10^{-2} (T - 1500) - 6.3 \times 10^{-5} (T - 1500)^2 \\ + 7.9 \times 10^{-8} (T - 1500)^3 \pm 0.02 \quad (1573 - 1973 \text{ K})$$

No data for the solid solubility of molybdenum in beryllium are known. It is probably defect-controlled.

The molybdenum solvus in bismuth is given by

$$\ln x_{\text{Mo}} = 2.4 - 22300 T^{-1} \pm 1$$

Elliott [68] has reviewed earlier work. Weeks [260] and Jensen et al. [126] have more recently examined the Bi-Mo system. No solubility could be detected. The solubility of molybdenum in bismuth at 1300 K is given as less than 1 ppm. The estimated thermodynamic values from Part I yield

The molybdenum liquidus curve of Fig. II-2 between 1837 and 544.5 K, the boiling and melting points of bismuth. The solubility of bismuth in solid molybdenum is calculated to be so small that it is not a thermodynamic quantity, as it is determined by the quenched defect concentration rather than by temperature.

## Mo-Bk: molybdenum-berkelium (Fig.II-2)

No data were found. The normal boiling point of berkelium is estimated to be  $2430 \pm 100$  K. The phase boundaries of Fig.II-2 have been calculated from the estimated thermodynamic equations of Part I. The eutectic is calculated to be at  $1517 \pm 10$  K and  $x_{\text{Mo}} = 0.04 \pm 0.01$ . Above 1517 K the berkelium liquidus is represented by the equation

$$x_{\text{Mo}} = 8 \times 10^{-4} (1560 - T) + 2 \times 10^{-6} (1560 - T)^2$$

with an uncertainty of 0.01 at 1517 K. The berkelium solidus above 1517 K is calculated to be

$$x_{\text{Mo}} = 7 \times 10^{-5} (1560 - T)$$

with an uncertainty of a factor of 5. Below 1517 K the solid solution phase boundaries are calculated to be

$$\ln x_{\text{Mo}} = -21.7 + 1.816 \times 10^{-2} T - 4.93 \times 10^{-6} T^2$$

and

$$\ln x_{\text{Bk}} = -22.3 + 1.863 \times 10^{-2} T - 5.06 \times 10^{-6} T^2$$

The solubility of molybdenum falls to  $10^{-4}$  at 900 K and that of berkelium falls to  $10^{-4}$  at 950 K, with uncertainties in the solubilities of a factor of 5.

Between 1517 and 2430 K the molybdenum solidus and liquidus are calculated as

$$x_{\text{Bk}} = 0.003 + 9 \times 10^{-6} (T - 1500) + 1.4 \times 10^{-8} (T - 1500)^2 - 10^{-11} (T - 1500)^3$$

$$x_{\text{Mo}} = 0.03 + 1.5 \times 10^{-4} (T - 1500) + 10^{-8} (T - 1500)^2 + 3 \times 10^{-10} (T - 1500)^3$$

The uncertainty in  $x_{\text{Bk}}$  is  $\pm 0.005$ , while that for  $x_{\text{Mo}}$  rises from  $\pm 0.03$  at 1517 K to  $\pm 0.12$  at 2400 K.

## Mo-Br: molybdenum-bromine (Fig.II-9)

The phase diagram was calculated from the thermodynamic values of Part I, which were largely based on the disproportionation pressures of  $\text{MoBr}_2$  and  $\text{MoBr}_3$  solids determined by Opperman [182] and the conditions for preparation and dissociation of  $\text{MoBr}_4(s)$  given by Carnell et al. [40]. The principal vapour species are calculated to be  $\text{MoBr}_4$  and the elemental bromine species are calculated to

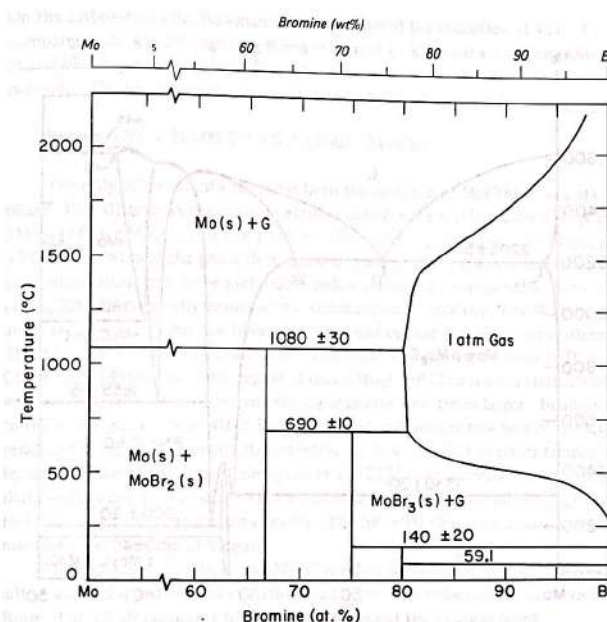


FIG.II-9. Phase diagram of the system molybdenum-bromine.

phase through a eutectic at 140 K. The gas at 1 atm, in equilibrium with Mo(s) at 1353 K, has 97 mol%  $\text{MoBr}_4$ , which drops at 2000 K to 13 mol%  $\text{MoBr}_4$ , with 3 mol%  $\text{MoBr}_3$ , 2 mol%  $\text{MoBr}_2$ , 10 mol%  $\text{Br}_2$  and 72 mol% Br. Atomic bromine increases to 96 mol% at 2500 K and 99 mol% at 2890 K. Golub et al. [96] have prepared a  $\text{MoBr}_5$  phase which is believed to be metastable. If the solubility of  $\text{MoBr}_4$  in liquid bromine is described in terms of  $\text{MoBr}_5$ , the maximum mole fraction of  $\text{MoBr}_5$  at 51°C is  $1.2 \times 10^{-3}$  [40]. The crystal structures of  $\alpha\text{MoBr}_2$  and  $\text{MoBr}_3$  are reviewed in Part III. Glicksman et al. [91, 92] review the preparation of a binuclear  $\beta\text{MoBr}_2$  phase which is assumed here to be unstable with respect to the hexanuclear  $\alpha\text{MoBr}_2$ . The occurrence of intermediate phases such as  $\text{W}_6\text{Br}_{14}$  and  $\text{W}_6\text{Br}_{16}$  in the Br-W system [223, 229] suggests the possibility of similar phases in the Br-Mo system. The solubility of bromine in solid molybdenum is believed to

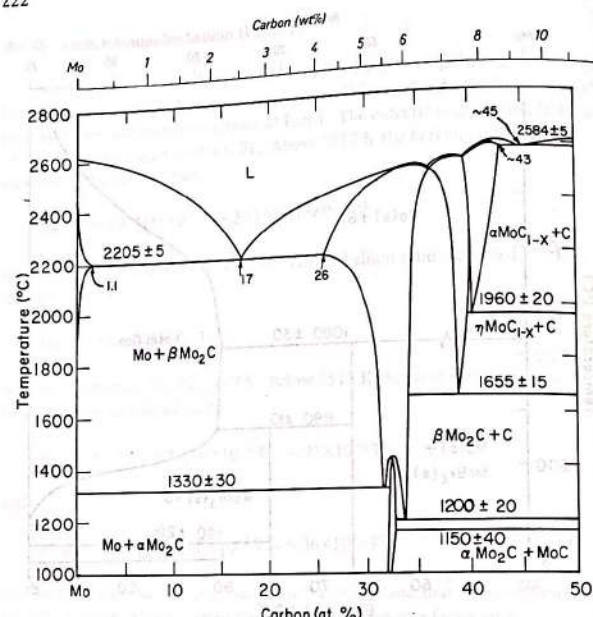


FIG.II-10. Phase diagram of the system molybdenum-carbon.

be defect-controlled. The homogeneous ranges of  $\text{MoBr}_2$  and  $\text{MoBr}_3$  are discussed in Part I. They are believed to be substantial, but they are not known and are not indicated in Fig.II-9.

#### Mo-C: molybdenum-carbon (Fig.II-10)

The phase diagram of Fig.II-10 is based essentially on the comprehensive study by Rudy et al. [205, 207, 209, 210]. Kempfer [134] has reviewed recent measurements of the molybdenum solvus boundary and the Mo-Mo<sub>2</sub>C eutectic, and confirms the diagram as given by Rudy et al. [205, 210]. Recent work at Los Alamos suggests minor temperature changes. On the basis of the work of Reavis et al. [200], the Mo-Mo<sub>2</sub>C eutectic temperature was increased by 5°C to 2205°C. The boundaries of the  $\alpha$ - $\beta$ Mo<sub>2</sub>C transformation are difficult to determine.

On the carbon-rich side, Bowman [27] has reported the transition at 1210°C, compared with 1190°C given by Rudy et al. and 1170°C given by Eremenko et al. [70]. Bowman gives 1330°C as the transition temperature on the molybdenum-rich side. The molybdenum solvus saturated by  $\beta\text{Mo}_2\text{C}$  is given by

$$\ln x_C = 3.97 - 21000 T^{-1} \pm 0.2 \quad (1603-2478 \text{ K})$$

The only other modification has been the addition of MoC(hP2) as a stable phase. Part III reviews the crystallographic data for the stable phases  $\alpha\text{Mo}_2\text{C}$ (oP12),  $\beta\text{Mo}_2\text{C}$ (hP3),  $\eta\text{Mo}_3\text{C}_2$  or  $\eta\text{MoC}_{1-x}$ (hP ~ 10),  $\alpha\text{MoC}_{1-x}$ (cF8), the metastable phase  $\gamma'\text{MoC}_{1-x}$ (hP8), and the phase designated as  $\gamma\text{MoC}_{1-x}$ (hP2), which had been previously considered to be metastable unless stabilized by impurities. Schuster et al. [224] have recently reviewed the stabilization of MoC(hP2) by W, Fe or Co and have concluded that the binary phase would be stable at low temperatures. The decomposition temperature is given in Fig.II-10 as an estimate of 1150 ± 40°C. Christensen [49] has recently reported that  $\alpha\text{Mo}_2\text{C}$ (oP12) has a superstructure with the b-parameter doubled and the c-parameter four times larger. In addition to the above phases, Note 40 of Part III presents references to a new Mo<sub>2</sub>C structure produced at high pressure and the retention of MoC<sub>1-x</sub>(cF8) to room temperature by high-pressure preparation. Shinyaev et al. [227] have recently demonstrated that pressure application of 25 kbar extends the stability range of MoC<sub>1-x</sub>(hP ~ 10) to 1380°C and to lower carbon content. The hP ~ 10 phase is stabilized by pressure more than the cF8 phase.

The transition of  $\beta\text{Mo}_2\text{C}$  to  $\alpha\text{Mo}_2\text{C}$  involves an ordering of the interstitial lattice and a displacive transformation leading to the orthorhombic distortion. Rudy et al. [210] propose a first-order transition at the singular point,  $32.5 \pm 0.1$  at.% C and  $1430 \pm 10^\circ\text{C}$ . At higher carbon contents the transition takes place through a two-phase region terminating at  $1200 \pm 10^\circ\text{C}$ , where  $\alpha\text{Mo}_2\text{C}$  ( $32.7 \pm 0.2$  at.% C),  $\beta\text{Mo}_2\text{C}$  ( $33.8 \pm 0.2$  at.% C) and graphite are in equilibrium. At carbon contents below 32.5 at.%, Rudy et al. propose that the interstitial ordering and the orthorhombic distortion take place separately through second-order transitions. However, Fig.II-10 follows Bowman [27] in showing two-phase regions on both sides of 32.5 at.%, and a eutectoid at  $1330 \pm 30^\circ\text{C}$  on the molybdenum-rich side, with the  $\beta$ -phase at  $31.0 \pm 0.5$  at.% C and the  $\alpha$ -phase at  $31.7 \pm 0.3$  at.% C.

The close relationship of the  $\text{Mo}_3\text{C}_2$ (hP ~ 10) and  $\alpha\text{MoC}_{1-x}$ (cF8) structures is pointed out in Note 40 of Part III, and miscibility of the two phases at higher temperatures might be expected. However, Rudy et al. were able to establish the existence of a small but finite composition gap as shown in Fig. II-10.

No data are available on the solubility of molybdenum in graphite. The graphite liquidus determined by Rudy et al. runs from 45 at.% C at the eutectic temperature of  $2584 \pm 5^\circ\text{C}$  to 60 at.% C at  $2675 \pm 20^\circ\text{C}$ , 70 at.% C at  $2950 \pm 50^\circ\text{C}$ ,

and 80 at % C at  $3500 \pm 50^\circ\text{C}$ . Kashin et al. [131] have recently reported measurements of the graphite liquidus, but their temperature calibration point was in error by  $1000^\circ\text{C}$  and their reported values were rejected.

Between  $2478 \pm 5$  and  $2890 \pm 8$  K the molybdenum solidus is given with an uncertainty of 50% by

$$x_C = 1.7 \times 10^{-5} (2890 - T) + 7 \times 10^{-9} (2890 - T)^2 + 3.4 \times 10^{-11} (2890 - T)^3$$

and the molybdenum liquidus is given with an uncertainty of  $\pm 0.03$  by

$$x_C = 5.6 \times 10^{-4} (2890 - T) - 3.8 \times 10^{-7} (2890 - T)^2 + 3 \times 10^{-10} (2890 - T)^3$$

The molybdenum-rich portions of the  $\text{Mo}_2\text{C}$  solidus and liquidus between  $2478 \pm 5$  and  $2795 \pm 5$  K are given with an accuracy of  $\pm 0.02$  by

$$x_C = 0.341 - 4.2 \times 10^{-4} (2795 - T) + 3.5 \times 10^{-7} (2795 - T)^2 + 6 \times 10^{-10} (2795 - T)^3$$

for the solidus and

$$x_C = 0.341 - 6 \times 10^{-4} (2795 - T) - 1.1 \times 10^{-6} (2795 - T)^2 + 4 \times 10^{-9} (2795 - T)^3$$

for the liquidus.

The carbon-rich portions are given between 2783 and 2795 K by

$$x_C = 0.341 + 2 \times 10^{-4} (2795 - T) + 1.1 \times 10^{-4} (2795 - T)^2 \pm 0.01$$

for the solidus and by

$$x_C = 0.341 + 3.4 \times 10^{-3} (2795 - T) - 1.2 \times 10^{-4} (2795 - T)^2 \pm 0.01$$

for the  $\text{Mo}_2\text{C}$  liquidus. The molybdenum-rich portions of the solidus and liquidus for  $\eta\text{Mo}_3\text{C}_2$  between 2783  $\pm$  3 and 2823  $\pm$  5 K are given with an accuracy of  $\pm 0.01$  by

$$x_C = 0.386 - 5 \times 10^{-4} (2823 - T) + 3 \times 10^{-6} (2823 - T)^2$$

for the solidus and by

$$x_C = 0.386 - 8.6 \times 10^{-4} (2823 - T) + 7 \times 10^{-6} (2823 - T)^2$$

for the liquidus. The carbon-rich solidus extends only between  $x_C = 0.386$  at  $2823 \pm 5$  K and  $x_C = 0.395$  at  $2820 \pm 3$  K, and the liquidus is within 0.005 of the

## PART II. PHASE DIAGRAMS

TABLE II-4. PHASES AND EUTECTICS OF THE Mo-C SYSTEM

Phase (structure)	Maximum composition range (at.% C)	Melting or decomposition temperature (K) Composition (at.% C)
Mo (cI2)	0-1.1	m2890 $\pm$ 8
$\beta\text{Mo}_2\text{C}$ (hP3)	26-36	m2795 $\pm$ 5, 34 $\pm$ 0.3%
$\alpha\text{Mo}_2\text{C}$ (oP12)	31.7-32.7	tr1703 $\pm$ 30, 32.5 $\pm$ 0.1%
$\eta\text{Mo}_3\text{C}_2$ (hP $\sim$ 10)	37.0-39.5	d1928 $\pm$ 15, 39 $\pm$ 0.5%
$\alpha\text{MoC}_{1-x}$ (cF8)	39.5-43	m2823 $\pm$ 5, 38.6 $\pm$ 0.3%
$\gamma\text{MoC}$ (hP2)	50	d2233 $\pm$ 20, 40.4 $\pm$ 0.4% m2873 $\pm$ 5, 42.0 $\pm$ 0.3% p1423 $\pm$ 40, 50%
<b>Eutectics</b>		
Solid phases	Temperature (K)	Liquid composition (at.% C)
Mo- $\beta\text{Mo}_2\text{C}$	2478 $\pm$ 5	17. $\pm$ 2
$\beta\text{Mo}_2\text{C}-\text{Mo}_3\text{C}_2$	2783 $\pm$ 5	36.3 $\pm$ 0.3
$\text{Mo}_3\text{C}_2-\alpha\text{MoC}_{1-x}$	2820 $\pm$ 5	39.5 $\pm$ 0.3
$\alpha\text{MoC}_{1-x}-\text{C}$	2857 $\pm$ 5	45. $\pm$ 1

solidus even at the eutectic. Rudy et al. [205, 210] report that the liquidus and solidus curves are so close for both  $\eta\text{Mo}_3\text{C}_2$  and  $\alpha\text{MoC}_{1-x}$  that all compositions appear to melt isothermally. The  $\alpha\text{MoC}_{1-x}$  solidus and liquidus extend from  $x_C = 0.395$  at 2820 K to the melting point at  $x_C = 0.42$  and 2873 K. At the  $\text{MoC}_{1-x}$  eutectic at  $2857 \pm 5$  K with graphite, the  $\text{MoC}_{1-x}$  solidus is at  $x_C = 0.430 \pm 0.004$  and the liquidus composition is  $x_C = 0.45 \pm 0.01$ .

To keep the diagram uncluttered, additional details of melting points, eutectic and decomposition temperatures, and composition ranges are given in Table II-4.

### Mo-Ca: molybdenum-calcium (Fig. II-2)

No data were found. The estimated thermodynamic equations of Part I have been used to calculate the solubility of molybdenum in liquid calcium. From 1112 to 1750 K,

$$\ln x_{\text{Mo}} = -17800 T^{-1} + 2.2$$

The solubility of molybdenum in the liquid rises from  $x_{\text{Mo}} = 10^{-6}$  at 1112 K to  $x_{\text{Mo}} = 3.5 \times 10^{-4}$  at 1750 K, with an uncertainty of a factor of 5. The solid solubilities are defect-controlled.

#### Mo-Cd: molybdenum-cadmium (Fig. II-2)

No data were found in the literature. The molybdenum liquidus of Fig. II-2 was calculated from the estimated thermodynamic data of Part I to be

$$\ln x_{\text{Mo}} = 3 - 19000 T^{-1} \pm 4 \quad (594-1040 \text{ K})$$

#### Mo-Ce: molybdenum-cerium (Fig. II-1)

Savitskij et al. [213] found the solubility of cerium in molybdenum to be between 0.10 and 0.15 at.% at an unspecified temperature. Gaume-Mahn and Blanchard [84] determined the solubility of molybdenum in liquid cerium to be 0.001 at.% at 1073 K, rising to 0.0175 at.% at 1473 K. Unreasonable values of thermodynamic properties are required for agreement with the values of Ref. [84], which have been discarded.

The estimated thermodynamic equations of Part I have been used to calculate the phase boundaries of Fig. II-1.

The monotectic is calculated to be at  $2800 \pm 10$  K and  $x_{\text{Ce}} = 3 \times 10^{-3}$ ,  $0.067 \pm 0.01$  and  $0.68 \pm 0.08$ . The molybdenum liquidus and solidus above the monotectic are represented by

$$x_{\text{Ce}} = 5.3 \times 10^{-4} (2890-T) + 2.4 \times 10^{-6} (2890-T)^2$$

with an uncertainty of  $\pm 1.1 \times 10^{-4}$  (2890-T) for the liquidus, and

$$x_{\text{Ce}} = 3.4 \times 10^{-5} (2890-T)$$

with an uncertainty of a factor of 5 for the solidus.

The two-liquid phase boundaries between 2800 and 3100 K are represented by

$$x_{\text{Mo}} = 0.32 + 3.1 \times 10^{-4} (T-2800) + 4 \times 10^{-10} (T-2800)^3$$

with uncertainties of  $\pm 0.08$  at 2800 K and  $\pm 0.10$  at 3100 K, and

$$x_{\text{Ce}} = 0.065 + 9 \times 10^{-5} (T-2800) + 4 \times 10^{-8} (T-2800)^2$$

with uncertainties of  $\pm 0.01$  at 2800 K and  $\pm 0.02$  at 3100 K.

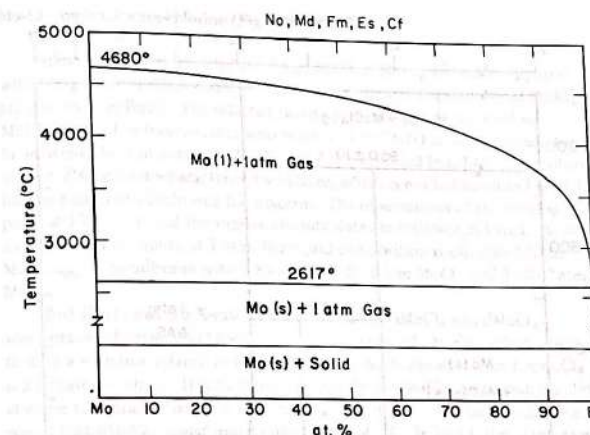


FIG. II-11. Phase diagram of a system Mo-EI, where EI is one of the actinides between nobelium and californium shown above.

The equilibrium between solid molybdenum and liquid from 1071 to 2800 K is calculated to be

$$x_{\text{Mo}} = -1.54 \times 10^{-3} + 3.5 \times 10^{-5} (T-1000) - 5.1 \times 10^{-8} (T-1000)^2 + 7.1 \times 10^{-11} (T-1000)^3$$

with uncertainties of  $\pm 4 \times 10^{-4}$  at 1071 K and  $\pm 0.08$  at  $2800 \pm 10$  K

$$x_{\text{Ce}} = 1.8 \times 10^{-5} - 2.7 \times 10^{-7} (T-1000) + 4 \times 10^{-10} (T-1000)^2 + 4 \times 10^{-13} (T-1000)^3$$

with an uncertainty of a factor of 5. The solubility of cerium in molybdenum falls to  $10^{-4}$  at 1630 K, below which temperature it is less than the quenched defect concentration. The solubility of molybdenum in solid cerium is below  $10^{-4}$ .

The eutectic is calculated to be at 1071 K and  $x_{\text{Mo}} = (7 \pm 1) \times 10^{-4}$ .

#### Mo-Cf: molybdenum-californium (Fig. II-11)

No data were found. The estimated normal boiling point of  $1350 \pm 50$  K is below the estimated melting point of 1700 K. The estimated thermodynamic

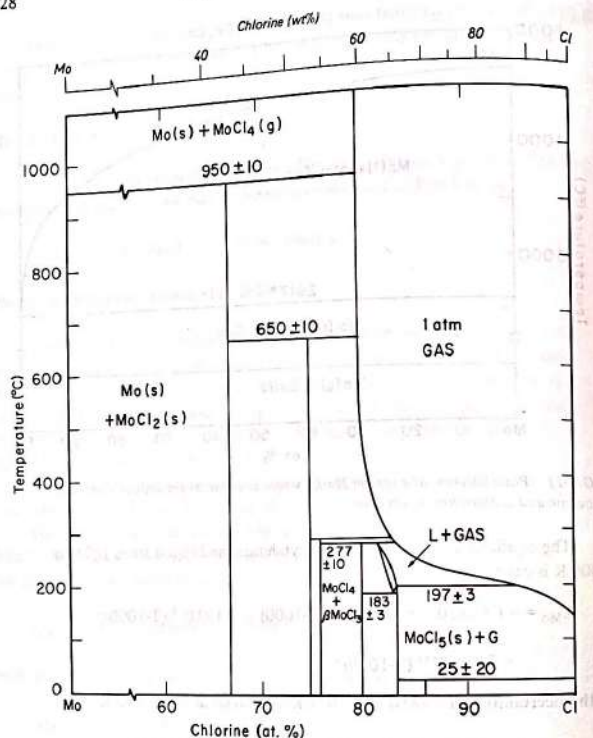


FIG.II-12. Phase diagram of the system molybdenum-chlorine.

equations of Part I have been used to calculate the solid-solution phase boundaries below 1350 K.

$$x_{\text{Mo}} = 4 \times 10^{-5} + 10^{-7}(T-1000) + 4.5 \times 10^{-9}(T-1000)^2$$

The solubility of molybdenum in californium falls to  $10^{-6}$  at 1100 K, with an uncertainty of a factor of 5. The solubility of californium in molybdenum is defect-controlled.

## Mo-Cl: molybdenum-chlorine (Fig. II-12)

Mercer [174] has reported the preparation of  $\text{MoCl}_6$  to be isomorphous with  $\text{WCl}_6(\text{hR}35)$ . The various observations relating to the stability of  $\text{MoCl}_6$  are discussed in Part I. The selected thermodynamic data correspond to  $\text{MoCl}_6(\text{s})$  which is barely stable with respect to  $\text{MoCl}_5(\text{s})$  at room temperature in an atmosphere of chlorine.  $\text{MoCl}_5(\text{mC}72)$  is reported [61, 148] to transform at  $98 \pm 2^\circ\text{C}$  to an uncharacterized structure, which is not indicated in Fig. II-12 for the reason of simplifying the diagram. The observations of the melting point at  $197 \pm 3^\circ\text{C}$  and the vapour pressure data are reviewed in Part I. At the melting point of  $\text{MoCl}_5$  at 1 atm, the liquid composition is calculated to be  $\text{MoCl}_{4.986}$ , in equilibrium with 0.84 atm  $\text{Cl}_2$ , 0.16 atm  $\text{MoCl}_5$  and  $3 \times 10^{-4}$  atm  $\text{MoCl}_4$ .

Part III reviews the X-ray diffraction data for  $\alpha\text{MoCl}_4$  and  $\beta\text{MoCl}_4$ . Westland and Uzelac [261] have recently characterized  $\gamma\text{MoCl}_4$ , which seems to have a structure related to that of  $\alpha\text{MoCl}_4$ . As discussed in Part I,  $\gamma\text{MoCl}_4$  is a metastable phase. It transforms irreversibly to  $\alpha\text{MoCl}_4$ , even upon grinding at room temperature or upon heating to around  $140^\circ\text{C}$ . Westland and Uzelac report that  $\alpha\text{MoCl}_4$  transforms to  $\beta\text{MoCl}_4$  at  $241^\circ\text{C}$ . In Part I, this is interpreted as an irreversible kinetically controlled transformation; the equilibrium transformation temperature is estimated at around  $80^\circ\text{C}$ . It is possible that small compositional differences may characterize the three forms of  $\text{MoCl}_4$  and that the low-temperature forms may be stabilized by incorporation of the halogenated hydrocarbons used for their preparation. To avoid the complexity of additional lines, Fig. II-12 does not indicate the  $\text{MoCl}_4$  transformation. Drobot and Sapranova [61] report the  $\text{MoCl}_4$ - $\text{MoCl}_4$  eutectic with  $\text{MoCl}_{4.9}$ ( $\text{l}$ ) to be  $14^\circ\text{C}$  below the melting point of  $\text{MoCl}_5$ , and the  $\text{MoCl}_4$  peritectic at  $272^\circ\text{C}$ , in equilibrium with  $\text{MoCl}_{4.5}$ ( $\text{l}$ ) and  $\text{MoCl}_3(\text{s})$ , which is taken to be  $\beta\text{MoCl}_{3.08}(\text{s})$  in Fig. II-12. Schäfer et al. [222] give a peritectic temperature of  $275^\circ\text{C}$ , and Westland and Uzelac [261] report the peritectic temperature at  $288^\circ\text{C}$ . A value of  $277 \pm 10^\circ\text{C}$  was selected for the  $\text{MoCl}_4$  peritectic. The vapour in equilibrium with the eutectic at 456 K is calculated to be 0.09 atm  $\text{MoCl}_5$ , 0.02 atm  $\text{Cl}_2$  and  $8 \times 10^{-4}$  atm  $\text{MoCl}_4$ . The  $\text{MoCl}_4$  liquidus determined by Drobot and Sapranova [61] is given by

$$\ln x_{\text{MoCl}_4} = 4.28 - (2580 + 455 x_{\text{MoCl}_4}^2) T^{-1} \pm 0.04 \quad (456-550 \text{ K})$$

where the mole fractions are based on  $\text{MoCl}_4$  and  $\text{MoCl}_5$  components. The vapour in equilibrium with the peritectic at 550 K is calculated to have a total pressure of  $1.17 \pm 0.2$  atm, with 1.02 atm  $\text{MoCl}_5$ , 0.13 atm  $\text{MoCl}_4$  and 0.02 atm  $\text{Cl}_2$ . Within the uncertainty of the calculations, the two three-phase equilibria

$\text{MoCl}_4$ -liquid-gas and  $\text{MoCl}_4\text{-MoCl}_{3.08}$ -gas coincide with the  $\text{MoCl}_4$  peritectic and are given in Fig. II-12 as an accidental four-phase equilibrium.

Part III reviews the X-ray data for  $\alpha\text{MoCl}_3(\text{mC16})$  and  $\beta\text{MoCl}_{3.08}(\text{mC32})$ . Schäfer et al. [222] have demonstrated the stability of  $\text{MoCl}_{3.08}$  in a pressurized system up to 375°C. Drobot and Sapranova [61] have gone to even higher pressure and have measured the liquidus up to 400°C as given by  $\ln(x_{\text{Cl}}/x_{\text{Mo}}) = 0.128 + 770 T^{-1} \pm 0.2$  (550–667 K). Because of the closeness in composition of  $\alpha\text{MoCl}_3$  and  $\beta\text{MoCl}_{3.08}$  and the lack of information about their homogeneous ranges the uncertainties of the thermodynamic data of Part I do not allow a reliable calculation of the temperature range of stability of  $\text{MoCl}_{3.08}$ . However, it is estimated to disproportionate at 1 atm total pressure, at a temperature only a few degrees above the peritectic temperature of  $\text{MoCl}_4$ . Based on the data of Oppermann and Stöver [183] and Schäfer et al. [222] the disproportionation of  $\text{MoCl}_3(\text{mC16})$  to  $\alpha\text{MoCl}_2(\text{oC72})$  is calculated to produce 1 atm of essentially pure  $\text{MoCl}_4(\text{g})$  at  $650 \pm 10^\circ\text{C}$ . Glicksman et al. [91, 92] review the preparation of binuclear  $\text{MoCl}_2$  which is assumed here to be unstable with respect to hexanuclear  $\text{MoCl}_6$ . Similarly, the amorphous  $\text{Mo}_6\text{Cl}_{15}$  prepared by Kepert et al. [135] is assumed to be unstable with respect to disproportionation. The disproportionation of  $\text{MoCl}_2(\text{s})$  to  $\text{Mo}(\text{s})$  and essentially pure  $\text{MoCl}_4(\text{g})$  takes place at 1 atm at  $950 \pm 10^\circ\text{C}$ . On further heating of  $\text{MoCl}_4(\text{g})$  in equilibrium with molybdenum metal, the gas at a total pressure of 1 atm is calculated to consist at 2000 K of 0.91 atm  $\text{MoCl}_4$ , 0.04 atm  $\text{MoCl}_3$ , 0.04 atm Cl, 0.007 atm  $\text{MoCl}_2$ , 0.003 atm  $\text{Cl}_2$ ,  $10^{-4}$  atm  $\text{MoCl}_5$  and  $10^{-6}$  atm  $\text{MoCl}$ . The solubility of chlorine in solid molybdenum is believed to be defect-controlled.

#### Mo-Cm: molybdenum-curium (Fig. II-2)

No data were found. Curium has been placed in Fig. II-2, with neighbouring americium and berkelium, although the thermodynamic estimates of Part I indicate that curium may be non-volatile enough and have a high enough internal pressure for the 1 atm diagram to extend above the melting point of molybdenum and may have a diagram more like that of lawrencium and plutonium shown in Figs II-24 and II-37.

The eutectic is calculated to be at  $1565 \pm 20$  K and  $x_{\text{Mo}} = 0.03 \pm 0.01$ . Above the eutectic the curium liquidus is represented by

$$x_{\text{Mo}} = 6.3 \times 10^{-4} (1611 - T) + 2.22 \times 10^{-6} (1611 - T)^2$$

with an uncertainty of  $2 \times 10^{-4} (1611 - T)$ , and the curium solidus by

$$x_{\text{Mo}} = 7.9 \times 10^{-5} (1611 - T)$$

with an uncertainty of a factor of 5.

#### PART II. PHASE DIAGRAMS

The molybdenum solidus and liquidus between 1565 and 2890 K are calculated to be

$$x_{\text{Cm}} = 7.04 \times 10^{-5} (2890 - T) - 1.03 \times 10^{-7} (2890 - T)^2 + 3.9 \times 10^{-11} (2890 - T)^3$$

with an uncertainty of a factor of 5 for the solidus, and

$$T = \frac{5081 + 7560x_{\text{Cm}}^2 - 4180x_{\text{Cm}}^3}{0.3x_{\text{Cm}}^2 + 1.758 - \ln(1 - x_{\text{Cm}})}$$

for the liquidus, with an uncertainty of  $\pm 70$  degrees at  $x_{\text{Cm}} = 0.97$  and  $\pm 50$  degrees at  $x_{\text{Cm}} = 0.66$ .

Below 1565 K the solid-solution phase boundaries are calculated to be

$$x_{\text{Mo}} = 1.6 \times 10^{-4} + 10^{-6} (T - 1000) + 5 \times 10^{-9} (T - 1000)^2 + 8 \times 10^{-12} (T - 1000)^3$$

and

$$x_{\text{Cm}} = 1.4 \times 10^{-4} + 10^{-6} (T - 1000) + 4 \times 10^{-9} (T - 1000)^2 + 7 \times 10^{-12} (T - 1000)^3$$

The solubility of molybdenum in curium falls to  $x_{\text{Mo}} = 10^{-4}$  at 950 K, and the solubility of curium in molybdenum falls to  $x_{\text{Cm}} = 10^{-4}$  at 970 K, with an uncertainty of a factor of 5. Below these temperatures the solubilities are defect-controlled.

#### Mo-Co: molybdenum-cobalt (Fig. II-13)

The structural data on the four intermediate phases,  $\sigma\text{Co}_2\text{Mo}_3(\text{tP30})$ ,  $\epsilon\text{Co}_7\text{Mo}_6(\text{hR39})$ ,  $\kappa\text{Co}_3\text{Mo}(\text{hP8})$  and  $\theta\text{Co}_9\text{Mo}_2(\text{hP2})$ , are reviewed in Part III. Hansen and Anderko [109] have presented a phase diagram based on previous work. Two alternative representations of the extension of  $\alpha\text{Co}(\text{hP2})$  were given. In one,  $\alpha\text{Co}$  was extended continuously to 980°C. In the other representation, following Sykes and Graff [244], Co(hP2) containing 17 at.% Mo existed as an isolated  $\theta$ -phase region between 1020 and 1200°C. Quinn and Hume-Rothery [195] have since then carefully investigated the system between 800 and 2300°C and have confirmed the results of Sykes and Graff. Figure II-13 is largely based on the results of Quinn and Hume-Rothery. Krajewski et al. [151] have reviewed previous data on the  $\alpha\text{-}\beta$  Co transformation and presented new data indicating that addition of molybdenum raises the transformation temperature. However, equilibrium is difficult to attain. For example, the work of Heijwegen and Rieck [114] with diffusion couples between 13.5 and 21 at.% Mo

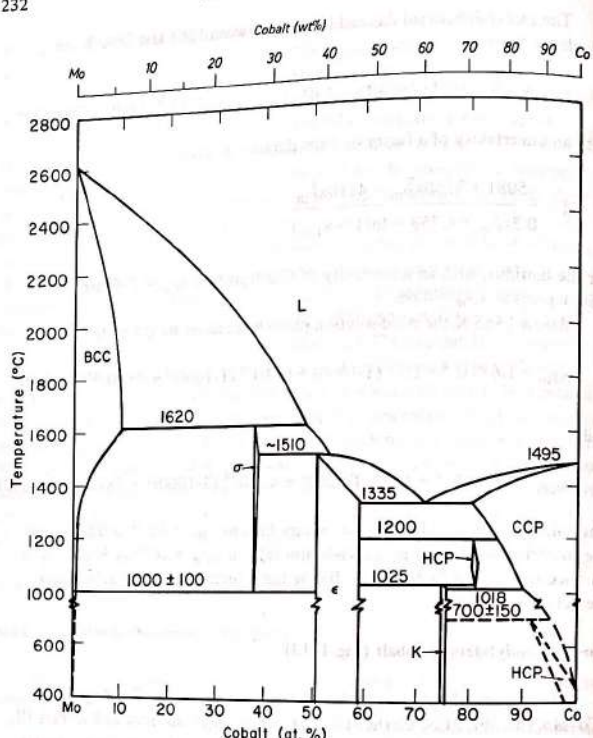


FIG.II-13. Phase diagram of the system molybdenum-cobalt.

suggests an extension of  $\alpha$ -Co(hP2) to 1000°C and 16 at.% Mo, but still separated from the  $\theta$ -boundary at 1020°C and 18.6 at.% Mo. On the other hand, Gust et al. [105] report only a two-phase mixture of  $\beta$ -Co(cF4) and  $\text{Co}_3\text{Mo}$ (hP8) between 700 and 950°C for 7–10 at.% Mo. Bibring and Graf [17] report  $\alpha$ -Co in equilibrium with the  $\kappa$ - $\text{Co}_3\text{Mo}$  phase up to 700°C, as indicated in Fig. II-13. There have been three recent determinations of the  $\beta$ -Co(cF4) boundary. Gust et al. [105] obtained a value of 950°C, 10% lower than that estimated by

Quinn and Hume-Rothery, and extended the boundary to 704°C. Katayama et al. [133] obtained values between 950 and 1150°C, which are 20% higher than those of Quinn and Hume-Rothery, and Heijwegen and Rieck [114] report values between 950 and 1300°C, i.e. 30% higher than those of Quinn and Hume-Rothery. The boundary of  $\beta$ -Co(cF4) saturated by  $\text{Co}_3\text{Mo}$  between 973 ± 150 and 1291 ± 5 K is given with an uncertainty in  $x_{\text{Mo}}$  of 10% by

$$\ln x_{\text{Mo}} = -6.02 - 1.37 \times 10^{-3} T + 3.36 \times 10^{-6} T^2$$

The boundary of  $\beta$ -Co(cF4) saturated by the  $\theta$ -phase between 1291 ± 5 K and 1473 ± 10 K is given with an uncertainty of 15% by

$$x_{\text{Mo}} = 0.016 + 3.9 \times 10^{-4} (T-1000) - 2.3 \times 10^{-7} (T-1000)^2$$

The boundary of  $\beta$ -Co(cF4) saturated by  $\epsilon$ - $\text{Co}_3\text{Mo}_6$  between 1473 ± 10 K and 1608 ± 2 K is given with an uncertainty of 15% by

$$x_{\text{Mo}} = -0.53 + 2.38 \times 10^{-3} (T-1000) - 1.96 \times 10^{-6} (T-1000)^2$$

The boundary of the  $\theta$ -phase (hP2) saturated by  $\beta$ -Co is given by

$$x_{\text{Mo}} = 0.254 + 1.3 \times 10^{-4} (T-1200) \pm 0.01 \quad (1291 \pm 5 \text{ to } 1473 \pm 10 \text{ K})$$

The lower limit of the stability range of the  $\sigma$ -phase has been extended from 1250°C, as reported by Quinn and Hume-Rothery [195], to 1000°C, as reported by both Katayama et al. [133] and Heijwegen and Rieck [114]. Heijwegen and Rieck have been followed here in showing the homogeneous range of the  $\epsilon$ -phase from 51.5 to 58.5 at.% Co, the range of the  $\kappa$ -phase from 75 to 76.5 at.% Co, and the range of the  $\theta$ -phase from 81 to 83 at.% Co. The range of the  $\sigma$ -phase is not well established, but is within the limits 36–40 at.% Co. The Mo(c12) boundary saturated by  $\epsilon$ - $\text{Co}_3\text{Mo}_6$  between 800 and 1000°C contains between 0.5 and 1 at.% Co [114]. The molybdenum boundary saturated by the  $\sigma$ -phase [114, 195] between 1273 ± 50 K and 1893 ± 3 K is given with an uncertainty of 10% by

$$\ln x_{\text{Co}} = -3.9 - 4.4 \times 10^{-3} (T-1000) + 7 \times 10^{-6} (T-1000)^2$$

The molybdenum solidus between 1893 ± 3 K and 2890 ± 8 K is given with an uncertainty of ±0.03 by

$$x_{\text{Co}} = 3 \times 10^{-4} (2890-T) - 5 \times 10^{-7} (2890-T)^2 + 3 \times 10^{-10} (2890-T)^3$$

The molybdenum liquidus is given by

$$x_{\text{Co}} = 7.7 \times 10^{-4} (2890 - T) - 3.7 \times 10^{-7} (2890 - T)^2 + 9 \times 10^{-11} (2890 - T)^3 \pm 0.03$$

$$(1893 - 2890 \text{ K})$$

The  $\alpha$ -liquidus is given by

$$x_{\text{Co}} = 0.56 - 3.6 \times 10^{-4} (T - 1700) \pm 0.02 \quad (1783 - 1893 \text{ K})$$

The  $\epsilon$ -liquidus is given by

$$x_{\text{Co}} = 0.26 + 1.9 \times 10^{-3} (T - 1600) - 3.9 \times 10^{-5} (T - 1600)^2$$

$$+ 1.92 \times 10^{-7} (T - 1600)^3 \pm 0.03 \quad (1608 \pm 2 \text{ to } 1783 \pm 3 \text{ K})$$

The  $\beta\text{Co(cF4)}$  solidus is given by

$$x_{\text{Mo}} = 2.0 \times 10^{-3} (1768 - T) - 1.26 \times 10^{-5} (1768 - T)^2 + 4.8 \times 10^{-8} (1768 - T)^3 \pm 0.02$$

The cobalt liquidus is given by

$$x_{\text{Mo}} = 3.0 \times 10^{-3} (1768 - T) - 1.3 \times 10^{-5} (1768 - T)^2 + 2.7 \times 10^{-8} (1768 - T)^3 \pm 0.03.$$

#### Mo-Cr: molybdenum-chromium (Fig. II-14)

Rudy [205] determined the solidus curve of Fig. II-14. Hansen and Anderko [109] have reviewed the earlier literature and presented a diagram with a minimum melting point at 12 at.% Mo based on the data of Putnam et al. [194] and Bloom and Grant [20]. The measurements of Rudy are close to those of the two earlier sets of measurements, but they do not show any evidence of a minimum melting point. Rudy [205] estimated the liquidus curve as shown in Fig. II-14 as much as 200 K above the temperature of collapse of his samples. Calculations using Rudy's solidus values and the thermodynamic values of Part I indicate a narrower solidus-liquidus gap. For the solidus,

$$T = 2133 + 230x_{\text{Mo}} - 234x_{\text{Mo}}^2 + 761x_{\text{Mo}}^3$$

with an uncertainty of  $\pm 20$  K. For the liquidus,

$$T = 2133 + 289x_{\text{Mo}} - 468x_{\text{Mo}}^2 + 936x_{\text{Mo}}^3$$

with an uncertainty of  $\pm 30$  K.

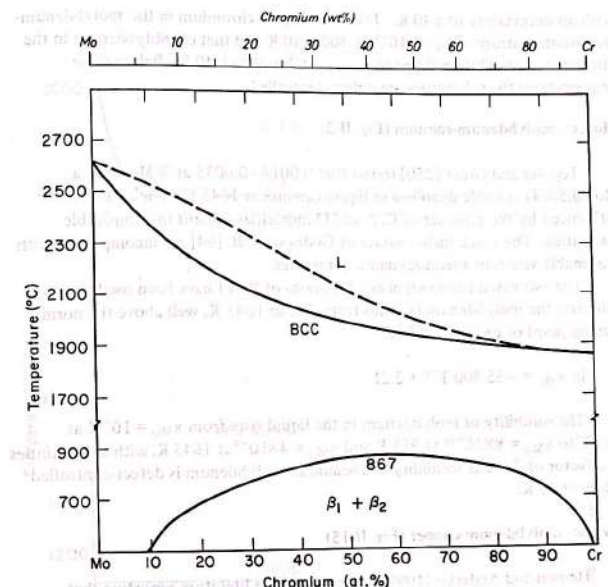


FIG. II-14. Phase diagram of the system molybdenum-chromium.

The miscibility gap was confirmed by Kubaschewski and Chart [154] who had predicted it from the thermodynamic data discussed in Part I. These data have been used to calculate the phase boundaries for the miscibility gap. For  $x_{\text{Cr}} < 0.51$  the boundary of the molybdenum-rich solid solution is given by

$$\ln x_{\text{Cr}} = 9.054 - 4180 T^{-1} - 1.358 \times 10^{-2} T + 6.96 \times 10^{-6} T^2$$

with an uncertainty of  $\pm 40$  K. From  $x_{\text{Cr}} = 0.51$  to  $x_{\text{Cr}} = 0.68$  the phase boundary is nearly flat at  $T = 1205 \pm 40$  K. At  $x_{\text{Cr}} \geq 0.68$  the boundary of the chromium-rich solid solution is given by

$$\ln x_{\text{Mo}} = -3.988 - 2840 T^{-1} + 4.910 \times 10^{-3} T - 5.2 \times 10^{-7} T^2$$

with an uncertainty of  $\pm 40$  K. The solubility of chromium in the molybdenum-rich solution drops to  $x_{Cr} = 10^{-4}$  at  $300 \pm 40$  K and that of molybdenum in the chromium-rich solution drops to  $x_{Mo} = 10^{-4}$  at  $400 \pm 40$  K. Below these temperatures the solubilities are defect-controlled.

#### Mo-Cs: molybdenum-caesium (Fig. II-2)

Teppler and Greer [250] found that 0.0014–0.0035 at.% Mo from a Mo–0.5% Ti crucible dissolved in liquid caesium at 1645 K. Their value is influenced by the presence of C, N and O impurities present in comparable quantities. The much higher values of Godneva et al. [94] are incompatible with reasonable values of thermodynamic properties.

The estimated thermodynamic functions of Part I have been used to calculate the molybdenum liquidus from 302 to 1645 K, well above the normal boiling point of caesium, 955 K,

$$\ln x_{Mo} = -35300 T^{-1} + 2.21$$

The solubility of molybdenum in the liquid rises from  $x_{Mo} = 10^{-50}$  at 302 K to  $x_{Mo} = 8 \times 10^{-16}$  at 955 K and  $x_{Mo} = 4 \times 10^{-9}$  at 1645 K, with uncertainties of a factor of 5. The solubility of caesium in molybdenum is defect-controlled below 1645 K.

#### Mo-Cu: molybdenum-copper (Fig. II-15)

Hansen and Anderko [109] have reviewed the literature reporting that copper and molybdenum are immiscible in both the liquid and solid states. The electrical resistivity measurements of Linde [162] clearly establish a solubility of molybdenum in copper at 900°C too small to produce any measurable resistivity change. The work of Dreibholz [60] on the ternary Cu-Mo-Ni system as well as direct measurements on the binary system indicate negligible solid solubility for the binary system. In contrast, Baskin et al. [14] report a solubility of copper in molybdenum at 950°C of less than 3 wt%, but possibly as much as 1.5 wt%, based on resistivity changes and X-ray lattice constant changes of 0.0006 Å. Kozlova et al. [149, 150] report lattice constant changes of 0.0004 Å. However, the lattice constant, after conversion from kX units, reported for pure molybdenum [149, 150] is 0.0004 Å lower than given in Part III of this monograph, thus suggesting that impurities may be responsible for the observed changes. The reported solubility is much higher than would be expected from the estimated thermodynamic data of Part I.

The phase diagram of Fig. II-15 was calculated from the thermodynamic data of Part I. The eutectic is calculated to be at  $1083.4 \pm 0.1^\circ\text{C}$ , with the

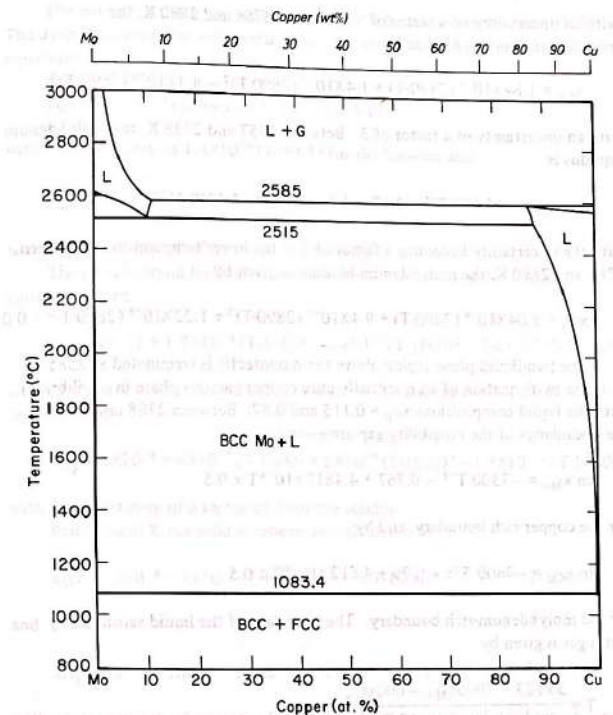


FIG. II-15. Phase diagram of the system molybdenum-copper.

solid compositions  $x_{Cu} = 6.3 \times 10^{-4}$  and  $x_{Mo} = 6.7 \times 10^{-4}$  in equilibrium with liquid  $x_{Mo} = 6.1 \times 10^{-4}$ , with uncertainties of a factor of 5. A monotectic is calculated at  $2515 \pm 100^\circ\text{C}$ , with the liquid compositions  $x_{Cu} = 0.105$  and  $0.882$  in equilibrium with solid  $x_{Cu} = 0.016$ . The molybdenum solidus between 1356 and 2788 K is given by

$$\ln x_{Cu} = -8424 T^{-1} - 1.36 + 2.12 \times 10^{-4} T - 4.8 \times 10^{-8} T^2$$

with an uncertainty of a factor of 5. Between 2788 and 2890 K, the molybdenum solidus is given by

$$x_{\text{Cu}} = 1.84 \times 10^{-4} (2890-T) + 1.4 \times 10^{-7} (2890-T)^2 - 4.4 \times 10^{-9} (2890-T)^3$$

with an uncertainty of a factor of 3. Between 1357 and 2788 K, the molybdenum liquidus is

$$\ln x_{\text{Mo}} = -12470 T^{-1} + 2.57 - 1.01 \times 10^{-3} T + 3.32 \times 10^{-7} T^2$$

with the uncertainty becoming a factor of 3 at the lower temperatures. Between 2788 and 2890 K, the molybdenum liquidus is given by

$$x_{\text{Cu}} = 8.04 \times 10^{-4} (2890-T) + 9.4 \times 10^{-7} (2890-T)^2 + 1.22 \times 10^{-8} (2890-T)^3 \pm 0.01$$

The two-liquid phase region above the monotectic is terminated at 2585°C at 1 atm by formation of an essentially pure copper gaseous phase in equilibrium with the liquid compositions  $x_{\text{Cu}} = 0.115$  and 0.87. Between 2788 and 2858 K, the boundaries of the miscibility gap are given by

$$\ln x_{\text{Mo}} = -7300 T^{-1} - 0.767 + 4.4817 \times 10^{-4} T \pm 0.5$$

for the copper-rich boundary, and by

$$\ln x_{\text{Cu}} = -7600 T^{-1} - 0.79 + 4.512 \times 10^{-4} T \pm 0.5$$

for the molybdenum-rich boundary. The boundary of the liquid saturated by 1 atm gas is given by

$$T = \frac{36123 - 7000x_{\text{Mo}}^2 - 600x_{\text{Mo}}^3}{\ln(1-x_{\text{Mo}}) + 12.737}$$

between 2858 and 3000 K, with an uncertainty of 100°. At 3000 K, the liquid composition is  $x_{\text{Cu}} = 0.05$ , with an uncertainty of a factor of 2, and the 1-atm gas contains  $10^{-4}$  atm Mo, with an uncertainty of 10%.

#### Mo-Dy: molybdenum-dysprosium (Fig. II-2)

No data were found. The estimated thermodynamic equations of Part I have been used to calculate the phase boundaries of Fig. II-2.

The eutectic is calculated to be at  $1650 \pm 10$  K and  $x_{\text{Mo}} = 0.020 \pm 0.005$ . The dysprosium liquidus and solidus above the eutectic are represented by the equations

$$x_{\text{Mo}} = 4.6 \times 10^{-4} (1684-T) + 2 \times 10^{-6} (1684-T)^2$$

with an uncertainty of  $1.4 \times 10^{-4}$  (1684-T) for the liquidus and

$$x_{\text{Mo}} = 8 \times 10^{-5} (1684-T)$$

with an uncertainty of a factor of 5 for the solidus.

The molybdenum liquidus and solidus between 1650 and 2835 K are calculated to be

$$x_{\text{Mo}} = 0.011 + 1.7 \times 10^{-4} (T-1600) - 2 \times 10^{-7} (T-1600)^2 + 2.4 \times 10^{-10} (T-1600)^3$$

with an uncertainty of  $\pm 0.008$  at 1650 K rising to  $\pm 0.05$  at 2450 K for the liquidus, and

$$x_{\text{Dy}} = 4 \times 10^{-4} + 6 \times 10^{-7} (T-1600) + 5 \times 10^{-9} (T-1600)^2 - 1.7 \times 10^{-12} (T-1600)^3$$

with an uncertainty of a factor of 5 for the solidus.

Below 1650 K the solid solutions are calculated to be

$$x_{\text{Mo}} = 4 \times 10^{-5} + 4 \times 10^{-7} (T-1000) + 10^{-9} (T-1000)^2 + 5 \times 10^{-12} (T-1000)^3$$

and

$$x_{\text{Dy}} = 10^{-7} (T-1000) - 3 \times 10^{-10} (T-1000)^2 + 2 \times 10^{-12} (T-1000)^3$$

with an uncertainty of a factor of 5. The mole fraction solubility of molybdenum in dysprosium falls to  $10^{-4}$  at 1100 K; that of dysprosium in molybdenum falls to  $10^{-4}$  at 1390 K. Below these temperatures the solubilities are defect-controlled.

#### Mo-Er: molybdenum-erbium (Fig. II-1)

No data were found. The estimated thermodynamic equations of Part I have been used to calculate the phase boundaries of Fig. II-1.

The monotectic is at  $2740 \pm 30$  K and  $x_{\text{Er}} = 5 \times 10^{-3}$ ,  $0.09 \pm 0.03$  and  $0.59 \pm 0.07$ . Above the monotectic the molybdenum liquidus and solidus are:

$$x_{\text{Er}} = 6 \times 10^{-4} (2890-T) - 2 \times 10^{-6} (2890-T)^2 + 1.3 \times 10^{-8} (2890-T)^3$$

with an uncertainty of  $\pm 2 \times 10^{-4}$  (2890-T) for the liquidus, and  
 $x_{\text{Er}} = 3 \times 10^{-5} (2890-T)$

with an uncertainty of a factor of 5 for the solidus.

The two-liquid phase boundaries from 2740 to 2890 K are described by  
the equations

$$x_{\text{Mo}} = 0.41 + 8 \times 10^{-4} (T-2740)$$

with an uncertainty of  $\pm 0.07$  at 2740 K, rising to  $\pm 0.2$  at 2890 K, and

$$x_{\text{Er}} = 0.093 + 10^{-4} (T-2740)$$

with an uncertainty of  $\pm 0.025$ .

The eutectic is calculated to be at  $1750 \pm 10$  K and  $x_{\text{Er}} = 0.96 \pm 0.01$ . The equilibrium between solid molybdenum and liquid between 1750 and 2740 K is represented by the equations

$$x_{\text{Mo}} = 0.025 + 2 \times 10^{-4} (T-1700) - 3 \times 10^{-7} (T-1700)^2 + 4.5 \times 10^{-10} (T-1700)^3$$

with an uncertainty rising from  $\pm 0.006$  at 1750 K to  $\pm 0.08$  at 2740 for the liquidus, and

$$x_{\text{Er}} = 6 \times 10^{-4} + 2 \times 10^{-6} (T-1700) + 4 \times 10^{-9} (T-1700)^2 - 2 \times 10^{-12} (T-1700)^3$$

with an uncertainty of a factor of 5 for the solidus.

The erbium liquidus and solidus above the eutectic are represented by

$$x_{\text{Mo}} = 6.5 \times 10^{-4} (1795-T) + 6 \times 10^{-6} (1795-T)^2$$

with an uncertainty of  $1.7 \times 10^{-4}$  (1795-T) for the liquidus, and

$$x_{\text{Mo}} = 10^{-4} (1795-T)$$

with an uncertainty of a factor of 5 for the solidus.

Below 1750 K the solid-solution phase boundaries are

$$x_{\text{Mo}} = 10^{-4} + 10^{-6} (T-1000) + 3 \times 10^{-9} (T-1000)^2 + 7 \times 10^{-12} (T-1000)^3$$

and

$$x_{\text{Er}} = 10^{-7} (T-1000) - 4 \times 10^{-10} (T-1000)^2 + 2 \times 10^{-12} (T-1000)^3$$

with uncertainties of a factor of 5. The solubility falls to  $x = 10^{-4}$  at 1400 K for erbium in molybdenum, and at 1000 K for molybdenum in erbium.

#### Mo-Es: molybdenum-einsteinium (Fig. II-11)

No data were found. The estimated normal boiling point of  $1200 \pm 50$  K is lower than the estimated melting temperature,  $1700 \pm 100$  K. The estimated thermodynamic equations of Part I have been used to calculate the solid-solution phase boundaries below 1200 K:

$$x_{\text{Mo}} = 1.7 \times 10^{-5} + 4 \times 10^{-8} (T-1000) + 1.6 \times 10^{-9} (T-1000)^2$$

The solubility of molybdenum in einsteinium falls to  $10^{-4}$  at 1215 K with an uncertainty of a factor of 5. Below this temperature the solubility is defect-controlled, as is the solubility of einsteinium in molybdenum at all temperatures up to 1200 K.

#### Mo-Eu: molybdenum-europium (Fig. II-2)

No data were found. The estimated thermodynamic equations of Part I have been used to calculate the phase boundaries of Fig. II-2. From 1090 to 1870 K the molybdenum liquidus is calculated to be

$$x_{\text{Mo}} = -3 \times 10^{-5} + 5.1 \times 10^{-7} (T-1000) - 2 \times 10^{-9} (T-1000)^2 + 2.6 \times 10^{-12} (T-1000)^3$$

with an uncertainty in  $x_{\text{Mo}}$  of  $\pm 10^{-6}$  at 1090 K, rising to  $\pm 2 \times 10^{-4}$  at 1870 K.

The solid solubilities are defect-controlled.

The eutectic temperature is calculated to be 0.001 K lower than the melting point of pure europium. The eutectic composition is  $x_{\text{Mo}} = 10^{-6}$ .

#### Mo-F: molybdenum-fluorine (Fig. II-16a, b)

This system is complicated by disproportionation reactions of all of the lower fluorides and by great sensitivity to water and oxygen resulting in the formation of oxyfluorides. Some of the reported phases, such as the solids with F/Mo less than one, prepared by Johnson and Siegel [128] by explosion of molybdenum wire in  $\text{SF}_6$ , are undoubtedly metastable. It has been suggested [221] that some of the reported phases such as  $\text{MoF}_3$  are metastable as pure phases but are stabilized by oxygen. The wide discrepancies between the melting points and vapour pressure reported for  $\text{MoF}_5$  [153] clearly show

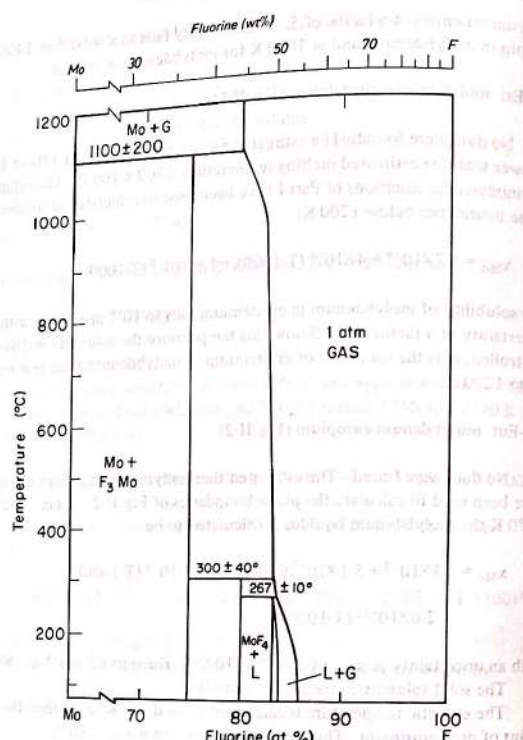


FIG.II-16a. Phase diagram of the system molybdenum-fluorine.

the influence of oxyfluoride impurities. Krause and Douglas [153] have reviewed previous determinations of the melting point of  $\text{MoF}_5$  which were about 20°C higher than the melting point at 45.7°C of their carefully prepared sample. They suggest that the previous samples were solid solutions of  $\text{MoOF}_4$  and  $\text{MoF}_5$  or that different crystalline forms of  $\text{MoF}_5$  nucleated, depending upon the method of sample preparation. Popov et al. [190] report a transition at 21.1°C for  $\text{MoF}_5$  and a liquidus curve for the low-temperature  $\alpha\text{MoF}_5$  which can be

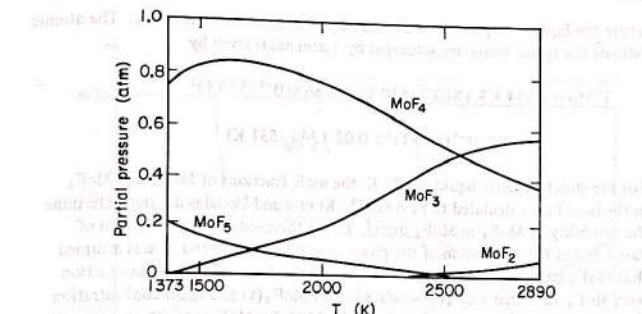


FIG.II-16b. Composition of molybdenum-fluorine 1-atm gas in equilibrium with molybdenum solid.

extrapolated to a melting point of 45°C; for  $\beta\text{MoF}_5$  they observe a melting point of 67.4°C. They suggest that lower reported melting points correspond to a metastable congruent melting of  $\alpha\text{MoF}_5$ . They also report the phases  $\text{Mo}_2\text{F}_{11}$  and  $\text{Mo}_4\text{F}_{23}$  melting congruently at  $40 \pm 1^\circ\text{C}$  and  $34 \pm 1^\circ\text{C}$ , respectively. As it would not be possible to show the details of their diagram on the scale of Fig. II-16a, which shows the high-temperature behaviour of the Mo-F phase diagram, their three eutectic points are listed here. The  $\text{MoF}_5\text{-Mo}_2\text{F}_{11}$  eutectic is at  $8.0 \pm 0.2^\circ\text{C}$ , with the liquid composition at  $\text{MoF}_{5.375}$ . The  $\text{Mo}_2\text{F}_{11}\text{-Mo}_4\text{F}_{23}$  eutectic is at  $0.7 \pm 0.1^\circ\text{C}$  and  $\text{MoF}_{5.625}$ . The  $\text{Mo}_4\text{F}_{23}\text{-MoF}_6$  eutectic is at  $7.8 \pm 0.3^\circ\text{C}$  and  $\text{MoF}_{5.892}$ .

Part I discusses the phases  $\text{MoF}_4$  and  $\text{MoF}_3$  and the metastable  $\text{Mo}_2\text{F}_9$ .  $\text{MoF}_4$  has not been well characterized, but Fukutomi and Corbett [80] have recently demonstrated the stability of  $\text{MoF}_3$  and the lack of stable phases between Mo and  $\text{MoF}_3$ . They have fixed the stoichiometry of  $\text{MoF}_3$  within an analytical uncertainty of 1%. The crystallographic data are reviewed in Part III. The recent studies of the vapour species by Alikhanyan et al. [6], Gotkis et al. [99] and Kleinschmidt et al. [143] are discussed in detail in Part I.

$\text{MoF}_6$  melts at 17.61°C and boils at 33.85°C [184]. Douglas [59] and Krause and Douglas [152, 153] have determined the  $\text{Mo}_2\text{F}_{10}$  partial pressure of  $\text{MoF}_5$  liquid as discussed in detail in Part I. Because of disproportionation to  $\text{MoF}_4$  and  $\text{MoF}_6$ , the vaporization of  $\text{MoF}_5$  liquid is complicated. Krause [152] has developed a model, discussed in detail in Part I, which allows calculation of the liquid and vapour compositions as a function of  $\text{MoF}_6$  partial pressure. The average F/Mo ratio for the gas, which is essentially 6 at low temperatures, becomes 5.976 at 400 K, 5.85 at 450 K, 5.49 at 500 K, and 5.21 at 531 K,

where the liquid composition is calculated to be stoichiometric  $\text{MoF}_5$ . The atomic ratio of the liquid boundary saturated by 1 atm gas is given by

$$\begin{aligned} F/\text{Mo} &= 4.954 + 3.1 \times 10^{-3} (550-T) - 3.86 \times 10^{-5} (550-T)^2 \\ &+ 1.59 \times 10^{-7} (550-T)^3 \pm 0.02 \quad (340-531 \text{ K}) \end{aligned}$$

For the stoichiometric liquid at 531 K, the mole fractions of  $\text{MoF}_4$  and  $\text{MoF}_6$  in the liquid are calculated to be  $6 \times 10^{-3}$ . Krause and Douglas did not determine the solubility of  $\text{MoF}_4$  in  $\text{MoF}_5$  liquid. In the thermodynamic evaluation of Part I and in the calculation of the phase diagram of Fig. II-16a, it was assumed that  $\text{MoF}_4$  has a sufficiently high melting point and a small enough interaction with  $\text{MoF}_5$  such that  $\text{MoF}_4(s)$  would saturate  $\text{MoF}_5(\ell)$  at a small concentration. From the data of Krause and Douglas [152, 153], for  $\text{MoF}_5(\ell)$  with an excess of  $\text{MoF}_4$  over  $\text{MoF}_6$ , the relation between the pressure of  $\text{MoF}_6$  in atm and the mole fraction of  $\text{MoF}_4$  is given by

$$\ln P_{\text{MoF}_6} x_{\text{MoF}_4} = 5.827 - 6400 T^{-1} \pm 0.03 \quad (340-540 \text{ K})$$

At 540 K, with 0.8 atm  $\text{Mo}_2\text{F}_{10}$  and 0.2 atm  $\text{MoF}_6$ ,  $x_{\text{MoF}_4} = 10^{-2}$ , which is taken as the solubility of  $\text{MoF}_4$  in  $\text{MoF}_5(\ell)$ . This fixes the  $\text{MoF}_5$  peritectic at  $267 \pm 10^\circ\text{C}$ , as indicated in Fig. II-16a.

As discussed in Part I, the selected thermodynamic data correspond to the disproportionation of  $\text{MoF}_4(s)$  at  $300 \pm 40^\circ\text{C}$  to  $\text{MoF}_3(s)$  and 1 atm gas containing 97 mol%  $\text{Mo}_2\text{F}_{10}(g)$  and 3 mol%  $\text{MoF}_6(g)$ . As the temperature increases, the molybdenum activity at the fluorine-rich boundary of the  $\text{MoF}_3$  homogeneous range increases and the  $\text{MoF}_4$  content of the gas begins to increase. It is calculated that there is a rather rapid change from the major species  $\text{Mo}_2\text{F}_{10}$  and  $\text{MoF}_6$  to  $\text{MoF}_4$  and  $\text{MoF}_5$  just below the disproportionation temperature of  $\text{MoF}_3$ . The 1-atm gas in equilibrium with  $\text{MoF}_3(s)$  and  $\text{Mo}(s)$  at  $1100 \pm 100^\circ\text{C}$  is calculated to contain  $75 \pm 5$  mol%  $\text{MoF}_4(g)$  and  $20 \pm 2$  mol%  $\text{MoF}_5(g)$  as shown in Fig. II-16b. Each of  $\text{MoF}_6(g)$  and  $\text{Mo}_2\text{F}_{10}(g)$  is calculated to be  $3 \pm 2$  mol%. These species are not shown in Fig. II-16b which indicates the variation with temperature of the gaseous species  $\text{MoF}_5$ ,  $\text{MoF}_4$ ,  $\text{MoF}_3$  and  $\text{MoF}_2$  in the 1-atm gas in equilibrium with molybdenum metal.  $\text{MoF}_4$  is seen to be the major species over a wide temperature range.  $\text{MoF}$  does not become significant until higher temperatures in the liquid molybdenum range.

#### Mo-Fe: molybdenum-iron (Fig. II-17)

Sinha et al. [231] have added to the previous work reviewed by Hansen and Anderko [109] to fix the main features of the Fe-Mo diagram. Hawkins

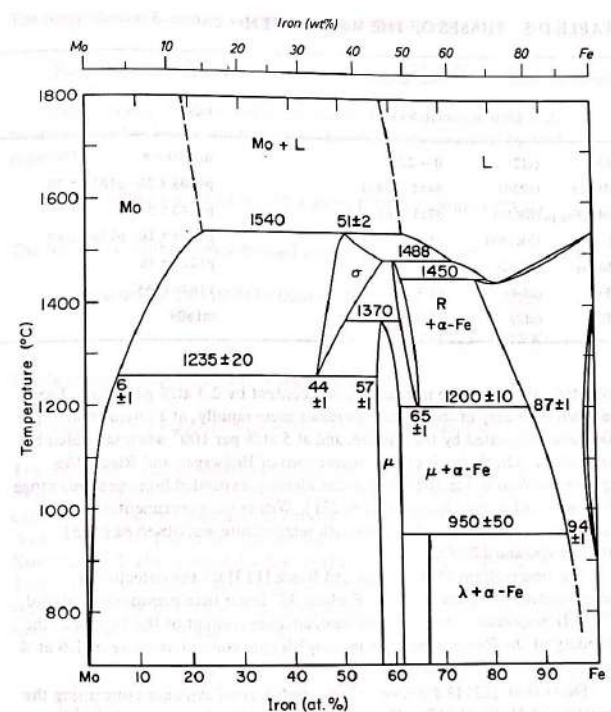


FIG. II-17. Phase diagram of the system molybdenum-iron.

and Hultgren [110] have reviewed the literature up to 1972 and their diagram has been used with modifications because of very recent data [1, 113, 117, 142].

The composition and temperature ranges of the phases are given in Table II-5. Many of the phase boundaries presented previously [109, 231] have been somewhat changed on the basis of the careful diffusion couple studies of Heijwegen and Rieck [113]. For example, the temperature of the eutectoidal decomposition of  $\sigma\text{MoFe}$  has increased by  $55^\circ$ . As the iron content of the bcc Mo boundary increases with increasing temperature, the molybdenum-rich

TABLE II-5. PHASES OF THE Mo-Fe SYSTEM

Phase (structure)	Maximum composition range (at.% Fe)	Peritectic or peritectoid temperature (K)
Mo (cI2)	0 - 22±2	m2890 ± 8
$\sigma$ MoFe (tP30)	44±1 - 58±1	p1508 ± 20; p1813 ± 20
$\mu$ Mo <sub>0.385</sub> Fe <sub>0.615</sub> (hR39)	57±1 - 61.5±1	p1643 ± 5
R (hR159)	61±1 - 65±1	p1473 ± 10; p1761 ± 10
MoFe <sub>2</sub> (hP12)	66.7 ± 0.2	p1223 ± 50
$\gamma$ Fe (cF4)	98.3±0.2 - 100	1184-1665
$\alpha$ Fe (cI2)	77±2 - 100	m1809

The boundary of the  $\sigma$ -phase increases in iron content by 2.3 at.% per 100°. The iron-rich boundary of the  $\sigma$ -phase increases more rapidly, at a rate of 6 at.% per 100° when saturated by the  $\mu$ -phase, and at 5 at.% per 100° when saturated by the R-phase. On the basis of the observations of Heijwegen and Rieck, the  $\mu$ -phase is shown in Fig. II-17 with a considerably expanded homogeneous range compared with earlier diagrams [109, 231]. Within the experimental error of 1 at.%, no change in the boundaries with temperature was observed [113] between 900 and 1250°C.

The observations of Heijwegen and Rieck [113] fix the eutectoidal decomposition temperature of the R-phase 45° lower than previously reported [231]. In response to the increasing molybdenum content of the Fe-phase, the boundary of the R-phase increases in molybdenum content at a rate of 1.6 at.% per 100° as the temperature rises.

Sinha et al. [231] have reviewed the controversial evidence concerning the formation of MoFe<sub>2</sub>(hP12). Their work indicated the formation of the phase with a very narrow homogeneous range below 950°C. However, Rawlings and Newey [199] and Heijwegen and Rieck [113] were unable to detect the phase in their recent diffusion couple studies. This appears to be a nucleation problem. Higgins and Wilkes [117] have studied the formation of MoFe<sub>2</sub> in a 12 at.% Mo alloy. No MoFe<sub>2</sub> could be obtained at 1300°C nor below 500°C. However, MoFe<sub>2</sub> precipitate was observed after 300 hours at 550°C or 500 hours at 500°C.

The data of Heijwegen and Rieck [113] and the earlier data given by Hansen and Anderko [109] fix the bcc molybdenum boundary saturated by the  $\mu$ -phase as

$$\ln x_{\text{Fe}} = -1.627 + 1.412 \times 10^{-3} T - 5326 T^{-1} \pm 0.15 \quad (1100-1508 \text{ K})$$

## PART II. PHASE DIAGRAMS

The molybdenum boundary saturated by the  $\sigma$ -phase is given by

$$\ln x_{\text{Fe}} = 4.19 + 3.877 \times 10^{-4} T - 11658 T^{-1} \pm 0.15 \quad (1508-1813 \text{ K})$$

Part I reviews the data used for fixing the thermodynamic data and boundaries of the bcc Fe solid solution. The boundary saturated by MoF<sub>2</sub> is given by

$$\ln x_{\text{Mo}} = -16.05 + 7.65 \times 10^{-3} T + 4830 T^{-1} \pm 0.1 \quad (800-1223 \text{ K})$$

The boundary saturated by  $\mu$ Mo<sub>0.385</sub>Fe<sub>0.615</sub>(hR39) is given by

$$x_{\text{Mo}} = 0.046 - 2.6 \times 10^{-5} (T-1000) + 4.3 \times 10^{-7} (T-1000)^2 \pm 0.005$$

(1223-1473 K)

The boundary saturated by the R-phase is given by

$$x_{\text{Mo}} = 0.09 + 6.3 \times 10^{-4} (T-1400) - 7 \times 10^{-7} (T-1400)^2 \pm 0.01 \quad (1473-1723 \text{ K})$$

The data fixing the boundaries of the gamma-loop are discussed in Part I. Recent measurements [1, 75, 113, 142] are in agreement that the gamma-loop extends to a higher molybdenum concentration than indicated by Hansen and Anderko [109]. The most accurate measurements appear to be those of Kirchner et al. [142] which fix the maximum extent at 1410 ± 20 K, with 1.69 ± 0.05 at.% Mo in fcc Fe and 2.26 ± 0.05 at.% Mo in bcc Fe. The fcc Fe boundary is given with an uncertainty in  $x_{\text{Mo}}$  of 3% for the lower branch between 1184 and 1410 K by

$$\frac{x_{\text{Mo}}}{T-1184} = 2.06 \times 10^{-4} - 1.025 \times 10^{-6} (T-1184) + 1.97 \times 10^{-9} (T-1184)^2$$

and for the upper branch between 1410 and 1665 K by

$$\frac{x_{\text{Mo}}}{1665-T} = 1.53 \times 10^{-4} - 5.3 \times 10^{-7} (1665-T) + 7.4 \times 10^{-10} (1665-T)^2$$

The bcc Fe boundary saturated by fcc Fe is given with an uncertainty of 5% for the lower branch between 1184 and 1410 K by

$$\frac{x_{\text{Mo}}}{T-1184} = 2.84 \times 10^{-4} - 1.41 \times 10^{-6} (T-1184) + 2.64 \times 10^{-9} (T-1184)^2$$

and for the upper branch between 1410 and 1665 K by

$$\frac{x_{\text{Mo}}}{1665-T} = 1.905 \times 10^{-4} - 5.3 \times 10^{-7} (1665-T) + 5.1 \times 10^{-10} (1665-T)^2$$

The bcc Fe solidus and liquidus are given with an uncertainty in  $x_{\text{Mo}}$  of 10% between 1718 and 1809 K by

$$\frac{x_{\text{Mo}}}{1809-T} = -0.012 + 2.25 \times 10^{-3} (1809-T) + 1.1 \times 10^{-6} (1809-T)^2$$

for the solidus, and

$$\frac{x_{\text{Mo}}}{1809-T} = 0.017 + 1.4 \times 10^{-3} (1809-T) + 7 \times 10^{-6} (1809-T)^2$$

for the liquidus. At higher  $x_{\text{Mo}}$ , the solidus and liquidus rise by 5° to  $x_{\text{Mo}} = 0.22$  for the solidus and  $x_{\text{Mo}} = 0.21$  for the liquidus. The R-liquidus is given by

$$\frac{x_{\text{Mo}}}{T-1700} = 0.20 - 4 \times 10^{-5} (T-1700) + 2.1 \times 10^{-5} (T-1700)^2 \pm 5\%$$

(1723–1761 K)

The  $\sigma$ -liquidus is given by

$$\frac{x_{\text{Mo}}}{T-1700} = 0.302 - 1.71 \times 10^{-3} (T-1700) + 2.06 \times 10^{-5} (T-1700)^2 \pm 3\%$$

(1761–1813 K)

Except for the values near the  $\sigma$ -peritectic, no measurements were found for either the molybdenum solidus or liquidus. From the thermodynamic data of Part I, the following equations were calculated. The molybdenum solidus and liquidus are given with an uncertainty in  $x_{\text{Fe}}$  of 10% between 1813 and 2890 K by

$$\frac{x_{\text{Fe}}}{2890-T} = 1.56 \times 10^{-4} - 3.5 \times 10^{-9} (2890-T) + 4.2 \times 10^{-11} (2890-T)^2$$

for the solidus, and

$$\frac{x_{\text{Fe}}}{2890-T} = 7.1 \times 10^{-4} - 2.44 \times 10^{-7} (2890-T) + 1.19 \times 10^{-10} (2890-T)^2$$

for the liquidus.

#### Mo-Fm: molybdenum-fermium (Fig. II-11)

No data were found. The estimated normal boiling point of  $1120 \pm 50$  K is below the estimated melting point of  $1600 \pm 200$  K. The estimated thermodynamic equations of Part I have been used to predict the solid-solution phase boundaries below 1120 K:

$$x_{\text{Fm}} = 7.4 \times 10^{-5} - 7.1 \times 10^{-7} (T-800) + 4.7 \times 10^{-9} (T-800)^2$$

$$x_{\text{Mo}} = 9.5 \times 10^{-5} + 1.1 \times 10^{-6} (T-800) + 4.7 \times 10^{-9} (T-800)^2 \\ + 1.3 \times 10^{-11} (T-800)^3$$

The solubilities drop to  $x_{\text{Fm}} = 10^{-4}$  at 1000 K and  $x_{\text{Mo}} = 10^{-4}$  at 800 K, with an uncertainty of a factor of 5. Below these temperatures the solubilities are defect-controlled.

#### Mo-Fr: molybdenum-francium (Fig. II-2)

No data were found. The estimated thermodynamic functions of Part I have been used to calculate the molybdenum liquidus from 300 to 955 K.

$$\ln x_{\text{Mo}} = -35560 T^{-1} + 2.21$$

The solubility of molybdenum in liquid francium rises from  $x_{\text{Mo}} = 10^{-51}$  at 300 K to  $x_{\text{Mo}} = 6 \times 10^{-16}$  at 955 K, with an uncertainty of a factor of 5. The solubility of francium in molybdenum is defect-controlled.

#### Mo-Ga: molybdenum-gallium (Fig. II-18)

As discussed in more detail in Part III, the five phases  $\text{GaMo}_3$  (cP8),  $\sim \text{GaMo}$ ,  $\text{Ga}_2\text{Mo}$ ,  $\text{Ga}_{31}\text{Mo}_6$  (mP37) and  $\text{Ga}_{41}\text{Mo}_8$  (hR147) have been reported [269]. An analysis of  $\text{Ga}_{31}\text{Mo}_6$ , which has defects on the gallium sites, yielded  $\text{Ga}/\text{Mo} = 5.1 \pm 0.1$ .  $\text{Ga}_{41}\text{Mo}_8$ , which has an excess of gallium, has  $\text{Ga}/\text{Mo} = 5.3 \pm 0.1$ .

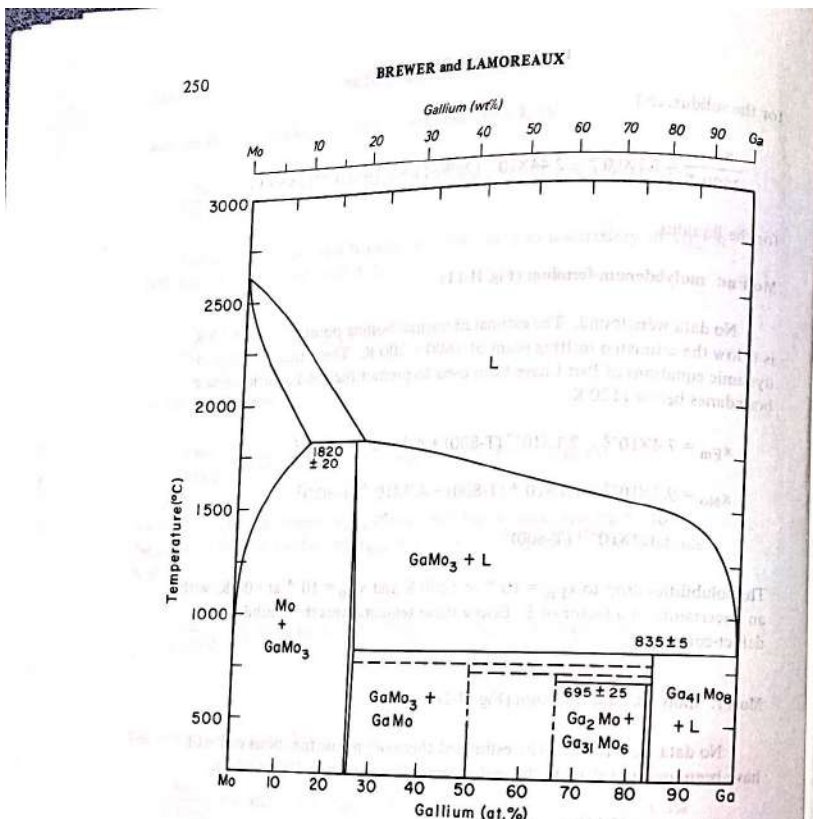


FIG.II-18. Phase diagram of the system molybdenum-gallium.

Bornand et al. [23] report a peritectic for  $\text{GaMo}_3$  at  $1830 \pm 20^\circ\text{C}$ , and a peritectic at  $835 \pm 5^\circ\text{C}$  for  $\text{Ga}_2\text{Mo}$  which is taken to correspond to  $\text{Ga}_{41}\text{Mo}_8$ , the most gallium-rich phase. No other phases have been observed at temperatures above  $800^\circ\text{C}$  and the remaining three phases are assumed to be unstable above  $800^\circ\text{C}$ .  $\text{Ga}_{31}\text{Mo}_6$  is observed to form from the liquid at  $700^\circ\text{C}$ ; thus it must be unstable with respect to  $\text{Ga}_2\text{Mo}$  and  $\text{Ga}_{41}\text{Mo}_8$  solids at temperatures higher than about  $690^\circ\text{C}$ . No information is available on the conditions of preparation of  $\text{GaMo}_3$  or  $\text{Ga}_2\text{Mo}$ . The molybdenum solidus is based on the measurements between

## PART II. PHASE DIAGRAMS

251

1548 and  $1973\text{ K}$  by Bornand et al. [23]. They also report  $x_{\text{Mo}} = 0.75$  at  $2168\text{ K}$  for the molybdenum liquidus. Yatsenko and Anikin [267] report  $x_{\text{Mo}} = 4 \times 10^{-3}$  at  $1220\text{ K}$  and  $x_{\text{Mo}} = 3 \times 10^{-3}$  at  $1150\text{ K}$  for the  $\text{GaMo}_3$  liquidus, and  $x_{\text{Mo}} = 1.4 \times 10^{-3}$  at  $1030\text{ K}$  for the  $\text{Ga}_{41}\text{Mo}_8$  liquidus.

The molybdenum solidus below  $2093\text{ K}$  is given by

$$\ln x_{\text{Ga}} = 4.31 - 12960 T^{-1} \pm 0.1$$

From  $2093$  to  $2890\text{ K}$ , it is given by

$$x_{\text{Ga}} = 6 \times 10^{-5} (2890-T) + 2.768 \times 10^{-7} (2890-T)^2 - 1.87 \times 10^{-10} (2890-T)^3 \\ + 5.99 \times 10^{-4} (2890-T)^4 \pm 0.01$$

The molybdenum liquidus is given by

$$x_{\text{Ga}} = 5.95 \times 10^{-4} (2890-T) - 1.04 \times 10^{-6} (2890-T)^2 + 1.58 \times 10^{-9} (2890-T)^3 \\ - 8.58 \times 10^{-13} (2890-T)^4 \pm 0.02 \quad (2093-2890\text{ K})$$

The  $\text{GaMo}_3$  liquidus between  $1108$  and  $2093\text{ K}$  is given by

$$T = \frac{8710 + \frac{1}{3} (6240 - 10^4 x_{\text{Mo}}) x_{\text{Mo}}^2 + \{10^4(1-x_{\text{Mo}}) - 8760\}(1-x_{\text{Mo}})^2}{3.235 - \frac{1}{3} \ln(1-x_{\text{Mo}}) - \ln x_{\text{Mo}} - 0.167 x_{\text{Mo}}^2 - 0.5(1-x_{\text{Mo}})^2}$$

with an uncertainty of  $15\text{ K}$  in  $T$  or  $\pm 0.05$  in  $x_{\text{Mo}}$  around  $2090\text{ K}$ , increasing to  $\pm 0.1$  at  $1900\text{ K}$ , to  $\pm 0.2$  at  $1800\text{ K}$  and up to  $\pm 0.3$  at  $1700\text{ K}$ . See Part I for a discussion of the uncertainty. The liquid boundary in equilibrium with gallium gas at  $1\text{ atm}$  is estimated to be  $x_{\text{Ga}} = 0.3 \pm 0.1$  at  $2300^\circ\text{C}$  and  $0.5 \pm 0.2$  at  $2500^\circ\text{C}$ .

## Mo-Gd: molybdenum-gadolinium (Figs II-1 and II-19)

Savitskij et al. [213] report the solubility of gadolinium in molybdenum to be less than  $0.1\text{ wt\%}$  at an unspecified temperature. The only other publication found was that of Chuang et al. [50] who report that the molybdenum solidus increases from  $0.09\text{ wt\% Gd}$  at  $2570^\circ\text{C}$  to  $1.53\text{ wt\%}$  at  $2510^\circ\text{C}$  and then decreases to  $0.15\text{ wt\%}$  at  $1600^\circ\text{C}$ . The only information reported on the liquidus is that an addition of molybdenum lowered the melting point of gadolinium by about  $14^\circ$  and that a metallographical examination of samples with up to  $24\text{ wt\% Mo}$ , which had been melted, indicated that immiscible liquid phases had formed with a monotectic composition around  $14.5\text{ wt\%}$ . The monotectic

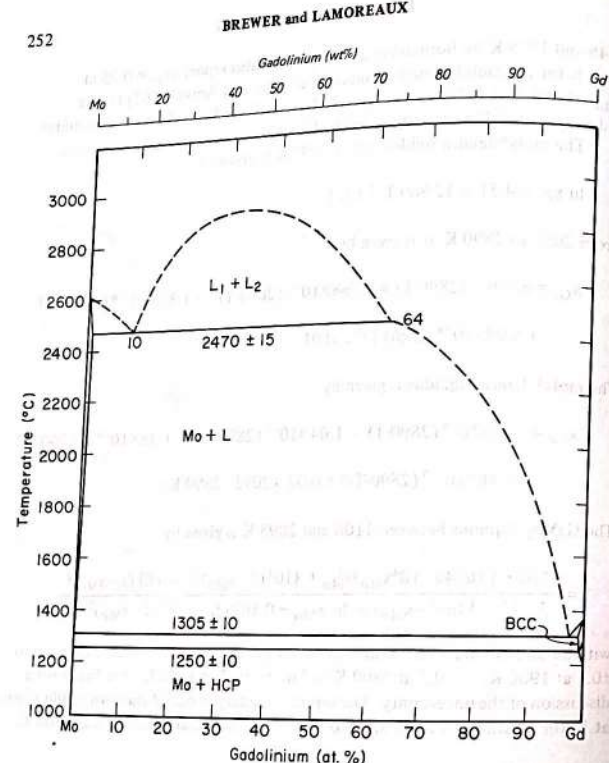


FIG.II-19. Phase diagram of the system molybdenum-gadolinium.

temperature was fixed between 2457 and 2470°C. These observations have been utilized in Part I to generate thermodynamic equations that were then used to calculate the phase diagram of Fig.II-19. The two-liquid phase boundaries between 2740 and 3100 K are calculated to be

$$x_{\text{Gd}} = 0.10 + 2 \times 10^{-4} (T - 2700) + 4 \times 10^{-10} (T - 2700)^3 \quad (\text{high molybdenum})$$

$$\text{and } x_{\text{Mo}} = 0.35 + 4 \times 10^{-4} (T - 2700) \quad (\text{low molybdenum})$$

with an uncertainty of ±0.03 for the high molybdenum boundary and of ±0.09 for the low molybdenum boundary. The molybdenum solidus above the monotectic is represented between 2890 and 2740 K by

$$x_{\text{Gd}} = 5.6 \times 10^{-5} (2890 - T) + 6 \times 10^{-7} (2890 - T)^2 + 4.5 \times 10^{-9} (2890 - T)^3$$

Between 2740 and 1580 K,

$$x_{\text{Gd}} = 2.3 \times 10^{-4} + 3 \times 10^{-6} (T - 1500) + 2 \times 10^{-9} (T - 1500)^2$$

Below 1580 K,

$$x_{\text{Gd}} = 4.5 \times 10^{-5} - 4 \times 10^{-7} (T - 1000) + 2 \times 10^{-9} (T - 1000)^2$$

The uncertainty of the molybdenum solidus is ±0.002. The molybdenum liquidus between 2890 and 2740 K is given by

$$x_{\text{Gd}} = 4.0 \times 10^{-4} (2890 - T) + 9 \times 10^{-6} (2890 - T)^2 - 4.8 \times 10^{-8} (2890 - T)^3 \pm 0.09$$

and between 2740 and 1580 K by

$$x_{\text{Mo}} = 0.03 - 4 \times 10^{-5} (T - 1500) + 2.4 \times 10^{-7} (T - 1500)^2 \pm 0.03$$

The gadolinium solidus is calculated to be  $x_{\text{Mo}} = 0.001 \pm 0.005$  at 1570 K, dropping to a value of  $10^{-4}$  with an uncertainty of a factor of 2 around 1200 K.

#### Mo-Ge: molybdenum-germanium (Fig.II-20)

Section III reviews the literature on the structures of the five characterized stable phases,  $\text{GeMo}_3(\text{cP}8)$ ,  $\text{Ge}_3\text{Mo}_5(\text{tI}32)$ ,  $\text{Ge}_{13}\text{Mo}_{13}(\text{P} \sim 144)$ ,  $\text{Ge}_{16}\text{Mo}_9(\text{tP} \sim 100)$  and  $\alpha\text{Ge}_2\text{Mo}(\text{oP}12)$ , as well as the metastable  $\beta\text{Ge}_2\text{Mo}(\text{tI}6)$ . Shunk [228] has presented a phase diagram based on the literature through 1964, which is largely based on the measurements of Stecher et al. [236]. Steinmetz et al. [239] present confirming results. Two more recently reported phases [258],  $\text{Ge}_{16}\text{Mo}_9(\text{Ge}_{1.778}\text{Mo})$  and  $\text{Ge}_{41}\text{Mo}_{23}(\text{Ge}_{1.783})$ , are not shown. The diagram is reproduced in Fig.II-20, with only a single line shown at the composition  $\text{Ge}_{23}\text{Mo}_{13}(\text{Ge}_{1.769}\text{Mo})$ ,

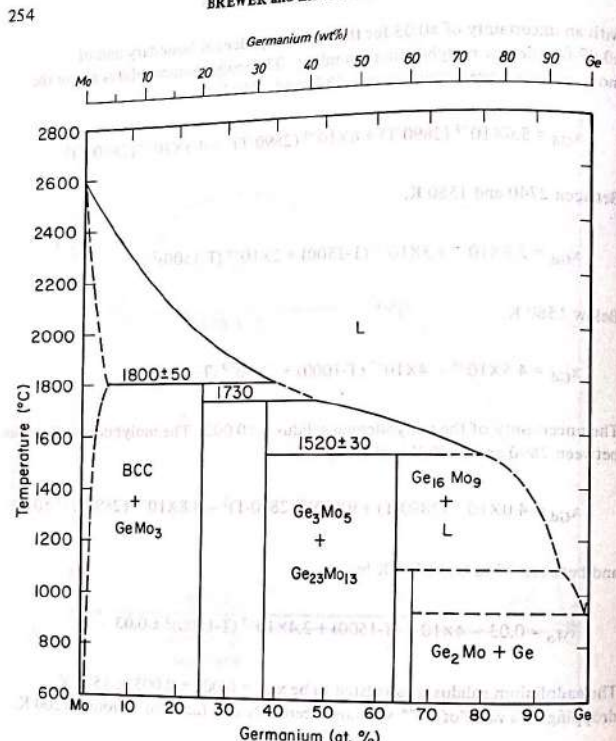


FIG.II-20. Phase diagram of the system molybdenum-germanium.

since the phases are so closely spaced in composition that it is impractical to show them as separate phases. The peritectic temperatures for each of the phases have not been distinguished and it is possible that they merge into a single homogeneous phase region at high temperatures.

The thermodynamic values selected in Part I indicate that the molybdenum liquidus in Fig.II-20 from Shunk [228] should be up to 100° higher in the middle

of its range. The calculated boundary is given between 2073 and 2890 K, with an uncertainty in  $x_{\text{Ge}}$  of 20%, by

$$\frac{x_{\text{Ge}}}{2890-T} = 5.92 \times 10^{-4} - 2.19 \times 10^{-7} (2890-T) + 9.42 \times 10^{-11} (2890-T)^2$$

The calculated solidus is given by

$$\ln \frac{x_{\text{Ge}}}{2890-T} = 2700 T^{-1} - 8.768 - 1.27 \times 10^{-3} T + 10^{-7} T^2 \pm 0.2 \quad (2073-2890 \text{ K}),$$

The Mo<sub>3</sub>Ge liquidus is given by

$$x_{\text{Ge}} = 0.47 - 10^{-3} (T-2000) \pm 0.02 \quad (2003-2073 \text{ K})$$

The Mo<sub>9</sub>Ge<sub>16</sub> liquidus is given by

$$x_{\text{Mo}} = 0.145 + 3 \times 10^{-4} (T-1700) + 3.15 \times 10^{-6} (T-1700)^2 \pm 0.02$$

(1793-2003 K)

The Mo<sub>9</sub>Ge<sub>16</sub> liquidus is given by

$$x_{\text{Mo}} = 0.07 - 2.5 \times 10^{-4} (T-1300) + 10^{-6} (T-1300)^2 \pm 0.03 \quad (1363-1793 \text{ K})$$

The MoGe<sub>2</sub> liquidus is given by

$$x_{\text{Mo}} = 0.01 + 10^{-5} (T-1200) + 1.7 \times 10^{-6} (T-1200)^2 \pm 0.01 \quad (1203-1363 \text{ K})$$

Mo-H: molybdenum-hydrogen (Fig. II-4)

Solubility measurements of hydrogen in molybdenum have been reported for temperatures between 400 and 2300°C [63, 118, 158, 171, 173, 179, 230, 272] and for pressures up to 100 atm [173]. Within experimental error the solubility is proportional to the square root of the hydrogen pressure. The solubility is given by

$$\ln x_{\text{H}} = -3300 T^{-1} + \ln T - 14.6 + \ln P_{\text{H}_2}^{1/2} \pm 0.3$$

The low-temperature data are particularly difficult to obtain. The data of Martin [171] between 450 and 1200°C were generally too high and were given

little weight. The value at 400°C by Zakharov and Sharapov [272] was higher by a factor of 1.6 than the equation value, and their value at 800°C was lower by a factor of 4. The values by Sieverts and Brüning [230] were higher by factors of 5 and 1.6 at 420 and 667°C, but ranged from 4% lower to 15% higher between 763 and 1095°C, except for one value at 983°C which was lower by 48%. The data by Eguchi and Morozumi [63] between 600 and 1200°C were mostly close to the calculated values, with some values lower by as much as 13% but most ranging on the high side. With the exception of a few very high points, the main portion of their results was within 20%. The data of Oates and McLellan [179] between 905 and 1521°C were generally lower than the calculated values. One value at 1460°C was higher by 2%. The other values above 1229°C were lower by 2 to 13%. The deviation increased at lower temperatures, ranging from 12 to 52% lower. The data of Hill [118] from 1280 to 1700°C were almost parallel to the calculated curve, ranging from 16 to 18% higher. The data of Mazaev et al. [173] from 1100 to 2300°C are higher by 5% than the calculated value at 1100°C and range over a few per cent on either side at 1900, 2100 and 2300°C. However, their values at 1300–1700°C range from 30% to over 60% below the calculated curve or determinations by other investigators. The data of Lange and Schenck [158] from 1340 to 1950°C are lower by 10 to 35% at the lower temperatures and cross the calculated curve to become increasingly higher at the upper end.

#### Mo-He: molybdenum-helium (Fig. II-4)

No experimental data were found; see Mo-Ar for details of the calculation of Fig. II-4. The order of magnitude of the mole fraction of helium in liquid molybdenum at 2890 K saturated with 1 atm gas is calculated to be  $10^{-10}$ .

#### Mo-Hf: molybdenum-hafnium (Fig. II-21)

The phase diagram literature for the Mo-Hf system was reviewed by Rudy [205] who confirmed the essential observations of Taylor et al. [247] and gave a more detailed description of the hafnium-rich region. Garg and Ackermann [82] have presented a less detailed phase diagram, in reasonable agreement with the above references. The phase diagram in Fig. II-21 has been determined by a critical evaluation of the literature and is consistent with the approximate thermodynamic equations of Part I.

The  $\text{HfMo}_2$  phase forms peritectically at  $2170 \pm 40^\circ\text{C}$  from bcc molybdenum containing 27 ± 1 at.% Hf, and liquid molybdenum containing 40 ± 3 at.% Hf

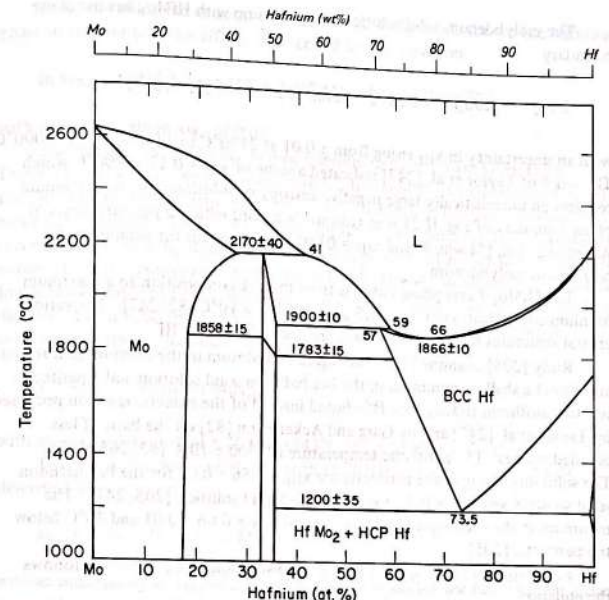


FIG.II-21. Phase diagram of the system molybdenum-hafnium.

[205, 247]. Above the peritectic the molybdenum solidus is described by the equation

$$\frac{\ln x_{\text{Hf}}}{2890-T} = -2391T^{-1} + 4.333 - 7.436 \times 10^{-3}T + 1.240 \times 10^{-6}T^2$$

with an uncertainty in  $x_{\text{Hf}}$  of  $\pm 2 \times 10^{-5}(2890-T)$ . The molybdenum liquidus is given by

$$\frac{\ln x_{\text{Hf}}}{2890-T} = -6.107 - 1.084 \times 10^{-3}T + 2.90 \times 10^{-7}T^2$$

with an uncertainty in  $x_{\text{Hf}}$  of  $\pm 7 \times 10^{-5}(2890-T)$ .

The molybdenum solid solution in equilibrium with  $\text{HfMo}_2$  has the phase boundary

$$\ln x_{\text{Hf}} = -2200 T^{-1} + 0.6592 - 1.466 \times 10^{-3} T + 4.205 \times 10^{-7} T^2$$

with an uncertainty in  $x_{\text{Hf}}$  rising from  $\pm 0.01$  at  $2170^\circ\text{C}$  to a factor of 2 at  $1000^\circ\text{C}$ . The work of Taylor et al. [247] indicated a value of  $x_{\text{Hf}} = 0.17$  at  $900^\circ\text{C}$  which requires an unrealistically large negative entropy of solution. The molybdenum phase boundary of Fig. II-21 is in reasonable accord with the measurements of Alfintseva et al. [5] who found  $x_{\text{Hf}} = 0.095$  at  $1200^\circ\text{C}$  for the solubility of hafnium in molybdenum.

The  $\text{HfMo}_2$  Laves phase extends from the 2:1 composition to a maximum hafnium concentration of  $36\text{--}37.5$  at.% at  $1900 \pm 10^\circ\text{C}$  [82, 247]. The various crystal structures reported for  $\text{HfMo}_2$  are discussed in Part III.

Rudy [205] examined the solid-liquid equilibrium in the hafnium-rich region and found a shallow minimum in the bcc hafnium solid solution and a peritectic reaction isotherm  $\text{HfMo}_2$ -bcc Hf-liquid instead of the eutectic reaction proposed by Taylor et al. [247] and by Garg and Ackermann [82] on the basis of less detailed studies. The peritectic temperature is  $1900 \pm 10^\circ\text{C}$  [82, 205, 247]. The solubility limits at the peritectic are  $x_{\text{Hf}} = 0.56 \pm 0.02$  for the bcc hafnium solid solution and  $x_{\text{Hf}} = 0.59 \pm 0.02$  for the liquid solution [205, 247]. The minimum in the solid-liquid equilibrium is at  $x_{\text{Hf}} = 0.66 \pm 0.01$  and  $34^\circ\text{C}$  below the peritectic [205].

From  $x_{\text{Hf}} = 0.56$  to  $x_{\text{Hf}} = 1.00$  the solid-solution phase boundary follows the equation

$$T = 2500 - 2369x_{\text{Mo}} + 4114x_{\text{Mo}}^2 - 951x_{\text{Mo}}^3$$

with an uncertainty in  $T$  of  $\pm 10$  K. From  $x_{\text{Hf}} = 0.59$  to  $x_{\text{Hf}} = 1.00$  the boundary for liquid in equilibrium with hafnium is given by

$$T = 2500 - 798x_{\text{Mo}} - 4899x_{\text{Mo}}^2 + 11948x_{\text{Mo}}^3$$

with an uncertainty of  $\pm 10$  K.

Between  $1900$  and  $2170^\circ\text{C}$  the liquid phase limit in equilibrium with  $\text{HfMo}_2$  is represented by

$$T = 3762 - 8287x_{\text{Hf}} + 18770x_{\text{Hf}}^2 - 15746x_{\text{Hf}}^3$$

with an uncertainty rising from  $\pm 10$  K at  $1900^\circ\text{C}$  to  $\pm 40$  K at  $2170^\circ\text{C}$ .

## PART II. PHASE DIAGRAMS

From the eutectoid at  $1200 \pm 35^\circ\text{C}$  to  $1900^\circ\text{C}$  the limits for the bcc hafnium phase in equilibrium with  $\text{HfMo}_2$  is described by the equation

$$\ln x_{\text{Mo}} = -3935 T^{-1} + 3.757 - 2.407 \times 10^{-3} T + 5.22 \times 10^{-7} T^2$$

with an uncertainty in  $x_{\text{Mo}}$  of 0.02.

The boundaries for the bcc-hcp equilibrium in hafnium are taken from Taylor et al. [247]. To be consistent with the thermodynamic equations of Part I, the rather high value of  $\Delta H_{\text{tr}}/R = 1550$  K was used for the hcp-bcc transition. Since the experimental phase boundaries appear to have been carefully determined, this high value for  $\Delta H_{\text{tr}}/R$  may be necessitated, at least in part, by the approximate nature of the thermodynamic equations of Part I. It was considered most practical to use these simple equations which are consistent with the remainder of the phase diagram. From  $1200$  to  $1743 \pm 20^\circ\text{C}$  the limit of the bcc hafnium phase in equilibrium with hcp hafnium is given by

$$T = 952 - 276x_{\text{Hf}} + 1340x_{\text{Hf}}^2$$

with an uncertainty in  $T$  of  $\pm 20$  K at  $1743^\circ\text{C}$  and  $\pm 35$  K at  $1200^\circ\text{C}$ .

The hcp hafnium in equilibrium with bcc hafnium from  $1200$  to  $1743^\circ\text{C}$  is described by

$$\ln x_{\text{Mo}} = 3.315 \times 10^{-5} (2016-T) - 3.392 \times 10^{-8} (2016-T)^2$$

with an uncertainty in  $x_{\text{Mo}}$  of a factor of 2. The limits for the hcp hafnium phase in equilibrium with  $\text{HfMo}_2$  are given from  $480$  to  $1200^\circ\text{C}$  by the equation

$$\ln x_{\text{Mo}} = -5.32 \times 10^{-6} T + 7.30 \times 10^{-9} T^2$$

with an uncertainty in  $x_{\text{Mo}}$  of a factor of 2. The solubility of molybdenum in hcp hafnium falls to  $10^{-4}$  at  $480^\circ\text{C}$ , below which temperature it is a function of defect structure rather than thermodynamics.

### Mo-Hg: molybdenum-mercury (Fig. II-2)

Irvin and Russell [121] report a solubility of molybdenum in mercury at room temperature of  $2 \times 10^{-5}$  wt%. Strachan and Harris [242] and Bowersox and Leary [25] report a limit of less than 0.001 g molybdenum per litre of mercury at  $350^\circ\text{C}$  that excludes the value of Irvin and Russell. The molybdenum liquidus of Fig. II-2 between  $234$  and  $630$  K was calculated from the estimated thermodynamic data of Part I to be  $\ln x_{\text{Mo}} = 3 - 20000 T^{-1} \pm 5$ .

**Mo-Ho: molybdenum-holmium (Fig. II-1)**

No data were found. The estimated thermodynamic equations of Part I have been used to calculate the phase boundaries of Fig. II-1.

The monotectic is at  $2790 \pm 10$  K and  $x_{\text{Ho}} = 6 \times 10^{-3}$ ,  $0.08 \pm 0.02$  and  $0.65 \pm 0.06$ . The molybdenum liquidus and solidus above the monotectic temperature are represented by

$$x_{\text{Ho}} = 4.8 \times 10^{-4} (2890 - T) + 3.2 \times 10^{-6} (2890 - T)^2$$

with an uncertainty of  $2.0 \times 10^{-4}$  (2890-T) for the liquidus, and

$$x_{\text{Ho}} = 6 \times 10^{-5} (2890 - T)$$

with an uncertainty of a factor of 5 for the solidus.

The two-liquid region phase boundary between 2790 and 3000 K are represented by

$$x_{\text{Mo}} = 0.315 + 4 \times 10^{-4} (T - 2700) + 10^{-9} (T - 2700)^3$$

with an uncertainty rising from  $\pm 0.06$  at 2790 K to  $\pm 0.10$  at 3000 K, and

$$x_{\text{Ho}} = 0.075 + 10^{-4} (T - 2700)$$

with an uncertainty of  $\pm 0.02$ . The eutectic is determined to be at  $1705 \pm 10$  K and  $x_{\text{Ho}} = 0.97 \pm 0.01$ . The holmium liquidus and solidus are

$$x_{\text{Mo}} = 7 \times 10^{-4} (1743 - T)$$

with an uncertainty of a factor of 2 for the liquidus, and

$$x_{\text{Mo}} = 10^{-4} (1743 - T)$$

with an uncertainty of a factor of 5 for the solidus.

The equilibrium between solid molybdenum and liquid solution between 1705 and 2790 K determines the phase boundaries

$$x_{\text{Mo}} = 0.025 + 1.5 \times 10^{-4} (T - 1700) - 1.3 \times 10^{-7} (T - 1700)^2 + 2.47 \times 10^{-10} (T - 1700)^3$$

with an uncertainty of  $\pm 0.01$  at 1705 K, rising to  $\pm 0.06$  at 2790 K for the liquidus, and

$$x_{\text{Ho}} = 6 \times 10^{-4} + 2 \times 10^{-6} (T - 1700) + 5 \times 10^{-9} (T - 1700)^2 - 2 \times 10^{-12} (T - 1700)^3$$

for the solidus, with an uncertainty of a factor of 5.

**PART II. PHASE DIAGRAMS**

The solid-solution phase boundaries below 1710 K are calculated to be

$$x_{\text{Mo}} = 7 \times 10^{-5} + 5 \times 10^{-7} (T - 1000) + 2 \times 10^{-9} (T - 1000)^2 + 5 \times 10^{-12} (T - 1000)^3$$

and

$$x_{\text{Ho}} = -3.5 \times 10^{-7} (T - 1000) + 1.4 \times 10^{-9} (T - 1000)^2 \quad (1400 - 1710 \text{ K})$$

with uncertainties of a factor of 5. The solubility falls to  $x = 10^{-4}$  at 1310 K for holmium in molybdenum and at 1050 K for molybdenum in holmium. Below these temperatures the solubilities are defect-controlled.

**Mo-I: molybdenum-iodine (Fig. II-22)**

The phase diagram was calculated from the thermodynamic values of Part I. The crystal structure data for  $\alpha\text{MoI}_2$  (oC72) and  $\text{MoI}_3$  (oP16) are reviewed in Part III. Glicksman and Walton [92] have prepared a binuclear  $\beta\text{MoI}_2$ , in contrast to the hexanuclear  $\alpha\text{MoI}_2$ . It is assumed here to be unstable with respect to the  $\alpha$ -phase. Guichard [104] has reported the preparation of  $\text{MoI}_4$ . However, it was not pure and Lewis et al. [161] could prepare only  $\text{MoI}_3$  upon heating molybdenum with excess iodine in a sealed tube to 300°C.  $\text{MoI}_4$  was assigned an enthalpy of formation corresponding to stability only up to 20°C.  $\text{MoI}_3(s)$  is calculated to decompose to  $\text{MoI}(s)$  and 1 atm  $\text{I}_2(g)$  at 355 ± 50°C.  $\text{MoI}_2(s)$  is calculated to decompose to  $\text{Mo}(s)$  and vapour consisting of 0.63 atm  $\text{I}_2$  and 0.37 atm  $\text{I}$  at 1023 ± 70°C. The partial pressures of  $\text{MoI}_4$ ,  $\text{MoI}_3$ ,  $\text{MoI}_2$  and  $\text{MoI}$  gases are calculated to total  $10^{-5}$  atm, in agreement with Schäfer et al. [220]. Even for molybdenum metal in equilibrium with 1 atm iodine vapour at 2000 K, the calculated partial pressure of  $\text{MoI}_2$  is only  $10^{-4}$  atm, and for the other molybdenum species it is even lower. The solid solubilities of molybdenum and iodine in one another are believed to be defect-controlled.

**Mo-In: molybdenum-indium (Fig. II-2)**

Bruckhart et al. [37] report 0.025 at.% indium in molybdenum to be single phase at an undesignated temperature. Dieva [57] and Yatsenko and Dieva [268] measured the solubility of molybdenum in liquid indium between 600 and 1240 K. The molybdenum liquidus of Fig. II-2 is represented by

$$T = \frac{5285 + 4100 x_{\text{In}}^2}{1.86 - 0.41 x_{\text{In}}^2 - \ln(1 - x_{\text{In}})} \pm 30 \text{ K} \quad (430 - 2365 \text{ K})$$

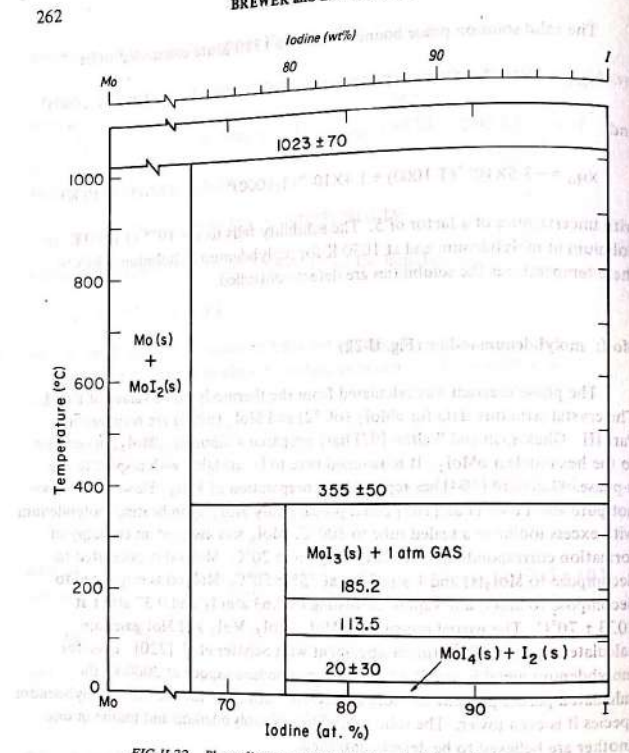


FIG.II-22. Phase diagram of the system molybdenum-iodine.

$x_{\text{Mo}}$  varies from  $10^{-9}$  at 430 K to  $3.6 \times 10^{-4}$  at 1000 K to 0.14 at 2365 K where the liquid is in equilibrium with 1 atm gas. The molybdenum solidus of Fig II-2 is represented by

$$\ln x_{\text{In}} = -1.1 - 14500 T^{-1} \pm 1 \quad (1400-2365 \text{ K})$$

At 2365 K,  $x_{\text{In}}$  in the solid molybdenum is calculated to be  $7 \times 10^{-4}$ . Below 1400 K, the calculated solubility is smaller than the quenched defect concentration and is no longer fixed by temperature alone.

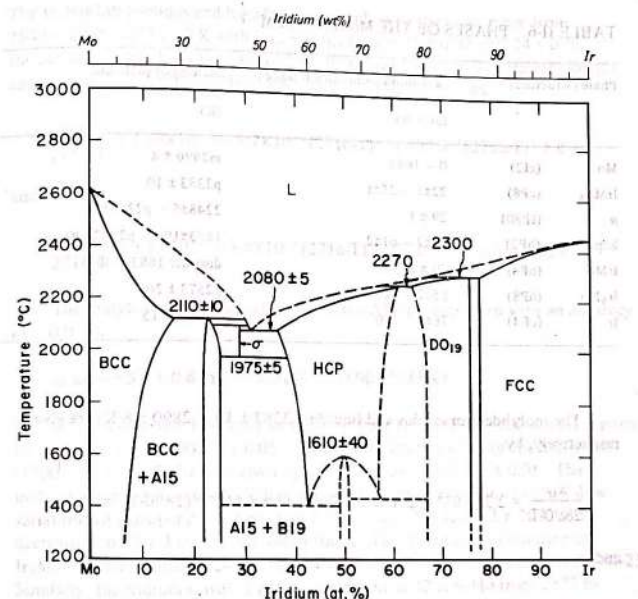


FIG.II-23. Phase diagram of the system molybdenum-iridium.

## Mo-Ir: molybdenum-iridium (Fig. II-23)

Knapton [145] has reviewed the literature and has presented the diagram shown in Fig. II-23. The eutectic liquid at  $2080 \pm 15^\circ\text{C}$  with  $31 \pm 1$  at.% Ir is saturated by the  $\sigma$ -phase with  $29 \pm 1$  at.% Ir and the hcp phase with  $37 \pm 2$  at.% Ir. The  $\text{IrMo}_3$  peritectic liquid at  $2110 \pm 10^\circ\text{C}$  contains  $30 \pm 1$  at.% Ir, and at the  $2270 \pm 20^\circ\text{C}$  peritectic of the hcp phase the liquid contains  $58 \pm 2$  at.% Ir. The liquid at the  $\text{Ir}_3\text{Mo}$  ( $\text{D}0_{19}$ , hP8) peritectic contains  $68 \pm 2$  at.% Ir. The crystal structures of the solid phases are reviewed in Part III. The composition and temperature ranges are given in Table II-6.

TABLE II-6. PHASES OF THE Mo-Ir SYSTEM

Phase (structure)	Maximum composition range (at.% Ir)	Melting or peritectic temperature (K)
Mo (d2)	0 - 16±2	m2890 ± 8
Ir <sub>3</sub> Mo <sub>3</sub> (cP8)	22±1 - 25±1	p2383 ± 10
$\alpha$ (fP30)	29 ± 1	2248±5 - p2368±10
hcp (hP2)	37±2 - 61±2	1673±100 - p2543±20
IrMo (oP4)	50 ± 2	disorder 1883 ± 40
Ir <sub>3</sub> Mo (hP8)	65±2 - 76±1	p2573 ± 20
Ir (cF4)	78±1 - 100	m2716 ± 15

The molybdenum solidus and liquidus ( $2383 \pm 10$  -  $2890 \pm 8$  K) are given, respectively, by

$$\frac{x_{\text{Ir}}}{2890-T} = 2.3 \times 10^{-4} - 2.4 \times 10^{-7}(2890-T) + 8 \times 10^{-10}(2890-T)^2 \pm 10\%$$

and

$$\frac{x_{\text{Ir}}}{2890-T} = 8.1 \times 10^{-4} - 2.4 \times 10^{-7}(2890-T) - 4 \times 10^{-10}(2890-T)^2 \pm 15\%$$

The A15-liquidus ( $2368 \pm 10$  -  $2383 \pm 10$  K) extends only from  $x_{\text{Ir}} = 0.295$  to  $0.30 \pm 0.01$ . The  $\alpha$ -liquidus ( $2353 \pm 15$  -  $2368 \pm 10$  K) extends from  $0.30$  to  $0.31 \pm 0.01$ . The hcp solidus and liquidus ( $2353 \pm 15$  -  $2543 \pm 20$  K) are given, respectively, by

$$\begin{aligned} x_{\text{Mo}} &= 0.39 + 1.66 \times 10^{-3}(2543-T) - 1.5 \times 10^{-6}(2543-T)^2 \\ &\quad - 3 \times 10^{-9}(2543-T)^3 \pm 0.02 \end{aligned}$$

and

$$\begin{aligned} x_{\text{Mo}} &= 0.422 + 2.96 \times 10^{-3}(2543-T) - 1.37 \times 10^{-5}(2543-T)^2 \\ &\quad + 2.9 \times 10^{-8}(2543-T)^3 \pm 0.03 \end{aligned}$$

## PART II. PHASE DIAGRAMS

The Ir<sub>3</sub>Mo(hP8) solidus and liquidus extend only over the small range from  $2543 \pm 20$  to  $2573 \pm 20$  K with  $x_{\text{Mo}}$  varying from  $0.35 \pm 0.02$  to  $0.24 \pm 0.01$  for the solidus and from  $0.42$  to  $0.32 \pm 0.03$  for the liquidus. The iridium solidus and liquidus ( $2573 \pm 20$  -  $2716 \pm 15$  K) are given, respectively, by

$$\frac{x_{\text{Mo}}}{2716-T} = 2.33 \times 10^{-3} - 7.7 \times 10^{-6}(2716-T) + 1.6 \times 10^{-8}(2716-T)^2 \pm 8\%$$

and

$$\frac{x_{\text{Mo}}}{2716-T} = 3.1 \times 10^{-3} - 7.4 \times 10^{-6}(2716-T) + 9 \times 10^{-9}(2716-T)^2 \pm 10\%$$

The molybdenum solvus saturated by the A15-phase is given with an accuracy of  $\pm 0.02$  by

$$\ln x_{\text{Ir}} = -5.9 + 0.8 \ln T - 5380 T^{-1} \quad (1600-2383 \text{ K})$$

The molybdenum-rich boundary of the hcp phase ( $1673 \pm 100$  -  $2353 \pm 5$  K) is given by  $\ln x_{\text{Ir}} = -1.37 + 900 T^{-1} \pm 0.05$ . The iridium-rich boundary of the hcp phase ( $1700 \pm 100$  -  $2543 \pm 20$  K) is given by  $\ln x_{\text{Ir}} = -0.38 - 330 T^{-1} \pm 0.05$ . The molybdenum-rich boundary of the (D<sub>0.19</sub>)Ir<sub>3</sub>Mo phase (hP8) shows only a slow variation with temperature starting with  $35 \pm 2$  at.% Mo at  $2543 \pm 20$  K and decreasing to  $33 \pm 3$  at.% Mo around 1700 K. The iridium-rich boundary of Ir<sub>3</sub>Mo is given as close to 24 at.% Mo over the entire temperature range of Fig. II-23. Similarly, the iridium solvus is shown as constant at 22 at.% Mo from 2573 to below 1700 K, but an equilibrated system must surely show a reduction in molybdenum content at the lower temperatures.

Mo-K: molybdenum-potassium (Fig. II-2)

Several studies of the solubility of molybdenum in liquid potassium have been made [54, 65, 166, 237]. The apparent solubilities found by the various investigators are functions of the carbon, nitrogen and oxygen impurity levels. The two determinations [65, 237] that have appeared since Anthropic [11] surveyed the literature in 1967 do not change his evaluation of the data of Cleary et al. [54] as being the most reliable. These investigators found the solubility of molybdenum in liquid potassium to be  $x_{\text{Mo}} < 8.2 \times 10^{-8}$  up to 1478 K. The thermodynamic equations estimated in Part I have been used to calculate phase boundaries for this system in agreement with Ref. [54]. Along the molybdenum liquidus,

$$\ln x_{\text{Mo}} = -33870 T^{-3} + 2.21$$

The solubility of molybdenum in potassium rises from  $x_{Mo} = 10^{-43}$  at 336 K to  $x_{Mo} = 1.4 \times 10^{-9}$  at 1500 K, with an uncertainty of a factor of 5. The solubility of potassium in molybdenum is defect-controlled.

#### Mo-Kr: molybdenum-krypton (Fig. II-4)

No experimental data were found; see Mo-Ar for details of the calculation of Fig. II-4. The order of magnitude of the mole fraction of krypton in liquid molybdenum at 2890 K saturated with 1 atm gas is calculated to be  $10^{-17}$ .

#### Mo-La: molybdenum-lanthanum (Fig. II-1)

Savitskij et al. [213] determined the solubility of lanthanum in solid molybdenum as less than 0.07 at.% at an unspecified temperature. No other data were found. The estimated thermodynamic functions of Part I have been used to calculate the phase boundaries of Fig. II-1.

The monotetic temperature was calculated to be  $2820 \pm 10$  K, with  $x_{La} = 0.0013$ ,  $0.04 \pm 0.01$  and  $0.79 \pm 0.04$ . Above this temperature the molybdenum liquidus and solidus are calculated to be

$$x_{La} = 5.57 \times 10^{-4}(2890-T) + 4.08 \times 10^{-7}(2890-T)^2$$

with an uncertainty of  $\pm 1.4 \times 10^{-4}(2890-T)$  for the liquidus, and

$$x_{La} = 3.4 \times 10^{-5}(2890-T) - 2.1 \times 10^{-7}(2890-T)^2$$

with an uncertainty of a factor of 5 for the solidus. The eutectic is calculated to be at 1193 K and  $x_{Mo} = 9 \times 10^{-4}$ .

The two-liquid phase boundaries from 2820 to 3120 K are given by

$$x_{Mo} = 0.21 + 2.1 \times 10^{-4}(T-2800) - 1.2 \times 10^{-7}(T-2800)^2 + 3 \times 10^{-10}(T-2800)^3$$

and

$$x_{La} = 0.040 + 5.6 \times 10^{-5}(T-2800) + 5 \times 10^{-8}(T-2800)^2$$

with an uncertainty in  $x_{Mo}$  of  $\pm 0.04$  and an uncertainty in  $x_{La}$  of  $\pm 0.01$ . Between 1193 and 2820 K the molybdenum solidus and liquidus are calculated to be

$$x_{La} = -8.672 \times 10^{-4} + 1.956 \times 10^{-6}T - 1.48 \times 10^{-9}T^2 + 3.77 \times 10^{-13}T^3$$

with an uncertainty of a factor of 5 for the solidus, and

$$x_{Mo} = -8.59 \times 10^{-2} + 1.925 \times 10^{-4}T - 1.51 \times 10^{-7}T^2 + 4.245 \times 10^{-11}T^3$$

with an uncertainty of  $\pm 0.004$  for the liquidus. The solidus falls to  $x_{La} = 10^{-4}$  at 1900 K, below which temperature the solubility is defect-controlled.

The solubility of molybdenum in La(s) is calculated to be below  $10^{-4}$ , with an uncertainty of a factor of 5.

#### Mo-Li: molybdenum-lithium (Fig. II-2)

Measurements of the solubility of molybdenum in liquid lithium [38, 54, 160] were reviewed by Anthropic [11] in 1967. Subsequent studies [41, 64, 65] do not alter his conclusion that the most reliable solubility value is that of Cleary et al. [54] who found the atomic fraction of molybdenum in Li(l)  $\leq 7.3 \times 10^{-8}$  at 1590 K. The estimated thermodynamic equations of Part I have been used to calculate the molybdenum liquidus from 454 to 1597 K:

$$\ln x_{Mo} = -29770T^{-1} + 2.21$$

The solubility of molybdenum in the liquid rises from  $x_{Mo} = 10^{-28}$  at 454 K to  $x_{Mo} = 7 \times 10^{-8}$  at 1597 K, with an uncertainty of a factor of 5. The solubility of lithium in molybdenum is defect-controlled.

#### Mo-Lr: molybdenum-lawrencium (Fig. II-24)

No data were found. The estimated thermodynamic equations of Part I have been used to calculate the phase boundaries. The eutectic is calculated to be at  $1660 \pm 40$  K and  $x_{Lr} = 0.88 \pm 0.03$ . Above 1660 K the lawrencium liquidus and solidus are given by

$$x_{Mo} = 3.96 \times 10^{-4}(1900-T) + 5.21 \times 10^{-7}(1900-T)^2$$

with an uncertainty of  $\pm 0.02$  for the liquidus, and

$$x_{Mo} = 2.2 \times 10^{-4}(1900-T) + 3.02 \times 10^{-7}(1900-T)^2$$

with an uncertainty of a factor of 5 for the solidus.

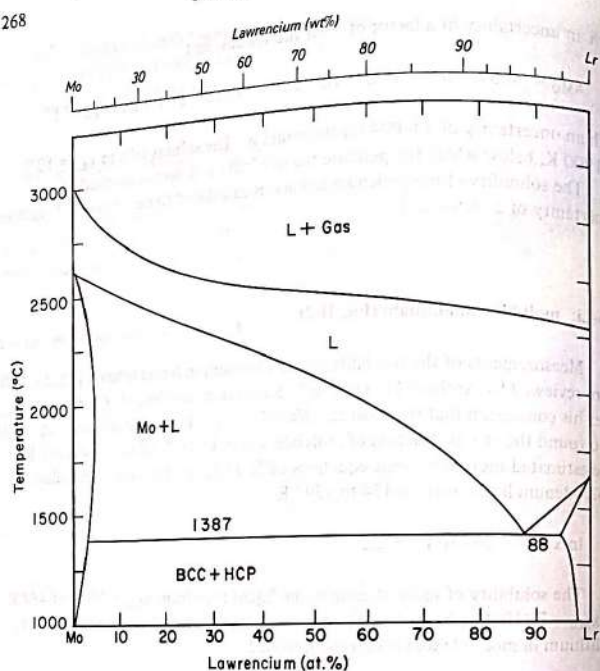


FIG.II-24. Phase diagram of the system molybdenum-lawrencium.

Between 1660 and 2890 K the molybdenum liquidus and solidus are calculated to be

$$x_{Lr} = 9.3 \times 10^{-4} (2890-T) + 7 \times 10^{-8} (2890-T)^2 - 2 \times 10^{-10} (2890-T)^3$$

with an uncertainty of  $\pm 0.03$  at 1660 K, rising to  $\pm 0.04$  at 2570 K, for the liquidus, and

$$x_{Lr} = 1.4 \times 10^{-4} (2890-T) - 1.4 \times 10^{-7} (2890-T)^2 + 3.4 \times 10^{-11} (2890-T)^3$$

with an uncertainty of a factor of 5 for the solidus.

Below 1660 K the solid-solution phase boundaries are calculated to be

$$x_{Lr} = 3 \times 10^{-9} (T-600)^2 + 2 \times 10^{-11} (T-600)^3$$

and

$$x_{Mo} = 10^{-4} + 5 \times 10^{-7} (T-600) + 10^{-8} (T-600)^2 + 3 \times 10^{-11} (T-600)^3$$

with an uncertainty of a factor of 5. The solubility of molybdenum in lawrencium falls to  $x_{Mo} = 10^{-4}$  at 600 K and that of lawrencium in molybdenum falls to  $x_{Lr} = 10^{-4}$  at 730 K. Below these temperatures the solubilities are defect-controlled.

#### Mo-Lu: molybdenum-lutetium (Fig. II-25)

No data were found. The estimated thermodynamic equations of Part I have been used to calculate the phase boundaries of Fig. II-25. The eutectic is at  $1818 \pm 30$  K,  $x_{Lu} = 0.91 \pm 0.03$ . The molybdenum liquidus between 1818 and 2890 K is calculated to be

$$T = \frac{4996 + 7750x_{Lu}^2 - 4600x_{Lu}^3}{1.729 + 0.3x_{Lu}^2 - \ln(1-x_{Lu})}$$

with an uncertainty of  $\pm 150^\circ$  at  $x_{Lu} = 0.91$  and  $\pm 70^\circ$  at  $x_{Lu} = 0.54$ . The corresponding solidus is given by

$$x_{Lu} = 7 \times 10^{-5} (2890-T) - 1.2 \times 10^{-7} (2890-T)^2 + 5.6 \times 10^{-11} (2890-T)^3$$

with an uncertainty of a factor of 5.

The lutetium liquidus above 1818 K is calculated to be

$$x_{Mo} = 5.88 \times 10^{-4} (1936-T) + 1.39 \times 10^{-6} (1936-T)^2$$

with an uncertainty of  $\pm 0.01$ . The lutetium solidus in this temperature range is

$$x_{Mo} = 1.2 \times 10^{-4} (1936-T)$$

with an uncertainty of a factor of 5.

Below 1818 K the solid-solution phase boundaries are calculated to be

$$x_{Mo} = 10^{-4} + 10^{-6} (T-850) + 4 \times 10^{-9} (T-850)^2 + 10^{-11} (T-850)^3$$

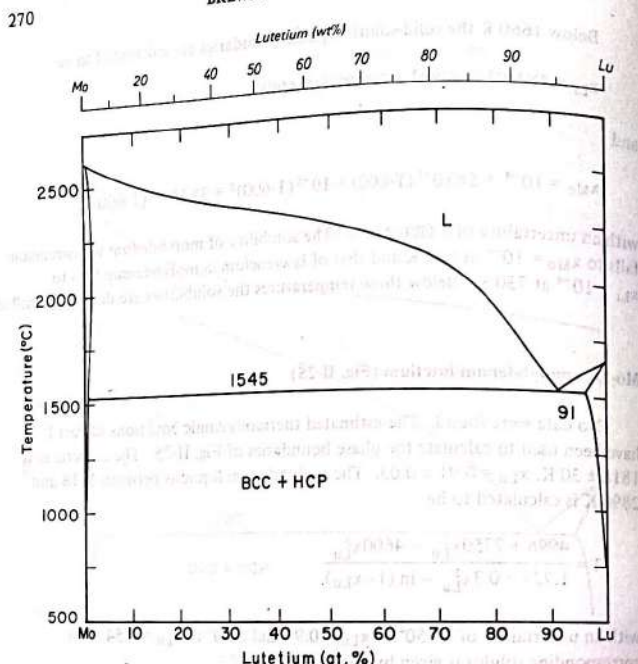


FIG.II-25. Phase diagram of the system molybdenum-lutetium.

and

$$x_{Lu} = 10^{-4} + 7 \times 10^{-7}(T-1000)^2 + 3.5 \times 10^{-9}(T-1000)^3 + 6 \times 10^{-12}(T-1000)^4$$

The solid solubilities, which are uncertain by a factor of 5, fall to  $10^{-4}$  at 1010 K for lutetium in molybdenum and at 850 K for molybdenum in lutetium.

#### Mo-Md: molybdenum-mendelevium (Fig. II-11)

No data were found. The estimated normal boiling point of  $900 \pm 50$  K is below the estimated melting point of 1100 K. At 900 K the solid solubilities are defect-controlled.

#### Mo-Mg: molybdenum-magnesium (Fig. II-2)

No data were found. The thermodynamic equations estimated in Part I have been used to calculate phase boundary conditions for the molybdenum-magnesium system. The molybdenum liquidus from 922 to 1400 K is calculated to be given by

$$\ln x_{Mo} = -27600 T^{-1} + 1.91$$

The solubility of molybdenum in the liquid rises from  $x_{Mo} = 10^{-12}$  at 922 K to  $x_{Mo} = 3 \times 10^{-8}$  at 1400 K, with an uncertainty of a factor of 5. The solid solubility of magnesium in molybdenum is less than the quenched defect concentration up to 1400 K. The solubility of molybdenum in solid magnesium is also defect-controlled.

#### Mo-Mn: molybdenum-manganese (Fig. II-26)

The results of early work by Eremenko and Zhel'vis [71] for 0–8 at.% Mo have been disproved by later work. Hellawell [115] established a maximum of 0.6 at.% Mo in  $\gamma$ Mn (cF4) at 1112°C, in equilibrium with  $\delta$ Mn (cI2) with 0.9 at.% Mo and  $\beta$ Mn (cP20) with 0.8 at.% Mo. The  $\delta$ Mn solidus and liquidus rose with temperature to 1255 and 1267°C, respectively, at 2.5 at.% Mo. The boundaries of the  $\delta$ Mn and  $\beta$ Mn two-phase region were very close together and decreased gradually with temperature to an extrapolated eutectoid decomposition of  $\delta$ Mn at  $1010 \pm 10$ °C and 2.5 at.% Mo. No data have been reported on the extension to higher temperatures of the molybdenum-rich  $\delta$ Mn boundary. At 800°C, Telegus et al. [249] report the maximum extent of  $\beta$ Mn at about 2 at.% Mo, but they find stabilization of  $\alpha$ Mn with a range of 4–14 at.% Mo.

The only well-characterized intermediate phase is the  $\sigma$ -phase (tP30) which has a narrow homogeneous range near 64 at.% Mn [55, 132]. Kasper et al. [132] report the  $\sigma$ -phase to be unstable below 1115°C, but Hellawell indicates that both  $\beta$ Mn and  $\delta$ Mn are in equilibrium with the  $\sigma$ -phase, which would place the decomposition temperature of the  $\sigma$ -phase below 1112°C. Another intermediate phase has been reported between 80 and 88 at.% Mn [55, 100] at 1000°C, but this is not stable at 1125°C. In Fig. II-26, this phase is shown as an extension of the  $\alpha$ Mn phase region reported by Telegus et al. at 800°C; they also report another intermediate phase between 50 and 60 at.% Mn at 800°C of uncharacterized structure. This may be a phase related to  $Mo_6Fe_7$  (hR39).

Pipitz and Kieffer [189] report that bcc Mo dissolves up to almost 30 at.% Mn at 1800°C and more than 15 at.% Mn at 1000°C. Telegus et al. [249] report around 16 at.% Mn in Mo at 800°C.

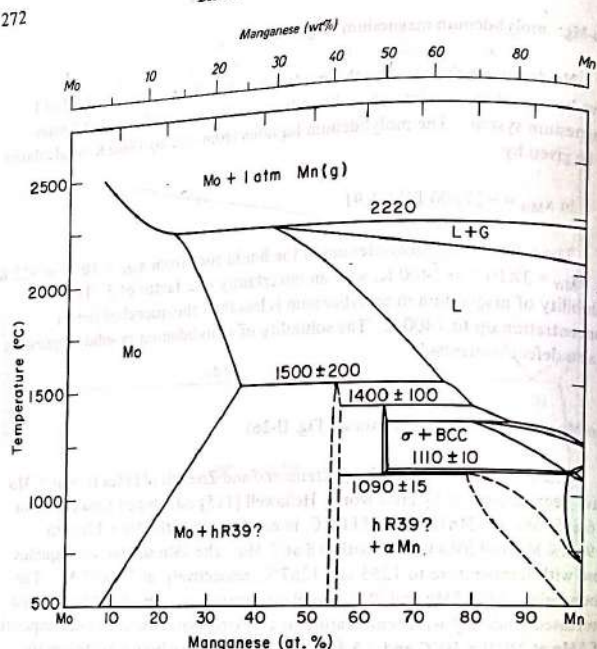


FIG.II-26. Phase diagram of the system molybdenum-manganese.

The liquid boundary saturated by 1 atm Mn gas over the interval  $x_{\text{Mn}} = 0.42 - 1.0$  and at  $T = 2335 - 2490$  K is given by

$$T = \frac{27000 + 2000x_{\text{Mn}}^2 - 1000x_{\text{Mn}}^3}{\ln x_{\text{Mn}} + 11.563 + 1.25x_{\text{Mn}}^2 - 0.5x_{\text{Mn}}^3} \pm 30 \text{ K}$$

The bcc solid boundary saturated by 1 atm Mn gas over the interval  $x_{\text{Mn}} = 0.065 - 0.22$  and at  $T = 2490 - 3880$  K is given by

$$T = \frac{28450 - 3000x_{\text{Mn}}^2 - 3900x_{\text{Mn}}^3}{\ln x_{\text{Mn}} + 12.52 - x_{\text{Mn}}^2 - x_{\text{Mn}}^3} \pm 100 \text{ K}$$

## PART II. PHASE DIAGRAMS

TABLE II-7. PHASES OF THE Mo-Mn SYSTEM

Phase (structure)	Maximum composition range (at.% Mn)	Melting, peritectic or peritectoid temperature (K)
Mo (cI2)	0-30	2890 ± 8
$\mu?$ (hR39?)	55 ± 5?	p1770 ± 200
$\sigma$ (tP30)	64 ± 1	1365 ± 15 - 1670 ± 100
$\delta\text{Mn}$ (cI2)	80 ± 10 - 100	1383 ± 10 - 1600 ± 100
$\gamma\text{Mn}$ (cF4)	99.4 - 100	1360 ± 10 - 1410 ± 5
$\beta\text{Mn}$ (cP20)	97.4 - 100	980 ± 20 - p1383 ± 10
$\alpha\text{Mn}$ (cI8)	83 ± 3 - 100	p1370 ± 50

The composition and temperature ranges of the phases are given in Table II-7. The molybdenum solidus is given by

$$x_{\text{Mn}} = 0.38 - 2.3 \times 10^{-4}(T-1700) + 2.2 \times 10^{-7}(T-1700)^2 - 2.2 \times 10^{-10}(T-1700)^3 \pm 0.05 \quad (1773-2490 \text{ K})$$

The molybdenum liquidus is given by

$$x_{\text{Mn}} = 0.77 - 3 \times 10^{-4}(T-1700) - 2 \times 10^{-10}(T-1700)^3 \pm 0.1 \quad (1773-2490 \text{ K})$$

The molybdenum solvus saturated by  $\text{MoMn}_{1.2}(\text{hR39?})$  is given by

$$\ln x_{\text{Mn}} = -2200 T^{-1} + 0.22 \pm 0.05 \quad (900-1773 \text{ K})$$

The extension of  $\alpha\text{Mn}$  up to 1370 K and 21 at.% Mo which is predicted in Fig. II-26 can be represented by

$$x_{\text{Mo}} = 0.105 + 5.3 \times 10^{-4}(T-1000) - 6.7 \times 10^{-7}(T-1000)^2$$

for the boundary saturated by  $\text{MoNi}_{1.2}(\text{hR39?})$ , and by

$$x_{\text{Mo}} = 0.044 - 1.8 \times 10^{-4}(T-1000) + 1.7 \times 10^{-6}(T-1000)^2$$

for the boundary saturated by  $\beta\text{Mn}$ .

If the interpretation is correct, the boundaries should be accurate to  $\pm 0.03$  between 1000 and 1370 K. The  $\beta$ Mn boundary saturated by  $\alpha$ Mn is given by

$$x_{\text{Mo}} = 3.1 \times 10^{-4} (T-980) - 10^{-6} (T-980)^2 + 9.3 \times 10^{-10} (T-980)^3 \pm 0.01$$

$$(980-1370 \text{ K})$$

$\beta$ Mn is saturated by the  $\sigma$ -phase over a very small interval between 1370 and 1383 K, with a composition of  $x_{\text{Mo}} = 0.024 \pm 0.005$ . As discussed earlier, over a very small temperature interval where  $\beta$ Mn is saturated by  $\delta$ Mn, the boundary varies from  $x_{\text{Mo}} = 0.024$  at 1383 K to 0.008 at 1385 K where it is in equilibrium with  $\gamma$ Mn. The boundaries of  $\delta$ Mn above 2.5 at.% Mo are rather uncertain. As shown in Fig. II-26, the boundary saturated by the  $\sigma$ -phase varies from 2.5 at.% Mo at 1383 K to 20 at.% Mo at  $1600 \pm 100$  K, with the uncertainty in molybdenum composition increasing from  $\pm 0.5$  at.% to  $\pm 10$  at.%. Similarly, the boundary saturated by liquid varies from  $2.5 \pm 0.5$  at.% Mo at 1528 K to  $14 \pm 8$  at.% Mo at  $1600 \pm 100$  K.

#### Mo-N: molybdenum-nitrogen (Fig. II-27)

Part I reviews the various measurements that were used to evaluate the thermodynamic properties of the various phase regions. These thermodynamic properties were used to calculate the 850 atm phase diagram shown in Fig. II-27. Equations for the boundaries at 1 atm and 850 atm are given below.

The various reported molybdenum nitride phases are listed in Part III. The low-temperature tetragonal  $\beta$ Mo<sub>2</sub>N and the high-temperature cubic  $\gamma$ Mo<sub>2</sub>N are closely related and become indistinguishable at high nitrogen content [73, 122]. Figure II-27 follows Ettmayer [73] in showing a miscibility gap between the  $\beta$ - and  $\gamma$ -phases for stoichiometric compositions from 850°C down to a critical point around 400°C and 34.5 at.% N which has not been accurately fixed because of the slow rate of equilibration. The molybdenum-rich boundary is reported to extend from 28.7 at.% N at 1100°C to 27 at.% N in equilibrium with the eutectic liquid of 19 at.% N [122]. The calculations based on the thermodynamic treatment of Part I indicate the eutectic at  $1894 \pm 25^\circ\text{C}$  in equilibrium with 563  $\pm$  90 atm of N<sub>2</sub> gas and liquid with  $x_N = 0.20 \pm 0.01$ . The molybdenum solidus at the eutectic is calculated to be  $x_N = 0.011 \pm 0.002$ . The somewhat more rigorous thermodynamic treatment of the data used here yields the eutectic temperature 34° higher, the nitrogen pressure 107 atm lower and the molybdenum solidus point 2% higher than calculated by Jahn and Ettmayer [122].

For molybdenum solid saturated with nitrogen gas at 1 atm,  $\ln x_N = -8900T^{-1} + 0.7 \ln T - 9.0$  represents the data reviewed in Part I. Between 1600 and 2500 K, the uncertainty in  $x_N$  is 5%, increasing to 10% between 1400 and 1600 K and

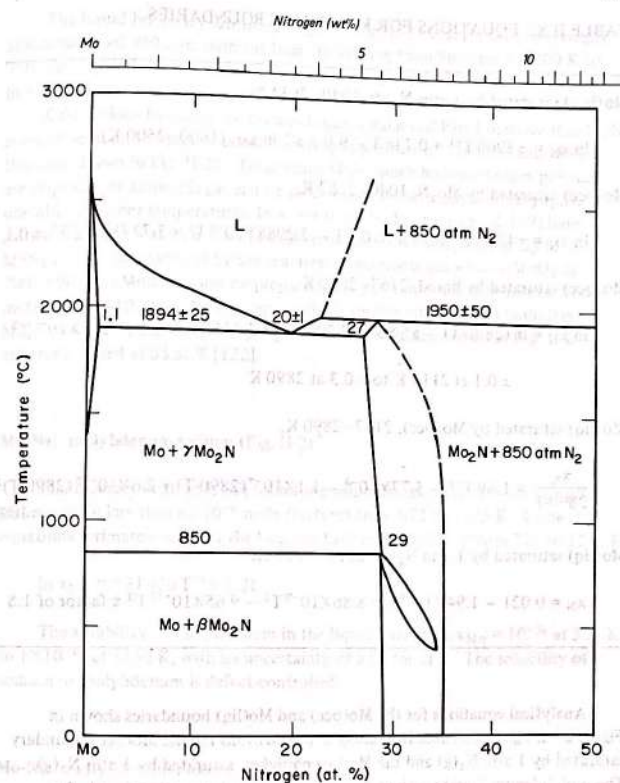


FIG. II-27. Phase diagram of the system molybdenum-nitrogen.

between 2500 and 2634 K, where the molybdenum solid phase with  $x_N = 0.001$  is in equilibrium with 1 atm N<sub>2</sub> and the liquid phase has  $x_N = 0.01$ . The values calculated below 1400 K are uncertain by 20%, down to 1040 K where molybdenum solid with  $x_N = 3 \times 10^{-6}$  is calculated to be in equilibrium with 1 atm N<sub>2</sub> gas and  $\beta$ Mo<sub>2</sub>N.

TABLE II-8. EQUATIONS FOR Mo-N PHASE BOUNDARIES

Mo(bcc) saturated by 1 atm N <sub>2</sub> (g), 1040–2634 K,
$\ln x_N = -8900 T^{-1} + 0.7 \ln T - 9.0 \pm 5\% \text{ in } x_N \quad (1600-2500 \text{ K})$
Mo(bcc) saturated by Mo <sub>2</sub> N, 1040–2167 K,
$\ln x_N = -45.931 + 5.1466 \times 10^{-2} T - 2.2968 \times 10^{-5} T^2 + 3.717 \times 10^{-9} T^3 \pm 0.1$
Mo(bcc) saturated by liquid, 2167–2890 K,
$\ln x_N = \ln(2890-T) - 51.56 + 22.700 T^{-1} + 2.435 \times 10^{-2} T - 4.812 \times 10^{-6} T^2$ $\pm 0.1 \text{ at } 2110 \text{ K to } \pm 0.3 \text{ at } 2890 \text{ K}$
Mo(liq) saturated by Mo(bcc), 2167–2890 K,
$\frac{x_N}{2890-T} = 1.69 T^{-1} - 5.77 \times 10^{-4} - 1.1 \times 10^{-7}(2890-T) + 2.6 \times 10^{-10}(2890-T)^2$ $\pm 10\%$
Mo(liq) saturated by 1 atm N <sub>2</sub> (g), 2634–4300 K,
$x_N = 0.021 - 1.94 \times 10^{-5} T + 8.86 \times 10^{-9} T^2 - 9.65 \times 10^{-13} T^3 \pm \text{factor of 1.8}$

Analytical equations for the Mo(bcc) and Mo(liq) boundaries shown in Fig. II-27 are given in Table II-8, along with equations for the Mo(bcc) boundary saturated by 1 atm N<sub>2</sub>(g) and the Mo(liq) boundary saturated by 1 atm N<sub>2</sub>(g). The molybdenum liquidus values calculated here can be compared with the calculated values of Jahn and Ettmayer [122] who assumed ideal solution behaviour and a different entropy of solution. Their values are within 10% of those given here near the eutectic, but become steadily smaller with increasing temperature. At temperatures of 2700–2800 K, their values are lower by a factor of two. The equation for the liquid-gas boundary at 1 atm, which has an accuracy of better than a factor of two, is given only from 2634 K, where contact is made with the molybdenum liquidus, to 4300 K, where x<sub>N</sub> reaches a maximum of 0.025 and then decreases at higher temperatures as molybdenum vapour contributes increasingly to the pressure.

## PART II. PHASE DIAGRAMS

The liquid boundary saturated by gas in Fig. II-27 is given for nitrogen gas at a pressure of 850 atm, with the fugacity varying from 980 atm at 2300 K to 950 atm at 2800 K. The liquid boundaries for x<sub>N</sub> > 0.2 are uncertain by 50% in x or 50–100 K in T.

Calculations based on the thermodynamic values of Part I indicate that MoN is unstable at all temperatures, with a nitrogen pressure of 850 atm, and MoN is thus not shown in Fig. II-27. To produce MoN, much higher nitrogen pressures are required, or ammonia gas can be used, which is thermodynamically quite unstable at higher temperatures. In a recent study, Bliznakov et al. [19] have shown that δMoN as well as metastable portions of the Mo<sub>2</sub>N range up to MoN<sub>0.68</sub> can be produced by the reaction of ammonia gas with H<sub>2</sub>MoO<sub>4</sub> at 700–800°C. δMoN can also be prepared [122] by ammonia with molybdenum metal at 700–1000°C. No data are available on the nitrogen-rich boundary of Mo<sub>2</sub>N in equilibrium with nitrogen gas, and the boundary shown in Fig. II-27 is arbitrarily fixed at 35 at.% [122].

## Mo-Na: molybdenum-sodium (Fig. II-2)

Eichelberger et al. [64, 65] found the solubility of molybdenum in liquid sodium to be less than 6 × 10<sup>-6</sup> mole fractions from 973 to 1273 K. Using the equations estimated in Part I the liquidus has been calculated from 371 to 1156 K.

$$\ln x_{Mo} = -31420 T^{-1} + 2.21$$

The solubility of molybdenum in the liquid rises from x<sub>Mo</sub> = 10<sup>-36</sup> at 371 K to 1 × 10<sup>-11</sup> at 1156 K, with an uncertainty of a factor of 5. The solubility of sodium in molybdenum is defect-controlled.

## Mo-Nb: molybdenum-niobium (Fig. II-28)

Hultgren et al. [119] reviewed the phase diagram literature and selected the diagram given in Fig. II-28 from Rudy [205], who estimated the liquidus curve. Earlier diagrams showing a minimum melting point were rejected by Hultgren et al. Calculations based on the thermodynamic data of Part I indicate that the liquidus curve should be closer to the solidus than shown in Fig. II-28. The solidus curve is given by

$$\frac{x_{Nb}}{2890-T} = 4.45 \times 10^{-3} - 1.38 \times 10^{-5}(2890-T) + 2.1 \times 10^{-7}(2890-T)^2$$

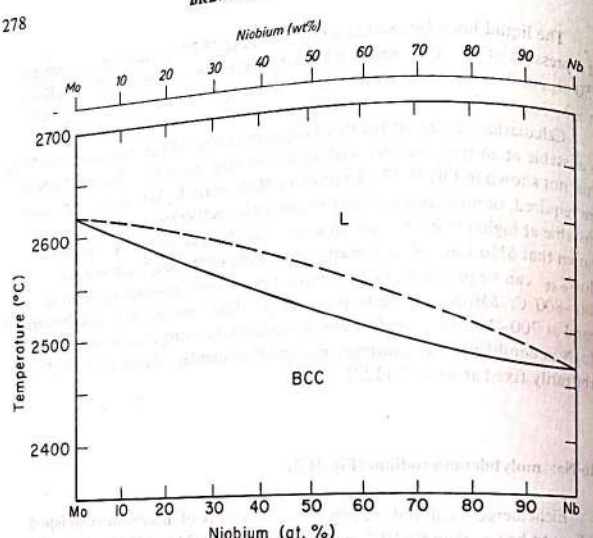


FIG.II-28. Phase diagram of the system molybdenum-niobium.

with an uncertainty in  $T$  of  $\pm 10$  K. The liquidus curve

$$\frac{x_{Nb}}{2890-T} = 4.28 \times 10^{-3} + 3.54 \times 10^{-5}(2890-T) - 1.2 \times 10^{-7}(2890-T)^2$$

with an uncertainty in  $T$  of  $\pm 20$  K, which lies closer to the solidus, is recommended in preference to the liquidus of Fig. II-28.

#### Mo-Nd: molybdenum-neodymium (Fig. II-1)

Savitskij et al. [213] report the solubility of neodymium in molybdenum to be  $\geq 0.046$  at.% at an unspecified temperature. No other data were found. The estimated thermodynamic equations of Part I have been used to calculate the phase boundaries of Fig. II-1.

The monotectic is calculated to be at  $2820 \pm 10$  K,  $x_{Nd} = 3 \times 10^{-3}$ ,  $0.04 \pm 0.01$  and  $0.75 \pm 0.08$ . Above the monotectic the molybdenum liquidus and solidus are represented by

$$x_{Nd} = 5.6 \times 10^{-4}(2890-T) + 3 \times 10^{-7}(2890-T)^2$$

with an uncertainty of  $\pm 1.2 \times 10^{-4}(2890-T)$  for the liquidus, and

$$x_{Nd} = 4.8 \times 10^{-5}(2890-T)$$

with an uncertainty of a factor of 5 for the solidus.

The two-liquid phase boundaries between 2805 and 3000 K are calculated to be

$$x_{Nd} = 4.06 \times 10^{-2} + 5.7 \times 10^{-5}(T-2800) + 3 \times 10^{-8}(T-2800)^2$$

with an uncertainty of  $\pm 0.001$  for the molybdenum-rich liquid, and

$$x_{Mo} = 0.250 + 2.4 \times 10^{-4}(T-2800)$$

with an uncertainty of  $\pm 0.08$  for the neodymium-rich liquid.

From 1285 to 2805 K the phase boundaries are described by the equations

$$x_{Mo} = 2.93 \times 10^{-5}(T-1200) - 1.32 \times 10^{-8}(T-1200)^2 + 5.56 \times 10^{-11}(T-1200)^3$$

with an uncertainty of  $\pm 0.002$  at 1285 K, rising to  $\pm 0.08$  at 2805 K, for the liquidus, and

$$\ln x_{Nd} = -20.31 + 9.24 \times 10^{-3}T - 1.44 \times 10^{-6}T^2$$

for the solidus, with an uncertainty of a factor of 5. The solubility of neodymium in molybdenum falls to  $x_{Nd} = 10^{-4}$  at 1600 K, below which temperature it is less than the quenched defect concentration.

The solubility of molybdenum in solid neodymium is less than the quenched defect concentration.

The eutectic is calculated to be at 1285 K and  $x_{Mo} = (2.4 \pm 2.0) \times 10^{-3}$ .

#### Mo-Ne: molybdenum-neon (Fig. II-4)

No experimental data were found; see Mo-Ar for details of the calculation of Fig. II-4. The order of magnitude of the mole fraction of neon in liquid molybdenum at 2890 K, saturated with 1 atm gas, is calculated to be  $10^{-12}$ .

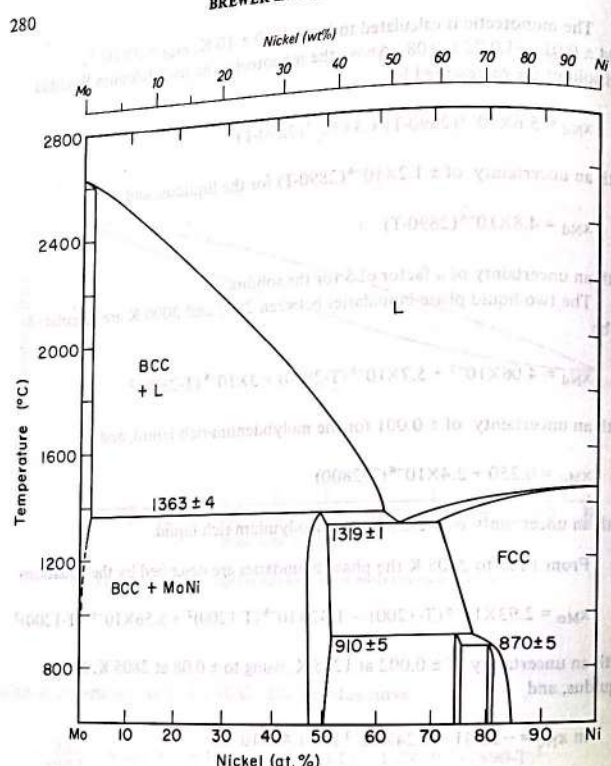


FIG. II-29. Phase diagram of the system molybdenum-nickel.

## Mo-Ni: molybdenum-nickel (Fig. II-29)

Casselton and Hume-Rothery [42] have reviewed earlier phase diagram studies and have added new data. Kurilo et al. [156] have presented metallographic evidence for the Mo-Ni eutectic at 64.2 at.% Ni, but the liquidus thermal arrest for 63.7 at.% Ni observed by Casselton and Hume-Rothery 14 degrees above the eutectic temperature of  $1318 \pm 4^\circ\text{C}$  would fix the eutectic liquid at  $65 \pm 0.5$  at.% Ni.

TABLE II-9. STABLE PHASES OF THE Mo-Ni SYSTEM

Phase (structure)	Maximum composition range (at.% Ni)	Melting, peritectic or peritectoid temperature (K)
Mo (cl2)	0-1.8	m2890 ± 8
MoNi (oP112)	47.5-52.3	p1635 ± 4
MoNi <sub>3</sub> (oP8)	75 ± 1	p1183 ± 5
MoNi <sub>4</sub> (tI10)	80.0-81.1	p1143 ± 5
Ni (cF4)	71.6-100	m1726 ± 4

The MoNi peritectic is at  $1363 \pm 4^\circ\text{C}$  and the peritectic liquid is at  $61.6 \pm 0.5$  at.% Ni. Heijwegen and Rieck [112] have confirmed the diagram between 800 and  $1295^\circ\text{C}$  and have established the solid phase boundaries somewhat more accurately. Other measurements [106, 253] also indicate that MoNi<sub>4</sub> undergoes an order-disorder transformation or a peritectoid reaction about 5 degrees lower than indicated by Casselton and Hume-Rothery.

Part III reviews the crystallographic data for the reported phases, including the three metastable phases MoNi<sub>2</sub>(oI6), MoNi<sub>3</sub>(tI8) and Mo<sub>3</sub>Ni<sub>1</sub>. The ordering reactions involving the metastable phases upon cooling the fcc nickel-rich phase are quite complicated. The extensive literature is reviewed in Part III and in two recent papers by Ruedl [211] and Van Tendeloo [253]. The properties of the stable solid phases are given in Table II-9.

The MoNi boundary saturated by nickel is given by

$$x_{\text{Ni}} = 0.515 + 9 \times 10^{-6}(T-1000) \pm 0.005 \quad (1183-1592 \text{ K})$$

The MoNi boundary saturated by molybdenum is given by

$$x_{\text{Ni}} = 0.4805 - 4.8 \times 10^{-6}(T-1000) \pm 0.005 \quad (1000-1636 \text{ K})$$

The nickel solvus saturated by MoNi<sub>4</sub> is given by

$$\ln x_{\text{Mo}} = -19.70 + 8080T^{-1} + 9.58 \times 10^{-3}T + 3 \times 10^{-11}T^3 \pm 0.04 \quad (800-1143 \text{ K})$$

The nickel solvus saturated by  $\text{MoNi}_3$  is given by

$$x_{\text{Mo}} = 0.303 - 4.2 \times 10^{-3}(T-1100) + 3.9 \times 10^{-5}(T-1100)^2 \pm 0.007$$

(1143–1183 K)

The nickel solvus saturated by  $\text{MoNi}$  is given by

$$x_{\text{Mo}} = 0.220 + 10^{-5}T(T-1100) + 2.5 \times 10^{-7}(T-1100)^2 \pm 0.006$$

(1183–1591 K)

The nickel solidus is given to  $\pm 0.01$  in  $x$  by

$$\frac{x_{\text{Mo}}}{1726-T} = 6.7 \times 10^{-3} - 7.5 \times 10^{-5}(1726-T) + 3.03 \times 10^{-7}(1726-T)^2$$

(1591–1726 K)

The nickel liquidus is given by

$$\frac{x_{\text{Mo}}}{1726-T} = 7.64 \times 10^{-3} - 7.9 \times 10^{-5}(1726-T) + 3.1 \times 10^{-7}(1726-T)^2 \pm 0.03 \text{ in } x_{\text{Mo}}$$

(1591–1726 K)

The  $\text{MoNi}$  liquidus extends only from 61.6 at.% Ni at  $1362^\circ\text{C}$  to 65 at.% Ni at  $1318^\circ\text{C}$ . The molybdenum solvus saturated by  $\text{MoNi}$  is given by

$$\ln x_{\text{Ni}} = -8.82 + 1180T^{-1} + 2.57 \times 10^{-3}T \pm 0.1 \quad (1100-1635 \text{ K})$$

Casselton and Hume-Rothery [42] show the molybdenum solidus to be essentially constant at 2 at.% Ni, up to  $2500^\circ\text{C}$ . The thermodynamic data selected in Part I indicate that the solidus reaches a maximum value of 2.1 at.% Ni between  $1500$  and  $1600^\circ\text{C}$  and then gradually drops to 1 at.% Ni at  $2350^\circ\text{C}$ . The solidus mole fraction is given with an uncertainty of  $\pm 0.004$  by

$$\frac{\ln x_{\text{Ni}}}{2890-T} = -3920T^{-1} - 7.07 - 1.5 \times 10^{-3}T + 3.4 \times 10^{-7}T^2 \quad (1635-2890 \text{ K})$$

The molybdenum liquidus mole fraction is given with an uncertainty of  $\pm 0.02$  by

$$\frac{x_{\text{Ni}}}{2890-T} = 1.487 T^{-1} - 6.5 \times 10^{-4} - 1.5 \times 10^{-7}T + 1.8 \times 10^{-10}T^2$$

(1635–2890 K)

#### Mo-No: molybdenum-nobelium (Fig.II-11)

No data were found. The estimated normal boiling point of nobelium,  $900 \pm 50$  K, is below the estimated melting point of  $1100$  K. At  $900$  K the solid solubilities are calculated to be  $x < 10^{-6}$ , less than the quenched defect concentration.

#### Mo-Np: molybdenum-neptunium (Fig.II-30)

Smith and Hill [232] studied a sample of  $\text{Np}_{0.82}\text{Mo}_{0.18}$ , probably a metastable quenched phase, at low temperature. No other phase diagram data were found for the Mo-Np system. The thermodynamic equations of Part I have been used to calculate the phase boundaries of Fig.II-30.

The orthorhombic  $\alpha$ -phase of neptunium transforms to the tetragonal  $\beta$ -phase at  $553 \pm 5$  K,  $\beta\text{Np}$  transforms to the bcc  $\gamma$ -phase at  $850 \pm 3$  K, and melting of neptunium takes place at  $910 \pm 2$  K [120].

The eutectic is calculated to be at  $770 \pm 80$  K and  $x_{\text{Np}} = 0.91 \pm 0.02$ . The molybdenum liquidus from  $770$  to  $2890$  K is described by

$$T = \frac{1485 x_{\text{Np}}^2 + 3890 x_{\text{Np}}^3 - 5242}{\ln(1-x_{\text{Np}}) + 2.493 x_{\text{Np}}^2 + x_{\text{Np}}^3 - 1.814}$$

with an uncertainty in  $T$  of  $\pm 100$  K.

The molybdenum solidus above  $770$  K is given by

$$\frac{\ln x_{\text{Np}}}{2890-T} = -5.367 - 8 \times 10^{-3}T^{-1} - 2.180 \times 10^{-3}T + 7.19 \times 10^{-7}T^2$$

with an uncertainty in  $x_{\text{Np}}$  of a factor of 3.

The solubility of neptunium in molybdenum falls to  $x_{\text{Np}} = 10^{-4}$  at  $780$  K, below which temperature the solubility is defect-controlled.

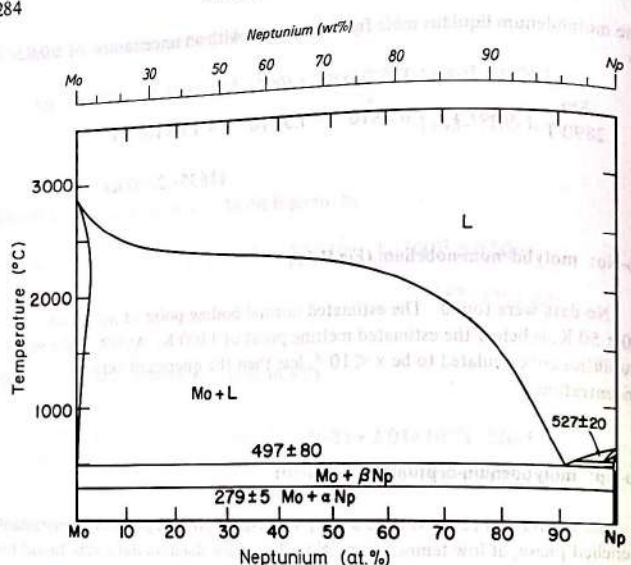


FIG.II-30. Phase diagram of the system molybdenum-neptunium.

The neptunium liquidus from 770 to 910 K is given by

$$x_{\text{Mo}} = 7.29 \times 10^{-4} (910 - T) - 6.1 \times 10^{-7} (910 - T)^2$$

with an uncertainty in  $x_{\text{Mo}}$  of  $\pm 1.4 \times 10^{-4}$  (910-T). The phase boundary for  $\gamma\text{Np}$  in equilibrium with the liquid from  $800 \pm 20$  K to 910 K is given by  $x_{\text{Mo}} = 2 \times 10^{-4}$  (910-T). The boundary for  $\gamma\text{Np}$  in equilibrium with  $\beta\text{Np}$  from  $800 \pm 20$  K to 850 K is given by  $x_{\text{Mo}} = 4.4 \times 10^{-4}$  (850-T). The boundary for  $\beta\text{Np}$  in equilibrium with  $\gamma\text{Np}$  or  $\text{Np}(l)$  from 770 to 850 K is given by

$$x_{\text{Mo}} = 7.4 \times 10^{-5} (850 - T) - 3.1 \times 10^{-7} (850 - T)^2$$

and the boundary for  $\beta\text{Np}$  in equilibrium with molybdenum from 552 ± 5 K to 770 K is given by

$$\ln x_{\text{Mo}} = 6.8 \times 10^{-2} - 4300 T^{-1} - 3.1 \times 10^{-4} T + 3.6 \times 10^{-7} T^2$$

The small two-phase region of  $\alpha\text{Np}$  and  $\beta\text{Np}$  is bounded by the points  $x_{\text{Mo}} = 0$  at  $553 \pm 5$  K and  $x_{\text{Mo}} = 4 \times 10^{-4}, 2 \times 10^{-5}$  at  $552 \pm 5$  K. The solubility of molybdenum

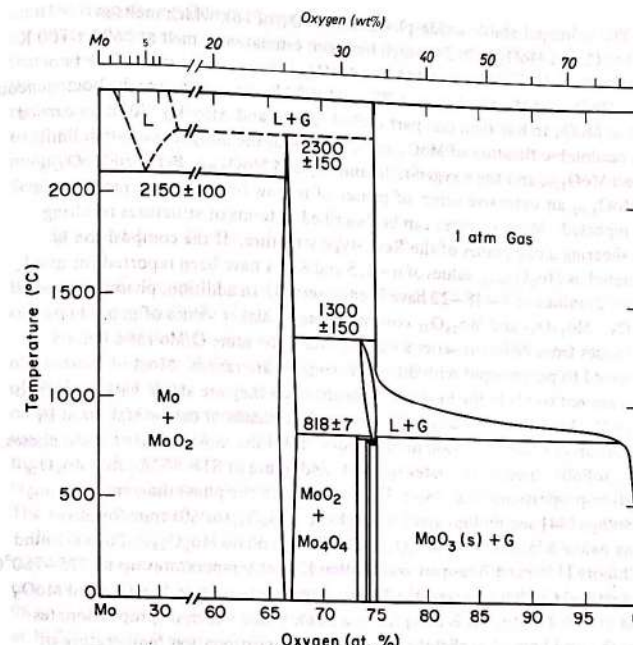


FIG.II-31. Phase diagram of the system molybdenum-oxygen.

in  $\alpha\text{Np}$  is defect-controlled. The uncertainty in the solid solubilities for molybdenum in neptunium is a factor of 3.

A  $\text{MoNp}_2$  phase may be present below about 500 K, but the uncertainty in the enthalpy of formation precludes the calculation of definite phase boundaries.

#### Mo-O: molybdenum-oxygen (Fig.II-31)

Part III reviews the various stable and metastable oxides of molybdenum. The Gmelin Handbuch [93] has recently presented a thorough summary of the literature dealing with the phase diagram and the properties of the oxide phases. The extensive bibliography will not be repeated here. This summary may be supplemented by the paper by Ekstrom and Tilley [66] which reviews Ekstrom's work as well as the earlier work of Kihlborg on the phases of the Mo-O system.

The principal stable oxide phases are  $\text{MoO}_3$  (oP16), which melts at  $800 \pm 5^\circ\text{C}$ , and  $\text{MoO}_2$  (mP12), which has been estimated to melt at  $2600 \pm 100\text{ K}$ . Zhukovskij et al. [275] have stated that  $\text{MoO}_{2.99}$  samples consisted of the two phases  $\text{MoO}_3$  and  $\text{Mo}_9\text{O}_{26}$  between  $773$  and  $1023\text{ K}$ , thus restricting the homogeneous range of  $\text{MoO}_3$  to less than one part in  $300$ . Zador and Alcock [270] have carried out a coulombic titration of  $\text{MoO}_2$  at  $1273\text{ K}$ , with the molybdenum-rich limit beyond  $\text{MoO}_{1.99}$  and the oxygen-rich limit beyond  $\text{MoO}_{2.03}$ . Between  $\text{MoO}_{1.75}$  and  $\text{MoO}_{1.92}$  an extensive series of phases of narrow homogeneous ranges have been reported. Many of them can be described in terms of structures resulting from shearing along planes of the  $\text{ReO}_3$ -type structure. If the composition is designated as  $\text{Mo}_n\text{O}_{3n-m}$ , values of  $n = 4, 5$  and  $8-14$  have been reported for  $m = 1$ . For  $m = 2$ , values of  $n = 18-22$  have been observed. In addition, phases such as  $\text{Mo}_{12}\text{O}_{33}$ ,  $\text{Mo}_{17}\text{O}_{47}$ , and  $\text{Mo}_{26}\text{O}_{75}$  corresponding to higher values of  $m$  are known.

Phases from different series sometimes have the same O/Mo ratio and correspond to polymorphs with different temperature ranges. Most of these phases are not stable in the binary system although they are stable with respect to  $\text{MoO}_2 + \text{MoO}_3$  and can be produced as metastable phases or can be stabilized by the addition of other transition metal oxides. Even the most stable of these phases,  $\text{Mo}_4\text{O}_{11}$  (oP60), disproportionates to  $\text{MoO}_2$  and liquid at  $818 \pm 7^\circ\text{C}$ , and  $\text{Mo}_9\text{O}_{26}$  (mP70) disproportionates at  $780 \pm 5^\circ\text{C}$  according to the phase diagram of Chang and Phillips [44] and Phillips and Chang [188].  $\text{Mo}_4\text{O}_{11}$  (oP60) transforms on cooling below  $875 \pm 50\text{ K}$  to  $\text{Mo}_4\text{O}_{11}$  (mP60). The phase  $\text{Mo}_8\text{O}_{23}$  (mP62) is found by Kihlborg [139] and Bousquet and Guillon [24] at temperatures up to  $775-780^\circ\text{C}$ . Bousquet and Guillon observed  $\text{Mo}_8\text{O}_{23}$  to disproportionate to  $\text{Mo}_4\text{O}_{11}$  and  $\text{MoO}_3$  vapour at  $780^\circ\text{C}$ .  $\text{Mo}_8\text{O}_{23}$  is accepted as a stable phase which disproportionates to  $\text{Mo}_4\text{O}_{11}$  and liquid just slightly above the disproportionation temperature of  $\text{Mo}_9\text{O}_{26}$ .

The Gmelin Handbuch reviews reports stating that  $\text{MoO}_2 + \text{MoO}_3$  or  $\text{Mo} + \text{MoO}_3$  mixtures yield  $\text{Mo}_{18}\text{O}_{52}$  (aP140) at temperatures up to  $760^\circ\text{C}$ . Phillips and Chang [188] obtained  $\text{Mo}_9\text{O}_{26}$  (mP70) from  $\text{Mo} + \text{MoO}_3$  at  $770^\circ\text{C}$ . On this basis, they presented the phase diagram showing a transformation from  $\text{Mo}_9\text{O}_{26}$  (mP70) to  $\text{Mo}_{18}\text{O}_{52}$  (aP140) at  $765^\circ\text{C}$ . However, the Gmelin Handbuch presents other observations indicating the formation of  $\text{Mo}_9\text{O}_{26}$  (mP70) at  $750^\circ\text{C}$  and even as low as  $700^\circ\text{C}$ .  $\text{Mo}_{18}\text{O}_{52}$  (aP140) transforms to  $\text{Mo}_9\text{O}_{26}$  (mP70) in two hours at  $780^\circ\text{C}$ , but the reverse transformation does not take place after three days at  $700^\circ\text{C}$  or a week at  $648^\circ\text{C}$ . It is concluded that there is no firm basis for  $\text{Mo}_{18}\text{O}_{52}$  (aP140) in the equilibrium phase diagram and it has been excluded as being a metastable phase.

The other phases have been prepared at lower temperatures where equilibrium is difficult to attain. On the basis of the present information, all of the other solid phases, including  $\text{Mo}_3\text{O}$ , which can be prepared by hydrogen reduction of  $\text{MoO}_3$ , and  $\text{Mo}_2\text{O}_5$ , which can be prepared by dehydration of  $\text{MoO}(\text{OH})_3$  [136], are

## PART II. PHASE DIAGRAMS

omitted from the equilibrium phase diagram. Srivastava and Seigle [235] find the solubility of oxygen in zone-refined molybdenum solid saturated by  $\text{MoO}_2$  to vary from  $x_O = (2 \pm 0.5) \times 10^{-5}$  at  $1673\text{ K}$  to  $x_O = (1 \pm 0.2) \times 10^{-7}$  at  $2190\text{ K}$ . They review the literature and assign larger uncertainties to the earlier measurements which did not extend to the high-temperature range where oxygen solubilities are large enough to be measured accurately. Also the higher purity of the zone-refined molybdenum minimized the effect of impurities. For the molybdenum solvus, Srivastava and Seigle give

$$\ln x_O = 5.86 - 27900 T^{-1} \pm 0.2 \quad (1700-2200\text{ K})$$

Below  $1700\text{ K}$ , the solubility of oxygen in molybdenum metal is undoubtedly controlled by quenched defects and impurities.

Except for the exclusion of  $\text{Mo}_{18}\text{O}_{52}$  and the addition of  $\text{Mo}_8\text{O}_{23}$ , the portion of Fig.II-31 between  $\text{MoO}_2$  and  $\text{MoO}_3$  below  $1000^\circ\text{C}$  is based on the observations of Phillips and Chang. Their melting point of  $\text{MoO}_3$  was increased to  $800 \pm 5^\circ\text{C}$  on the basis of the measurement by King et al. [141]. The  $\text{MoO}_3-\text{Mo}_9\text{O}_{26}$  eutectic was accepted at  $775 \pm 5^\circ\text{C}$ , with the liquid composition at  $74.6 \pm 0.1$  at.% O. From the work of Perry et al. [187], a Mo-MoO<sub>2</sub> eutectic at  $2150 \pm 100^\circ\text{C}$  is expected, but Chang and Phillips [44] predict a liquid miscibility gap rather than a eutectic. The thermodynamic data of Part I indicate that the liquid phase, which at  $800^\circ\text{C}$  – the melting point of  $\text{MoO}_3$  – extends from  $75.0$  at.% O to  $74.3 \pm 0.1$  at.% O, moves up in temperature as shown by the narrow band in Fig.II-31. The oxygen-rich boundary is determined at 1 atm total pressure by the vapour containing 98 at.% O at  $800^\circ\text{C}$  and becoming essentially pure ( $\text{MoO}_3$ ) vapour of 75.0 at.% O at  $1125^\circ\text{C}$ , with 9 mol%  $\text{Mo}_5\text{O}_{15}$ , 46 mol%  $\text{Mo}_4\text{O}_{12}$ , 45 mol%  $\text{Mo}_3\text{O}_9$  and only 0.3 mol%  $\text{O}_2$ . The composition of the 1-atm vapour saturating the liquid between  $1073$  and  $1400\text{ K}$  is expressed in terms of  $x_O$ , the mole fraction of oxygen, considering all oxygen species, by

$$\ln x_O = 0.075 - 1.376 \times 10^{-3}(T-1000) + 1.17 \times 10^{-6}(T-1000)^2 \pm 0.03$$

Above  $1400\text{ K}$ , the composition of the vapour remains very close to  $x_O = 0.75$ . The liquid boundary saturated by the vapour is within 0.001 of  $x_O = 0.750$  from  $1073\text{ K}$  to almost  $1400\text{ K}$ , where  $x_O$  is calculated to be 0.748. Above  $1400\text{ K}$ , the oxygen content begins to drop more rapidly, reaching  $x_O = 0.735 \pm 0.005$  at  $1573 \pm 150\text{ K}$ .

As discussed in Part I, the thermodynamic data cannot fix accurately the upper temperature limit of the liquid phase and it is possible that this phase might extend several hundred degrees higher, but the best present estimates indicate that the  $\text{MoO}_2$  liquidus and the vapour-saturated boundary of the liquid come together around  $1300^\circ\text{C}$ , as indicated in Fig.II-31. The  $\text{MoO}_2$  liquidus between  $1091$  and  $1573\text{ K}$  is calculated to vary only from 74.2 at.% O to 73.5 at.% O.

As described in Part I, the thermodynamic data obtained by Zador and Alcock [270] for the  $\text{MoO}_2$  homogeneous range were used to calculate the boundaries. The value of  $x$  for the  $\text{MoO}_{2+x}$  boundary saturated by liquid is given by

$$x = 0.095 - 6.6 \times 10^{-5} (T-1000) - 3.7 \times 10^{-8} (T-1000)^2$$

with an uncertainty of a factor of 1.5 in  $x$  between 1091 and 1573 K. The variation is from  $x = 0.09$  at 1091 K to  $x = 0.05$  at 1573 K. The boundary for  $\text{MoO}_{2+x}$  saturated by 1 atm gas is given by

$$\ln x = -3.13 + 2.8 \times 10^{-3} (T-1500) - 1.7 \times 10^{-5} (T-1500)^2$$

with an uncertainty of a factor of 1.7 in  $x$  between 1573 and 2000 K. The variation is from  $x = 0.05$  at 1573 K to  $x = 0.0025$  at 2000 K. The 1-atm gas saturating  $\text{MoO}_2$  is calculated to consist mainly of polymers of  $\text{MoO}_3$ , with the following percentages for the dimer, trimer, tetramer and pentamer, respectively: 2, 57, 36 and 4 mol% at 1573 K, and 14, 67, 18 and 1 mol% at 2000 K.

The oxygen pressure is of the order of  $10^{-6}$  atm at 1573 K and  $10^{-5}$  atm at 2000 K. The boundary of  $\text{MoO}_{2-x}$  saturated by molybdenum metal is given by

$$\ln x = -1.73 - 3.7 \times 10^{-3} (T-1000) + 1.7 \times 10^{-6} (T-1000)^2 \pm 0.6 \quad (1200-2000 \text{ K})$$

From the thermodynamic data reviewed in Part I, the molybdenum solidus was calculated to be

$$\frac{x_0}{2890-T} = 1.04 \times 10^{-5} - 8.3 \times 10^{-9} (2890-T) + 4 \times 10^{-13} (2890-T)^2$$

and the liquidus was calculated to be

$$\frac{x_0}{2890-T} = 5.68 \times 10^{-4} - 1.56 \times 10^{-7} (2890-T) + 6 \times 10^{-11} (2890-T)^2$$

These values apply between 2890 K and the eutectic, which is estimated to be 2423  $\pm$  150 K, with  $x_0 = 0.24 \pm 0.1$  for the liquid. The values of  $x_0$  for the solidus have an uncertainty of a factor of 2; for the liquidus, the uncertainty is 50%. There are no experimental values for comparison.

No data of any kind exist for the behaviour of oxygen in liquid molybdenum other than at low concentration. If the thermodynamic relations from Part I, used to calculate the molybdenum liquidus, are extrapolated to higher oxygen contents, the liquid boundary saturated by 1 atm gas can be calculated to rise very steeply from  $x_0 = 0.40 \pm 0.05$  at 2573  $\pm$  150 K, where it contacts the  $\text{MoO}_2$  liquidus, to

$x_0 = 0.37 \pm 0.05$  at 1850 K. The gas at 2573 K consists of over 80%  $\text{MoO}_3$  and over 10%  $\text{MoO}_2$ , with smaller amounts of  $(\text{MoO}_3)_n$  and diatomic and atomic oxygen. With increasing temperature the proportion of  $\text{MoO}_3$  drops, while the proportions of  $\text{Mo}_2$ ,  $\text{MoO}_2$ , O and  $\text{O}_2$  in the 1-atm gas increase. It is particularly difficult to accurately predict the contributions of the  $(\text{MoO}_3)_n$  polymers as their enthalpies and entropies were determined at low temperatures and are believed to be rather inaccurate; thus extrapolations to 1000–2000° higher are very uncertain.

#### Mo-Os: molybdenum-osmium (Fig.II-32)

The phase diagram was determined by Taylor et al. [248]. Erley and Wagner [72] confirmed the elemental phase boundaries. The eutectic liquid of 21  $\pm$  1 at.% Os at 2380°C is in equilibrium with bcc Mo with 19.5  $\pm$  0.5 at.% Os and  $\text{Mo}_2\text{Os}$  (tP30) with 29.6  $\pm$  0.5 at.% Os. At the peritectic temperature of 2430  $\pm$  50°C, hcp Os with 52  $\pm$  1 at.% Mo and  $\text{Mo}_2\text{Os}$  (tP30) with 37 at.% Os are in equilibrium with  $\text{Mo}(l)$  of 22  $\pm$  1 at.% Os.  $\text{Mo}_3\text{Os}$  (cP8) with a maximum composition range of 24–25.5 at.% Os is formed by a peritectoid reaction at 2210  $\pm$  20°C from Mo with 16  $\pm$  1 at.% Os and  $\text{Mo}_2\text{Os}$  with 30  $\pm$  1 at.% Os. The osmium-rich boundary of  $\text{Mo}_2\text{Os}$  increases in osmium content with decreasing temperature, reaching 39  $\pm$  1 at.% Os at 1200°C.

The osmium solvus (1000–2703 K) is given by

$$\ln x_{\text{Mo}} = -2.17 + 0.2 \ln T - 300 T^{-1} \pm 0.06$$

The osmium solidus and liquidus (2703–3300  $\pm$  20 K) are given, respectively, by

$$\frac{x_{\text{Mo}}}{3300-T} = 1.37 \times 10^{-3} - 2.4 \times 10^{-6} (3300-T) + 2.65 \times 10^{-9} (3300-T)^2 \pm 5\%$$

and

$$\frac{x_{\text{Mo}}}{3300-T} = 3.03 \times 10^{-3} - 4.16 \times 10^{-6} (3300-T) + 2.13 \times 10^{-9} (3300-T)^2 \pm 10\%$$

The molybdenum solvus is given by the two equations

$$\ln x_{\text{Os}} = -2.33 + 0.16 \ln T - 2030 T^{-1} \pm 0.1 \quad (1300-2483 \text{ K})$$

and

$$\ln x_{\text{Os}} = 1.25 - 7700 T^{-1} \pm 0.1 \quad (2483-2653 \text{ K})$$

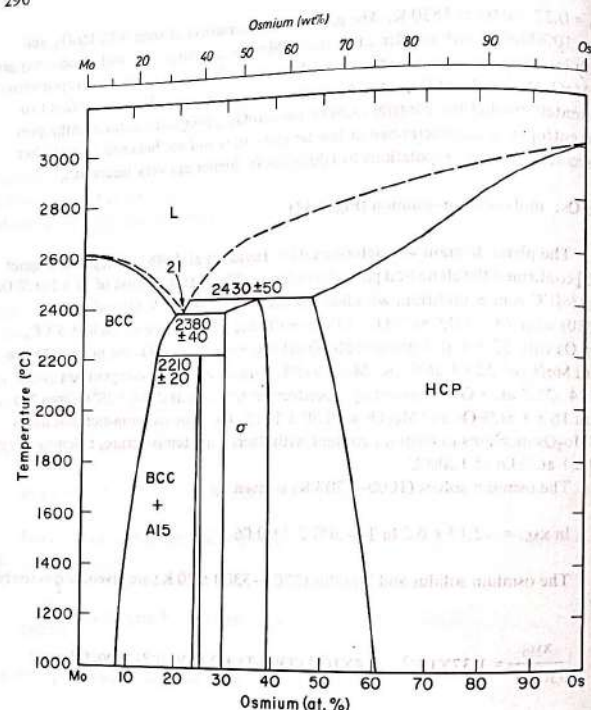


FIG.II-32. Phase diagram of the system molybdenum-osmium.

The molybdenum solidus and liquidus (2653–2890 K) are given, respectively, by

$$\frac{x_{Os}}{2890-T} = 1.2 \times 10^{-3} - 1.1 \times 10^{-6}(2890-T) - 2 \times 10^{-9}(2890-T)^2 \pm 5\%$$

and

$$\frac{x_{Os}}{2890-T} = 1.3 \times 10^{-3} - 1.8 \times 10^{-6}(2890-T) \pm 15\%$$

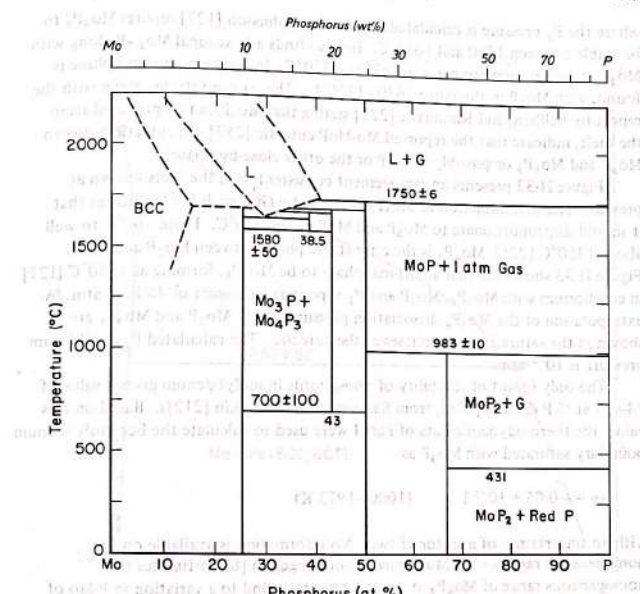


FIG.II-33. Phase diagram of the system molybdenum-phosphorus.

## Mo-P: molybdenum-phosphorus (Fig.II-33)

Details of the structures of  $Mo_3P$ (tI32),  $Mo_8P_5$ (mP13),  $Mo_4P_3$ (oP56),  $MoP(hP2)$ ,  $MoP_2(oC12)$  and  $MoP_4(mC20)$  are given in Part III. Jeitschko and Donohue [123] prepared  $MoP_4$  at pressures over 15 kbar; they conclude that it is thermodynamically unstable at 1 atm.  $MoP_2$  is calculated to dissociate to 1 atm phosphorus vapour and  $MoP$  at 983°C according to the dissociation pressure measurements of Faller et al. [74]. Vogel and Horstmann [257] report a  $Mo$ - $MoP$  eutectic at 29.7 at. % P and 1650°C and a melting point for  $MoP$  of over 1700°C. The extrapolation of the dissociation pressure measurements of Gingerich [89] indicate that  $MoP$  would decompose to  $Mo_4P_3$  and 1 atm  $P_2$  gas at 1760°C, but  $Mo_4P_3$  is predicted to reach the peritectic with the liquid and  $MoP$  at 1700°C.

where the  $P_2$  pressure is calculated as 0.5 atm. Johnsson [127] reports  $\text{Mo}_8\text{P}_5$  to be stable between 1580 and 1680°C. He also finds a hexagonal  $\text{Mo}_{1.7}\text{P}$  along with  $\text{Mo}_3\text{P}$  at preparation temperatures above 1720°C. In addition, another phase is found, with  $\text{Mo}_3\text{P}$  in the range 1670–1720°C. These observations, along with the report by Sellberg and Rundqvist [225] stating that  $\text{Mo}_3\text{P}$  can be prepared from the melt, indicate that the reported Mo-MoP eutectic [257] is a eutectic between  $\text{Mo}_3\text{P}$  and  $\text{Mo}_8\text{P}_5$  or possibly  $\text{Mo}_{1.7}\text{P}$  or the other close-by phase.

Figure II-33 presents an arrangement consistent with the facts known at present. The determination of  $\text{Mo}_4\text{P}_3$  stability by Gingerich [89] indicates that it should disproportionate to  $\text{Mo}_3\text{P}$  and MoP below 700°C. From 700°C to well above 1350°C [225],  $\text{Mo}_4\text{P}_3$  is the only stable phase between  $\text{Mo}_3\text{P}$  and MoP. Figure II-33 shows the first additional phase to be  $\text{Mo}_8\text{P}_5$ , forming at 1580°C [127] in equilibrium with  $\text{Mo}_3\text{P}$ ,  $\text{Mo}_3\text{P}$  and  $\text{P}_2$  vapour at a pressure of  $4 \times 10^{-3}$  atm, by extrapolation of the  $\text{Mo}_3\text{P}_4$  dissociation pressures [89].  $\text{Mo}_3\text{P}$  and  $\text{Mo}_8\text{P}_5$  are shown as the saturating solid phases at the eutectic. The calculated  $\text{P}_2$  equilibrium pressure is  $10^{-2}$  atm.

The only report of solubility of phosphorus in molybdenum gives a value of 14–19 at.% P (Shunk [228], from Samsonov and Vereikin [212]). Based on this value, the thermodynamic data of Part I were used to calculate the bcc molybdenum boundary saturated with  $\text{Mo}_3\text{P}$  as

$$x_P = -0.05 + 10^{-5} T \quad (1000-1973 \text{ K})$$

with an uncertainty of a factor of two. No information is available on the homogeneous range of the  $\text{Mo}_3\text{P}$  phase, but Gingerich [89] estimates the homogeneous range of  $\text{Mo}_4\text{P}_3$  at 1500 K to correspond to a variation in P-Mo of less than 0.02. For the MoP phase, he fixes the variation in P-Mo as less than 0.001.

The molybdenum solidus is calculated to be

$$\ln x_P = 3300 T^{-1} - 7.18 + 8.34 \times 10^{-3} (2890-T) - 4.94 \times 10^{-6} (2890-T)^2 \pm 0.7 \quad (1973-2890 \text{ K})$$

The molybdenum liquidus is calculated to be

$$\frac{x_P}{2890-T} = 1.71 T^{-1} - 9.9 \times 10^{-5} - 5.3 \times 10^{-7} (2890-T) + 6 \times 10^{-11} (2890-T)^2$$

with an uncertainty in  $x_P$  of 30%. The liquid boundary saturated with 1 atm  $\text{P}_2$  gas is given by

$$x_P = 0.426 - 2.86 \times 10^{-4} (T-2000) + 1.56 \times 10^{-7} (T-2000)^2 - 8.2 \times 10^{-11} (T-2000)^3 \pm 0.1 \quad (2020-2600 \text{ K})$$

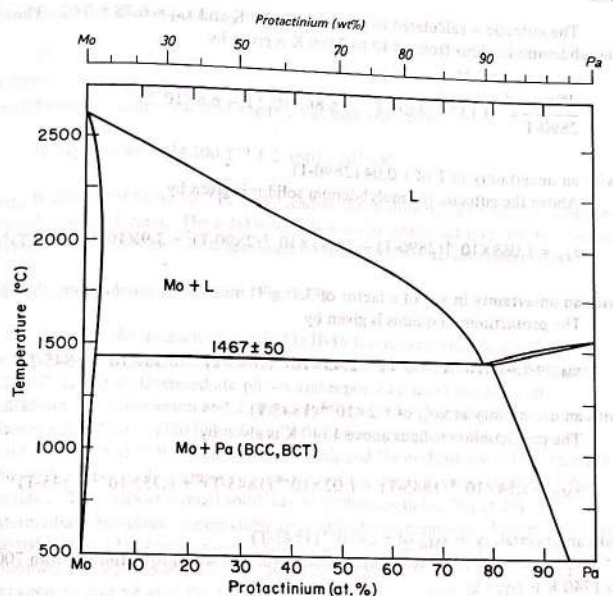


FIG.II-34. Phase diagram of the system molybdenum-protactinium.

Fowler et al. [79] studied a  $\text{Mo}_{0.15}\text{Pa}_{0.85}$  sample, probably a metastable quenched phase, at low temperature. No other phase diagram data were found for the Mo-Pa system. The thermodynamic equations of Part I have been used to calculate the phase boundaries of Fig.II-34.

The room-temperature bct structure of protactinium changes to bcc at about 1450 K [188]. The change in symmetry takes place by the variation of lattice constants with temperature rather than by a discontinuous structural change; both bct and bcc are considered as a continuous phase in Fig.II-34.

The eutectic is calculated to be at  $1740 \pm 50$  K and  $x_{\text{Pa}} = 0.78 \pm 0.02$ . The molybdenum liquidus from 1740 to 2890 K is given by

$$\frac{\ln x_{\text{Pa}}}{2890-T} = -3.137 - 4800 T^{-1} - 6.86 \times 10^{-4} T - 6.8 \times 10^{-8} T^2$$

with an uncertainty in T of  $\pm 0.04$  (2890-T)

Above the eutectic the molybdenum solidus is given by

$$x_{\text{Pa}} = 1.068 \times 10^{-4} (2890-T) - 1.235 \times 10^{-7} (2890-T)^2 + 3.9 \times 10^{-11} (2890-T)^3$$

with an uncertainty in  $x_{\text{Pa}}$  of a factor of 3.

The protactinium liquidus is given by

$$x_{\text{Mo}} = 1.41 \times 10^{-3} (1845-T) - 2.45 \times 10^{-6} (1845-T)^2 + 8.55 \times 10^{-8} (1845-T)^3$$

with an uncertainty in  $x_{\text{Mo}}$  of  $\pm 2 \times 10^{-4}$  (1845-T).

The protactinium solidus above 1740 K is given by

$$x_{\text{Mo}} = 1.14 \times 10^{-3} (1845-T) - 1.02 \times 10^{-5} (1845-T)^2 + 1.75 \times 10^{-7} (1845-T)^3$$

with an uncertainty in  $x_{\text{Mo}}$  of  $\pm 2 \times 10^{-4}$  (1845-T).

The phase boundary for molybdenum saturated with protactinium from 700 to 1740 K is given by

$$\ln x_{\text{Pa}} = 0.025 - 6800 T^{-1} - 1.33 \times 10^{-4} T + 5.5 \times 10^{-8} T^2$$

with an uncertainty in  $x_{\text{Pa}}$  of a factor of 3. The solubility of protactinium in molybdenum falls to  $10^{-4}$  at  $740 \pm 50$  K. Below this temperature the solubility is a function of the quenched defect concentration.

The phase boundary for protactinium in equilibrium with molybdenum below 1740 K is given by

$$\ln x_{\text{Mo}} = -1.000 - 1500 T^{-1} - 1.52 \times 10^{-4} T + 1.87 \times 10^{-7} T^2$$

with an uncertainty in  $x_{\text{Mo}}$  of  $\pm 0.02$  at 1740 K and rising to a factor of 3 at 300 K.

A  $\text{MoPa}_3$  intermediate phase may be present below about 650 K, but the uncertainty in the enthalpy of formation precludes the calculation of definite phase boundaries. The presence of this phase will lower the solubility of molybdenum in protactinium by less than the stated uncertainty.

## PART II. PHASE DIAGRAMS

### Mo-Pb: molybdenum-lead (Fig.II-2)

The only data found were an upper limit of 0.005 wt% Mo in lead at 1200°C [2] and an upper limit of  $10^{-4}$  wt% Mo in lead at 1110°C [185]. The molybdenum liquidus curve of Fig.II-2 was estimated to be

$$\ln x_{\text{Mo}} = 2.89 - 24300 T^{-1} \pm 2 \quad (601-2023 \text{ K})$$

$x_{\text{Mo}}$  is calculated to be  $10^{-4}$  in liquid lead at the boiling point of 2023 K saturated by solid molybdenum. The solid solubilities are so small that they are not thermodynamic quantities but are determined by the quenched defect concentration.

### Mo-Pd: molybdenum-palladium (Fig.II-35)

Although the diagram shown in Fig.II-35 is relatively simple, substantial features are in dispute. Raub [197], who studied the system between 800 and 1200°C, found no intermediate phases and reported a small solubility of palladium in molybdenum and a large solubility of molybdenum in palladium. Greenfield and Beck [101] also found no intermediate phases but reported a solubility of 25 at.% Pd in bcc Mo. Haworth and Hume-Rothery [111] extended the study of the molybdenum-rich portion of the diagram from 1100°C to the liquidus. They report a small solubility of palladium in bcc Mo and find an intermediate hcp phase region stable only at high temperatures. Anderson [8] and Savitskij et al. [216] have made additional measurements. They agree on the intermediate hcp phase, restricted to a narrow composition range somewhere between 52 and 54 at.-% Pd, between roughly 1400 and 1750°C. However, Savitskij et al. [216] indicate a solubility of palladium in bcc Mo as high as 16 at.% and their liquidus is displaced to higher palladium concentrations. Thus they show a peritectic for fcc Pd at 1700°C compared with the maximum melting point and formation of a eutectic reported by Anderson. In the lower temperature region, Maldonado and Schubert [168] have found that the disordered fcc phase at 67 at.% Pd undergoes an order-disorder transformation at around 1000°C to  $\text{MoPd}_2(\text{oI6})$ . Recently, Zaiss et al. [273] have carried out diffusion studies indicating a solubility of molybdenum in fcc Pd higher than reported in earlier studies and they were unable to detect the hcp intermediate phase.

Figure II-35 attempts to reconcile the discordant results. It is assumed that Zaiss et al. [273] did not see the hcp phase in their diffusion studies because of nucleation difficulties, but their higher solubilities of molybdenum in palladium have been incorporated in Fig.II-35, with a maximum extent of  $56 \pm 2$  at.% Pd at 1600°C. At  $1755 \pm 10^\circ\text{C}$  – the peritectic temperature for the hcp phase – the liquid with  $53 \pm 2$  at.% Pd is in equilibrium with bcc Mo having the maximum solubility of  $7 \pm 2$  at.% Pd, which is consistent with the observations of both

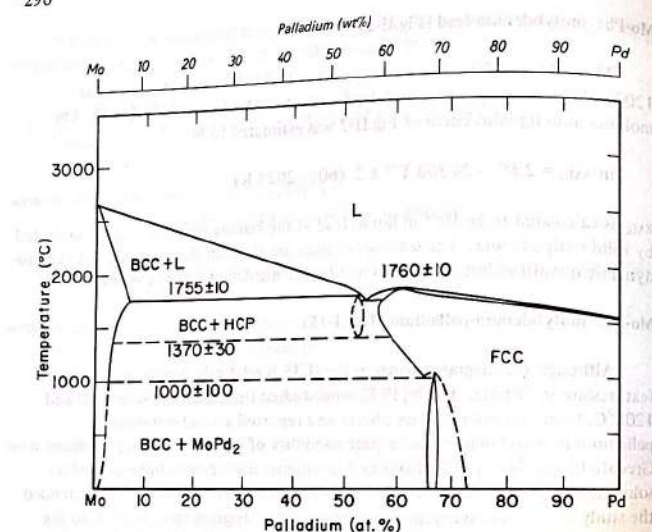


FIG.II-35. Phase diagram of the system molybdenum-palladium.

Anderson and Haworth/Hume-Rothery. The reported higher solubilities are attributed to metastable quenched phases. A eutectic is shown at  $1700 \pm 30^\circ\text{C}$ , between the hcp phase at  $52 \pm 2$  at.% Pd, the fcc phase at  $57 \pm 2$  at.% Pd, and the liquid phase at  $54 \pm 2$  at.% Pd. The fcc phase is shown to reach a maximum melting point at  $1762 \pm 10^\circ\text{C}$  at 61 at.% Pd.

The palladium solidus and liquidus between 1825 K – the melting point of palladium – and 2033 K – the maximum melting point of the fcc solid solution – are given for the solidus by

$$\frac{x_{\text{Mo}}}{T-1825} = 1.37 \times 10^{-3} + 1.26 \times 10^{-5}(T-1825) - 4.9 \times 10^{-8}(T-1825)^2$$

and for the liquidus by

$$\frac{x_{\text{Mo}}}{T-1825} = 0.001 + 4 \times 10^{-6}(T-1825) + 5 \times 10^{-10}(T-1825)^2$$

## PART II. PHASE DIAGRAMS

The uncertainty in the boundaries is  $\pm 15$  K. The boundary of fcc Pd saturated by hcp Pd ( $1643 \pm 30$  to  $1973 \pm 30$  K) is given by

$$x_{\text{Mo}} = 0.404 + 2.5 \times 10^{-4}(T-1600) - 4.87 \times 10^{-7}(T-1600)^2 \pm 0.02$$

The boundary of fcc Pd saturated by Mo ( $1273 \pm 100$  to  $1643 \pm 30$  K) is given by

$$x_{\text{Mo}} = 0.344 + 7 \times 10^{-5}(T-1200) + 2 \times 10^{-7}(T-1200)^2 \pm 5\%$$

There are no data for the palladium solidus saturated by MoPd<sub>2</sub> and any values calculated from estimated thermodynamic values are very uncertain at such a low temperature. The estimated curve shown in Fig.II-35 is uncertain by  $\pm 5$  at.% even above 800 K.

The molybdenum solidus is given by

$$\frac{x_{\text{Pd}}}{2890-T} = 9.1 \times 10^{-5} + 5 \times 10^{-9}(2890-T) - 1.2 \times 10^{-11}(2890-T)^2$$

and the molybdenum liquidus is given by

$$\frac{x_{\text{Pd}}}{2890-T} = 6.725 \times 10^{-4} - 7.1 \times 10^{-8}(2890-T) - 4.3 \times 10^{-12}(2890-T)^2$$

over the temperature interval  $2028 \pm 10$  to  $2890 \pm 8$  K, with the uncertainty in  $x_{\text{Pd}}$  increasing with temperature from 4% to 30% for the solidus and from 4% to 10% for the liquidus. The molybdenum solvus saturated by hcp Pd ( $1643 \pm 30$  to  $2028 \pm 10$  K) is given by

$$x_{\text{Pd}} = 0.037 - 6.7 \times 10^{-5}(T-1600) + 3.3 \times 10^{-7}(T-1600)^2 \pm 0.002$$

The molybdenum solvus saturated by fcc Pd ( $1273 \pm 100$  to  $1643 \pm 30$  K) is given by

$$x_{\text{Pd}} = 0.030 + 8 \times 10^{-6}(T-1200) \pm 10\%$$

The molybdenum solvus saturated by MoPd<sub>2</sub> is given by

$$x_{\text{Mo}} = 0.023 + 3 \times 10^{-5}(T-1000) \pm 20\% \quad (1000-1273 \text{ K})$$

**Mo-Pm: molybdenum-promethium (Fig.II-1)**

No data were found. The estimated thermodynamic equations of Part I have been used to calculate the phase boundaries of Fig.II-1.

The monotetic is at  $2830 \pm 10$  K and  $x_{Pm} = 3 \times 10^{-3}$ ,  $0.04 \pm 0.01$  and  $0.76 \pm 0.05$ . Above the monotetic the molybdenum liquidus and solidus are represented by

$$x_{Pm} = 5.83 \times 10^{-4} (2890 - T) + 1.67 \times 10^{-6} (2890 - T)^2$$

with an uncertainty of  $\pm 1.7 \times 10^{-4} (2890 - T)$  for the liquidus and

$$x_{Pm} = 7.3 \times 10^{-5} (2890 - T)$$

with an uncertainty of a factor of 5 for the solidus.

The two-liquid phase-region phase boundaries between 2830 and 3100 K are calculated to be

$$x_{Pm} = 0.039 + 5.7 \times 10^{-5} (T - 2800) + 2.8 \times 10^{-8} (T - 2800)^2$$

with an uncertainty of  $\pm 0.01$  at 2830 K, rising to  $\pm 0.02$  at 3100 K, and

$$x_{Mo} = 0.234 + 2.10 \times 10^{-4} (T - 2800) + 7.5 \times 10^{-8} (T - 2800)^2$$

with an uncertainty of  $\pm 0.05$ . The eutectic is calculated to be at 1346 K and  $x_{Mo} = (3 \pm 1) \times 10^{-3}$ .

The molybdenum liquidus and solidus between 1346 and 2830 K are calculated to be

$$x_{Mo} = 3.2 \times 10^{-3} + 3.0 \times 10^{-5} (T - 1346) + 6 \times 10^{-9} (T - 1346)^2 + 5.4 \times 10^{-11} (T - 1346)^3$$

with an uncertainty rising from  $\pm 1 \times 10^{-3}$  at 1346 K to  $\pm 0.05$  at 2830 K for the liquidus, and

$$\ln x_{Pm} = -20.84 + 9.50 \times 10^{-3} T - 1.50 \times 10^{-6} T^2$$

with an uncertainty of a factor of 5 for the solidus. The solubility of promethium in molybdenum falls to  $x_{Pm} = 10^{-4}$  at 1660 K, below which temperature it is less than the quenched defect concentration.

The solid solubility of molybdenum in promethium is

$$x_{Mo} = 7 \times 10^{-5} + 5.2 \times 10^{-7} (T - 1200) + 2.4 \times 10^{-9} (T - 1200)^2$$

falling to  $x_{Mo} = 10^{-4}$  at 1250 K, with an uncertainty of a factor of 5.

**Mo-Po: molybdenum-polonium**

The only observation is that of Witterman et al. [263] that molybdenum solid and polonium vapour do not react up to 700°C. It was not possible in Part I to estimate the thermodynamic data accurately enough to fix the phase diagram. It is most likely that the phase diagram is of the type given in Fig.II-2.

**Mo-Pr: molybdenum-praseodymium (Fig.II-1)**

Savitskij et al. [213] have reported that the solubility of praseodymium in solid molybdenum is between 0.02 and 0.047 at.% at an unspecified temperature. No other data were found. The estimated thermodynamic equations of Part I have been used to calculate the phase boundaries of Fig.II-1.

The monotetic is calculated to be at  $2820 \pm 10$  K and  $x_{Pr} = 3 \times 10^{-3}$ ,  $0.05 \pm 0.01$  and  $0.72 \pm 0.08$ . The molybdenum liquidus above the eutectic is represented by

$$x_{Mo} = 5 \times 10^{-4} (2890 - T) + 3 \times 10^{-6} (2890 - T)^2$$

with an uncertainty of  $1 \times 10^{-4} (2890 - T)$ . The molybdenum solidus above 2820 K is calculated to be

$$x_{Pr} = 4.7 \times 10^{-5} (2890 - T)$$

with an uncertainty of a factor of 5.

The two-liquid phase boundaries between 2820 and 3000 K are calculated to be

$$x_{Pr} = 0.0548 + 4.6 \times 10^{-5} (T - 2800) + 7.4 \times 10^{-8} (T - 2800)^2$$

and

$$x_{Mo} = 0.272 + 2.5 \times 10^{-4} (T - 2800) + 1.4 \times 10^{-7} (T - 2800)^2$$

with uncertainties of  $\pm 0.001$  for  $x_{Pr}$  and  $\pm 0.08$  for  $x_{Mo}$ .

The molybdenum liquidus and solidus from 1204 to 2820 K are represented by

$$x_{Mo} = 1.5 \times 10^{-3} + 2.84 \times 10^{-5} (T - 1200) - 1.58 \times 10^{-8} (T - 1200)^2 + 6.33 \times 10^{-11} (T - 1200)^3$$

with an uncertainty rising from  $\pm 5 \times 10^{-4}$  at 1204 K to  $\pm 0.08$  at 2820 K for the liquidus, and

$$\ln x_{\text{Pt}} = -20.89 + 9.80 \times 10^{-3}T - 1.56 \times 10^{-6}T^2$$

with an uncertainty of a factor of 5 for the solidus. The solubility of praseodymium in molybdenum drops to  $10^{-4}$  at 1600 K, below which temperature the solubility is defect-controlled. The solubility of molybdenum in solid praseodymium is defect-controlled.

The eutectic is at 1204 K and  $x_{\text{Mo}} = 1.0 \times 10^{-3} \pm 5 \times 10^{-4}$ .

#### Mo-Pt: molybdenum-platinum (Fig.II-36)

Ocken and Van Vucht [180] have presented a phase diagram, based on their own and earlier work, with five intermediate phases. Flükiger et al. [77] have reviewed the earlier studies and have presented new data which confirm the five phases but which fix somewhat different composition ranges. The crystal structures are reviewed in Part III. The composition and temperature ranges are given in Table II-10.

There is a considerable range in the values reported for the boundaries of the phases of the Mo-Pt system. The uncertainties cited for each boundary equation are mainly based on those listed by Flükiger et al., as their study emphasized the accurate fixing of the phase boundaries. With an uncertainty in  $x_{\text{Pt}}$  of  $\pm 0.02$ , the molybdenum solidus and liquidus (2353–2890 K) are given, respectively, by

$$\frac{x_{\text{Pt}}}{2890-T} = 1.52 \times 10^{-4} + 1.6 \times 10^{-7}(2890-T) + 1.5 \times 10^{-10}(2890-T)^2$$

and

$$\frac{x_{\text{Pt}}}{2890-T} = 7.8 \times 10^{-4} - 1.16 \times 10^{-6}(2890-T) + 1.14 \times 10^{-9}(2890-T)^2$$

Within the uncertainty of the values, the molybdenum solvus saturated by the hcp phase can be combined with the small range of the boundary saturated by the ordered hP8 phase as

$$\ln x_{\text{Pt}} = -0.430 - 3400 T^{-1} \pm 0.07 \quad (2053-2353 \text{ K})$$

For molybdenum saturated by the A15 phase (1553–2053 K),

$$\ln x_{\text{Pt}} = 1.57 - 7600 T^{-1} \pm 0.2$$

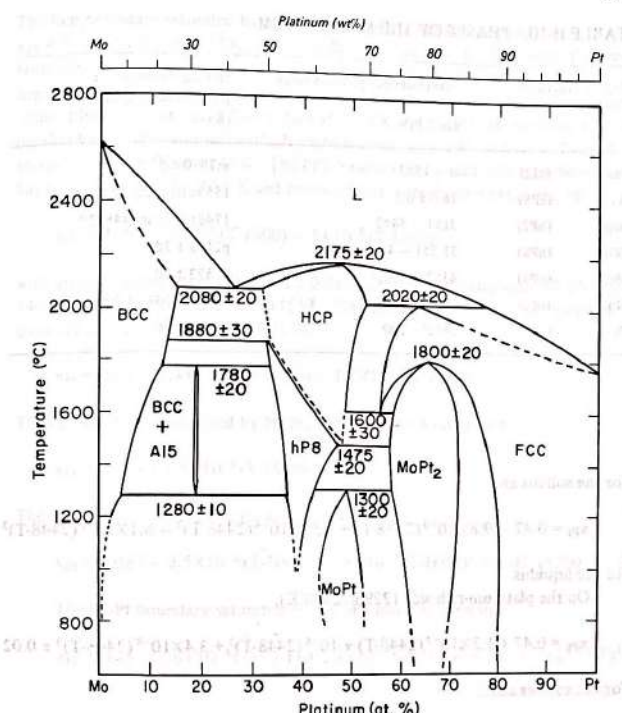


FIG.II-36. Phase diagram of the system molybdenum-platinum.

For molybdenum saturated by the hP8 phase (1300–1553 K),

$$\ln x_{\text{Pt}} = 0.42 - 6040 T^{-1} \pm 0.3$$

The hcp phase solidus and liquidus (2353–2448 K) on the molybdenum-rich side of the melting-point maximum are given with an uncertainty of  $\pm 0.02$  by

$$x_{\text{Pt}} = 0.47 - 6.8 \times 10^{-3}(2448-T) + 1.1 \times 10^{-4}(2448-T)^2 - 5.9 \times 10^{-7}(2448-T)^3$$

TABLE II-10. PHASES OF THE Mo-Pt SYSTEM

Phase (structure)	Maximum composition range (at.% Pt)	Melting, peritectic or peritectoid temperature (K)
Mo	(cI2)	0 - 15±1
A15	(cP8)	18.5 ± 0.5
hcp	(hP2)	31±1 - 54±2
D0 <sub>19</sub>	(hP8)	31.5±1 - 45±2
MoPt	(oP4)	43±2 - 53±2
MoPt <sub>2</sub>	(oI6)	58±2 - 72±2
Pt	(cF4)	56±2 - 100

for the solidus and

$$x_{\text{Pt}} = 0.47 - 9.8 \times 10^{-3}(2448-T) + 1.57 \times 10^{-4}(2448-T)^2 - 8.1 \times 10^{-7}(2448-T)^3$$

for the liquidus.

On the platinum-rich side (2293-2448 K),

$$x_{\text{Pt}} = 0.47 + 1.2 \times 10^{-3}(2448-T) + 10^{-5}(2448-T)^2 + 3.4 \times 10^{-8}(2448-T)^3 \pm 0.02$$

for the solidus and

$$x_{\text{Pt}} = 0.47 + 4.8 \times 10^{-3}(2448-T) - 3.5 \times 10^{-5}(2448-T)^2 \\ + 1.1 \times 10^{-7}(2448-T)^3 \pm 0.03$$

for the liquidus. The hcp boundary saturated by molybdenum (2153-2353 K) is given by

$$x_{\text{Pt}} = 0.345 - 10^{-4}(T-2000) \pm 0.02$$

The hcp boundary saturated by fcc Pt (1873-2293 K) is given by

$$x_{\text{Pt}} = 0.508 - 1.6 \times 10^{-4}(T-1500) + 2.5 \times 10^{-7}(T-1500)^2 \pm 0.03$$

## PART II. PHASE DIAGRAMS

The hcp boundary saturated by MoPt<sub>2</sub> shows only a slight variation from  $x_{\text{Pt}} = 0.485 \pm 0.02$  at 1873 K to  $x_{\text{Pt}} = 0.48 \pm 0.03$  at 1748 K. The order-disorder boundary between the hcp phase and the hP8 phase is not well defined for the hcp phase; it is given in Fig.II-36 as estimated by Flükiger et al. [77] as an almost straight line between  $x_{\text{Pt}} = 0.33 \pm 0.02$  at 2153 K and  $x_{\text{Pt}} = 0.48 \pm 0.03$  at 1748 K, parallel to the hP8 boundary which extends from  $x_{\text{Pt}} = 0.315 \pm 0.01$  at 2153 K to  $x_{\text{Pt}} = 0.45 \pm 0.02$  at 1748 K. The hP8 boundary saturated with molybdenum has two ranges, 2153-2053 K and below 1553 K, which are represented by

$$x_{\text{Pt}} = 0.39 - 7 \times 10^{-6}(T-1000) - 5 \times 10^{-8}(T-1000)^2$$

with an uncertainty increasing from  $\pm 0.01$  at 2153 K to greater than  $\pm 0.03$  below 1400 K. The intermediate range (1553-2053 K) saturated by the A15 phase is given with an uncertainty of  $\pm 0.02$  by

$$x_{\text{Pt}} = 0.37 - 1.48 \times 10^{-5}(T-1500) - 1.1 \times 10^{-7}(T-1500)$$

The hP8 boundary saturated by MoPt<sub>2</sub> (1573-1748 K) is given by

$$x_{\text{Pt}} = 0.414 + 1.5 \times 10^{-4}(T-1500) \pm 0.03$$

The hP8 boundary saturated by MoPt is given by

$$x_{\text{Pt}} = 0.387 - 3.5 \times 10^{-5}(T-1000) + 1.8 \times 10^{-7}(T-1000)^2 \pm 0.03 \quad (1300-1573 \text{ K})$$

The MoPt boundary saturated by the hP8 phase is given by

$$x_{\text{Pt}} = 0.48 - 2.6 \times 10^{-4}(1573-T) + 2.5 \times 10^{-7}(1573-T)^2 + 2 \times 10^{-10}(1573-T)^3 \\ \pm 0.02 \quad (1200-1573 \text{ K})$$

The MoPt boundary saturated by MoPt<sub>2</sub> is given by

$$x_{\text{Pt}} = 0.48 + 1.7 \times 10^{-4}(1573-T) + 2.3 \times 10^{-7}(1573-T)^2 - 9 \times 10^{-10}(1573-T)^3 \\ \pm 0.02 \quad (1200-1573 \text{ K})$$

The MoPt<sub>2</sub> boundary saturated by MoPt is given by

$$\ln x_{\text{Mo}} = -1.775 + 390 T^{-1} + 4.2 \times 10^{-4}T \pm 0.03 \quad (1100-1573 \text{ K})$$

The MoPt<sub>2</sub> boundary saturated by the hP8 phase (1573-1748 K) is essentially constant at  $x_{\text{Mo}} = 0.42 \pm 0.02$ . The boundary saturated by the hcp phase

(1748–1873 K) varies from  $x_{\text{Mo}} = 0.42$  at 1573 K to  $x_{\text{Mo}} = 0.405$  at 1873 K, with an uncertainty of  $\pm 0.02$ . The molybdenum-rich boundary of  $\text{MoPt}_2$  saturated by fcc Pt (1873–2073 K) is given by

$$\begin{aligned} x_{\text{Mo}} &= 0.333 + 1.28 \times 10^{-3}(2073-T) - 7.6 \times 10^{-6}(2073-T)^2 \\ &\quad + 1.5 \times 10^{-8}(2073-T)^3 \pm 0.03 \end{aligned}$$

The platinum-rich boundary is given by

$$\begin{aligned} x_{\text{Mo}} &= 0.333 - 2.74 \times 10^{-4}(2073-T) + 4.07 \times 10^{-7}(2073-T)^2 \\ &\quad - 1.6 \times 10^{-10}(2073-T)^3 \pm 0.03 \quad (1100–2073 \text{ K}) \end{aligned}$$

The solidus and liquidus of fcc Pt (2073–2293 K) are given, respectively, by

$$\frac{x_{\text{Mo}}}{T-2042} = 2 \times 10^{-3} - 3.9 \times 10^{-6}(T-2042) + 7.7 \times 10^{-9}(T-2042)^2 \pm 10\%$$

and

$$\frac{x_{\text{Mo}}}{T-2042} = 5.6 \times 10^{-4} + 1.3 \times 10^{-6}(T-2042) \pm 15\%$$

The boundary saturated by the hcp phase (1873–2293 K) is given by

$$\begin{aligned} x_{\text{Mo}} &= 0.375 + 5.3 \times 10^{-4}(2293-T) - 1.5 \times 10^{-6}(2293-T)^2 \\ &\quad + 1.45 \times 10^{-9}(2293-T)^3 \pm 0.03 \end{aligned}$$

The molybdenum-rich boundary of the fcc phase saturated by  $\text{MoPt}_2$  (1873–2073 K) is given by

$$\begin{aligned} x_{\text{Mo}} &= 0.333 + 1.83 \times 10^{-3}(2073-T) - 1.1 \times 10^{-5}(2073-T)^2 \\ &\quad + 2.3 \times 10^{-8}(2073-T)^3 \pm 0.03 \end{aligned}$$

The platinum-rich fcc boundary saturated by  $\text{MoPt}_2$  is given by

$$\begin{aligned} x_{\text{Mo}} &= 0.333 - 7.4 \times 10^{-4}(2073-T) + 1.6 \times 10^{-6}(2073-T)^2 \\ &\quad - 1.22 \times 10^{-9}(2073-T)^3 \pm 0.03 \quad (1100–2073 \text{ K}) \end{aligned}$$

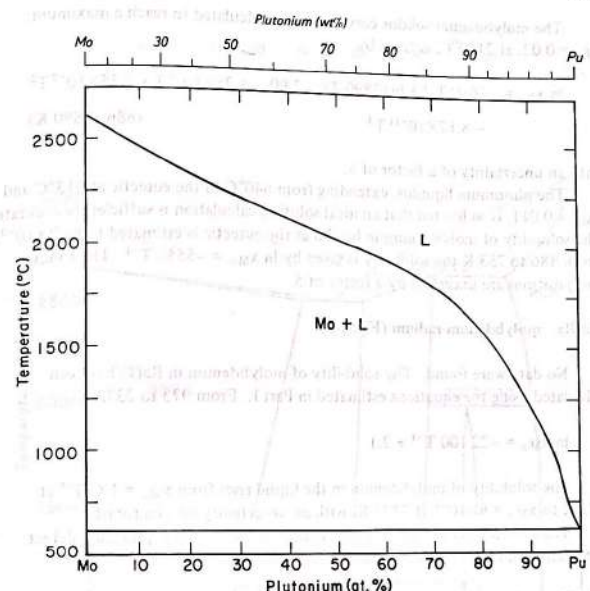


FIG.II-37. Phase diagram of the system molybdenum-plutonium.

#### Mo-Pu: molybdenum-plutonium (Fig.II-37)

Ellinger et al. [67] have summarized earlier publications [21, 169] as well as unpublished Los Alamos work on the solubility of molybdenum in plutonium liquid. Bowersox and Leary [26] have since published their Los Alamos work (700–1000°C). Figure II-37 is based on these data and the thermodynamic values of Part I.

The molybdenum liquidus curve from 613 to 2617°C is given by

$$T = \frac{5207 + 3550(1-x_{\text{Mo}})^2 - 4600(1-x_{\text{Mo}})^3}{1.79 + 0.64(1-x_{\text{Mo}})^2 - 2.13(1-x_{\text{Mo}})^3 - 0.99 \ln x_{\text{Mo}}}$$

with the uncertainty in T of the order of  $10^\circ\text{C}$ .

The molybdenum solidus curve, which is calculated to reach a maximum,  $x_{\text{Pu}} = 0.02$ , at 2100°C, is given by

$$\ln x_{\text{Pu}} = -7660 T^{-1} + \ln(2890-T) - 7.90 - 4.35 \times 10^{-4} T + 5.55 \times 10^{-7} T^2 - 8.17 \times 10^{-11} T^3 \quad (886-2890 \text{ K})$$

with an uncertainty of a factor of 5.

The plutonium liquidus, extending from 640°C to the eutectic at 613°C and  $x_{\text{Mo}} = 0.011$ , is so limited that an ideal solution calculation is sufficiently accurate. The solubility of molybdenum in bcc Pu at the eutectic is estimated to be  $2 \times 10^{-3}$ . From 886 to 753 K the solubility is given by  $\ln x_{\text{Mo}} = -5550 T^{-1}$ . The solidus compositions are uncertain by a factor of 5.

#### Mo-Ra: molybdenum-radium (Fig.II-2)

No data were found. The solubility of molybdenum in Ra( $\ell$ ) has been calculated using the equations estimated in Part I. From 973 to 2373 K

$$\ln x_{\text{Mo}} = -22100 T^{-1} + 2.1$$

The solubility of molybdenum in the liquid rises from  $x_{\text{Mo}} = 1 \times 10^{-9}$  at 973 K to  $x_{\text{Mo}} = 8 \times 10^{-4}$  at 2373 K, with an uncertainty of a factor of 5.

The solubility of radium in molybdenum is less than the quenched defect concentration and is thus not a thermodynamic quantity.

#### Mo-Rb: molybdenum-rubidium (Fig.II-2)

No data were found. The estimated thermodynamic equations of Part I have been used to calculate the liquidus from 313 to 967 K.

$$\ln x_{\text{Mo}} = -34660 T^{-1} + 2.21$$

The solubility of molybdenum in the liquid rises from  $x_{\text{Mo}} = 10^{-47}$  at 313 K to  $x_{\text{Mo}} = 3 \times 10^{-15}$  at 967 K, with an uncertainty of a factor of 5. The solubility of rubidium in molybdenum is defect-controlled.

#### Mo-Re: molybdenum-rhenium (Fig.II-38)

Dickinson and Richardson [56], Knapton [144], and Savitskij et al. [218] have independently evaluated the Mo-Re system. Knapton [144] has discussed the differences between the first two studies. Hultgren et al. [119] present additional

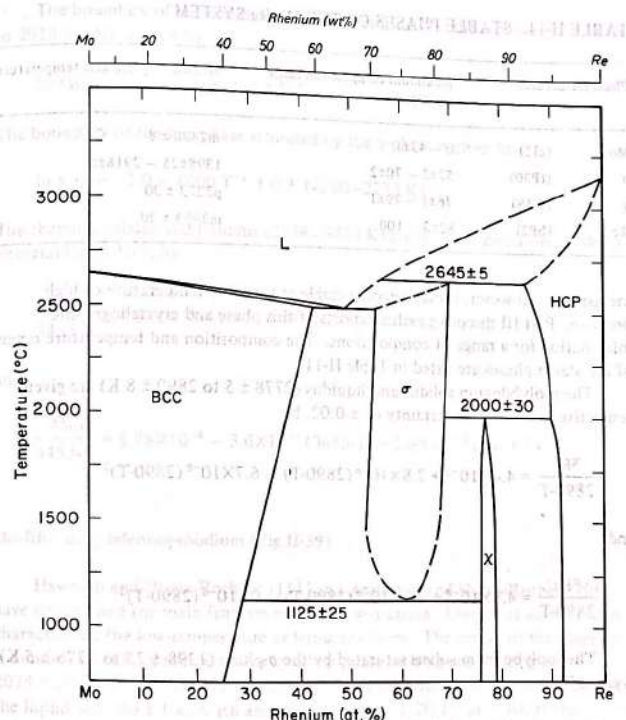


FIG.II-38. Phase diagram of the system molybdenum-rhenium.

observations up to 1967. The diagram in Fig.II-38 was selected as being consistent with the reported data within their experimental uncertainties. Matveeva et al. [172] report diffusion couple results at 1500°C which are in agreement with Fig.II-38, but with a 2 at.% higher solubility of rhenium in molybdenum and a wider homogeneous range for the  $\chi$ -phase. Savitskij et al. [215, 217] have presented additional data on the solubilities of molybdenum and rhenium in each other, and Witcomb and Dew-Hughes [262] have observations on the precipitation of the  $\sigma$ -phase. Gavalier et al. [85] report an A15-type phase which is believed to be

TABLE II-11. STABLE PHASES OF THE Mo-Re SYSTEM

Phase (structure)	Maximum composition range (at.% Re)	Melting or peritectic temperature (K)
Mo (cI2)	0 - 43±1	m2890 ± 8
$\sigma$ (tP30)	52±2 - 70±2	1398±25 - 2918±5
X (cI58)	76±1 - 79±1	p2273 ± 30
Re (hP2)	82±3 - 100	m3453 ± 20

metastable. However, it may become stable at very low temperature or high pressure. Part III discusses earlier reports of this phase and crystallographic information for a range of compositions. The composition and temperature ranges of the stable phases are listed in Table II-11.

The molybdenum solidus and liquidus ( $2778 \pm 5$  to  $2890 \pm 8$  K) are given, respectively, with an uncertainty of  $\pm 0.02$ , by

$$\frac{x_{\text{Re}}}{2890-\text{T}} = 4.4 \times 10^{-3} + 2.8 \times 10^{-6}(2890-\text{T}) - 6.7 \times 10^{-8}(2890-\text{T})^2$$

and

$$\frac{x_{\text{Re}}}{2890-\text{T}} = 4.8 \times 10^{-3} + 5.8 \times 10^{-6}(2890-\text{T}) - 9 \times 10^{-8}(2890-\text{T})^2$$

The molybdenum solvus saturated by the  $\sigma$ -phase ( $1398 \pm 25$  to  $2778 \pm 5$  K) is given by

$$\ln x_{\text{Re}} = -2.18 + 0.2 \ln \text{T} - 733 \text{T}^{-1} \pm 0.04$$

The molybdenum solvus saturated by the X-phase is given by

$$\ln x_{\text{Re}} = -0.61 - 865 \text{T}^{-1} \pm 0.1 \quad (1100-1398 \text{ K})$$

Table II-11 gives the compositions of the  $\sigma$ -phase at the eutectic temperature of  $2778 \pm 5$  K with molybdenum and at its peritectic. The homogeneous range must decrease with decreasing temperature, but the available observations indicate only a very small change until below 1700 K. The X-phase expands from a homogeneous range of 1.5 at.% at 1800 K to 3 at.% at 1500 K and is expected to decrease at lower temperatures.

## PART II. PHASE DIAGRAMS

The boundary of the hcp rhenium phase saturated by the  $\sigma$ -phase ( $2273 \pm 30$  to  $2918 \pm 5$  K) is given by

$$\ln x_{\text{Mo}} = -0.22 - 5000 \text{T}^{-1} \pm 0.2$$

The boundary of the hcp phase saturated by the X-phase is given by

$$\ln x_{\text{Mo}} = -2.0 - 1000 \text{T}^{-1} \pm 0.3 \quad (1200-2273 \text{ K})$$

The rhenium solidus and liquidus (2918-3453 K) are given, respectively, with an uncertainty of 10%, by

$$\frac{x_{\text{Mo}}}{3453-\text{T}} = 3.8 \times 10^{-4} - 1.7 \times 10^{-7}(3453-\text{T}) + 1.7 \times 10^{-10}(3453-\text{T})^2$$

and

$$\frac{x_{\text{Mo}}}{3453-\text{T}} = 8.78 \times 10^{-4} - 3.6 \times 10^{-7}(3453-\text{T}) + 2.6 \times 10^{-10}(3453-\text{T})^2$$

## Mo-Rh: molybdenum-rhodium (Fig.II-39)

Haworth and Hume-Rothery [111] and Anderson and Hume-Rothery [9] have determined the main features of the phase diagram. Giessen et al. [87] have characterized the low-temperature ordering reactions. The centre of the diagram is dominated at high temperatures by a hcp phase melting congruently at  $2075 \pm 10^\circ\text{C}$ , with a maximum extent of 43-82 at.% Rh. It is in equilibrium with the liquid with  $40 \pm 1$  at.% Rh and with bcc Mo with  $20 \pm 1$  at.% Rh at the eutectic temperature of  $1940 \pm 15^\circ\text{C}$ . The melting point of fcc Rh is increased by adding molybdenum to a maximum concentration of  $15 \pm 1$  at.% Mo at the peritectic temperature of  $2000 \pm 10^\circ\text{C}$ . The hcp phase undergoes a peritectoid decomposition at  $1100 \pm 100^\circ\text{C}$  to Rh and to the ordered phase  $\text{MoRh}_3$ , which probably has a range of 1 at.% on either side of 75 at.% Rh. At  $1000 \pm 100^\circ\text{C}$ , the hcp phase undergoes a peritectoid decomposition to  $\text{MoRh}_3$  and  $\text{MoRh}_{(0)4}$ , which also probably has a narrow range of about 1 at.% on each side of 50 at.% Rh. The order-disorder transformation of the disordered hcp phase to the ordered  $\text{MoRh}_3$  phase takes place at  $1200 \pm 200^\circ\text{C}$ .

The miscibility gap between the hcp and ccp phases widens only very slowly with decreasing temperature until precipitation of  $\text{MoRh}_3$  near  $1100^\circ\text{C}$ . At lower temperatures the molybdenum content of the fcc phase drops much more rapidly.

The rhodium-rich boundaries of the hcp phase between 2273 and 2348 K, with an uncertainty of  $\pm 0.02$ , are given by

$$x_{\text{Mo}} = 0.345 - 1.38 \times 10^{-2}(2348-T) + 3.24 \times 10^{-4}(2348-T)^2 - 2.24 \times 10^{-6}(2348-T)^3$$

for the liquidus and

$$x_{\text{Mo}} = 0.345 - 2.1 \times 10^{-3}(2348-T)$$

for the solidus. The boundary of the hcp phase saturated by bcc Mo between 1323 and 2213 K is given by

$$x_{\text{Rh}} = 0.697 - 7.1 \times 10^{-4}(T-1000) + 5.97 \times 10^{-7}(T-1000)^2 - 1.56 \times 10^{-10}(T-1000)^3$$

with an uncertainty of  $\pm 0.01$  at higher temperatures and increasing to  $\pm 0.05$  at the lower temperatures. The hcp solvus saturated by fcc Rh (1373  $\pm$  100 to 2273  $\pm$  10 K) is given by

$$x_{\text{Mo}} = 0.09 - 10^{-5}(2273-T) \pm 0.01$$

The molybdenum solvus saturated by the hcp phase (1323  $\pm$  75 to 2213  $\pm$  15 K) is given by

$$\ln x_{\text{Rh}} = -3.64 + 1.46 \times 10^{-3}T - 2600 T^{-1}$$

with an uncertainty in  $x_{\text{Rh}}$  of  $\pm 10\%$ . The molybdenum solidus and liquidus (2213–2890 K) are given, with an uncertainty in  $x_{\text{Rh}}$  of 5%, by

$$\frac{x_{\text{Rh}}}{2890-T} = 2.5 \times 10^{-4} - 3.7 \times 10^{-8}(2890-T) + 1.5 \times 10^{-10}(2890-T)^2 - 5.2 \times 10^{-13}(2890-T)^3$$

for the solidus and

$$\frac{x_{\text{Rh}}}{2890-T} = 4.8 \times 10^{-4} + 1.6 \times 10^{-7}(2890-T)$$

for the liquidus.

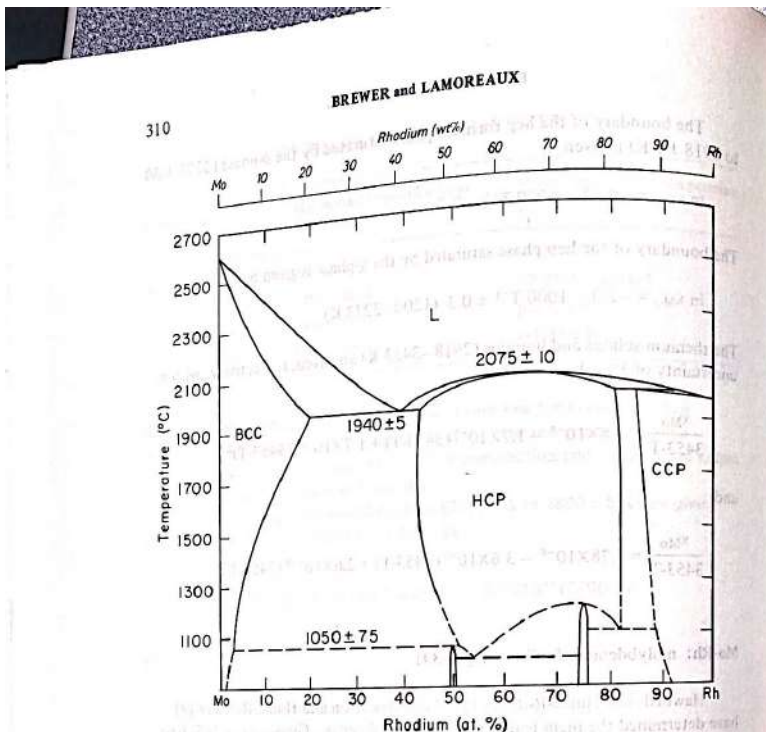


FIG.JI-39. Phase diagram of the system molybdenum-rhodium.

The molybdenum-rich boundary of the hcp phase with 43.5 at.% Rh at the eutectic temperature goes to 43 at.% Rh at 1500°C and then increases to more than 50 at.% Rh at the peritectoid. The liquidus of the hcp phase is given by

$$x_{\text{Rh}} = 0.655 - 9.13 \times 10^{-3}(2348-T) + 1.24 \times 10^{-4}(2348-T)^2 - 5.2 \times 10^{-7}(2348-T)^3 \pm 0.02 \quad (2213-2348 \text{ K})$$

for the molybdenum-rich portion of the boundary. The corresponding solidus of the hcp phase is given by

$$x_{\text{Rh}} = 0.655 - 4.6 \times 10^{-3}(2348-T) + 4.6 \times 10^{-5}(2348-T)^2 - 1.77 \times 10^{-7}(2348-T)^3 \pm 0.02 \quad (2213-2348 \text{ K})$$

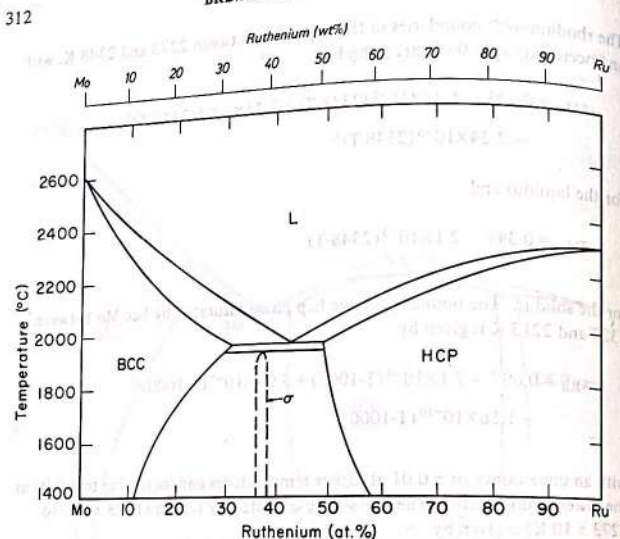


FIG.II-40. Phase diagram of the system molybdenum-ruthenium.

## Mo-Rn: molybdenum-radon (Fig.II-4)

No experimental data were found; see Mo-Ar for details of the calculation of Fig.II-4. The mole fraction of radon in liquid molybdenum at 2890 K, saturated with 1 atm gas, is calculated to be  $6 \times 10^{-20}$ .

## Mo-Ru: molybdenum-ruthenium (Fig.II-40)

Anderson and Hume-Rothery [10] have reviewed earlier observations and have extended the diagram to the liquidus.  $\text{Mo}_5\text{Ru}_3$ (tP30), the only intermediate phase, is formed by a peritectoid reaction at  $1920 \pm 20^\circ\text{C}$  and extends from 35 to 38 at.% Ru. At the eutectic temperature of  $1945 \pm 20^\circ\text{C}$ , the liquid with  $41.6 \pm 0.5$  at.% Ru is in equilibrium with bcc Mo with  $30 \pm 1$  at.% Ru and with hcp Ru with  $50 \pm 2$  at.% Mo.

The molybdenum liquidus and solidus ( $2218$ – $2890$  K) are given, respectively, by

$$\frac{x_{\text{Ru}}}{2890-\text{T}} = 3.35 \times 10^{-4} + 7.3 \times 10^{-7}(2890-\text{T}) - 4.5 \times 10^{-10}(2890-\text{T})^2 \pm 7\%$$

and

$$\frac{x_{\text{Ru}}}{2890-\text{T}} = 2.07 \times 10^{-4} + 2.7 \times 10^{-7}(2890-\text{T}) + 1.2 \times 10^{-10}(2890-\text{T})^2 \pm 5\%$$

The ruthenium liquidus and solidus ( $2218$ – $2603$  K) are given, respectively, by

$$\frac{x_{\text{Mo}}}{2603-\text{T}} = 3.6 \times 10^{-3} - 1.09 \times 10^{-5}(2603-\text{T}) + 1.43 \times 10^{-8}(2603-\text{T})^2 \pm 10\%$$

and

$$\frac{x_{\text{Mo}}}{2603-\text{T}} = 2.84 \times 10^{-3} - 7.54 \times 10^{-6}(2603-\text{T}) + 9.3 \times 10^{-9}(2603-\text{T})^2 \pm 10\%$$

The solvus boundary of molybdenum is given by

$$x_{\text{Ru}} = 0.080 + 10^{-4}(\text{T}-1500) + 2.7 \times 10^{-7}(\text{T}-1500)^2 \pm 0.01 \quad (1500-2193 \text{ K})$$

The solvus boundary of ruthenium is given by

$$x_{\text{Mo}} = 0.378 + 3.3 \times 10^{-4}(\text{T}-1500) - 2.2 \times 10^{-7}(\text{T}-1500)^2 \pm 0.01 \quad (1500-2193 \text{ K})$$

## Mo-S: molybdenum-sulphur (Fig. II-41)

There are two stable phases,  $\text{Mo}_2\text{S}_3$ (mP10) and  $\text{MoS}_2$ (hP6).  $\text{MoS}_2$ (hR3) is a metastable phase with a structure close to hP6. Clark [53] reports that it is richer in molybdenum than  $\text{MoS}_2$ (hP6); it may be stable at higher pressures. Various compositions between  $\text{MoS}_2$  and  $\text{Mo}_2\text{S}_3$  have been prepared by decomposition of sulphomolybdates. Mering and Levialdi [175] have shown that these higher sulphides have essentially the hP6 structure, with expansion and distortion of the lattice up to  $\text{MoS}_{2.59}$ . Amorphous phases are obtained with higher sulphur contents. Biltz and Köcher [18] demonstrated their metastability by showing that their decomposition could not be prevented by high sulphur pressures. Schaefer et al. [219] have established that the equilibrium homogeneous range of  $\text{MoS}_2$  extends to  $\text{MoS}_{2.2}$  at  $1100^\circ\text{C}$ . The sulphur pressure in atmospheres

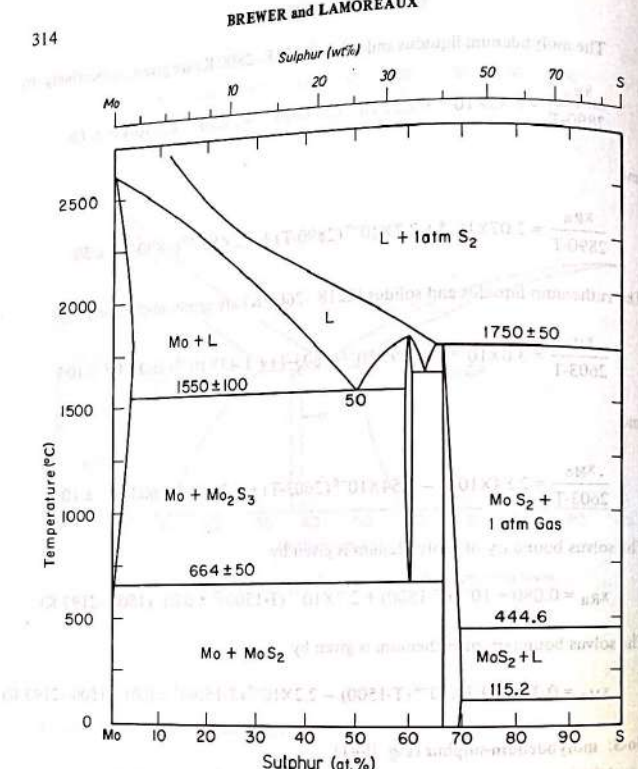


FIG.II-41. Phase diagram of the system molybdenum-sulfur.

in equilibrium with  $\text{MoS}_2+x$  at 1100°C was found to be  $\ln P = -7.83 + 28.16 x$  for  $0.02 < x < 0.23$ .

Chevrel et al. [47] have prepared  $\text{Mo}_3\text{S}_4$  (hR14) by acid extraction of the ternary compounds  $\text{M}_x\text{Mo}_3\text{S}_4$ . It could not be prepared from the elements and decomposes upon heating. It is not a stable phase in the binary system [76].

Stempok and Kullerud [240] present Bi-Mo-S and Fe-Mo-S diagrams, with  $\text{Mo}_2\text{S}_3$  unstable below 610°C, based on the observations of Morimoto and Kullerud [176] that a mixture of the elements forms only  $\text{Mo} + \text{MoS}_2$  until

$610 \pm 5^\circ\text{C}$  is reached, when  $\text{Mo}_2\text{S}_3$  appears. Starting with  $\text{Mo} + \text{MoS}_2$ ,  $\text{Mo}_2\text{S}_3$  cannot be obtained even after a month at 650°C nor can it be decomposed upon heating for a month at 600°C. Morimoto and Kullerud found that even above 900°C up to a week is required to attain equilibrium. These observations, which confirm that  $\text{Mo}_2\text{S}_3$  is stable with respect to the elements at 610°C (and at all other temperatures between 0 K and the melting point), do not clearly fix the stability of  $\text{Mo}_2\text{S}_3$  with respect to disproportionation to  $\text{Mo} + \text{MoS}_2$  at temperatures below 800°C. The observation by Pouillard and Perrot [193] that the  $\text{H}_2\text{S}/\text{H}_2$  ratios in equilibrium with  $\text{Mo} + \text{MoS}_2$  and  $\text{Mo}_2\text{S}_3 + \text{MoS}_2$  between 760 and 1000°C extrapolate to equal values at 664°C seems to be more definitive but, as discussed in Part I, it is considerably uncertain because of the difficulty of reaching equilibrium. The disproportionation temperature was selected as  $627 \pm 40^\circ\text{C}$ . McCabe [165] reports an analysis corresponding to  $\text{Mo}_{2.06}\text{S}_3$ , but he indicates that the 3% deviation from stoichiometry could be within experimental error. Morimoto and Kullerud [176] also report the composition  $\text{Mo}_{2.06}\text{S}_3$  and no detectable change in the X-ray pattern across the homogeneous range at 935°C. At 1100°C, a sample of 60.5 at.% S showed two phases [219]. At the eutectic temperatures of 1550–1630°C, where the range would be largest, it would be expected to be less than 59–60.5 at.% S.

Cannon [39] has presented evidence that earlier reported melting points of  $\text{MoS}_2$  were too low and that the melting point is over 1800°C. The thermodynamic values given in Part I indicate that  $4 \pm 2$  atm  $\text{S}_2$  gas would be required to prevent the decomposition of  $\text{MoS}_2$  to a liquid poorer in sulphur at 1900°C. With 1 atm  $\text{S}_2$ ,  $\text{MoS}_2$  is calculated to decompose at  $1750 \pm 50^\circ\text{C}$  to a liquid with 65 at.% S. Other high-temperature studies are those of Zelikman and Belyaevskaya [274], Gorokh et al. [98] and Eremenko et al. [69]. Flükiger et al. [76] have established that  $\text{Mo}_2\text{S}_3$  melts congruently around 1800°C and forms eutectics with both Mo and  $\text{MoS}_2$ . The  $\text{MoS}_2$ - $\text{Mo}_2\text{S}_3$  eutectic at  $1630 \pm 50^\circ\text{C}$  and 63 at.% S and the  $\text{Mo}-\text{Mo}_2\text{S}_3$  eutectic at  $1550 \pm 100^\circ\text{C}$  and 50 at.% S are consistent with the thermodynamic data of Part I and the literature cited above. The  $\text{Mo}_2\text{S}_3$  liquidus is given for 1825–2080 K and  $x_S = 0.5$  to 0.6 by

$$x_S = 0.60 - 2.7 \times 10^{-4}(2080-T) - 5 \times 10^{-7}(2080-T)^2 \pm 0.02 \quad (1825-2080 \text{ K})$$

and for 1900–2080 K and  $x_S = 0.6$  to 0.63 by

$$x_S = 0.60 + 1.4 \times 10^{-4}(2080-T) \pm 0.02 \quad (1900-2080 \text{ K})$$

The  $\text{MoS}_2$  liquidus is given by

$$x_S = 0.667 - 1.7 \times 10^{-4}(2180-T) + 9 \times 10^{-8}(2180-T)^2 \pm 0.02 \quad (1900-2180 \text{ K})$$

The molybdenum liquidus is given by

$$x_S = 6.8 \times 10^{-4} (2890-T) - 3.88 \times 10^{-7} (2890-T)^2 + 2.68 \times 10^{-10} (2890-T)^3 - 8.3 \times 10^{-14} (2890-T)^4 \pm 0.03 \quad (1825-2890 \text{ K})$$

Schaefer et al. [219] report that molybdenum saturated with  $\text{Mo}_2\text{S}_3$  at 1100°C has  $x_S = 0.015$ . For the temperature range 900–1825 K, the molybdenum solvus is given by

$$\ln x_S = -5900 T^{-1} + 0.1 \pm 0.09$$

with  $x_S$  varying from 0.002 at 900 K to 0.04 at 1825 K. Above 1825 K, the molybdenum solidus is given by

$$x_S = 8.8 \times 10^{-5} (2890-T) - 3.72 \times 10^{-8} (2890-T)^2 - 1.19 \times 10^{-11} (2890-T)^3 \pm 0.005 \quad (1825-2890 \text{ K})$$

$x_S$  is calculated to reach a maximum of 0.042 at 2065 K. The liquid boundary saturated by 1 atm  $\text{S}_2$  gas is calculated to be

$$x_{\text{Mo}} = 0.314 + 7.36 \times 10^{-4} (T-2000) - 1.36 \times 10^{-7} (T-2000)^2 \pm 0.05 \quad (2020-3000 \text{ K})$$

#### Mo-Sb: molybdenum-antimony (Fig. II-42)

A single intermediate phase  $\text{Mo}_3\text{Sb}_7$  (cI40) exists in the system. Part III reviews the literature related to its crystal structure. Boller and Nowotny [22] and Jensen et al. [126] provide fragmentary phase diagram information which indicates that  $\text{Mo}_3\text{Sb}_7$  is stable with respect to  $\text{Mo}(s)$  and  $\text{Sb}(l)$  at  $650 \pm 20^\circ\text{C}$ , but has become unstable at  $800^\circ\text{C}$ .

From the thermodynamic data estimated in Part I, the molybdenum liquidus curve is given by

$$\ln x_{\text{Mo}} = -13000 T^{-1} + 1.2 \pm 1 \quad (1053-1862 \text{ K})$$

The liquidus is terminated at 1862 K where solid molybdenum is in equilibrium with liquid,  $x_{\text{Mo}} = 3 \times 10^{-3}$ , and antimony vapour at 1 atm containing about 12 mol%  $\text{Sb}_4$ , 83 mol%  $\text{Sb}_2$  and 5 mol% Sb. The molybdenum concentration

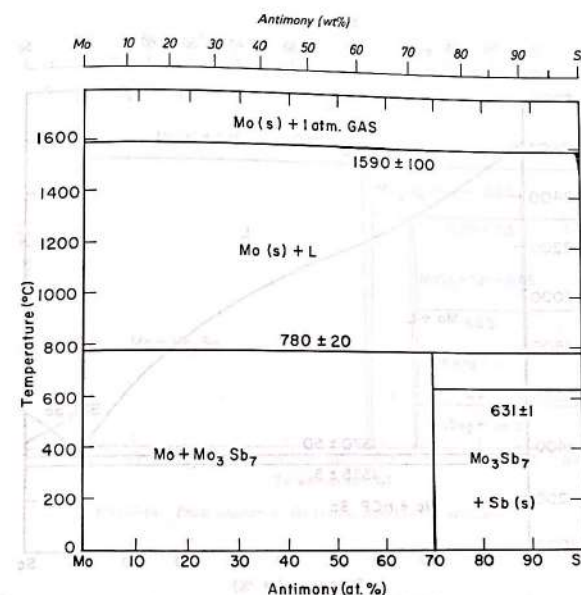


FIG.II-42. Phase diagram of the system molybdenum-antimony.

of the solid solution  $\text{Mo}_3\text{Sb}_7$  drops with decreasing temperature to 1053 K where Mo and  $\text{Mo}_3\text{Sb}_7$  solids are in equilibrium with  $x_{\text{Mo}} = 1.4 \times 10^{-5}$  liquid. The  $\text{Mo}_3\text{Sb}_7$  liquidus is given by

$$\ln x_{\text{Mo}} = -19700 T^{-1} + 7.53 \pm 1 \quad (904-1053 \text{ K})$$

Solid Sb and  $\text{Mo}_3\text{Sb}_7$  are in equilibrium with the eutectic liquid,  $x_{\text{Mo}} = 10^{-6}$ , at 904 K. The estimated solid solubilities are smaller than the defect concentrations.

#### Mo-Sc: molybdenum-scandium (Fig. II-43)

The only observation found in the literature was that of Taylor [245] who reports the solubility of scandium in molybdenum at 1900 K to be less than

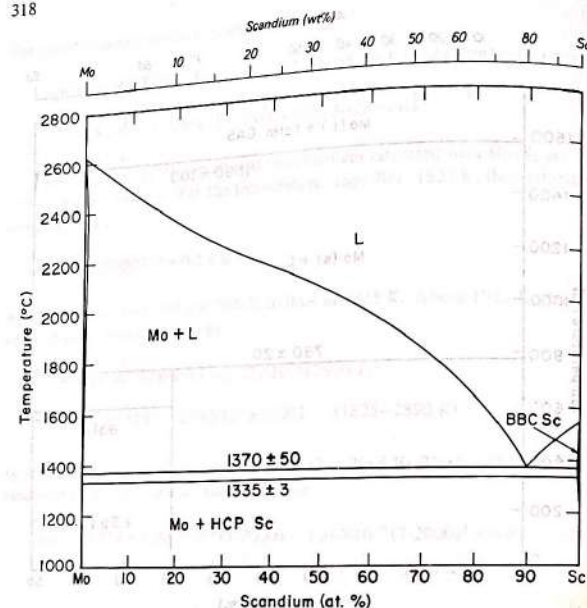


FIG.II-43. Phase diagram of the system molybdenum-scandium.

1 ppm. A comparison with the solidus determined for gadolinium and other metals indicates that this limit is much too low, and it was discarded. The diagram in Fig. II-43 is based upon the thermodynamic equations obtained from bonding considerations that are tabulated in Part I.

The molybdenum solidus from 2890 to 1645 K is given by

$$x_{Sc} = 3.44 \times 10^{-6}(2890-T) - 4.83 \times 10^{-8}(2890-T)^2 + 1.79 \times 10^{-11}(2890-T)^3$$

The mole fraction of scandium, which is uncertain by a factor of 1.5, is calculated to increase to a maximum value of 0.007 at 2400 K and then to drop off to 0.002 at 1645 K. The molybdenum liquidus from 2890 to 1645 K is given by

$$x_{Sc} = 6.25 \times 10^{-4}(2890-T) + 7.76 \times 10^{-7}(2890-T)^2 - 5.62 \times 10^{-10}(2890-T)^3$$

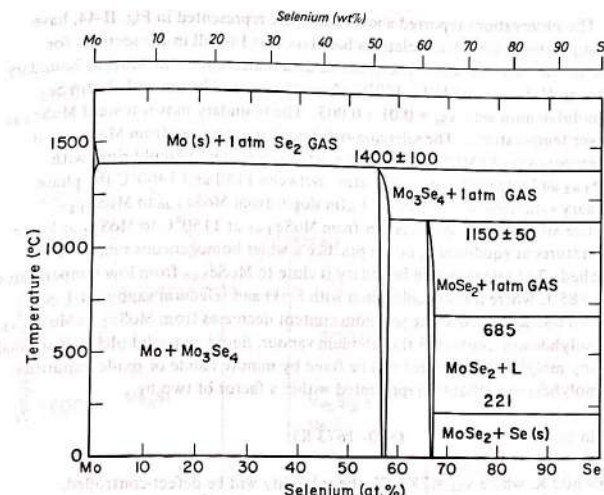


FIG.II-44. Phase diagram of the system molybdenum-selenium.

The uncertainty, which is  $\pm 0.01$  between 2890 and 2500 K, gradually increases with decreasing temperature and becomes  $\pm 0.09$  at 1645 K.

On the scandium-rich side, the mole fraction of molybdenum in bcc Sc is calculated to be  $0.002 \pm 0.001$  at 1725 K, in equilibrium with  $x_{Mo} = 0.05 \pm 0.01$  liquid and  $x_{Mo} = 0.004 \pm 0.002$  at the eutectic temperature of  $1645 \pm 50$  K, in equilibrium with  $x_{Mo} = 0.1 \pm 0.03$  liquid.

#### Mo-Se: molybdenum-selenium (Fig. II-44)

Spiesser et al. [233] have reviewed the earlier literature of the Mo-Se system and have presented their results on the phase regions  $MoSe_{2-x}(hP6)$  and  $Mo_{3}Se_{4+x}(hR14)$ . Towle et al. [252] have reported  $MoSe_2$  to be isostructural with  $Mo_2S_2(hR3)$  and produced at 40 kbar and 1500°C. Bars et al. [13] have given structural information for  $Mo_{3}Se_{4+x}(hR14)$ . Glazunov et al. [90] have measured the dissociation pressure of  $MoSe_2$  between 1233 and 1353 K. The solubility of selenium in molybdenum is discussed in Part I.

The observations reported above, which are represented in Fig. II-44, have been supplemented with calculations based on Part I to fill in the sections for which no data are available. The available data indicate that the  $\text{Mo}_3\text{Se}_4$  boundary is close to  $\text{MoSe}_{1.27}$  at  $1400 \pm 100^\circ\text{C}$  where it is in equilibrium with 1 atm  $\text{Se}_2$  and molybdenum with  $x_{\text{Se}} = 0.01 \pm 0.005$ . The boundary moves toward  $\text{MoSe}_{1.33}$  at lower temperatures. The selenium-rich boundary increases from  $\text{MoSe}_{1.34}$  at low temperatures to  $\text{MoSe}_{1.40}$  at  $1150 \pm 50^\circ\text{C}$  where it is in equilibrium with  $\text{MoSe}_{1.93}$  and selenium vapour at 1 atm. Between  $1150$  and  $1400^\circ\text{C}$  the phase boundary saturated with vapour at 1 atm slopes from  $\text{MoSe}_{1.40}$  to  $\text{MoSe}_{1.27}$ .

The  $\text{MoSe}_2$  boundary increases from  $\text{MoSe}_{1.93}$  at  $1150^\circ\text{C}$  to  $\text{MoSe}_2$  at lower temperatures at equilibrium, but in practice a wider homogeneous range will be quenched. The selenium-rich boundary is close to  $\text{MoSe}_{2.00}$  from low temperatures up to  $685^\circ\text{C}$  where it is in equilibrium with  $\text{Se}(\text{l})$  and selenium vapour at 1 atm. Between  $685$  and  $1150^\circ\text{C}$  the selenium content decreases from  $\text{MoSe}_2$  to  $\text{MoSe}_{1.93}$ . The molybdenum content in the selenium vapour, liquid and solid phases is so small that any molybdenum content will be fixed by minute halide or oxide impurities. The molybdenum solidus is represented within a factor of two by

$$\ln x_{\text{Se}} = -7700 T^{-1} \quad (800-1673 \text{ K})$$

Below  $800 \text{ K}$ , where  $x_{\text{Se}} = 7 \times 10^{-5}$ , the solubility will be defect-controlled. Figure II-44 represents the 1-atm diagram. The work of Flükiger et al. [76] indicates that at higher pressures of selenium vapour, used to prevent dissociation, eutectics are formed between Mo and  $\text{Mo}_3\text{Se}_4$  and between  $\text{Mo}_3\text{Se}_4$  and  $\text{MoSe}_2$ , with congruent melting points of  $1600-1700^\circ\text{C}$ .

#### Mo-Si: molybdenum-silicon (Fig. II-45)

Part III summarizes the crystallographic data for the four phases  $\text{Mo}_3\text{Si}(\text{cP}8)$ ,  $\text{Mo}_5\text{Si}_3(\text{tI}32)$ ,  $\text{MoSi}_2(\text{tI}6)$  and  $\text{MoSi}_2(\text{hP}9)$ .

Hultgren et al. [119] have presented a phase diagram based on a review of the literature to 1968. Chart [45] has considered more recent work, particularly that of Kocherzhinskij [146] and Svechnikov et al. [243]. The diagram given by Chart has been used in Fig. II-45, and the observation of Nechiporenko et al. [177] that  $\text{MoSi}_2(\text{tI}6)$  has a homogeneous range of several per cent at  $1200-1500^\circ\text{C}$  which increases with temperature has also been taken into account. A high-temperature form  $\text{MoSi}_2(\text{hP}9)$ , which undergoes a eutectoidal decomposition to  $\text{MoSi}_2(\text{tI}6)$  and  $\text{Mo}_5\text{Si}_3(\text{tI}32)$  upon cooling below  $1850 \pm 20^\circ\text{C}$  and thus must have a lower silicon content than the low-temperature modification, is reported in Refs [146, 243]. The eutectoid line is not shown in Fig. II-45 as it lies too close to the eutectic line at  $1900^\circ\text{C}$ . Both  $\text{Mo}_3\text{Si}(\text{cP}8)$  and  $\text{Mo}_5\text{Si}_3(\text{tI}32)$  are believed to have narrow homogeneous ranges, but the reported composition [159] of  $\text{Mo}_5\text{Si}_3$  is 2.5 at.-%

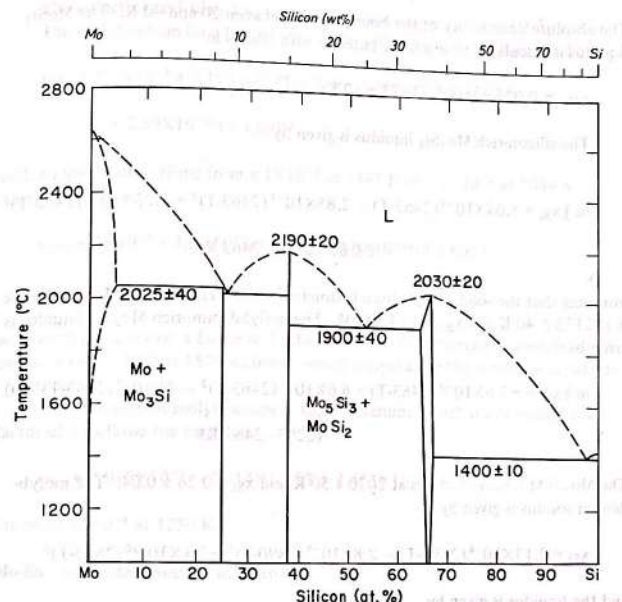


FIG. II-45. Phase diagram of the system molybdenum-silicon.

higher in silicon than the stoichiometric composition. The solubility of silicon in molybdenum is based on the measurements of Lassner et al. [159] which extend from 0.3 wt% Si at  $1300^\circ\text{C}$  to 1.5 wt% Si at  $2200^\circ\text{C}$ .

The silicon-rich  $\text{MoSi}_2$  liquidus calculated from the thermodynamic data of Part I is fitted by

$$\ln 3x_{\text{Mo}} = -6.44 \times 10^{-3}(2303-T) + 1.105 \times 10^{-5}(2303-T)^2 - 1.26 \times 10^{-8}(2303-T)^3$$

to better than 9% in the range  $1673-2303 \text{ K}$ . The molybdenum-rich liquidus is given by

$$\ln 3x_{\text{Mo}} = 0.0107(2303-T) - 1.15 \times 10^{-4}(2303-T)^2 + 4.1 \times 10^{-7}(2303-T)^3 \pm 0.09 \quad (2173-2303 \text{ K})$$

The absolute uncertainty of the boundaries is between 20 and 40 K. The  $\text{MoSi}_2$  liquidus is calculated to reach the eutectic with silicon at

$$x_{\text{Mo}} = 0.021 \pm 0.005 \quad (1673 \pm 10 \text{ K})$$

The silicon-rich  $\text{Mo}_5\text{Si}_3$  liquidus is given by

$$\ln \frac{1}{2} x_{\text{Si}} = 5.04 \times 10^{-3} (2463 - T) - 2.85 \times 10^{-5} (2463 - T)^2 + 5.25 \times 10^{-8} (2463 - T)^3 \\ \pm 0.08 \quad (2173 - 2463 \text{ K})$$

assuming that the solid composition is stoichiometric. The  $\text{Mo}_5\text{Si}_3$ - $\text{MoSi}_2$  eutectic is at  $2173 \pm 40$  K and  $x_{\text{Si}} = 0.53 \pm 0.04$ . The molybdenum-rich  $\text{Mo}_5\text{Si}_3$  liquidus is given by

$$\ln \frac{1}{2} x_{\text{Si}} = -7.6 \times 10^{-3} (2463 - T) + 6.6 \times 10^{-5} (2463 - T)^2 - 2 \times 10^{-7} (2463 - T)^3 \pm 0.1 \\ (2293 - 2463 \text{ K})$$

The  $\text{Mo}_3\text{Si}$ - $\text{Mo}_5\text{Si}_3$  eutectic is at  $2020 \pm 50$  K and  $x_{\text{Si}} = 0.26 \pm 0.04$ . The molybdenum solidus is given by

$$x_{\text{Si}} = 2.13 \times 10^{-4} (2890 - T) - 2.8 \times 10^{-7} (2890 - T)^2 + 2.1 \times 10^{-10} (2890 - T)^3$$

and the liquidus is given by

$$x_{\text{Si}} = 7.32 \times 10^{-4} (2890 - T) - 8.5 \times 10^{-7} (2890 - T)^2 + 5.76 \times 10^{-10} (2890 - T)^3$$

The uncertainty in  $x_{\text{Si}}$  is  $\pm 40\%$  for both the solidus and liquidus in the range 2890 K to the  $\text{Mo}_3\text{Si}$  peritectic at  $2298 \pm 40$  K, with  $x_{\text{Si}} = 0.255 \pm 0.05$  for the liquid and  $x_{\text{Si}} = 0.07 \pm 0.04$  for the solid. The uncertainties cited reflect in part the conclusion from the thermodynamic treatment of Part I that the phase diagram of Hultgren et al. [119], which shows a Mo- $\text{Mo}_3\text{Si}$  eutectic rather than the  $\text{Mo}_3\text{Si}$ - $\text{Mo}_5\text{Si}_3$  eutectic from Chart [45] shown in Fig. II-45, is more consistent with reasonable thermodynamic values.

#### Mo-Sm: molybdenum-samarium (Fig. II-2)

No data were found. The estimated thermodynamic equations of Part I have been used to calculate the phase boundaries of Fig. II-2.

#### PART II. PHASE DIAGRAMS

The eutectic is calculated to be at 1341 K and  $x_{\text{Mo}} = (3 \pm 1) \times 10^{-3}$ . The molybdenum liquidus between 1341 and 2064 K is calculated to be

$$x_{\text{Mo}} = 2.2 \times 10^{-3} + 1.19 \times 10^{-5} (T - 1300) + 3.88 \times 10^{-8} (T - 1300)^2 \\ + 2.59 \times 10^{-11} (T - 1300)^3$$

with an uncertainty rising from  $\pm 1 \times 10^{-3}$  at 1341 K to  $\pm 1 \times 10^{-2}$  at 2064 K. Along the solidus,

$$x_{\text{Sm}} = 2 \times 10^{-5} + 1.3 \times 10^{-7} (T - 1300) + 4.0 \times 10^{-10} (T - 1300)^2 \\ + 8.3 \times 10^{-13} (T - 1300)^3$$

with an uncertainty of a factor of 5. The solubility of samarium in molybdenum drops to  $x_{\text{Sm}} = 10^{-4}$  at 1575 K, below which temperature the solubility is defect-controlled.

The solubility of molybdenum in solid samarium, which is uncertain by a factor of 5, follows the equation

$$x_{\text{Mo}} = 2.918 \times 10^{-3} - 5.314 \times 10^{-6} T + 2.453 \times 10^{-9} T^2$$

dropping to  $10^{-4}$  at 1250 K.

#### Mo-Sn: molybdenum-tin (Fig. II-46)

Brown [35] has been able to overcome the inertness of tin-coated molybdenum by mixing molybdenum powder with 75 at.% tin in evacuated vitrosil ampoules that were simultaneously heated and shaken at temperatures of 600–900°C for 24 hours [36]. Single crystals of  $\text{MoSn}_2$ (hP6) were obtained at 600°C. At 900°C, no  $\text{MoSn}_2$  remained, but X-ray powder patterns indicated a phase with a tetragonal P4/mmb structure similar to  $\text{U}_3\text{Si}_2$ (tP4). It was not possible to distinguish between the compositions  $\text{Mo}_2\text{Sn}_3$  and  $\text{Mo}_3\text{Sn}_2$ . At 900°C, traces of a third unidentified phase were also observed.

Killpatrick [140] prepared the A15-type phase  $\text{Mo}_3\text{Sn}$ (cP8) at temperatures above 1000°C and at 35 kbar and found the phase boundary to have a slope of 30°/kbar. An extrapolation to 1 atm indicates a peritectic temperature of  $300 \pm 100$ °C.

Aleksandrov et al. [4] report less than  $5 \times 10^{-3}$  wt% Mo in liquid tin at 1450°C. The liquidus of Fig. II-46 is based mainly on the larger solubility measurements of Allen [7] between 1200 and 2000°C. The molybdenum liquidus is given by

$$\ln x_{\text{Mo}} = -0.41 - 12.700 T^{-1} + 3.44 \times 10^{-4} T \pm 0.3 \quad (1473 - 2879 \text{ K})$$

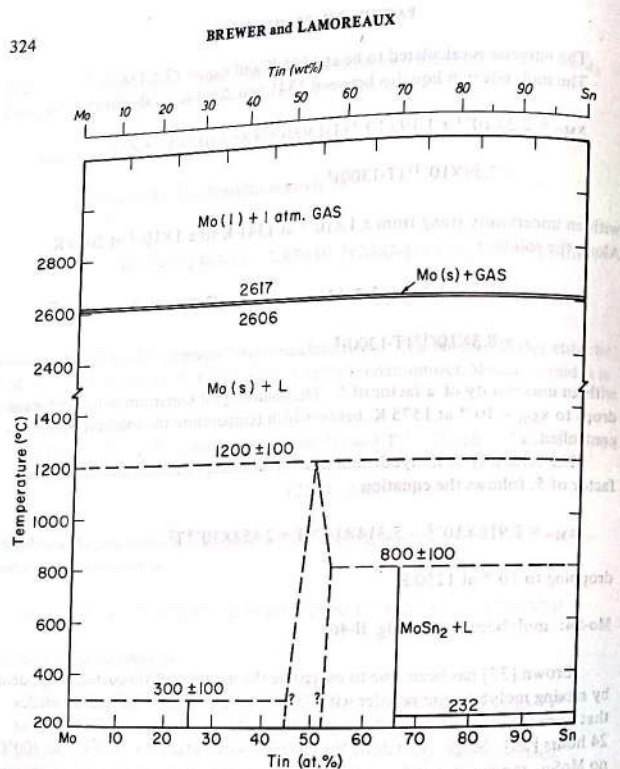


FIG.II-46. Phase diagram of the system molybdenum-tin.

At 2879 K, 1 atm Sn gas is in equilibrium with  $x_{\text{Mo}} = 0.02$  liquid and with  $x_{\text{Sn}} = 3 \times 10^{-3}$  solid molybdenum. The order of magnitude of the solubility of tin in solid molybdenum is calculated from the estimated thermodynamic enthalpy of solution from Part I to be

$$\ln x_{\text{Sn}} = -17000 T^{-1} \quad (1800-2879 \text{ K})$$

Below 1800 K the solubility is defect-controlled.

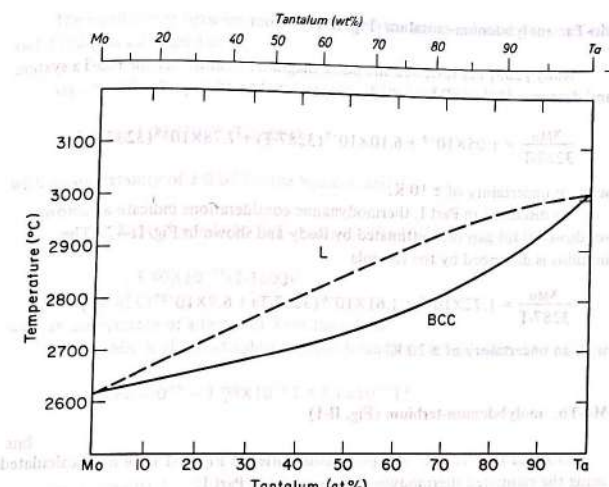


FIG.II-47. Phase diagram of the system molybdenum-tantalum.

## Mo-Sr: molybdenum-strontium (Fig. II-2)

No data were found. The solubility of molybdenum in liquid strontium has been calculated using the estimated thermodynamic equations of Part I. From 1042 to 1640 K,

$$\ln x_{\text{Mo}} = -20230 T^{-1} + 2.21$$

The solubility of molybdenum in the liquid rises from  $x_{\text{Mo}} = 3 \times 10^{-8}$  at 1042 K to  $x_{\text{Mo}} = 4 \times 10^{-5}$  at 1640 K, with an uncertainty of a factor of 5.

The solubilities of strontium in molybdenum and of molybdenum in strontium below 1042 K are less than the quenched defect concentrations and are not thermodynamic quantities.

## Mo-Ta: molybdenum-tantalum (Fig. II-47)

Rudy [205] has reviewed the phase diagram literature for the Mo-Ta system and determined the solidus, which is represented by the equation

$$\frac{x_{\text{Mo}}}{3287-T} = 1.05 \times 10^{-3} + 6.10 \times 10^{-7}(3287-T) + 7.78 \times 10^{-9}(3287-T)^2$$

with an uncertainty of  $\pm 10$  K.

As discussed in Part I, thermodynamic considerations indicate a narrower solidus-liquidus gap than estimated by Rudy and shown in Fig. II-47. The liquidus is described by the formula

$$\frac{x_{\text{Mo}}}{3287-T} = 1.72 \times 10^{-3} + 1.61 \times 10^{-6}(3287-T) + 6.9 \times 10^{-10}(3287-T)^2$$

with an uncertainty of  $\pm 20$  K.

## Mo-Tb: molybdenum-terbium (Fig. II-1)

No data were found. The phase boundaries of Fig. II-1 have been calculated using the estimated thermodynamic equations of Part I.

The monotectic is at  $2790 \pm 10$  K and  $x_{\text{Tb}} = 7 \times 10^{-3}$ ,  $0.07 \pm 0.02$  and  $0.67 \pm 0.05$ . The molybdenum liquidus and solidus above this temperature are calculated to be

$$x_{\text{Tb}} = 6.1 \times 10^{-4}(2890-T) + 6 \times 10^{-7}(2890-T)^2$$

with an uncertainty of  $\pm 2 \times 10^{-4}$  (2890-T) for the liquidus and

$$x_{\text{Tb}} = 7 \times 10^{-5}(2890-T)$$

with an uncertainty of a factor of 5 for the solidus.

The two-liquid region phase boundaries from 2790 to 3000 K are

$$x_{\text{Mo}} = 0.285 + 2.58 \times 10^{-4}(T-2600) + 2.63 \times 10^{-7}(T-2600)^2$$

with an uncertainty rising from  $\pm 0.05$  at 2790 K to  $\pm 0.08$  at 3000 K, and

$$x_{\text{Tb}} = 0.056 + 8.7 \times 10^{-5}(T-2600) + 3.3 \times 10^{-8}(T-2600)^2$$

with an uncertainty of  $\pm 0.01$  at 2790 K and  $\pm 0.02$  at 3000 K. The eutectic is determined to be at  $1600 \pm 10$  K and  $x_{\text{Tb}} = 0.98 \pm 0.01$ . The terbium liquidus and solidus above the eutectic are represented by  $x_{\text{Mo}} = 6.7 \times 10^{-4}(1630-T)$  for the liquidus and by  $x_{\text{Mo}} = 1.626 \times 10^{-5}(1630-T)$  for the solidus, with uncertainties of a factor of 5.

## PART II. PHASE DIAGRAMS

The equilibrium between molybdenum and the liquid solution between 1600 and 2790 K is calculated to be

$$x_{\text{Mo}} = 1.6 \times 10^{-2} + 1.16 \times 10^{-4}(T-1600) - 7.9 \times 10^{-8}(T-1600)^2 \\ + 1.72 \times 10^{-10}(T-1600)^3$$

with an uncertainty of  $\pm 0.05$  for the liquidus, and

$$x_{\text{Tb}} = 3.7 \times 10^{-4} + 9.7 \times 10^{-7}(T-1600) + 4.79 \times 10^{-9}(T-1600)^2 \\ - 1.40 \times 10^{-12}(T-1600)^3$$

with an uncertainty of a factor of 5 for the solidus.

Below 1600 K the solid-solution phase boundaries are calculated to be

$$x_{\text{Mo}} = 5.86 \times 10^{-3} - 1.09 \times 10^{-5}T + 5.1 \times 10^{-9}T^2$$

and

$$x_{\text{Tb}} = 1.9 \times 10^{-3} - 3.38 \times 10^{-6}T + 1.53 \times 10^{-9}T^2$$

with an uncertainty of a factor of 5. The solid solubility of molybdenum in terbium drops to  $x_{\text{Mo}} = 10^{-4}$  at 1200 K, and that of terbium in molybdenum drops to  $10^{-4}$  at 1370 K. Below these temperatures the solubilities are less than the quenched defect concentrations and are no longer thermodynamically determined quantities.

## Mo-Tc: molybdenum-technetium (Fig. II-48)

Shunk [228] has reviewed the phase diagram work through 1963 and has presented a provisional phase diagram with two intermediate phases: the A15-type phase at  $55 \pm 5$  at.% Tc and the  $\sigma$ -phase between 65 and 75 at.% Tc. No measurements in the liquid range have been made. Alekseevskij et al. [3] have reported larger solubilities, with up to 55 wt% Tc in Mo and 30 wt% Mo in Tc at 1000°C. The  $\sigma$ -phase is placed at 60 wt% Tc. Part III reviews the crystallographic data for the phases.

The thermodynamic values estimated in Part I were used to calculate the solidus and liquidus boundaries of Fig. II-48. The molybdenum solidus and liquidus between 2300 and 2890 K are given for the solidus by

$$x_{\text{Tc}} = 6.1 \times 10^{-4}(2890-T) - 2.3 \times 10^{-6}(2890-T)^2 + 4.6 \times 10^{-9}(2890-T)^3 \pm 0.05$$

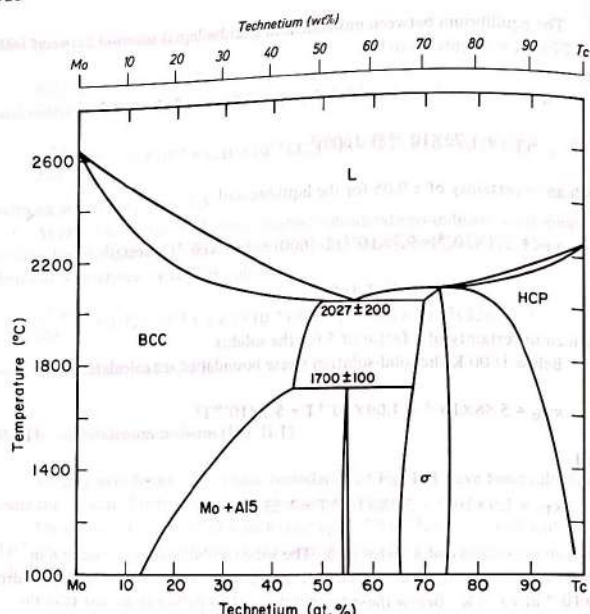


FIG.II-48. Phase diagram of the system molybdenum-technetium.

and for the liquidus by

$$x_{Tc} = 9.6 \times 10^{-4}(2890-T) - 8.2 \times 10^{-7}(2890-T)^2 + 1.34 \times 10^{-9}(2890-T)^3 \pm 0.07$$

The σ-phase liquidus extends from the eutectic, with bcc Mo at 2300 ± 100 K and 56 ± 5 at. % Tc, to the peritectic at 2350 ± 100 K and 72 ± 5 at. % Tc. The σ-phase solidus is estimated to extend from 70 ± 3 at. % Tc at 2300 K to 73 ± 3 at. % Tc at 2350 ± 100 K, the peritectic temperature. The σ-phase boundary saturated by hcp Tc, as shown in Fig. II-48, increases to about 74 at. % Tc as the temperature drops to 1000°C and would be expected to decrease in technetium content upon additional cooling if equilibration could be attained. Figure II-48 shows the molybdenum-rich boundary of the σ-phase to range from 68 ± 5 at. % Tc at the

## PART II. PHASE DIAGRAMS

A15 peritectic to a minimum of 65 ± 5 at. % Tc at 1200°C and is then expected to increase in technetium content at lower temperatures.

It is difficult to estimate the homogeneous range of the A15 phase. It is shown to decompose at 1700 ± 100°C. The thermodynamic equations from Part I for the bcc Mo and hcp Tc solid solutions were selected to yield reasonable values for calculating the liquidus and solidus curves, and the extrapolation to lower temperatures becomes increasingly uncertain. If those equations are accepted, and if the A15 phase is assumed to have a fixed composition at 55 at. % Tc, the molybdenum solvus is calculated to be

$$\ln x_{Tc} = 970 T^{-1} - 3.4 + 2.15 \times 10^{-3}(T-1000)$$

with an average uncertainty of ± 0.5 over the range 1200–1973 K. The calculation of the technetium solvus saturated by the σ-phase yields

$$\ln x_{Mo} = -3.21 + 1.88 \times 10^{-3}(T-1000) - 1800 T^{-1} \pm 0.5 \quad (1200-2350 \text{ K})$$

It is likely that the temperature coefficients are too large and that the solubilities do not drop off so rapidly, but the correct values should be within the average uncertainty limits indicated.

## Mo-Te: molybdenum-tellurium (Fig. II-49)

Spiesser et al. [233] have reviewed the earlier literature of the Mo-Te system and have presented their results on the phase regions  $MoTe_{2-x}$  and  $Mo_3Te_{4+x}$ . More recently, Vellinga et al. [255] have used a more sensitive method of fixing the phase boundaries and have narrowed the homogeneous range to  $MoTe_{1.90-1.99}$  between 750 and 950°C, with a transition from the low-temperature hP6 form to the mP12 form, at 820°C for tellurium-rich samples and at 880°C for molybdenum-rich samples. Opalovskij et al. [181] have measured dissociation pressures of  $MoTe_{2-x}$  at 909–81°C. Their results extrapolate to 1180 ± 40°C for  $Mo_3Te_4$  and  $MoTe_{1.9}$  in equilibrium with 1 atm Te<sub>2</sub> gas. Yanaki and Obolonchik [266] have reported weight losses on heating for the Mo-Te system. The solubility of tellurium in molybdenum is discussed in Part I.

By comparison with the Mo-Se system, the molybdenum-rich boundary of  $Mo_3Te_4$  in Fig. II-49 ranges from  $MoTe_{1.3}$  at low temperatures to  $MoTe_{1.27}$  at 1300 ± 70°C, where it is in equilibrium with 1 atm Te<sub>2</sub> gas and molybdenum with  $x_{Te} = 0.015 \pm 0.01$ . The tellurium-rich boundary ranges from  $MoTe_{1.35}$  at low temperatures to  $MoTe_{1.4}$  at 1180 ± 40°C, where it is in equilibrium with  $MoTe_{1.90}$ .

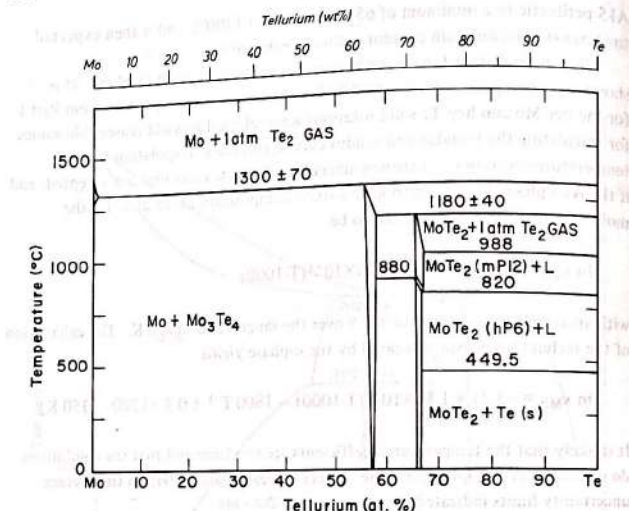


FIG.II-49. Phase diagram of the system molybdenum-tellurium.

(mP12) and  $\text{Te}_2$  gas at 1 atm. Between 1180 and 1300°C, the phase boundary saturated with gas at 1 atm varies from  $\text{MoTe}_{1.4}$  to  $\text{MoTe}_{1.27}$ . The molybdenum-rich boundary of  $\text{MoTe}_2$  (mP12) is close to  $\text{MoTe}_{1.90}$  between 1180 and 880°C, where it is in equilibrium with  $\text{MoTe}_{1.4}$  and  $\text{MoTe}_{1.89}$  (hP6). The tellurium-rich boundary of  $\text{MoTe}_2$  (mP12) increases from  $\text{MoTe}_{1.90}$  at 1180°C to  $\text{MoTe}_{1.99}$ , at 988°C, where it is in equilibrium with  $\text{Te}(\text{l})$  and  $\text{Te}_2$  gas at 1 atm. The  $\text{MoTe}_2$  (mP12) boundary increases slightly from  $\text{MoTe}_{1.99}$  to  $\text{MoTe}_{2.0}$  between 988 and 820°C, where it is in equilibrium with  $\text{MoTe}_{1.99}$  (hP6) and  $\text{Te}(\text{l})$ . The equilibrium boundaries of  $\text{MoTe}_2$  (hP6) should move toward  $\text{MoTe}_{2.00}$  as the temperature is lowered, but usual quenching procedures will retain wider homogeneous range.

The molybdenum content in the tellurium vapour, liquid and solid is so small that any molybdenum content would in practice be fixed by minute halide or oxide impurities. The molybdenum solvus is represented within a factor of three by

$$\ln x_{\text{Te}} = -6600 T^{-1} \quad (700-1573 \text{ K})$$

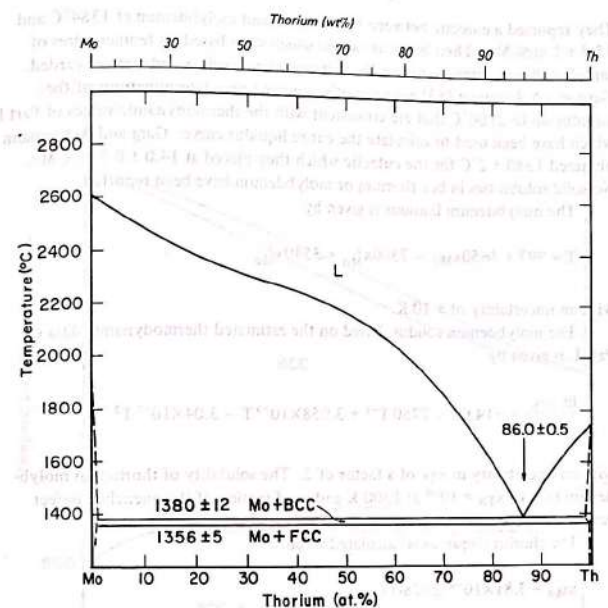


FIG.II-50. Phase diagram of the system molybdenum-thorium.

Below 700 K, where  $x_{\text{Te}} = 8 \times 10^{-5}$ , the concentration will be defect-controlled. Above 1573 K,  $x_{\text{Te}}$  will decrease, becoming 0.01 at 1900 K. Figure II-49 represents the 1-atm diagram. From the work of Flükiger et al. [76] on the Mo-S and Mo-Se systems at high pressures, it is expected that the high-pressure Mo-Te system will show Mo-Mo<sub>3</sub>Te<sub>4</sub> and Mo<sub>3</sub>Te<sub>4</sub>-MoTe<sub>2</sub> eutectics around 1400°C, with congruent melting points of 1500–1600°C.

#### Mo-Th: molybdenum-thorium (Fig. II-50)

McMasters et al. [167] found no intermediate phases and reported that on the addition of molybdenum the fcc-bcc transformation of thorium is lowered by 7°C to 1356 ± 5°C, with 0.06–0.12 at.% Mo in fcc thorium at 1225–1325°C.

They reported a eutectic between bcc thorium and molybdenum at 1384°C and 15.5 ± 1 at.% Mo. Their liquidus values, which were based on temperatures of sample collapse, implied impossible thermodynamic values and were discarded. Garg and Ackermann [83] have recently reported new determinations of the liquidus up to 2100°C that are consistent with the thermodynamic values of Part I which have been used to calculate the entire liquidus curve. Garg and Ackermann obtained 1380 ± 2°C for the eutectic which they placed at 14.0 ± 0.5 at.% Mo. No solid solubilities in bcc thorium or molybdenum have been reported.

The molybdenum liquidus is given by

$$T = 997 + 5650x_{Mo} - 7300x_{Mo}^2 + 3540x_{Mo}^3$$

with an uncertainty of ± 10 K.

The molybdenum solidus, based on the estimated thermodynamic data of Part I, is given by

$$\frac{\ln x_{Th}}{2890-T} = -14.03 - 7750T^{-1} + 3.058 \times 10^{-3}T - 3.04 \times 10^{-7}T^2$$

with an uncertainty in  $x_{Th}$  of a factor of 2. The solubility of thorium in molybdenum falls to  $x_{Th} = 10^{-4}$  at 1300 K and is a function of the quenched defect concentration below this temperature.

The thorium liquidus is calculated to be

$$x_{Mo} = 3.81 \times 10^{-4} (2028-T)$$

with an uncertainty of ± 3 × 10<sup>-5</sup> (2028-T). Above the eutectic the solubility of molybdenum in bcc thorium is calculated to be

$$x_{Mo} = 2.4 \times 10^{-5} (2028-T)$$

with an uncertainty of a factor of 2. The solubility in bcc thorium in equilibrium with solid molybdenum is  $x_{Mo} = 8 \times 10^{-3}$ , with an uncertainty of a factor of 2. The fcc thorium solidus is described by the equation

$$\ln(10^4 x_{Mo}) = -6.34 + 5.5 \times 10^{-3}T$$

with an uncertainty in  $x_{Mo}$  of a factor of 2. The solubility of molybdenum falls to  $10^{-4}$  at 1150 K.

The small two-phase region between fcc and bcc thorium is bounded by the points  $x_{Mo} = 8 \times 10^{-3}$  and  $1 \times 10^{-3}$  at 1358°C and the point  $x_{Mo} = 0$  at 1363°C.

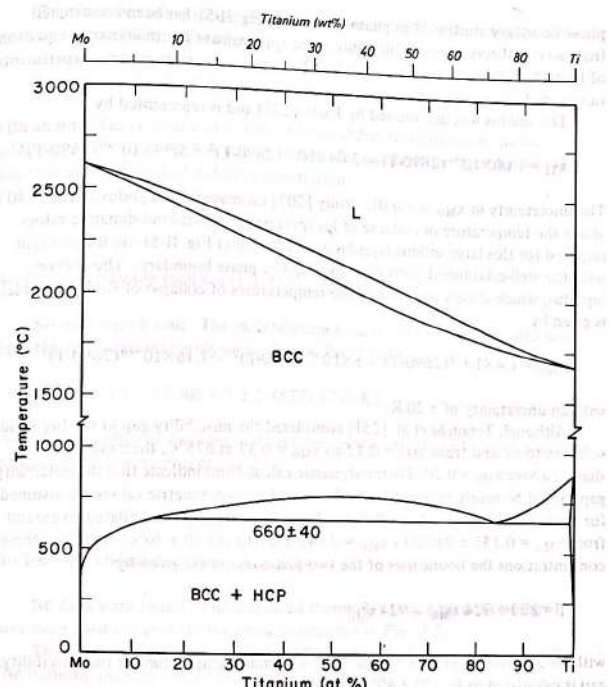


FIG.II-51. Phase diagram of the system molybdenum-titanium.

Mo-Ti: molybdenum-titanium (Fig. II-51)

The phase diagram for the Mo-Ti system, for which the literature was reviewed by Rudy [205], has not been changed by subsequent studies of the hcp-bcc boundaries [29, 31, 43, 46, 203, 204]. Terauchi et al. [251] investigated the solid-solution regions up to  $x_{Mo} = 0.225$  and found evidence of a miscibility gap in the bcc phase. This miscibility gap had been predicted at a lower temperature by Chernov and Shinyaev [46] on the basis of thermodynamic values derived from

phase boundary studies. The phase diagram of Fig. II-51 has been constructed from a critical review of the literature. The approximate thermodynamic equations of Part I have been used to predict phase boundaries where no reliable experimental values are known.

The solidus was determined by Rudy [205] and is represented by

$$x_{Ti} = 1.00 \times 10^{-3}(2890-T) - 5.04 \times 10^{-7}(2890-T)^2 + 5.94 \times 10^{-10}(2890-T)^3$$

The uncertainty in  $x_{Mo}$  is  $\pm 0.01$ . Rudy [205] estimated the liquidus as about 40 K above the temperature of collapse of his specimens. The thermodynamic values required for this large solidus-liquidus gap as shown in Fig. II-51 are inconsistent with the well-established portion of the hcp-bcc phase boundary. The chosen liquidus, which closely agrees with the temperatures of collapse of Rudy's samples, is given by

$$x_{Mo} = 1.4 \times 10^{-3}(2890-T) - 8 \times 10^{-7}(2890-T)^2 - 7.16 \times 10^{-10}(2890-T)^3$$

with an uncertainty of  $\pm 20$  K.

Although Terauchi et al. [251] considered the miscibility gap in the bcc solid solution to extend from  $x_{Mo} = 0.12$  to  $x_{Mo} = 0.33$  at 675°C, their evidence is slightly above  $x_{Mo} = 0.20$ . Thermodynamic calculations indicate that the miscibility gap should be nearly symmetrical unless very large asymmetric values are assumed for strain energies in the bcc solution. The miscibility gap is calculated to extend from  $x_{Mo} = 0.155 \pm 0.030$  to  $x_{Mo} = 0.845 \pm 0.030$  at 660  $\pm 40$ °C. Between these concentrations the boundaries of the two-phase region are given by

$$T = 809 + 924 x_{Mo} - 924 x_{Mo}^2$$

with an uncertainty in  $T$  of  $\pm 40$  K. The maximum temperature of the miscibility gap is calculated to be 770  $\pm 40$ °C at  $x_{Mo} = 0.50$ .

The phase limit for the hcp solution above 660°C is given by

$$x_{Mo} = 2.2 \times 10^{-5}(1156-T) - 2.2 \times 10^{-8}(1156-T)^2$$

with an uncertainty in  $x$  of  $4 \times 10^{-6}(1156-T)$ . Below 660°C the hcp phase boundary is described by

$$\ln x_{Mo} = -0.468 - 5100T^{-1} + 1.60 \times 10^{-3}T - 1.24 \times 10^{-6}T^2$$

with a maximum uncertainty in  $x_{Mo}$  of  $\pm 0.001$  at 660°C. The solubility of molybdenum in the hcp phase falls to  $x_{Mo} = 10^{-4}$  at 550  $\pm 5$  K; below this temperature it is a function of the quenched defect concentration.

The phase boundary of the bcc solid solution in equilibrium with the hcp solution below 660°C is given by

$$\ln x_{Ti} = 1.250 - 4390T^{-1} - 2.362 \times 10^{-4}T + 2.041 \times 10^{-6}T^2$$

with an uncertainty in  $\ln x$  of  $\pm 0.03$ . The solubility of titanium in the bcc solution falls to  $x_{Ti} = 10^{-4}$  at 420 K. Below this temperature the solubility is a function of the quenched defect concentration.

#### Mo-Tl: molybdenum-thallium (Fig. II-2)

No data were found. The molybdenum liquidus of Fig. II-2 was calculated from the estimated thermodynamic data of Part I to be

$$\ln x_{Mo} = 2.9 - 19300T^{-1} \pm 2 (577-1746 K)$$

The solid solubility of thallium in molybdenum was calculated to be smaller than the quenched defect concentration.

#### Mo-Tm: molybdenum-thulium (Fig. II-2)

No data were found. The estimated thermodynamic equations of Part I have been used to calculate the phase boundaries of Fig. II-2.

The eutectic is calculated to be at 1750  $\pm 10$  K and  $x_{Mo} = 0.05 \pm 0.015$ . The thulium liquidus above the eutectic is calculated to be

$$x_{Mo} = 5.5 \times 10^{-4}(1820-T) + 3.44 \times 10^{-6}(1820-T)^2$$

with an uncertainty of  $1.4 \times 10^{-4}(1820-T)$ . The thulium solidus in this temperature range is

$$x_{Mo} = 9.4 \times 10^{-5}(1820-T)$$

with an uncertainty of a factor of 5.

The molybdenum liquidus between 1750 and 2220 K is represented by

$$\ln x_{Mo} = -3.14 - 5040T^{-1} + 2.22 \times 10^{-3}T - 2.77 \times 10^{-6}T^2$$

with an uncertainty rising from  $\pm 0.015$  at 1750 K to  $\pm 0.035$  at 2220 K. The molybdenum solidus in this temperature range is calculated to be

$$\ln x_{Tm} = -15.23 + 7.44 \times 10^{-3} T - 1.33 \times 10^{-6} T^2$$

with an uncertainty of a factor of 5.

Below 1750 K the solid-solution phase boundaries are calculated to be

$$\ln x_{Mo} = -20.67 + 1.52 \times 10^{-2} T - 3.6 \times 10^{-6} T^2$$

and

$$\ln x_{Tm} = -26.01 + 1.95 \times 10^{-2} T - 4.7 \times 10^{-6} T^2$$

The mole fraction solubility of thulium in molybdenum falls to  $10^{-4}$  at 1220 K, and that of molybdenum in thulium falls to  $10^{-4}$  at 980 K, with uncertainties of a factor of 5. Below these temperatures the solubilities are defect-controlled.

#### Mo-U: molybdenum-uranium (Fig. II-52)

Hawkins and Hultgren [110] and Hultgren et al. [119] present a phase diagram based on data up to 1967. The only stable intermediate phase reported is  $MoU_2$  (tl6). Part III of this monograph reviews the various metastable phases that can be quenched from high temperatures. Gomozov et al. [97] have added data on the solubility of molybdenum in  $\alpha U$ , and Garg and Ackermann [83] have characterized the bcc uranium solidus, up to the peritectic composition of  $40 \pm 1$  at.% molybdenum at  $1284 \pm 2$  °C, and the molybdenum liquidus, from  $70.0 \pm 0.5$  at.% U at  $1284 \pm 2$  °C to  $42.4$  at.% U at  $2006$  °C. The remainder of the diagram presented as Fig. II-52 has been calculated from the thermodynamic equations given in Part I.

The molybdenum solidus from  $1557 \pm 2$  K to 2890 K is given by

$$x_U = 2.32 \times 10^{-4} (2890-T) - 2.71 \times 10^{-7} (2890-T)^2 + 8.6 \times 10^{-11} (2890-T)^3$$

and below 1557 K the boundary for molybdenum saturated with uranium is given by

$$x_U = 1.56 \times 10^{-2} - 4.66 \times 10^{-5} T + 3.67 \times 10^{-8} T^2$$

The uncertainty for the saturated molybdenum boundary is a factor of 2.

#### PART II. PHASE DIAGRAMS

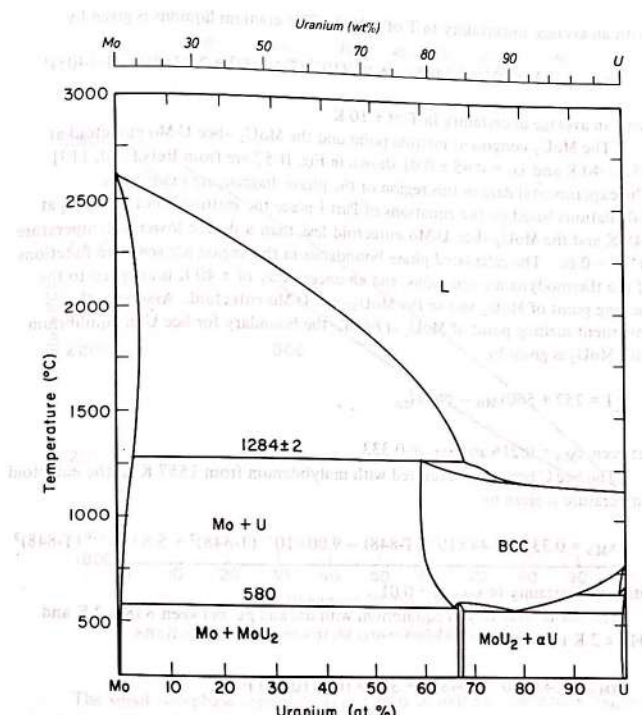


FIG.II-52. Phase diagram of the system molybdenum-uranium.

The molybdenum liquidus from  $1557 \pm 2$  K to 2890 K is given by

$$x_U = 8.80 \times 10^{-4} (2890-T) - 2.68 \times 10^{-7} (2890-T)^2$$

with an uncertainty in  $x_U$  of  $\pm 2 \times 10^{-5} (2890-T)$ .

The bcc uranium solidus is given by

$$x_{Mo} = 5.25 \times 10^{-3} (T-1405) - 1.71 \times 10^{-5} (T-1405)^2$$

with an average uncertainty in  $T$  of  $\pm 10$  K. The uranium liquidus is given by

$$x_{\text{Mo}} = 7.38 \times 10^{-3} (T - 1405) - 6.93 \times 10^{-5} (T - 1405)^2 + 2.23 \times 10^{-7} (T - 1405)^3$$

with an average uncertainty in  $T$  of  $\pm 10$  K.

The  $\text{MoU}_2$  congruent melting point and the  $\text{MoU}_2$ -bcc U-Mo eutectoid at  $853 \pm 40$  K and  $x_U = 0.65 \pm 0.01$  shown in Fig. II-52 are from Refs [110, 119]. The experimental data in this region of the phase diagram are inadequate. Calculations based on the equations of Part I place the melting point of  $\text{MoU}_2$  at 848 K and the  $\text{MoU}_2$ -bcc U-Mo eutectoid less than a degree lower in temperature at  $x_U = 0.66$ . The calculated phase boundaries in this region are sensitive functions of the thermodynamic equations, and an uncertainty of  $\pm 40$  K is assigned to the melting point of  $\text{MoU}_2$  and to the  $\text{MoU}_2$ -bcc U-Mo eutectoid. Assuming the congruent melting point of  $\text{MoU}_2$  at 848 K, the boundary for bcc U in equilibrium with  $\text{MoU}_2$  is given by

$$T = 757 + 560x_{\text{Mo}} - 863x_{\text{Mo}}^2$$

between  $x_{\text{Mo}} = 0.216$  and  $x_{\text{Mo}} = 0.333$ .

The bcc U boundary saturated with molybdenum from 1557 K to the eutectoid temperature is given by

$$x_{\text{Mo}} = 0.337 + 4.44 \times 10^{-4} (T - 848) - 9.00 \times 10^{-7} (T - 848)^2 + 5.8 \times 10^{-10} (T - 848)^3$$

with an uncertainty in  $x_{\text{Mo}}$  of  $\pm 0.01$ .

The bcc U boundary in equilibrium with  $\alpha\text{U}$  and  $\beta\text{U}$  between  $838 \pm 2$  K and  $1048 \pm 2$  K is given by

$$x_{\text{Mo}} = 3.43 \times 10^{-4} (1048 - T) + 3.26 \times 10^{-6} (1048 - T)^2$$

with an uncertainty in  $x_{\text{Mo}}$  of  $\pm 5 \times 10^{-6} (1048 - T)$ .

The boundary for  $\beta\text{U}$  between  $918 \pm 2$  K and  $1048 \pm 2$  K is given by

$$x_{\text{Mo}} = 1.3 \times 10^{-4} (1048 - T) - 10^{-7} (1048 - T)^2$$

with an uncertainty in  $x_{\text{Mo}}$  of  $\pm 4 \times 10^{-5} (1048 - T)$ .

The boundary for  $\beta\text{U}$  saturated with molybdenum below 918 K is given by

$$x_{\text{Mo}} = -2.2 \times 10^{-3} + 3.0 \times 10^{-6} T + 1.7 \times 10^{-9} T^2$$

with an uncertainty in  $x_{\text{Mo}}$  of a factor of 2. The solubility of molybdenum in  $\beta\text{U}$  falls to  $10^{-4}$  at 580 K; below this temperature the solubility is defect-controlled.

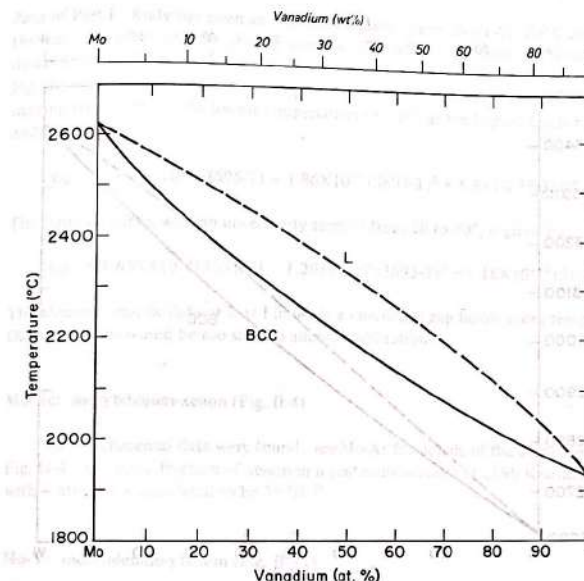


FIG. II-53. Phase diagram of the system molybdenum-vanadium.

The small two-phase region of  $\alpha\text{U}$  and  $\beta\text{U}$  is bounded by the points  $x_{\text{Mo}} = 0.015$  and  $x_{\text{Mo}} = 2 \times 10^{-3}$  at 918 K, and  $x_{\text{Mo}} = 0$  at  $941 \pm 2$  K.

#### Mo-V: molybdenum-vanadium (Fig. II-53)

Rudy [205] has reviewed previous data and has presented new solidus values, as shown in Fig. II-53, which are consistent with the thermodynamic data of Part I. Rudy estimated that the liquidus curve was  $10-40^\circ$  above the temperature he observed for the collapse of specimens. The calculation of the liquidus curve from the thermodynamic data of Part I indicates that Rudy's estimate of the liquidus curve as shown in Fig. II-53 lies somewhat too high. The enthalpy of fusion of vanadium is rather uncertain [16] and a larger value would raise the calculated values. As a compromise, the liquidus of Fig. II-53 is lowered to the

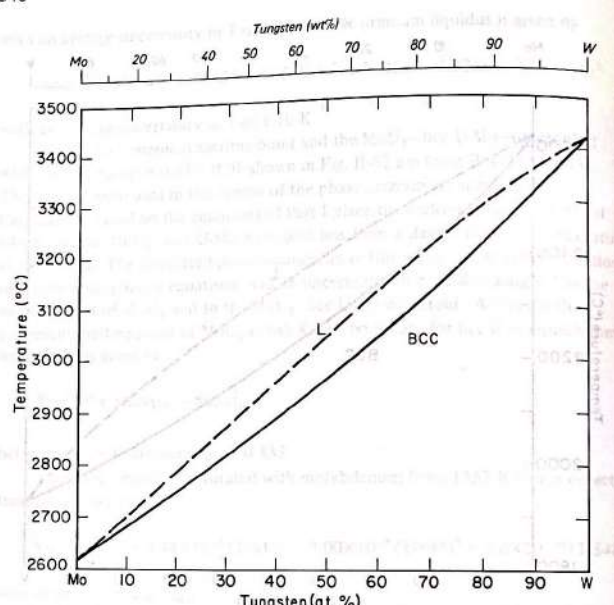


FIG.II-54. Phase diagram of the system molybdenum-tungsten.

temperature of collapse of Rudy's samples and is represented with an uncertainty of  $\pm 25^\circ$  by

$$x_{\text{W}} = 1.86 \times 10^{-3} (2890 - T) + 5.9 \times 10^{-8} (2890 - T)^2 - 9.5 \times 10^{-10} (2890 - T)^3$$

The solidus curve, which has an uncertainty of  $\pm 10^\circ$ , is given by

$$x_{\text{W}} = 7.4 \times 10^{-4} (2890 - T) + 2.076 \times 10^{-6} (2890 - T)^2 - 1.52 \times 10^{-9} (2890 - T)^3$$

#### Mo-W: molybdenum-tungsten (Fig. II-54)

The solidus of Fig. II-54 is from Rudy [205] whose measurements agree within experimental error with the calculations based on the thermodynamic

data of Part I. Rudy has given an estimated liquidus curve about 40–65°C above the temperature of collapse of alloy samples. Calculations based on the thermodynamic data of Part I indicate that the liquidus curve should be drawn, as in Fig. II-54, just above the collapse temperatures. The solidus curve has an uncertainty ranging from  $\pm 10^\circ$  at the lowest temperatures to  $\pm 30^\circ$  at the highest temperatures and is given by

$$x_{\text{Mo}} = 1.046 \times 10^{-3} (3695 - T) - 1.86 \times 10^{-7} (3695 - T)^2 + 5.5 \times 10^{-10} (3695 - T)^3$$

The liquidus curve, with an uncertainty ranging from 20 to 40°, is given by

$$x_{\text{Mo}} = 1.655 \times 10^{-3} (3695 - T) - 1.203 \times 10^{-6} (3695 - T)^2 + 9.16 \times 10^{-10} (3695 - T)^3$$

The thermodynamic data of Part I indicate a miscibility gap below room temperature. Diffusion rates would be too slow to allow equilibration.

#### Mo-Xe: molybdenum-xenon (Fig. II-4)

No experimental data were found; see Mo-Ar for details of the calculation of Fig. II-4. The mole fraction of xenon in liquid molybdenum at 2890 K saturated with 1 atm gas is calculated to be  $3 \times 10^{-19}$ .

#### Mo-Y: molybdenum-yttrium (Fig. II-55)

Unpublished data by Lundin and Klodt have been used by Gschneidner [102] to prepare a phase diagram showing liquid miscibility and a eutectic at 10 at.% Mo, with 0.02 at.% Mo in solid yttrium. Apparently all of the liquidus curve was estimated except for the eutectic point. Gschneidner suggests that the indicated eutectic temperature might be too high by as much as 50°. Taylor [245] reports a solubility of  $10^{-4}$  at.% yttrium in solid molybdenum at 1858 K, while Savitskij et al. [213, 214] report 0.03–0.065 at.% yttrium in solid molybdenum at 1723 K, with two liquid phases at 11 at.% yttrium. These data have been incorporated into the thermodynamic evaluation of Part I, and the phase diagram given in Fig. II-55 has been calculated from the resulting thermodynamic equations.

The molybdenum curve is represented by

$$x_{\text{Y}} = 8.53 \times 10^{-6} (2890 - T) - 1.281 \times 10^{-8} (2890 - T)^2 + 4.95 \times 10^{-12} (2890 - T)^3$$

between 1700 and 2890 K. The values are uncertain by a factor of 3. As the temperature drops below the melting point of molybdenum, the solubility of

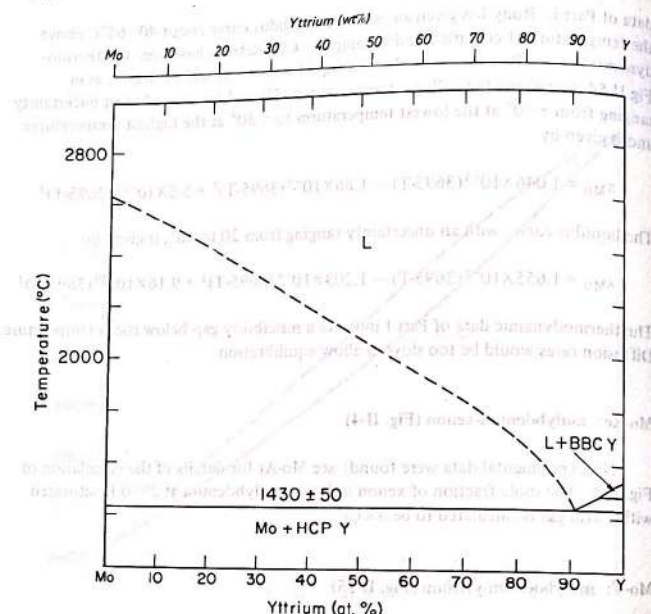


FIG.II-55. Phase diagram of the system molybdenum-yttrium.

(101) *Calculated*. FIG.II-55. Phase diagram of the system molybdenum-yttrium. The diagram shows the phase boundaries for the system Mo-Y. The liquidus curve is calculated to be linear with a slope of  $-1.3 \times 10^{-3}$  K<sup>-1</sup>. The solidus curve is calculated to be constant at  $1430 \pm 50$  K. The eutectic point is located at  $1430 \pm 50$  K and  $14.3 \pm 0.5$  at. % Y. The solubility of yttrium in solid molybdenum is calculated to increase to a maximum mole fraction of  $x_{Yt} = 2 \times 10^{-3}$  at 2400 K and then to drop to  $x_{Yt} = 4 \times 10^{-4}$  by 1700 K.

The molybdenum liquidus curve is given by

$$x_{Mo} = 5.40 \times 10^{-4}(2890-T) + 6.73 \times 10^{-7}(2890-T)^2 - 3.98 \times 10^{-10}(2890-T)^3$$

with the probable error increasing with decreasing temperature to  $\pm 0.04$  at 1700 K. On the yttrium side, the mole fraction of molybdenum decreases with increasing temperature along both the liquidus and solidus curves, reaching  $x_{Mo} = 0.025$  in the liquid and  $x_{Mo} = 0.001$  in the solid at around 1750 K.

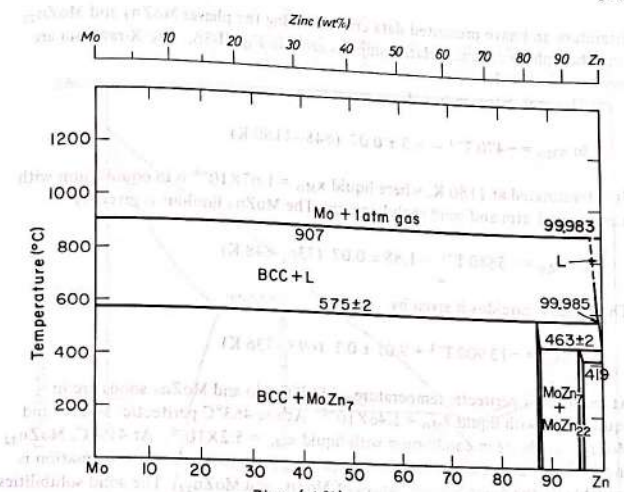


FIG.II-56. Phase diagram of the system molybdenum-zinc.

#### Mo-Yb: molybdenum-ytterbium (Fig. II-2)

No data were found. The estimated thermodynamic equations of Part I have been used to calculate the phase boundaries of Fig. II-2. From 1097 to 1467 K, the molybdenum liquidus is calculated to be

$$\ln x_{Mo} = -12.36 + 1.30 \times 10^{-2}(T-1000) - 7.0 \times 10^{-6}(T-1000)^2$$

with an uncertainty in  $x_{Mo}$  rising from  $\pm 1 \times 10^{-5}$  at 1098 K to  $\pm 2 \times 10^{-4}$  at 1467 K.

The solid solubilities are defect-controlled.

The eutectic is approximately 0.01° below the melting point of ytterbium, 1097 K, at  $x_{Mo} = (1.4 \pm 1.0) \times 10^{-5}$ .

#### Mo-Zn: molybdenum-zinc (Fig. II-56)

Martin et al. [170] have determined the solubility of molybdenum in liquid zinc between 422 and 730°C. Heumann et al. [116] have reviewed the previous

literature and have presented data characterizing the phases MoZn<sub>7</sub> and MoZn<sub>22</sub> and their phase diagram relationships as given in Fig. II-56. The X-ray data are reviewed in Part III.

The molybdenum liquidus is given by

$$\ln x_{\text{Mo}} = -470 T^{-1} - 8.3 \pm 0.07 \quad (848-1180 \text{ K})$$

It is terminated at 1180 K, where liquid  $x_{\text{Mo}} = 1.67 \times 10^{-4}$  is in equilibrium with zinc gas at 1 atm and solid molybdenum. The MoZn<sub>7</sub> liquidus is given by

$$\ln x_{\text{Mo}} = -5880 T^{-1} - 1.88 \pm 0.07 \quad (736-848 \text{ K})$$

The MoZn<sub>22</sub> liquidus is given by

$$\ln x_{\text{Mo}} = -13900 T^{-1} + 9.01 \pm 0.1 \quad (693-736 \text{ K})$$

At the MoZn<sub>7</sub> peritectic temperature of 575°C, Mo and MoZn<sub>7</sub> solids are in equilibrium with liquid  $x_{\text{Mo}} = 1.46 \times 10^{-4}$ . At the 463°C peritectic, MoZn<sub>7</sub> and MoZn<sub>22</sub> solids are in equilibrium with liquid  $x_{\text{Mo}} = 5.2 \times 10^{-5}$ . At 419°C, MoZn<sub>22</sub> and Zn solids are in equilibrium with liquid  $x_{\text{Mo}} = 1.6 \times 10^{-5}$ . No information is available on the homogeneous ranges of MoZn<sub>7</sub> and MoZn<sub>22</sub>. The solid solubilities of Zn and Mo are estimated to be smaller than defect concentrations.

#### Mo-Zr: molybdenum-zirconium (Fig. II-57)

The phase diagram literature for the Mo-Zr system has been reviewed by Kubaschewski-Von Goldbeck [155]. The phase boundaries of Fig. II-57, which are based on a critical evaluation of the literature, are consistent with the approximate thermodynamic equations of Part I.

The boundary of the ZrMo<sub>2</sub>(cF24) Laves phase is uncertain on the zirconium-rich side. Brauer and Liebbrandt [28] proposed a maximum zirconium concentration of ~40 at.%, while Garg and Ackermann [82] found a limit of ~36 at.% Zr, and Rudy [205] proposed a very small homogeneity range for ZrMo<sub>2</sub>. The studies of Rudy and Garg/Ackermann indicate that the Mo-ZrMo<sub>2</sub>-liquid peritectic is at 1950 ± 40°C. In his lattice parameter study, Rudy found a solid solubility of zirconium in molybdenum of  $x_{\text{Zr}} = 0.18 \pm 0.01$  at the peritectic, whereas other investigators [58, 155] have reported lower values. The liquid phase at the peritectic has a composition  $x_{\text{Zr}} = 0.42 \pm 0.02$  [58, 205].

The molybdenum liquidus above the peritectic temperature is given by

$$\frac{\ln x_{\text{Zr}}}{2890-T} = -6.68 - 8.0 \times 10^{-4} T + 2.2 \times 10^{-7} T^2$$

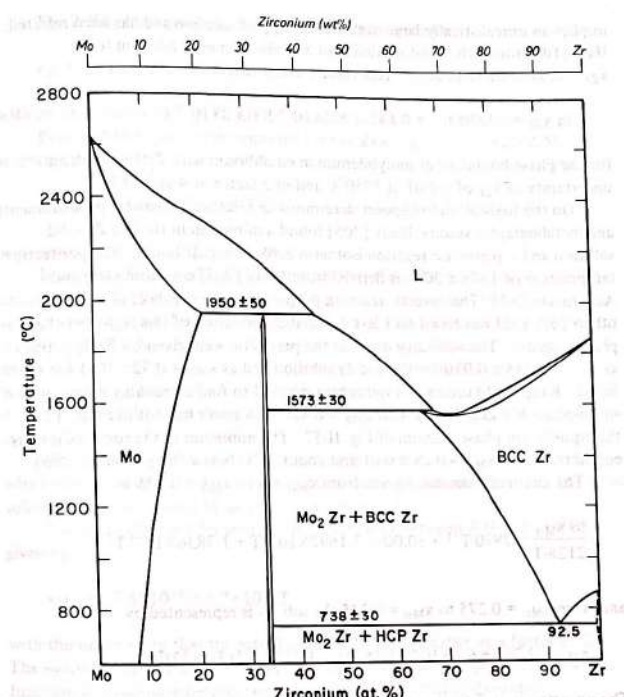


FIG. II-57. Phase diagram of the system molybdenum-zirconium.

with an uncertainty in  $x_{\text{Zr}}$  of  $\sim 3 \times 10^{-5}$  (2890-T). The molybdenum solidus above the peritectic follows the equation

$$\frac{\ln x_{\text{Zr}}}{2890-T} = -1200 T^{-1} - 1.45 - 4.20 \times 10^{-3} T + 6.29 \times 10^{-7} T^2$$

with an uncertainty in  $x_{\text{Zr}}$  of  $\pm 2 \times 10^{-5}$  (2890-T). Pipitz and Kieffer [189] reported the solubility of zirconium in bcc Mo as  $x_{\text{Zr}} = 0.07$  at 600°C. This value

implies an unrealistically large negative entropy of solution and has been rejected. Ham [107] found the solid solubility of zirconium in molybdenum to be  $x_{Zr} = 0.04 \pm 0.01$  at  $1100^\circ C$ . This value is consistent with the equation

$$\ln x_{Zr} = -3370 T^{-1} + 0.142 - 8.2 \times 10^{-4} T + 3.0 \times 10^{-7} T^2$$

for the phase boundary of molybdenum in equilibrium with  $ZrMo_2$ , with an uncertainty in  $x_{Zr}$  of  $\pm 0.01$  at  $1950^\circ C$  and of a factor of 4 at  $600^\circ C$ .

On the basis of melting-point determinations, lattice parameter measurements and metallographic studies, Rudy [205] found a minimum in the bcc Zr solid solution and a peritectic reaction isotherm  $ZrMo_2$ -bcc Zr liquid. The peritectic temperature of  $1575 \pm 30^\circ C$  is derived from Rudy [205] and from Garg and Ackermann [82]. The eutectic reaction proposed by Domagala et al. [58] and others [82, 155] was based on a less detailed examination of this region of the phase diagram. The solubility limits at the peritectic were given by Rudy [205] as  $x_{Mo} = 0.345 \pm 0.010$  for the bcc Zr solution and as  $x_{Mo} = 0.32 \pm 0.01$  for the liquid. Rapp [196] used a fast quenching method to find a probably metastable single-phase bcc Zr solution with  $x_{Mo} = 0.41$ . This result has not been used for the equilibrium phase diagram of Fig. II-57. The minimum in the solidus-liquidus equilibrium is at  $x_{Mo} = 0.28 \pm 0.01$  and about  $20^\circ C$  below the peritectic [205].

The zirconium solidus is given from  $x_{Mo} = 0$  to  $x_{Mo} = 0.275$  by

$$\frac{\ln x_{Mo}}{2128-T} = 7990 T^{-1} + 60.00 - 7.1692 \times 10^{-2} T + 1.7836 \times 10^{-5} T^2$$

and from  $x_{Mo} = 0.275$  to  $x_{Mo} = 0.345$  the solidus is represented by

$$x_{Mo} = 0.269 + 6.1 \times 10^{-3} (T-1823) - 1.22 \times 10^{-4} (T-1823)^2$$

The uncertainty in T for the solidus is  $\pm 5 K$ , within the uncertainty in the peritectic.

The zirconium liquidus is given from  $x_{Mo} = 0$  to  $x_{Mo} = 0.275$  by

$$\frac{\ln x_{Mo}}{2128-T} = 1.774 T^{-1} + 21.035 - 2.8393 \times 10^{-2} T + 7.129 \times 10^{-6} T^2$$

and from  $x_{Mo} = 0.275$  to  $x_{Mo} = 0.32$  by

$$x_{Mo} = 0.269 + 3.5 \times 10^{-3} (T-1823) - 6.7 \times 10^{-5} (T-1823)^2$$

The uncertainty in T for the liquidus is  $\pm 5 K$ , within the uncertainty of the peritectic.

## PART II. PHASE DIAGRAMS

The  $ZrMo_2$  liquidus above the peritectic is represented by

$$x_{Zr} = 5.968 - 8.501 \times 10^{-3} T - 4.788 \times 10^{-6} T^2 - 9.39 \times 10^{-10} T^3$$

with an uncertainty of  $\pm 10 K$ , within the uncertainties of the peritectics.

Below  $1848^\circ C$  the phase boundary for bcc Zr in equilibrium with  $ZrMo_2$  is given by

$$\ln x_{Mo} = -3370 T^{-1} + 1.643 \times 10^{-2} + 4.239 \times 10^{-4} T - 1.19 \times 10^{-8} T^2$$

with an uncertainty in  $x_{Mo}$  of  $\pm 0.01$ .

Braun and Rogozinskaya [30] reported that the addition of molybdenum to zirconium lowers the temperature of the hcp-bcc transition to  $738 \pm 15^\circ C$ . This temperature and the thermodynamic properties of Part I have been used to predict a composition of  $x_{Mo} = 0.055 \pm 0.010$  for bcc Zr in equilibrium with  $ZrMo_2$  and hcp Zr at  $738^\circ C$ . The phase boundary for bcc Zr in equilibrium with hcp Zr is represented by  $x_{Mo} = 4.4 \times 10^{-4} (1137-T)$ , with an uncertainty in  $x_{Mo}$  of  $\pm 1 \times 10^{-4} (1137-T)$ . The phase boundary for hcp Zr in equilibrium with bcc Zr is given by  $x_{Mo} = 1.6 \times 10^{-5} (1137-T)$ .

This boundary is based on the solubility measurements of Domagala et al. [58] which placed an upper limit on the solubility of molybdenum in hcp Zr. The actual solubility may be smaller by as much as a factor of 5.

The solubility limit for molybdenum in hcp Zr between  $400$  and  $738^\circ C$  is given by

$$x_{Mo} = -3.8 \times 10^{-3} + 5.7 \times 10^{-6} T$$

with the uncertainty that the actual solubility may be smaller by a factor of 5.

The solubility falls to  $x_{Mo} = 10^{-4}$  at  $400^\circ C$ , below which temperature it is a function of solid-state defects rather than equilibrium thermodynamics.

## REFERENCES TO PART II

- [1] ALBERRY, P.J., HAWORTH, C.W., Met. Sci. 9 (1975) 140.
- [2] ALDEN, T., STEVENSON, D.A., WULFF, J., Massachusetts Inst. of Tech., Cambridge, Metallurgy Report 8, No. 2 (Feb. 1957).
- [3] ALEKSEEVSKIJ, N.E., BALAKHOVSKIJ, O.A., KIRILLOV, I.V., Fiz. Met. Metalloved. 40 (1975) 50-54.
- [4] ALEKSANDROV, B.N., DUKIN, V.V., DEREVYANCHENKO, V.V., Phys. Met. Metallogr. 33 (1972) 124-32; Fiz. Met. Metalloved. 33 3 (1972) 584-92.
- [5] ALFINTSEVA, R.A., SHISHKIN, E.A., SHURIN, A.F., Fazovye Prevarshch. 129 (1967).
- [6] ALIKHANYAN, A.S., PERVOV, V.S., MALKEROVA, I.P., BUTSKIJ, V.D., GORGORAKI, V.I., Zh. Neorg. Khim. 23 (1978) 1483-85.

- [7] ALLEN, B.C., Trans. Metall. Soc. AIME 239 (1967) 1026-29.
- [8] ANDERSON, E., J. Less-Common Met. 6 (1964) 81-84.
- [9] ANDERSON, E., HUME-ROTHERY, W., J. Less-Common Met. 2 (1960) 19-28.
- [10] ANDERSON, E., HUME-ROTHERY, W., J. Less-Common Met. 2 (1960) 443-50.
- [11] ANTHROP, D.F., California Univ., Berkeley, Lawrence Berkeley Lab., Rep. UCRL-50315 (1967).
- [12] ANTHROP, B., Acta Chem. Scand. 12 (1958) 31-37.
- [13] BARS, O., GUILLEVIE, J., GRANDJEAN, D., J. Solid State Chem. 6 (1973) 48-57.
- [14] BASKIN, M.L., SAVIN, A.V., TUMANOV, V.I., EYDUK, Yu.A., Izv. Akad. Nauk SSSR, Otd. Tekhn. Nauk, Met. Toplivo No. 4 (1961) 111-14.
- [15] BELYAEVA, G.I., ILYUSHCHENKO, N.G., ANFINOGENOV, A.I., Tr. Inst. Ehlektrokhim., Akad. Nauk SSSR, Ural. Filial, No. 10 (1967) 85-95.
- [16] BEREZIN, B.Ya., CHEKHOVSKOI, V.Ya., KATS, S.A., in Proc. 4th Int. Conf. Thermodyn. Chim., Vol.9, Centre Rech. Microcalorimétrie Thermochim. C.N.R.S., Marseille (1975) 77-84; Chem. Abstr. 84 (1976) 96272y.
- [17] BIBRING, H., GRAF, R., C.R. Hebd. Acad. Sci. 252 (1961) 4160-62.
- [18] BILTZ, W., KÖCHER, A., Z. Anorg. Allg. Chem. 248 (1941) 172-74.
- [19] BLIZNAKOV, G., PIPEROV, B., TSOLOVSKI, I., Izv. Khim. 8 4 (1975) 614-20.
- [20] BLOOM, D.S., GRANT, N.J., Trans. Metall. Soc. AIME 200 (1954) 261-68.
- [21] BOCHVAR, A.A., KONOBEVSKY, S.T., KUTAITSEV, V.I., MENSHKOVA, T.S., CHEBOTAREV, N.T., in Peaceful Uses of Atomic Energy (Proc. 2nd Int. Conf. Geneva, 1958) Vol.6, UN, Geneva (1958) 191.
- [22] BOLLER, H., NOWOTNY, H., Monatsh. Chem. 95 (1964) 1272.
- [23] BORNAND, J.D., SIEMENS, R.E., ODEN, L.L., J. Less-Common Met. 30 (1973) 205-9.
- [24] BOUSQUET, J., GUILLOU, A., Bull. Soc. Chim. Fr. (1966) 2250-53.
- [25] BOWERSOX, D.F., LEARY, J.A., Rep. LAMS-2518 (1961).
- [26] BOWERSOX, D.F., LEARY, J.A., J. Nucl. Mater. 27 (1968) 181-86; 33 (1969) 311-14.
- [27] BOWMAN, M.G., Proc. Conf. Nucl. Appl. Nonfissionable Ceram., Washington, DC (1966) 293-302; Chem. Abstr. 67 (1967) 36011b.
- [28] BRAUER, G., LIEBRANDT, F., Metals for the Space Age, Plansee Proc. (1964) 340.
- [29] BRAUN, S.M., Izv. Vyssh. Uchebn. Zaved., Tsvetn. Metall. 14 1 (1971) 109.
- [30] BRAUN, S.M., ROGOZINSKAYA, A.A., Izv. Vyssh. Uchebn. Zaved., Tsvetn. Metall. 15 6 (1972) 118.
- [31] BRAUN, S.M., SAMSONOV, G.V., Dopov. Akad. Nauk Ukr. RSR, Ser. A, 33 (1971) 1116.
- [32] BREWER, L., Estimation of Thermodynamic Data and Phase Diagrams, California Univ., Berkeley, Lawrence Berkeley Lab., Rep. LBL-4994 (1976).<sup>a</sup>
- [33] BREWER, L., The Cohesive Energies of the Elements, California Univ., Berkeley, Lawrence Berkeley Lab., Rep. LBL-3720 Rev. (4 May 1977).<sup>a</sup>
- [34] BREWER, L., HP-67 Calculator Programs for Thermodynamic Data and Phase Diagram Calculations, California Univ., Berkeley, Lawrence Berkeley Lab., Rep. LBL-5485 (1978) 90 pp.<sup>a</sup>
- [35] BROWN, A., Nature (London) 206 (1965) 502-3; and private communication, 21 Jan. 1976.
- [36] BROWN, A., WESTBROOK, J.H., in Intermetallic Compounds, Chapter 17 (WESTBROOK, J.H., Ed.), Wiley, New York (1967) 316.

<sup>a</sup> Available from National Technical Information Service, United States Dept. of Commerce, 5285 Port Royal Road, Springfield, VA 22161, USA.

## PART II. PHASE DIAGRAMS

- [37] BRUCKHART, W.L., LaCHANCE, M.H., CRAIGHEAD, C.M., JAFFEE, R.I., Trans. Am. Soc. Met. 45 (1953) 286-313.
- [38] BYCHKOV, Y.P., ROZANOV, A.N., YAKOVLEVA, V.B., At. Ehnerg. 7 (1959) 531.
- [39] CANNON, P., Nature (London) 183 (1959) 1612-13.
- [40] CARNELL, P.J.H., MCCARLEY, R.E., HOUGUE, R.D., Inorg. Synth. 10 (1967) 49-54.
- [41] CARPENTER, J.H., HELSPER, D., WEED, H.C., MARSH, K.V., unpublished work, 1969.
- [42] CASSELTON, R.E.W., HUME-ROTHERY, W., J. Less-Common Met. 7 (1964) 212-21.
- [43] CHANDRASEKARAN, V., TAGGARD, R., POLONIS, D.H., Metallography 5 (1972) 393.
- [44] CHANG, L.L.Y., PHILLIPS, B., J. Am. Ceram. Soc. 53 (1969) 527-33.
- [45] CHART, T.G., Met. Sci. 8 (1974) 344-48.
- [46] CHERNOV, D.B., SHINYAEV, A.Ya., Izv. Akad. Nauk SSSR, Met. No.5 (1975) 212.
- [47] CHEVREL, R., SERGENT, M., PRIGENT, J., Mater. Res. Bull. 9 (1974) 1487-98.
- [48] CRETIEN, A., HELGORSKY, J., C.R. Hebd. Acad. Sci. 252 (1961) 742-44.
- [49] CHRISTENSEN, J., Cryst. Growth 33 (1976) 58-60.
- [50] CHUANG, Yu-Chin, LI, Chao-Wu, CHUANG, Hsiang-Lin, KAO, Lien-Mei, Acta Metall. Sinica 9 (1966) 110-12.
- [51] CHUANG, Y.C., CHUANG, T.L., WU, C.H., Sci. Sinica (Peking) 13 (1964) 1851-60.
- [52] CLARE, J.S., J. Inst. Met. 89 (1960-61) 232-34.
- [53] CLARK, A.H., Neues Jahrb. Mineral., Monatsh. No.1 (1970) 33-38.
- [54] CLEARY, R.E., BLECKERMAN, S.S., CORLISS, J.E., USAEC Rep. TIM-850 (1965).
- [55] DECKER, B.F., WATERSTRAT, R.M., KASPER, J.S., Trans. Metall. Soc. AIME 197 (1953) 1476; 200 (1954) 1406-7.
- [56] DICKINSON, J.M., RICHARDSON, L.S., Trans. Am. Soc. Met. 51 (1959) 1055-67.
- [57] DIVEVA, E.N., Tr. Inst. Khim., Ural. Nauchn. Tsentr., Akad. Nauk SSSR 29 (1974) 105-10.
- [58] DOMAGALA, R.F., McPHERSON, D.J., HANSEN, M., Trans. Metall. Soc. AIME 197 (1953) 73.
- [59] DOUGLAS, T.B., J. Chem. Thermodyn. 9 (1977) 1165-79.
- [60] DREIBHOLZ, L., Z. Phys. Chem. 108 (1924) 1-50.
- [61] DROBOT, D.V., SAPRANOVA, E.A., Zh. Neorg. Khim. 19 (1974) 228-31; Russ. J. Inorg. Chem. 19 (1974) 125-27.
- [62] EDSHAMMAR, L.E., Univ. of Stockholm, Institute of Inorganic Chemistry, Data and Information Series No.2, Final Tech. Rep. No.1 for Contract DA-91-591-EUC-2734 (AD-426927) (1963) 41-42.
- [63] EGUCHI, T., MOROZUMI, S., Nippon Kinzoku Gakkai-Shi 38 (1974) 1019-25.
- [64] EICHELBERGER, R.L., MCKISSON, R.L., Atomics International, Canoga Park, CA, Rep. AI-AEC-12955 (1970).
- [65] EICHELBERGER, R.L., MCKISSON, R.L., JOHNSON, B.G., National Aeronautics and Space Administration, Washington, DC, Rep. NASA-CR-1371 (1969).
- [66] EKSTROM, T., TILLEY, R.J.D., J. Solid State Chem. 19 (1976) 125-33.
- [67] ELLINGER, F.H., MINER, W.N., O'BOYLE, D.R., SCHONFELD, F.W., Los Alamos Scientific Laboratory, Rep. 3870 (1968) 63-64.
- [68] ELLIOTT, R.P., Constitution of Binary Alloys, Supplement No.1, McGraw Hill, New York (1965).
- [69] EREMENKO, V.N., LISTOVNICHII, V.E., OPALOVSKII, A.A., FEDOROV, V.E., Khalbogenidy No.2 (1970) 92-97.
- [70] EREMENKO, V.N., VELIKANOVA, T.Y., LISTOVNICHII, V.E., KOMAROVA, S.A., Izv. Akad. Nauk SSSR, Neorg. Mater. 6 (1970) 11-14.
- [71] EREMENKO, V.N., ZHEL'VIS, E.F., Ukr. Khim. Zh. 16 (1950) 370-83.
- [72] ERLEY, W., WAGNER, H., Phys. Status Solidi A 19 (1973) K23-26.

- [73] ETTMAYER, P., Monatsh. Chem. 101 (1970) 127-40.
- [74] FALLER, F.E., BILTZ, W., MEISEL, K., ZUMBUSCH, M., Z. Anorg. Allg. Chem. 248 (1941) 214-28.
- [75] FISCHER, W.A., LORENZ, K., FABRITIUS, H., SCHLEGEL, D., Arch. Eisenhüttenwes. 41 (1970) 489-98.
- [76] FLÜKIGER, R., DEVANTAY, H., JORDA, J.L., MULLER, J., Inst. Electr. Electron. Eng. Trans. Mag. 13 (1977) 818; and FLÜKIGER, R., private communication, March 1977.
- [77] FLÜKIGER, R., YVON, K., SUSZ, C., ROGGEN, R., PAOLI, A., MULLER, J., J. Less-Common Met. 32 (1973) 207-25.
- [78] FORSYTH, J.B., GRAN, G., Acta Crystallogr. 15 (1962) 100-4.
- [79] FOWLER, R.D., ASPREY, L.B., LINDSAY, J.D., WHITE, R.W., in Low Temperature Physics (Proc. 13th Int. Conf., 1972) Vol.3 (TOMMERHAUS, K.D., O'SULLIVAN, W.J., HAMMEL, E.F., Eds), Plenum Press, New York (1974) 377-81.
- [80] FUKUTOMI, M., CORBETT, J.D., J. Less-Common Met. 55 (1977) 125-30.
- [81] GALASSO, F., PINTO, J., Trans. Metall. Soc. AIME 242 (1968) 754-55.
- [82] GARG, S.P., ACKERMANN, R.J., Metall. Trans. 8A (1977) 239.
- [83] GARG, S.P., ACKERMANN, R.J., J. Nucl. Mater. 64 (1977) 265-74.
- [84] GAUME-MAHN, F., BLANCHARD, M., C.R. Hebd. Acad. Sci. 254 (1962) 1082-83.
- [85] GAVALIER, J.R., JANOCKO, M.A., JONES, C.K., Appl. Phys. Lett. 21 (1972) 179-80.
- [86] GEACH, G.A., SUMMERS-SMITH, D., J. Inst. Met. 82 (1953-54) 471-74.
- [87] GIessen, B.C., JAEHNIGEN, U., GRANT, N.J., J. Less-Common Met. 10 (1965) 147-50.
- [88] GILLES, P.W., POLLOCK, B.D., J. Met. 5, AIME Trans. 197 (1953) 1537-39; and United States Atomic Energy Commission, Rep. AECU-2894 (1954).
- [89] GINGERICH, K.A., J. Phys. Chem. 68 (1964) 2514-22.
- [90] GLAZUNOV, M.P., MIKHAILOV, E.S., PISKAREV, N.V., CHUPAKHIN, M.S., Poroshk. Metall. No.11 (1976) 59-61.
- [91] GLICKSMAN, H.D., HAMER, A.D., SMITH, T.J., WALTON, R.A., Inorg. Chem. 15 (1976) 2205-9.
- [92] GLICKSMAN, H.D., WALTON, R.A., Inorg. Chem. 17 (1978) 200-1.
- [93] Gmelin Handbuch der Anorganischen Chemie, Main Series, 8th ed., Molbydän, System No.53, Ergänzungsband Teil B 1, Springer-Verlag, Berlin (1975).
- [94] GODNEVA, M.M., SEDEL'NIKOVA, N.D., GEIZLER, E.S., Zh. Prikl. Khim. 47 (1974) 2177.
- [95] GOLDBECK, O. von, Atomic Energy Review, Special Issue No.4, IAEA, Vienna (1973) 45-61.
- [96] GOLUB, A.M., TRACHEVSKIJ, V.V., UL'KO, N.V., Zh. Neorg. Khim. 23 (1978) 1832-35.
- [97] GOMOZOV, L.I., LYUTINA, E.M., IVANOV, O.S., Izv. Akad. Nauk SSSR, Met. No.2 (1970) 210-15.
- [98] GOROKH, A.V., KLOKOTINA, L.I., RISPTEL, K.N., Dokl. Akad. Nauk SSSR 158 (1964) 1183-85.
- [99] GOTKIS, I.S., GUSAROV, A.V., PERVOV, V.S., BUTSKII, V.D., Koord. Khim. 4 (1978) 720-24.
- [100] GREENFIELD, P., BECK, P.A., Trans. Metall. Soc. AIME 200 (1954) 253-57.
- [101] GREENFIELD, P., BECK, P.A., Trans. Metall. Soc. AIME 206 (1956) 265-76.
- [102] GSCHNEIDNER, K.A., Jr., in Rare Earth Alloys, Van Nostrand, Princeton, NJ (1961) 221-22.
- [103] GUERIN, R., SERGENT, M., PRIGENT, J., C.R. Hebd. Acad. Sci., Ser. C 274 (1972) 1278; Mater. Res. Bull. 10 (1975) 957-66.
- [104] GUICHARD, M., Ann. Chim. Phys., Ser. 7, 23 (1901) 498-574.

## PART II. PHASE DIAGRAMS

- [105] GUST, W., PREDEL, B., MEHRA, S.N., Mater. Sci. Eng. 21 (1975) 131-38.
- [106] GUTHRIE, P.V., STANSBURY, E.E., Oak Ridge National Lab., Tenn., Rep. ORNL-3078 (1961).
- [107] HAM, J.L., Trans. Am. Soc. Mech. Engrs. 73 (1951) 723.
- [108] HAM, J.L., Trans. Am. Soc. Mech. Engrs. 73 (1951) 727-28.
- [109] HANSEN, M., ANDERKO, K., Constitution of Binary Alloys, McGraw-Hill, New York (1958).
- [110] HAWKINS, D.T., HULTGREN, R., Constitution of Binary Alloys, Metals Handbook, Vol.8, 8th ed., American Society for Metals, Metals Park, Ohio (1973) 251-376.
- [111] HAWORTH, C.W., HUME-ROTHERY, W., J. Inst. Met. 87 (1959) 265-69.
- [112] HEIJWEGEN, C.P., RIECK, G.D., Z. Metallkd. 64 (1973) 450-53.
- [113] HEIJWEGEN, C.P., RIECK, G.D., J. Less-Common Met. 37 (1974) 115-21.
- [114] HEIJWEGEN, C.P., RIECK, G.D., J. Less-Common Met. 34 (1974) 309-14.
- [115] HELLA WELL, A., J. Less-Common Met. 1 (1959) 343-47.
- [116] HEUMANN, T., SCHLEICHER, H., VENKER, H., Z. Metallkd. 60 (1969) 438-41.
- [117] HIGGINS, J., WILKES, P., Philos. Mag. 25 (1972) 599-623.
- [118] HILL, M.L., J. Met. 12 (1960) 725-26.
- [119] HULTGREN, R., DESAI, P.D., HAWKINS, D.T., GLEISER, M., KELLEY, K.K., Selected Values of the Thermodynamic Properties of Binary Alloys, Mo-Nb, 10/67; Mo-Si, 2/68; Mo-Re, 10/67, American Society for Metals, Metals Park, Ohio (1973).
- [120] HULTGREN, R., DESAI, P.D., HAWKINS, D.T., GLEISER, M., KELLEY, K.K., WAGMAN, D.D., Selected Values of the Thermodynamic Properties of the Elements, American Society for Metals, Metals Park, Ohio (1973).
- [121] IRVIN, N.M., RUSSELL, A.S., J. Chem. Soc. (1932) 891-98.
- [122] JEHN, H., ETTMAYER, P., High Temp. - High Pressures 8 (1976) 83-94; J. Less-Common Met. 58 (1978) 85-98.
- [123] JEITSCHKO, W., DONOHUE, P.C., Acta Crystallogr., Sect. B, 28 (1972) 1893-98.
- [124] JENSEN, P., KJEKSHUS, A., Acta Chem. Scand. 20 (1966) 1309-13.
- [125] JENSEN, P., KJEKSHUS, A., SKANSEN, T., Acta Chem. Scand. 19 (1965) 1499; 20 (1966) 1003-15.
- [126] JENSEN, P., KJEKSHUS, A., SKANSEN, T., Acta Chem. Scand. 20 (1966) 403-16.
- [127] JOHANSSON, T., Acta Chem. Scand. 26 (1972) 365-82.
- [128] JOHNSON, R.L., SIEGEL, B., J. Inorg. Nucl. Chem. 31 (1969) 955-63.
- [129] KAMEI, K., NINOMIYA, T., TERAUCHI, S., Technol. Rep. Kansai Univ., Osaka, No.13 (1972) 93-106.
- [130] KANDLER, H., REISS, B., Z. Naturforsch., A 21 (1966) 549-54.
- [131] KASHIN, V.I., KLIBANOV, E.L., TSILOSANI, A.G., TYLKINA, M.A., KONIEVA, L.Z., Izv. Akad. Nauk SSSR, Met. No.2 (1971) 39-48; Russ. Met. No.2 (1971) 25-30.
- [132] KASPER, J.S., DECKER, B.F., BELANGER, J.R., J. Appl. Phys. 22 (1951) 361-62.
- [133] KATAYAMA, I., AOKI, M., KOZUKA, Z., Nippon Kinzoku Gakkaishi 39 (1975) 1210-14.
- [134] KEMPTER, C.P., Trans. Metall. Soc. AIME 242 (1968) 1483.
- [135] KEPERT, D.L., MARSHALL, R.E., TAYLOR, D., J. Chem. Soc. Dalton (1974) 506-9.
- [136] KHALDOYANIDI, K.A., GRANKINA, Z.A., Izv. Sib. Otd. Akad. Nauk SSSR, Ser. Khim. Nauk No.1 (1976) 47-50.
- [137] KHARITONOV, V.I., FEDOTOV, S.G., MAKUNIN, M.S., SHAMARAI, F.I., FALALEEVA, Z.S., SINDOVA, E.P., Izv. Akad. Nauk SSSR, Met. No.5 (1972) 133-37; Chem. Abstr. 78 (1973) 33174.
- [138] KHARITONOV, V.I., MAKUNIN, M.S., SHAMARAI, F.I., Tsvetn. Met. 41 (1968) 84-86; Chem. Abstr. 69 (1968) 100046; and Izv. Akad. Nauk SSSR, Met. (1971) 169-71; Chem. Abstr. 75 (1971) 112207.

- [139] KIHLBORG, L., *Acta Chem. Scand.* **13** (1959) 954-62.
- [140] KILLPATRICK, O.H., *J. Phys. Chem. Solids* **25** (1964) 1499-1500.
- [141] KING, E.G., WELLER, W.W., CHRISTENSEN, A.U., US Bureau of Mines Rep. Invest. 5664 (1960) 1-29.
- [142] KIRCHNER, G., HARVIG, H., UHRENJUS, B., *Metall. Trans.* **4** (1973) 1059-67.
- [143] KLEINSCHMIDT, P.D., LAU, K.H., HILDENBRAND, D.J., *J. Chem. Thermodyn.* **11** (1979) 765-72.
- [144] KNAPTON, A.G., *J. Inst. Met.* **87** (1958-59) 62-64; *Trans. Am. Soc. Met.* **51** (1959) 1067-68.
- [145] KNAPTON, A.G., in *Constitution of Binary Alloys* (HAWKINS, D.T., HULTGREN, R., Eds), Metals Handbook, 8th ed., American Society for Metals, Metals Park, Ohio (1973) 312, 365.
- [146] KOCHERZHINSKIJ, Y.A., *Colloq. Int. Cent. Nat. Rech. Sci.* No. 205 (1972) 47-51.
- [147] KOLOMITSSEV, P.T., MOSKALEVA, N.V., *Dokl. Akad. Nauk SSSR* **154** (1964) 1120-22.
- [148] KORSHUNOV, B.G., NIRSHA, B.M., *Zh. Neorg. Khim.* **14** (1969) 3143-46; Russ. J. Inorg. Chem. **14** (1969) 1656-58.
- [149] KOZLOVA, R.F., RABKIN, V.B., BLINOVA, N.V., *Poroshk. Metall.* No.2 (1973) 65-70.
- [150] KOZLOVA, R.F., RABKIN, V.B., LOSEV, L.Ya., PASHCHENKO, E.F., *Poroshk. Metall.* No.5 (1973) 56-60.
- [151] KRAJEWSKI, W., KRUEGER, J., WINTERHAGER, H., *Cobalt* **48** (1970) 120-28.
- [152] KRAUSE, R.F., Jr., in *Proc. Symp. High Temperature Metal Halide Chemistry* (HILDENBRAND, D.L., CUBICCIOTTI, D.D., Eds), Vol. 78-1, Electrochemical Society, Princeton, New Jersey (1978) 199-209.
- [153] KRAUSE, R.F., Jr., DOUGLAS, T.B., *J. Chem. Thermodyn.* **9** (1977) 1149-63.
- [154] KUBASCHEWSKI, O., CHART, T.G., *J. Inst. Met.* **93** (1965) 329.
- [155] KUBASCHEWSKI-von GOLDBECK, O., in *Zirconium: Physico-Chemical Properties of its Compounds and Alloys* (KUBASCHEWSKI, O., Ed.), Atomic Energy Review, Special Issue No.6, IAEA, Vienna (1976) 96-97.
- [156] KURILO, Y.P., SOMOV, A.I., TORTIKA, A.S., *Izv. Akad. Nauk. SSSR, Met.* No.1 (1973) 216-17.
- [157] LAMOREAUX, R.H., Melting Point Gram-Atomic Volumes and Enthalpies of Atomization for Liquid Elements, California Univ., Berkeley, Lawrence Berkeley Lab., Rep. LBL-4995 (1976).
- [158] LANGE, K.W., SCHENCH, H., *Z. Metallkd.* **60** (1969) 62-68.
- [159] LASSNER, E., PÜSCHEL, R., BENESOVSKY, F., *Planseeber. Pulvermetall.* **16** (1968) 91-103.
- [160] LEAVENWORTH, H., CLEARY, R.E., BRATTON, W.V., *Acta Metall.* **9** (1961) 519.
- [161] LEWIS, J., MACHIN, D.J., MYHOLM, R.S., PAULING, P., SMITH, P.W., *Chem. Ind.* (London) (1960) 259-60.
- [162] LINDE, J.O., *Ann. Physik* **15** (1932) 219-247, especially 231.
- [163] LINEL, F.V., *Trans. Metall. Soc. AIME* **175** (1948) 878-905.
- [164] LUNDSTRÖM, T., ROSENBERG, I., *J. Solid State Chem.* **6** (1973) 299-305.
- [165] McCABE, C.L., *Trans. Metall. Soc. AIME* **203** (1955) 61-63.
- [166] McKISSON, R.L., EICHELBERGER, R.L., DAHLEEN, R.C., SCARBOROUGH, J.M., ARGUE, G.R., Atomics International Div., Canoga Park, CA, Rep. AI-65-210 (1966).

<sup>a</sup> Available from National Technical Information Service, United States Dept. of Commerce, 5285 Port Royal Road, Springfield, VA 22161, USA.

## PART II. PHASE DIAGRAMS

- [167] McMASTERS, O.D., PALMER, P.E., LARSEN, W.L., *J. Nucl. Mater.* **7** (1962) 151-56.
- [168] MALDONADO, A., SCHUBERT, K., *Z. Metallkd.* **55** (1964) 619-26.
- [169] MARDON, P.G., EVANS, J.P., HODKIN, D.J., NORTH, J.M., PEARCE, J.H., in *Plutonium 1960* (GRISON, E., LORD, W.B.H., FOWLER, R.D., Eds), Cleaver-Hume Press, London (1961) 329-52.
- [170] MARTIN, A.E., KNIGHTON, J.B., FEDER, H.M., *J. Chem. Eng. Data* **6** (1961) 596-99.
- [171] MARTIN, E., *Arch. Eisenhüttenwes.* **3** (1929) 407-16.
- [172] MATVEEVA, M.P., VOLKOVA, R.M., MARCHUKOVA, I.D., BOZHENOV, V.A., *Fiz. Met. Metalloved.* **43** (1977) 657-60.
- [173] MAZAEV, A.A., AVARBE, R.G., VIL'K, Yu.N., *Zh. Fiz. Khim.* **42** (1968) 641-43; *Izv. Akad. Nauk SSSR, Met.* No.4 (1969) 255-56; *Russ. Metall.* No.4 (1969) 163-65.
- [174] MERCER, M., *Chem. Commun.* No.3 (1967) 119.
- [175] MERING, J., LEVIALDI, A., C.R. Hebd. Acad. Sci. **213** (1941) 798-800.
- [176] MORIMOTO, N., KULLERUD, G., in *Carnegie Institution of Washington, Year Book* **61** (1962) 143-44.
- [177] NECHIPORENKO, E.P., POLTAVTSEV, N.S., KAPUSTIN, V.L., KONDRATOV, Y.T., *Izv. Akad. Nauk SSSR, Neorg. Mater.* **9** (1973) 1829-30.
- [178] NOWOTNY, H., HASCHKE, H., BENESOVSKY, F., *Monatsh. Chem.* **98** (1967) 547-54.
- [179] OATES, W.A., MCLELLAN, R.B., *Scri. Metall.* **6** (1972) 349-52.
- [180] OCKEN, H., VAN VUCHT, J.H.N., *J. Less-Common Met.* **15** (1968) 193-200.
- [181] OPALOVSKIJ, A., FEDOROV, V.E., LOBKOV, E.U., TSIKANOVSKIJ, B.I., *Zh. Fiz. Chim.* **45** (1971) 1864.
- [182] OPPERMANN, H., *Z. Anorg. Allg. Chem.* **395** (1975) 249-61.
- [183] OPPERMANN, H., STÖVER, G., *Z. Anorg. Allg. Chem.* **387** (1972) 218-29.
- [184] OSBORNE, D.W., SCHREINER, F., MALM, J.G., SELIG, H., ROCHESTER, L., *J. Chem. Phys.* **44** (1966) 2802-9.
- [185] PARKMAN, R., SHEPARD, O.C., USAEC, Oak Ridge Operations Office, Tennessee, Rep. ORO-45 (1951).
- [186] PEARSON, W.B., *A Handbook of Lattice Spacings and Structures of Metals and Alloys*, Vol.2, Chapter 1, Pergamon Press, London, New York (1967).
- [187] PERRY, T., SPACIL, H.S., WULF, J., *Weld. J.* **33** (1954) 442-45.
- [188] PHILLIPS, B., CHANG, L.L.Y., *Trans. Metall. Soc. AIME* **233** (1965) 1433-36.
- [189] PIPITZ, E., KIEFFER, R., *Z. Metallkd.* **46** (1955) 187-94.
- [190] POPOV, A.P., TSVETNIKOV, A.K., GONCHARUK, V.K., *Zh. Neorg. Khim.* **23** (1978) 236-39.
- [191] PORTNOI, K.I., LEVINSKIJ, Y.V., ROMASHOV, V.M., MOROVIN, O.A., LEVINSKAYA, M.K., *Izv. Akad. Nauk SSSR, Met.* No.4 (1967) 171-76.
- [192] PÖTZSCHKE, M., SCHUBERT, K., *Z. Metallkd.* **53** (1962) 548-61.
- [193] POUILLARD, G., PERROT, P., C.R. Hebd. Acad. Sci., Ser. C, **281** (1975) 143-46.
- [194] PUTNAM, J.W., POTTER, R.D., GRANT, N.J., *Trans. Am. Soc. Met.* **43** (1951) 824-47.
- [195] QUINN, T.J., HUME-ROTHERY, W., *J. Less-Common Met.* **5** (1963) 314-24.
- [196] RAPP, O., *J. Less-Common Met.* **21** (1971) 27.
- [197] RAUB, E., *Z. Metallkd.* **45** (1954) 23-30.
- [198] RAUB, E., *Z. Metallkd.* **51** (1960) 290-91.
- [199] RAWLINGS, R.D., NEWHEY, C.W.A., *J. Iron Steel Inst.* **206** (1968) 723.
- [200] REAVIS, J.G., BREWER, G.R., COURT, D.B., SCHULTE, J.W., Los Alamos Scientific Lab., NM, Rep. LA-DC-12753 (1971).
- [201] REXER, J., *Z. Metallkd.* **62** (1971) 844-48.
- [202] RIEGER, W., NOWOTNY, H., BENESOVSKY, F., *Monatsh. Chem.* **95** (1964) 1502-3.

- [203] RONAMI, G.N., *Krist. Tech.* **7** (1972) 615.
- [204] RONAMI, G.N., KUZNETSOVA, S.M., FEDOTOV, S.G., KONSTANTINOV, K.M., *Vestn. Mosk. Univ., Ser. III, Fiz. Astron.* **11** 2 (1970) 186.
- [205] RUDY, E., *Compendium of Phase Diagram Data*, Air Force Materials Laboratory, Wright-Patterson AFB, Ohio, Rep. No. AFML-TR-65-2, Part V (June 1969)<sup>a</sup>.
- [206] RUDY, E., BENESOVSKY, F., TOTH, L.E., *Z. Metallkd.* **54** (1963) 345–53.
- [207] RUDY, E., WINDISCH, S., CHANG, Y.A., Air Force Materials Laboratory, Wright-Patterson, AFB, Ohio, Rep. No. AFML-TR-65-2, Part I, Vol. I (March 1965).
- [208] RUDY, E., WINDISCH, S., Air Force Materials Laboratory, Wright-Patterson, AFB, Ohio, Rep. No. AFML-TR-65-2, Part I, Vol. 3 (1965). (See also Rudy [205]).
- [209] RUDY, E., WINDISCH, S., HOFFMAN, J.R., Air Force Materials Laboratory, Wright-Patterson, AFB, Ohio, Rep. No. AFML-TR-65-2, Part I, Vol. 6 (Jan. 1966).
- [210] RUDY, E., WINDISCH, S., STOSICK, A.J., HOFFMAN, J.R., Air Force Materials Laboratory, Wright-Patterson, AFB, Ohio, Rep. No. AFML-TR-65-2, Part I, Vol. 11 (Apr. 1967); and *Trans. Metall. Soc. AIME* **239** (1967) 1247–67.
- [211] RUEDL, E., *Mater. Res. Bull.* **10** (1975) 267–72.
- [212] SAMSONOV, G.V., VEREIKIN, L.L., *Fosfidy, Izdatel. Akad. Nauk Ukr. SSR*, Kiev (1961).
- [213] SAVITSKIJ, E.M., BARON, V.Y., TAO, T.T., *Izv. Akad. Nauk SSSR, Otd. Tekh. Nauk, Met. Toplivo* No.1 (1962) 156–59.
- [214] SAVITSKIJ, E.M., TEREKHOVA, V.F., *Tsvetn. Met.* **32** 1 (1959) 48–53.
- [215] SAVITSKIJ, E.M., TYLKINA, M.A., in *Rhenium* (GONSER, B.W., Ed.), Elsevier, Amsterdam (1962) 67–83.
- [216] SAVITSKIJ, E.M., TYLKINA, M.A., KHAMIDOV, O.K., *Russ. J. Inorg. Chem.* **9** (1964) 1475–77.
- [217] SAVITSKIJ, E.M., TYLKINA, M.A., KHAMIDOV, O.K., *Izv. Akad. Nauk SSSR, Met.* **4** (1969) 200–8.
- [218] SAVITSKIJ, E.M., TYLKINA, M.A., POVAROVA, K.B., *Russ. J. Inorg. Chem.* **4** (1959) 190–95.
- [219] SCHAEFER, S.C., LARSON, A.H., SCHLECHTEN, A.W., *Trans. Metall. Soc. AIME* **230** (1964) 594–95.
- [220] SCHÄFER, H., GROFE, T., TRENKEL, M., *J. Solid State Chem.* **8** (1973) 14–28.
- [221] SCHÄFER, H., SCHNERING, H.-G. von, NIEHUES, K.-J., NIEDER-VAHRENHOLZ, H.G., *J. Less-Common Met.* **9** (1965) 100.
- [222] SCHÄFER, H., SCHNERING, H.-G. von, TILLACK, J., KUHNEN, F., WÖHRLE, H., BAUMANN, H., *Z. Anorg. Allg. Chem.* **353** (1967) 281–310.
- [223] SCHÄFER, H., SIEPMANN, R., *Z. Anorg. Allg. Chem.* **357** (1968) 273–88.
- [224] SCHUSTER, J., RUDY, E., NOWOTNY, H., *Monatsh. Chem.* **107** (1976) 1167–76.
- [225] SELLBERG, B., RUNDQVIST, S., *Acta Chem. Scand.* **19** (1965) 393–400, 760–62.
- [226] SEYBOLT, U., *Trans. Am. Soc. Met.* **52** (1960) 971–89.
- [227] SHINYAEV, A.Ya., FEDOROV, V.B., GORSHKOVA, L.V., CHERNOV, D.B., *Dokl. Akad. Nauk SSSR* **212** (1973) 1336–38.
- [228] SHUNK, F.A., *Constitution of Binary Alloys, Supplement No.2*, McGraw-Hill, New York (1969).
- [229] SIEPMANN, R., SCHÄFER, H., *Naturwiss.* **52** (1965) 344–45.

<sup>a</sup> Available from National Technical Information Service, United States Dept. of Commerce, 5285 Port Royal Road, Springfield, VA 22161, USA, as Publ. No. AD 689843/LL IPC(N) 268.

- [230] SIEVERTS, A., BRÜNING, K., *Arch. Eisenhüttenwes.* **7** (1934) 641–45.
- [231] SINHA, A.K., BUCKLEY, R.A., HUME-ROTHERY, W., *J. Iron Steel Inst.* **205** (1967) 191–95.
- [232] SMITH, J.L., HILL, H.H., *Bull. Am. Phys. Soc.* **21** (1976) 383.
- [233] SPIESSER, M., ROUXE, J., KERRIOU, M., GOUREAUX, M.G., *Bull. Soc. Chim.* No.5 (1969) 1427–31.
- [234] SPERNER, F., *Z. Metallkd.* **50** (1959) 588–91.
- [235] SRIVASTAVA, S.C., SEIGLE, L.L., *Metall. Trans.* **5** (1974) 49–52.
- [236] STECHER, P., BENESOVSKY, F., NOWOTNY, H., *Monatsh. Chem.* **94** (1963) 1154–62.
- [237] STECURA, S., National Aeronautics and Space Administration, Cleveland, Ohio, Rep. NASA-TN-D-5504 (1969).
- [238] STEINITZ, R., BINDER, I., MOSKOVITZ, D., *Trans. Metall. Soc. AIME, J. Met.* **4** (1952) 983–87.
- [239] STEINMETZ, P., DUPRE, B., ROQUES, B., *J. Less-Common Met.* **53** (1977) 43–53.
- [240] STEMPROK, M., KULLERUD, G., in *Carnegie Institution of Washington, Year Book 65* (1965–66) 336–42.
- [241] STORMS, E., MUELLER, B., *J. Phys. Chem.* **81** (1977) 318–24.
- [242] STRACHAN, J.F., HARRIS, N.L., *J. Inst. Met.* **85** (1956–57) 17–24.
- [243] SVECHNIKOV, V.N., KOCHERZHINSKII, Yu.A., YUPKO, L.M., *Dopov. Akad. Nauk Ukr. RSR, Ser. A* **32** (1970) 553–58.
- [244] SYKES, W.P., GRAFF, H.F., *Trans. Am. Soc. Met.* **23** (1935) 249–83.
- [245] TAYLOR, A., Tech. Rep. ASD-TDR-63-204 (AD-409434) (1963).
- [246] TAYLOR, J.B., CALVERT, L.D., HUNT, M.R., *Can. J. Chem.* **43** (1965) 3045–51.
- [247] TAYLOR, A., DOYLE, N.J., KAGLE, B.J., *J. Less-Common Met.* **3** (1961) 265.
- [248] TAYLOR, A., DOYLE, N.J., KAGLE, B.J., *J. Less-Common Met.* **4** (1962) 436–50.
- [249] TELEGUS, V.S., KUZ'MA, Y.B., MARKO, M.A., Sov. Powder Metall. Met. Ceram. **10** (1971) 898–903.
- [250] TEPLER, F., GREER, J., Air Force Materials Laboratory, Wright-Patterson, AFB, Ohio, Rep. AFML-TR-64-327 (1964).
- [251] TERAUCHI, S., MATSUMOTO, H., SUGIMOTO, T., KAMEI, K., *Nippon Kinzoku Gakkai-Shi* **41** (1977) 632.
- [252] TOWLE, L.C., OBERBECK, V., BROWN, B.E., STAJDODAR, R.E., *Science* **154** (1966) 895–96.
- [253] VAN TENDELOO, G., *Mater. Sci. Eng.* **26** (1976) 209–20.
- [254] VAN TENDELOO, G., VAN LANDUYT, J., AMELINCKX, S., *Mater. Res. Bull.* **10** (1975) 941–48.
- [255] VELLINGA, M.B., DEJONGE, R., HAAS, C.U., *Solid State Chem.* **220** (1970) 299–302.
- [256] VENGERNOVICH, R.D., PSAREV, V.I., *Izv. Akad. Nauk SSSR, Met.* No.5 (1970) 186–93.
- [257] VOGEL, R., HORSTMANN, D., *Arch. Eisenhüttenwes.* **24** (1953) 369–74.
- [258] VÖLLENKLE, H., WITTMANN, A., NOWOTNY, H., *Monatsh. Chem.* **95** (1964) 1544–49; **97** (1966) 506–16.
- [259] WALFORD, L.K., *Philos. Mag.* **9** (1964) 513–16; *Acta Crystallogr.* **17** (1964) 57–59.
- [260] WEEKS, J.R., *Trans. Am. Soc. Met.* **58** (1965) 302–22.
- [261] WESTLAND, A.D., UZELAC, V., *Inorg. Chim. Acta* **23** (1977) L37–39.
- [262] WITCOMB, M.J., DEW-HUGHES, D., *J. Less-Common Met.* **31** (1973) 197–209.
- [263] WITTEMAN, W.G., GIORGI, A.L., VIER, D.T., *J. Phys. Chem.* **64** (1960) 434–40.
- [264] WITTMANN, A., NOWOTNY, H., BOLLER, H., *Monatsh. Chem.* **91** (1960) 608–15.
- [265] YAMAGUCHI, K., SIMIZU, K., *Nippon Kinzoku Gakkai-Shi* **4** (1940) 390–92.

- [266] YANAKI, A.A., OBOLONCHIK, V.A., Zh. Prikl. Khim. 47 (1974) 1454-58; J. Appl. Chem. USSR 47 (1974) 1499-1503.
- [267] YATSENKO, S.P., ANIKIN, Yu.A., Fiz. Khim. Mekh. Mater. 6 (1970) 57-62.
- [268] YATSENKO, S.P., DIEVA, E.N., Zh. Fiz. Khim. 47 (1973) 2948.
- [269] YVON, K., Acta Crystallogr., Sect.B, 30 (1974) 853-56; 31 (1975) 117-20.
- [270] ZADOR, S., ALCOCK, C.B., J. Chem. Thermodyn. 2 (1970) 9-16.
- [271] ZAKHAROV, A.M., NOVIKOV, I.I., POL'KIN, V.C., Izv. Vyssh. Uchebn. Zaved., Tsvetn. Metall. 14 (1971) 126-29; Chem. Abstr. 76 (1972) 132161.
- [272] ZAKHAROV, A.P., SHARAPOV, V.M., Fiz.-Khim. Mekh. Mater. 7 6 (1971) 54-58.
- [273] ZAISS, W., STEEB, S., KRABICHLER, T., Z. Metallkd. 63 (1972) 180.
- [274] ZELIKMAN, A.N., BELYAEVSKAYA, L.V., Zh. Neorg. Khim. 1 (1956) 2239.
- [275] ZHUKOVSKIY, V.M., YANUSHKEVICH, T.M., LEBEDKIN, V.P., VOLKOV, V.L., NEUIMIN, A.D., Zh. Fiz. Khim. 46 (1972) 2688-89.